

# Advances

## in Clinical and Experimental Medicine

MONTHLY ISSN 1899-5276 (PRINT) ISSN 2451-2680 (ONLINE)

[www.advances.umw.edu.pl](http://www.advances.umw.edu.pl)

2022, Vol. 31, No. 1 (January)

Impact Factor (IF) – 1.727  
Ministry of Science and Higher Education – 70 pts  
Index Copernicus (ICV) – 166.39 pts



WROCLAW  
MEDICAL UNIVERSITY

Advances  
in Clinical and Experimental  
Medicine



# Advances in Clinical and Experimental Medicine

ISSN 1899-5276 (PRINT)

ISSN 2451-2680 (ONLINE)

[www.advances.umw.edu.pl](http://www.advances.umw.edu.pl)

**MONTHLY 2022**  
**Vol. 31, No. 1**  
**(January)**

Advances in Clinical and Experimental Medicine (*Adv Clin Exp Med*) publishes high quality original articles, research-in-progress, research letters and systematic reviews and meta-analyses of recognized scientists that deal with all clinical and experimental medicine.

## Editorial Office

ul. Marcinkowskiego 2–6  
50-368 Wrocław, Poland  
Tel.: +48 71 784 11 36  
E-mail: [redakcja@umw.edu.pl](mailto:redakcja@umw.edu.pl)

## Publisher

Wrocław Medical University  
Wybrzeże L. Pasteura 1  
50-367 Wrocław, Poland

© Copyright by Wrocław Medical University,  
Wrocław 2022

Online edition is the original version  
of the journal

## Editor-in-Chief

Prof. Donata Kurpas

## Deputy Editor

Prof. Wojciech Kosmala

## Managing Editor

Marek Misiak

## Scientific Committee

Prof. Sabine Bährer-Kohler  
Prof. Antonio Cano  
Prof. Breno Diniz  
Prof. Erwan Donal  
Prof. Chris Fox  
Prof. Naomi Hachiya  
Prof. Carol Holland  
Prof. Markku Kurkinen  
Prof. Christos Lionis

## Section Editors

### Basic Sciences

Prof. Iwona Bil-Lula  
Prof. Bartosz Kempisty  
Dr. Anna Lebedeva  
Dr. Mateusz Olbromski  
Dr. Maciej Sobczyński

### Biochemistry

Prof. Małgorzata Krzystek-Korpacka

### Clinical Anatomy, Legal Medicine, Innovative Technologies

Prof. Rafael Boscolo-Berto

### Dentistry

Prof. Marzena Dominiak  
Prof. Tomasz Gedrange  
Prof. Jamil Shibli

## Statistical Editors

Wojciech Bombała, MSc  
Katarzyna Giniewicz, MSc Eng.  
Anna Kopszak, MSc  
Dr. Krzysztof Kujawa

## Manuscript editing

Marek Misiak, Jolanta Krzyżak

Prof. Raimundo Mateos  
Prof. Zbigniew W. Ras  
Prof. Jerzy W. Rozenblit  
Prof. Silvina Santana  
Prof. James Sharman  
Prof. Jamil Shibli  
Prof. Michal Toborek  
Prof. László Vécsei  
Prof. Cristiana Vitale

## Dermatology

Prof. Jacek Szepietowski

## Emergency Medicine, Innovative Technologies

Prof. Jacek Smereka

## Gynecology and Obstetrics

Prof. Olimpia Sipak-Szmigiel

## Histology and Embryology

Prof. Marzena Podhorska-Okołów

## Internal Medicine

### Angiology

Dr. Angelika Chachaj

### Cardiology

Prof. Wojciech Kosmala  
Dr. Daniel Morris

### Endocrinology

Prof. Marek Bolanowski

### Gastroenterology

Prof. Piotr Eder

Assoc. Prof. Katarzyna Neubauer

### Hematology

Prof. Andrzej Deptała

Prof. Dariusz Wołowicz

### Nephrology and Transplantology

Assoc. Prof. Dorota Kamińska

Assoc. Prof. Krzysztof Letachowicz

### Pulmonology

Prof. Elżbieta Radzikowska

### Microbiology

Prof. Marzenna Bartoszewicz

Assoc. Prof. Adam Junka

### Molecular Biology

Dr. Monika Bielecka

Prof. Jolanta Sączko

Dr. Marta Sochocka

### Neurology

Assoc. Prof. Magdalena Koszewicz

Assoc. Prof. Anna Pokryszko-Dragan

Dr. Masaru Tanaka

### Oncology

Prof. Andrzej Deptała

Dr. Marcin Jędryka

Prof. Lucyna Kępka

#### Gynecological Oncology

Dr. Marcin Jędryka

### Ophthalmology

Prof. Marta Misiuk-Hojło

### Orthopedics

Prof. Paweł Reichert

### Otolaryngology

Assoc. Prof. Tomasz Zatoński

### Pediatrics

Pediatrics, Metabolic Pediatrics, Clinical Genetics, Neonatology, Rare Disorders

Prof. Robert Śmigiel

#### Pediatric Nephrology

Prof. Katarzyna Kiliś-Pstrusińska

#### Pediatric Oncology and Hematology

Assoc. Prof. Marek Ussowicz

### Pharmaceutical Sciences

Assoc. Prof. Maria Kepinska

Prof. Adam Matkowski

### Pharmacoeconomics, Rheumatology

Dr. Sylwia Szafraniec-Buryło

### Psychiatry

Prof. Istvan Boksay

Prof. Jerzy Leszek

### Public Health

Prof. Monika Sawhney

Prof. Izabella Uchmanowicz

### Qualitative Studies, Quality of Care

Prof. Ludmiła Marcinowicz

### Radiology

Prof. Marek Szaśniadek

### Rehabilitation

Prof. Jakub Taradaj

### Surgery

Assoc. Prof. Mariusz Chabowski

Prof. Renata Taboła

### Telemedicine, Geriatrics, Multimorbidity

Assoc. Prof. Maria Magdalena

Bujnowska-Fedak

---

## Editorial Policy

Advances in Clinical and Experimental Medicine (Adv Clin Exp Med) is an independent multidisciplinary forum for exchange of scientific and clinical information, publishing original research and news encompassing all aspects of medicine, including molecular biology, biochemistry, genetics, biotechnology and other areas. During the review process, the Editorial Board conforms to the "Uniform Requirements for Manuscripts Submitted to Biomedical Journals: Writing and Editing for Biomedical Publication" approved by the International Committee of Medical Journal Editors ([www.ICMJE.org/](http://www.ICMJE.org/)). The journal publishes (in English only) original papers and reviews. Short works considered original, novel and significant are given priority. Experimental studies must include a statement that the experimental protocol and informed consent procedure were in compliance with the Helsinki Convention and were approved by an ethics committee.

For all subscription-related queries please contact our Editorial Office:  
[redakcja@umw.edu.pl](mailto:redakcja@umw.edu.pl)

For more information visit the journal's website:  
[www.advances.umw.edu.pl](http://www.advances.umw.edu.pl)

Pursuant to the ordinance No. 134/XV R/2017 of the Rector of Wrocław Medical University (as of December 28, 2017) from January 1, 2018 authors are required to pay a fee amounting to 700 euros for each manuscript accepted for publication in the journal Advances in Clinical and Experimental Medicine.

Indexed in: MEDLINE, Science Citation Index Expanded, Journal Citation Reports/Science Edition, Scopus, EMBASE/Excerpta Medica, Ulrich's™ International Periodicals Directory, Index Copernicus

Typographic design: Piotr Gil, Monika Kołęda  
DTP: Wydawnictwo UMW  
Cover: Monika Kołęda  
Printing and binding: Soft Vision Mariusz Rajski

## Contents

### Editorials

- 5 Zbigniew Raś  
**Reduction of hospital readmissions**

### Original papers

- 9 Jun Yang, Youxin Liao, Yonghong Dai, Ling Hu, Yihong Cai  
**Prediction of prognosis in sepsis patients by the SOFA score combined with miR-150**
- 17 Conghui Zhu, Guanfeng Chen, Jiadi Yao, Wenji Lin  
**Effect of infection after liver cancer interventional therapy on T lymphocyte subsets and Toll-like receptors in peripheral blood mononuclear cells and its mechanism**
- 25 Małgorzata Godala, Ewa Sewerynek, Ewelina Gaszyńska  
**Vitamin D status in Polish women with endocrine and osteoporotic disorders in relation to diet, supplement use and exposure to ultraviolet radiation**
- 33 Agata Ewa Kaczyńska, Adam Kosiński, Katarzyna Bobkowska, Miłosz Andrzej Zajączkowski, Rafał Kamiński, Grzegorz Marek Piwko, Marta Gleinert-Rożek, Tomasz Gos, Karol Karnecki, Dariusz Kozłowski  
**Clinical anatomy of the spatial structure of the right ventricular outflow tract**
- 41 Joanna Budny-Wińska, Aleksandra Zimmer-Stelmach, Michał Pomorski  
**Impact of selected risk factors on uterine healing after cesarean section in women with single-layer uterine closure: A prospective study using two- and three-dimensional transvaginal ultrasonography**
- 49 Lifeng An, Dandan Zhu, Xin Zhang, Jingwen Huang, Guangbao Lu  
**Isoastilbin inhibits neuronal apoptosis and oxidative stress in a rat model of ischemia-reperfusion injury in the brain: Involvement of SIRT1/3/6**
- 59 Jingjing Guo, Zhu Wang, Ming Xue, Lei Mi, Mengpeng Zhao, Chao Ma, Jian Wu, Xinqiang Han  
**Metformin protects against abdominal aortic aneurysm by Atg7-induced autophagy**
- 71 Ayşegül Çopur Çiçek, Vicdan Şemen, Nebahat Aydoğan Ejder, Deniz Zehra Ulusan Gündoğdu, Sema Kocyiğit Kalcan, Fatma Tufan Köse, Osman Birol Özgümüş  
**Molecular epidemiological analysis of integron gene cassettes and *tetA/tetB/tetD* gene associations in *Escherichia coli* strains producing extended-spectrum  $\beta$ -lactamase (ESBL) in urine cultures**
- 81 Edyta Banaczewska-Duda, Alicja Bierkowska-Tokarczyk, Maciej Małecki  
**Gene capsules as functional pharmaceutical formulations for delivery of DNA as an active substance**

### Reviews

- 95 Grzegorz Charliński, Artur Jurczyszyn  
**Non-secretory multiple myeloma: Diagnosis and management**



# Reduction of hospital readmissions

Zbigniew Raś<sup>D</sup>

Computer Science Department, University of North Carolina, Charlotte, USA

A – research concept and design; B – collection and/or assembly of data; C – data analysis and interpretation;  
D – writing the article; E – critical revision of the article; F – final approval of the article

Advances in Clinical and Experimental Medicine, ISSN 1899–5276 (print), ISSN 2451–2680 (online)

*Adv Clin Exp Med.* 2022;31(1):5–8

## Address for correspondence

Zbigniew Raś  
E-mail: [ras@uncc.edu](mailto:ras@uncc.edu)

## Funding sources

None declared

## Conflict of interest

None declared

Received on November 23, 2021

Accepted on December 1, 2021

Published online on January 7, 2022

## Abstract

In recent years, healthcare spending has risen and become a burden on many governments. There are multiple reasons for this increase such as overtesting, long medical treatment path, ignoring doctors' orders, ineffective use of technologies, medical errors, many hospital readmissions, unnecessary emergency room (ER) visits, and medical treatment acquired side effects and infections. The first part of this editorial presents Healthcare Cost and Utilization Project (HCUP) datasets and their hierarchical partition used to build hierarchically structured personalized recommendation systems in healthcare domain. The second part outlines a simple strategy for reducing the number of readmissions using the concept of action rules to provide recommendations. First, we extract from HCUP datasets all possible procedure paths (course of treatments) for a given initial medical procedure. Then, we cluster patients according to the similarities in their diagnoses in order to increase the predictability of the course of treatment following this initial procedure. Finally, we present a novel algorithm that provides recommendations (actionable knowledge) to the physicians to put patients on a treatment path that would result in optimal reduction of the number of readmissions for these patients. There is not much research done on decreasing the number of readmissions to hospitals after initial procedure and almost none based on action rules.

**Key words:** recommendation systems, hospital readmissions, HCUP data, procedure graph, actionable knowledge

## Cite as

Raś Z. Reduction of hospital readmissions.  
*Adv Clin Exp Med.* 2022;31(1):5–8. doi:10.17219/acem/144413

## DOI

10.17219/acem/144413

## Copyright

© 2022 by Wrocław Medical University  
This is an article distributed under the terms of the  
Creative Commons Attribution 3.0 Unported (CC BY 3.0)  
(<https://creativecommons.org/licenses/by/3.0/>)

## Introduction

There are many papers focused on predicting hospital readmissions,<sup>1–4</sup> especially predicting hospital admissions and readmissions to emergency or intensive care units.<sup>5–11</sup> This editorial focuses on the basics of a knowledge-based recommendation system<sup>12,13</sup> for decreasing the number of readmissions to hospitals, based on actionable knowledge extracted from medical datasets, using the concept of action rules<sup>14–16</sup> to provide recommendations. There is not much research done on decreasing the number of readmissions to hospitals after initial procedure and almost none based on action rules.<sup>8</sup>

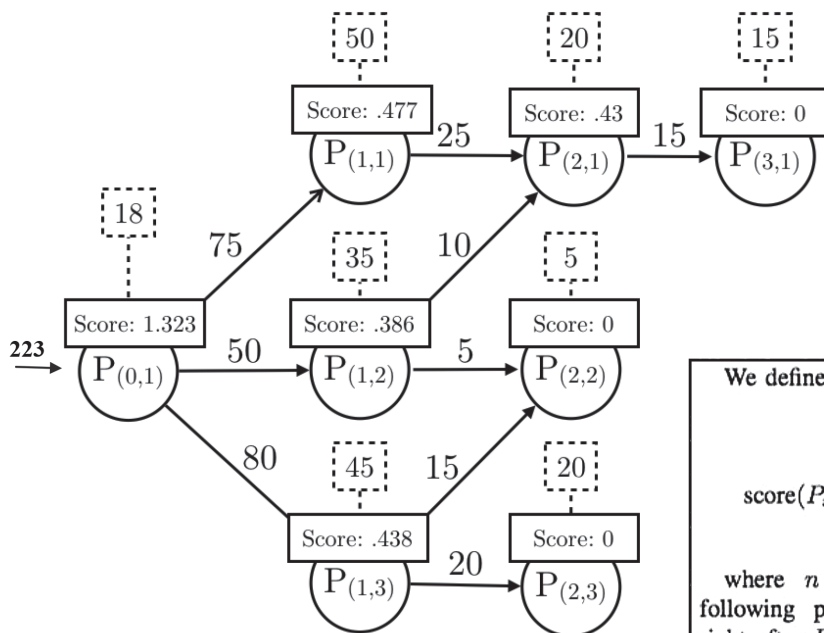
This editorial presents the results obtained from mining the Florida State Inpatient Database (SID) that is a part of the Healthcare Cost and Utilization Project (HCUP<sup>17</sup>). The SID datasets are primarily a state-level discharge data collected from nonfederal community hospitals constituting most of the hospitals in the USA. The SID includes patients' demographic data, such as race, age and gender. In addition to the demographic information, SID includes patients' medical data, such as diagnoses and medical procedures. The main table in SID is the core table that contains over 280 features. Two types of coding schemes are used in the core table for labeling and formatting: (1) The International Classification of Diseases, 9<sup>th</sup> Revision, Clinical Modification (ICD-9-CM), (2) The Clinical Classifications Software (CCS). The ICD-9-CM coding uses more codes to label the procedures and diagnoses, whereas the CCS is a generalized and collapsed version of the ICD-9-CM. There are 15,072 diagnosis categories and 3948 procedure categories in the ICD-9-CM. Clinical

Classifications Software clusters them into 285 diagnosis categories and 231 procedure categories.

## Procedure graph

The ordered sequence of primary medical procedures representing procedure  $P$  followed by all procedures a single patient had after procedure  $P$  during the whole course of treatment in a hospital is called a procedure path for  $P$ .<sup>13</sup>

By a procedure graph,<sup>13</sup> for a medical procedure  $P$ , we mean a directed graph representing a collection of all procedure paths for  $P$  extracted from the Florida SID, associated with patients during their course of treatment. The procedure graph can be used by physicians to visualize all possible outcomes which took place in Florida state hospitals after performing the initial procedure  $P$ . Nodes in the graph represent medical procedures that could be minor, such as breast biopsy, arthroscopy or laparoscopy, or that could be major, such as cesarean section, organ replacement or heart surgeries. The length of a path with a starting node  $P$  in a procedure graph gives the number of hospital readmissions after  $P$ . Figure 1 shows an example of the procedure graph for a procedure  $P_{(0,1)}$ . The numbers assigned to arrows represent the number of patients following that path and numbers in the dashed squares, above each procedure, represent the number of patients who had that procedure and did not come back to the hospital. Each node in a procedure graph is represented as term  $P_{(n,m)}$ , where  $n$  refers to the level of the node in a graph (distance from the initial node), which is the number of current readmissions, and  $m$  represents the path identifier.



We define the procedure score recurrence function as:

$$\text{score}(P_x) = \begin{cases} \sum_{k=1}^n \frac{|P_k|}{|P_x|} * (1 + \text{score}(P_k)) & \text{if } n \geq 1 \\ 0, & \text{otherwise} \end{cases}$$

where  $n$  denotes the number of procedures directly following procedure  $P_x$ ,  $P_k$  denotes the  $k^{\text{th}}$  procedure right after  $P_x$ , and  $|P_k|$  denotes the number of patients that underwent the  $k^{\text{th}}$  procedure.

Fig. 1. Procedure graph and score function



For example,  $P_{(1,3)}$  refers to the procedure node representing the 1<sup>st</sup> readmission to the hospital and belonging to the 3<sup>rd</sup> path in the procedure graph. Now, from the procedure graph, we can predict the most probable procedure path which follows the procedure  $P_{(i,j)}$  for any  $i$  and  $j$ . Function “score” is used to evaluate nodes in the procedure graph (see Fig. 1). The number of procedures directly following procedure  $P_x$  is denoted by  $n$ , and  $|P_k|$  denotes the number of patients who underwent the  $k^{\text{th}}$  procedure in a specific path. The  $P_k$  denotes the  $k^{\text{th}}$  procedure right after  $P_x$ .

The procedure score function assigned to a node in a procedure graph calculates the average number of readmissions after undergoing the procedure assigned to that node. It is a backward function which begins by assigning 0 score to all leaves of the procedure graph, which is the same as assigning 0 readmissions to them. Next, the procedure score function is calculated by moving backward until it reaches the starting node (initial procedure) of the graph. Figure 1 shows the scores assigned to all nodes in the procedure graph. The score 1.323 assigned to procedure  $P_{(0,1)}$  means that the average number of readmissions for all patients who underwent this procedure is 1.323. It also means that 1.323 is the expected number of readmissions for a new patient scheduled to take procedure  $P_{(0,1)}$ .

## Hierarchical clustering

The algorithm<sup>7</sup> is hierarchical and splits patients recorded in HCUP data into clusters using the concept of positive and negative sets. The positive set (P-Set), also called the included set, is a set of diagnoses that a patient must exhibit in order to belong to a certain cluster. Similarly, the negative set (N-Set), also called the excluded set, is a set of diagnoses a patient cannot exhibit in order to belong to a given cluster. From now on, we will use notation (P-Set, N-Set) to define a cluster of patients recorded in HCUP data. For example, taking CCS coding, the label  $\{157, \{-3, -48\}\}$  identifies patients (on the 3<sup>rd</sup> level of granularity – 3 diagnoses are listed) having positive diagnosis 157 (included set) and negative diagnoses 3 and 48 (excluded set). In CCS coding, diagnosis 3 means bacterial infection, 48 means thyroid disorders, while 157 means acute and unspecified renal failure. More diagnoses are used in the labels, smaller are constructed granules and personalization is deeper.

The main goal of this clustering is to partition the patients into subgroups using their common characteristics as the filtering tool. Such process is called personalization of patients, which increases the predictability of the following procedures in the procedure graph and decreases the value of procedure score function (decreases the anticipated number of readmissions). Higher level of personalization is achieved by using labels containing more diagnoses

and the same producing smaller granules. The number of generated clusters will keep increasing when granules are getting smaller. Therefore, there is a need to use a filtering technique to reduce the number of generated clusters. Clearly, if a majority of patients have a common diagnosis or do not have it, then this diagnosis will not play a significant role in determining the state in which the patients will end up. We tested 4 thresholds (5%, 10%, 15%, and 20%) and it looks like the optimal cut (in terms of generated clusters and time complexity) should be between 15% and 20%.

## Reducing the number of readmissions

In this section, we present a new method for constructing medical recommendations to be used by physicians for placing a patient on the shorter, more successful and safer procedure path. The number of anticipated hospital readmissions will be decreased as well. Let us present an example based on Florida State HCUP dataset and CCS coding to explain how these recommendations are constructed.

Figure 2 refers to kidney transplant procedure. If a new patient is assigned to cluster 1 identified by label  $\{106, \{-53, -156\}\}$ , then we cannot enhance the patient’s medical status, as this cluster has the minimum score among the 3 clusters shown in Fig. 2. However, if a patient belongs to any of the 2 remaining clusters, then we can provide a medical recommendation allowing the patient to follow the same path as patients in cluster 1. If we do that, the number of readmissions for this patient should decrease by 48%–52%.

The interpretation for all recommendation actions used in Fig. 2 is as follows:

- $(d \rightarrow d)$ : keep diagnostic code  $d$  for patients in the desired cluster;
- $(\sim \rightarrow -d)$ : patients in the desired cluster cannot have diagnostic code  $d$ ;
- $(d \rightarrow -d)$ : diagnostic code  $d$  has to be treated;
- $(\sim \rightarrow d)$ : patients in the desired cluster need to have diagnostic code  $d$ .

The largest gain in the procedure score is achieved by following the recommendations for patients assigned to cluster 3 identified by label  $\{53, 106, \{-3\}\}$ , which will move them to cluster 1. These patients additionally cannot have disorder 156.

The recommendation that the system will provide to the physician is to treat diagnostic code 53 ( $53 \rightarrow -53$ ) for patients in cluster 3 who do not have disorders identified by diagnostic code 156. By following this recommendation, patients in cluster 3 should end up with the same outcomes as patients in cluster 1. It is worth mentioning that lifestyle changes and drugs are sufficient to treat disorder 53. This will result in 0.5 reduction of hospital readmissions scoring function for these patients (see Fig. 2).

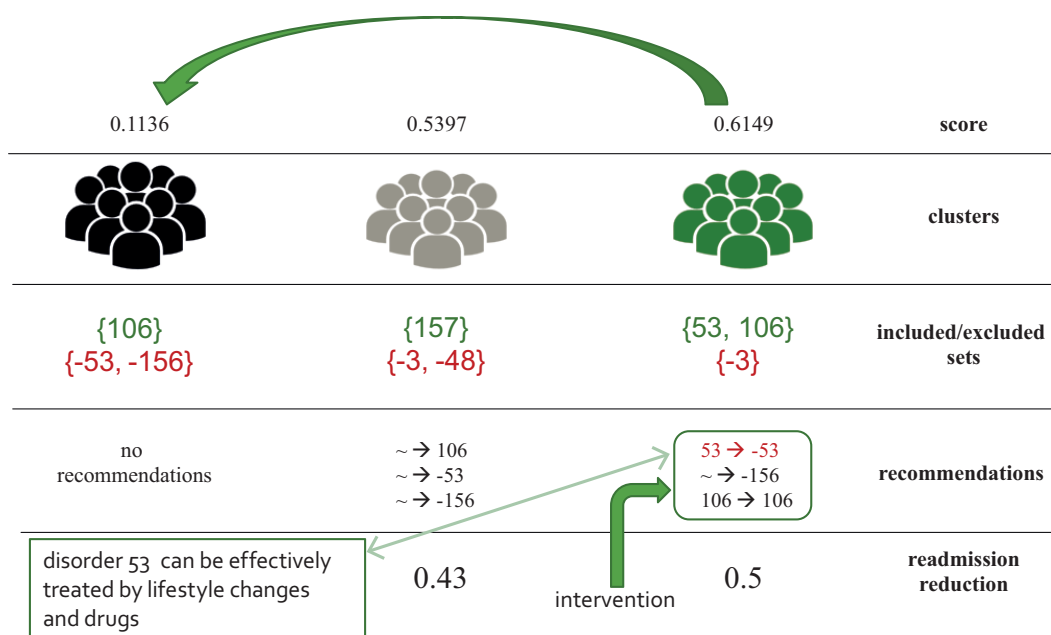


Fig. 2. Kidney transplant recommending actions

Meaning of the diagnostic codes provided in Healthcare Cost and Utilization Project (HCUP) data with Clinical Classifications Software (CCS) coding: 3 – bacterial infection; 48 – thyroid disorders; 53 – disorders of lipid metabolism; 106 – cardiac dysrhythmias; 156 – nephritis, nephrosis, renal sclerosis; 157 – acute and unspecified renal failure.

## ORCID iDs

Zbigniew Raś <https://orcid.org/0000-0002-8619-914X>

## References

- Almardini M, Raś ZW. A supervised model for predicting the risk of mortality and hospital readmissions for newly admitted patients. In: Kryszkiewicz M, Appice A, Ślęzak D, Rybinski H, Skowron A, Raś Z, eds. *Foundations of Intelligent Systems*. Cham, Switzerland: Springer; 2017:29–36. doi:10.1007/978-3-319-60438-1\_3
- Vedomske MA, Brown DE, Harrison JH. Random forests on ubiquitous data for heart failure 30-day readmissions prediction. Paper presented at: 12th International Conference on Machine Learning and Applications; December 4, 2013; Washington, USA. doi:10.1109/ICMLA.2013.158
- Veloso RF, Portela F, Santos MF, et al. Clustering approach for predicting readmissions in intensive medicine. *Procedia Technology*. 2014;16:1307–1316. doi:10.1016/J.PROT.CY.2014.10.147
- Vukicevic M, Radovanovic S, Kovacevic A, Stiglic G, Obradovic Z. Improving hospital readmission prediction using domain knowledge based virtual examples. *Lect Notes Bus Inf Process*. 2015;224:695–706. doi:10.1007/978-3-319-21009-451
- Fernandes MPB, Silva CF, Vieira SM, Sousa JMC. Multi-modeling for the prediction of patient readmissions in intensive care units. Paper presented at: 2014 IEEE International Conference on Fuzzy Systems (FUZZ-IEEE); July 6, 2014; Beijing, China. doi:10.1109/FUZZ-IEEE.2014.6891779
- Lisowska A, Szwamel K, Kurpas D. Somatic symptoms and level of anxiety and depression in self-referral patients at the emergency department. *Med Sci Pulse*. 2020;14(1):1–23. doi:10.5604/01.3001.0014.0685
- Rocha CN, Rodrigues F. Forecasting emergency department admissions. *J Intel Inf Syst*. 2021;56(3):509–528. doi:10.1007/s10844-021-00638-9
- Shams I, Ajorlou S, Yang K. A predictive analytics approach to reducing 30-day avoidable readmissions among patients with heart failure, acute myocardial infarction, pneumonia, or COPD. *Health Care Manag Sci*. 2015;18(1):19–34. doi:10.1007/s10729-014-9278-y
- Silva C, Vieira SM, Sousa JMC. Fuzzy decision tree to predict readmissions in intensive care unit. In: Moreira A, Matos A, Veiga G, eds. *Control'2014 – Proceedings of the 11th Portuguese Conference on Automatic Control*. Cham, Switzerland: Springer; 2015:365–373. doi:10.1007/978-3-319-10380-835
- Szwamel K, Kurpas D. Assessment of the health care system functioning in Poland in light of the analysis of the indicators of the hospital emergency department (ED) and primary health care (PHC) – proposals for systemic solutions. *Fam Med Prim Care Rev*. 2019;21(2):164–173. doi:10.5114/fmPCR.2019.84553
- Szwamel K, Kurpas D. Unmet needs in emergency department patients as an important aspect of the increasing number of hospitalizations. *Fam Med Prim Care Rev*. 2017;19(3):261–269. doi:10.5114/fmPCR.2017.68753
- Mardini M, Hashky A, Ras ZW. Personalizing patients to enable shared decision making. In: Ras ZW, Wieczorkowska A, Tsumoto S. *Recommender Systems for Medicine and Music*. Cham, Switzerland: Springer; 2021:75–90. doi:10.1007/978-3-030-66450-3\_5
- Mardini M, Ras ZW. Discovering primary medical procedures and their associations with other procedures in HCUP data. *Inf Sys Front*. 2020. doi:10.1007/s10796-020-10058-9
- Ras ZW, Dardzinska A, Tsay LS, Wasyluk H. Association action rules. Paper presented at: 2008 IEEE International Conference on Data Mining Workshops; December 15, 2008; Pisa, Italy. doi:10.1109/ICDMW.2008.66
- Ras ZW, Wieczorkowska A. Action-rules: How to increase profit of a company. In: Zighed DA, Komorowski J, Żytkow J, eds. *Principles of Data Mining and Knowledge Discovery. PKDD 2000*. Berlin, Germany: Springer; 2002:587–592. doi:10.1007/3-540-45372-5\_70
- Tsay LS, Ras ZW. Action rules discovery: System DEAR2, method and experiments. *J Exp Theor Artif*. 2004;17(1–2):119–128. doi:10.1080/09528130512331315855
- Agency for Healthcare Research and Quality. Healthcare Cost and Utilization Project (HCUP). <https://www.hcup-us.ahrq.gov/>. Accessed December 2, 2021.
- Hajja A, Touati H, Ras ZW, Studnicki J, Wieczorkowska A. Predicting negative side effects of surgeries through clustering. In: Appice A, Ceci M, Loglisci C, Manco G, Masciari E, Ras Z, eds. *New Frontiers in Mining Complex Patterns*. Cham, Switzerland: Springer; 2015:41–55. doi:10.1007/978-3-319-17876-9\_3

# Prediction of prognosis in sepsis patients by the SOFA score combined with miR-150

Jun Yang<sup>1,B-D</sup>, Youxin Liao<sup>2,C,E</sup>, Yonghong Dai<sup>1,B,C</sup>, Ling Hu<sup>1,A,C,E,F</sup>, Yihong Cai<sup>3,A,C,E</sup>

<sup>1</sup> Department of Critical Care Medicine, Central Hospital of Jiangjin District, Chongqing, China

<sup>2</sup> Department of Medical Administration, Central Hospital of Jiangjin District, Chongqing, China

<sup>3</sup> Department of Pediatrics, Central Hospital of Jiangjin District, Chongqing, China

A – research concept and design; B – collection and/or assembly of data; C – data analysis and interpretation;

D – writing the article; E – critical revision of the article; F – final approval of the article

Advances in Clinical and Experimental Medicine, ISSN 1899–5276 (print), ISSN 2451–2680 (online)

*Adv Clin Exp Med.* 2022;31(1):9–15

## Address for correspondence

Ling Hu

E-mail: huling00jiangjin@163.com

## Funding sources

None declared

## Conflict of interest

None declared

Received on July 28, 2021

Reviewed on September 5, 2021

Accepted on September 23, 2021

Published online on October 5, 2021

## Abstract

**Background.** The sequential organ failure assessment (SOFA) score, designed to evaluate sepsis-associated organ dysfunction in intensive care unit (ICU) patients, is associated with the prognosis of sepsis patients. MicroRNA-150 (miR-150) is one of the first miRNAs to be detected in patients with sepsis and other critical illnesses, and to have an association with the prognosis of critical illness and sepsis.

**Objectives.** To assess the predictive value of the combination of the SOFA score and miR-150 levels for the prognosis of sepsis patients.

**Materials and methods.** We retrospectively included 437 adult patients with sepsis who were divided into a death group (n = 138, 31.6%) and a survival group (n = 299, 68.4%), according to their survival status at the 28-day follow-up. Binary logistic regression was performed to identify independent associations. Receiver operator characteristic (ROC) curve was employed to assess the predictive values. The Z-test was used to compare the area under curve (AUC).

**Results.** Multivariate analysis demonstrated that miR-150 (odds ratio (OR): 0.549, 95% confidence interval (95% CI) [0.372, 0.826],  $p < 0.001$ ), the SOFA score (OR: 1.216, 95% CI [1.039, 1.807],  $p = 0.008$ ), age, procalcitonin (PCT), and septic shock were independently associated with 28-day mortality of sepsis patients following the adjustment for chronic renal failure, hypertension, diabetes mellitus, activated partial thromboplastin time (APTT), serum creatinine (SCr), blood urea nitrogen (BUN), and total bilirubin (TBil). The AUC of miR-150, the SOFA score and their combination in predicting the 28-day mortality of sepsis patients was 0.762 (standard error (SE): 0.023, 95% CI [0.717, 0.808]), 0.735 (SE: 0.025, 95% CI [0.687, 0.784]) and 0.886 (SE: 0.015, 95% CI [0.857, 0.916]), respectively. The AUC of their combined prediction was significantly greater than the independent prediction (0.886 compared to 0.762,  $Z = 4.516$ ,  $p < 0.001$ ; 0.886 compared to 0.735,  $Z = 5.179$ ,  $p < 0.001$ ). The sensitivity and specificity of combination prediction were 86.2% and 80.6%, respectively.

**Conclusions.** The combination of the SOFA score and miR-150 could improve the prediction of prognosis in sepsis patients.

**Key words:** prognosis, sepsis, prediction, sequential organ failure assessment score, miR-150

## Cite as

Yang J, Liao Y, Dai Y, Hu L, Cai Y. Prediction of prognosis in sepsis patients by the SOFA score combined with miR-150. *Adv Clin Exp Med.* 2022;31(1):9–15. doi:10.17219/acem/142536

## DOI

10.17219/acem/142536

## Copyright

© 2022 by Wrocław Medical University

This is an article distributed under the terms of the Creative Commons Attribution 3.0 Unported (CC BY 3.0) (<https://creativecommons.org/licenses/by/3.0/>)

## Background

Sepsis, defined as a life-threatening organ dysfunction, is induced by an altered systemic host response to infection.<sup>1</sup> It is the major cause of intensive care unit (ICU) admission and is correlated with concurrent multiple organ dysfunction syndrome.<sup>2,3</sup> Sepsis and subsequent multiple organ failure account for a large portion of morbidity and mortality in ICU patients.<sup>4,5</sup> In spite of advances in sepsis awareness and management, it still has a high mortality rate.<sup>6,7</sup> Thus, it is critical to precisely evaluate the prognosis of patients with sepsis.

The pathogenesis of sepsis is complex, and a variety of different factors may affect its prognosis. The sequential organ failure assessment (SOFA) score, designed to evaluate sepsis-associated organ dysfunction in ICU patients,<sup>8</sup> is associated with the prognosis of sepsis patients.<sup>9</sup> However, this scoring system does not include any factors associated with pathophysiology of sepsis itself, and only assesses relevant clinical parameters. Established biomarkers for sepsis patients mainly included procalcitonin (PCT), C-reactive protein (CRP) and interleukin-6 (IL-6), but they are nonspecific and have a limited diagnostic value. Considerable efforts have been made to identify new biomarkers in the context of sepsis. Recently, microRNAs (miRs) have received extensive attention in sepsis research. The miRs play a crucial role in both, innate and adaptive immunity in pathological disorders, such as bacterial infection, atherosclerosis, diabetes, and rheumatoid arthritis.<sup>10</sup> Many miRs regulate proinflammatory processes in sepsis through the direct targeting of the tumor necrosis factor (TNF) signaling pathway. In addition, miRs can modulate the expressions of sepsis-related genes, such as TNF and IL-6, 2 genes which can themselves regulate the expression of certain miRs, demonstrating their deep involvement in the pathogenesis of sepsis. The miR-150 is one of the first to be detected in patients with sepsis and critical illness. It has previously been confirmed that miR-150 is associated with the prognosis of critical illness and sepsis.<sup>11</sup>

## Objectives

Herein, we investigated whether a combination of the SOFA score and miR-150 could predict the prognosis of sepsis patients.

## Materials and methods

### Patients

A total of 487 adult patients with sepsis who were admitted to the Department of Critical Care Medicine of Central Hospital of Jiangjin District (Chongqing, China) according to the Sepsis-3 classification criteria,<sup>1</sup> were retrospectively

recruited between January 2018 and June 2020. All medical and nursing data were reviewed by the consulting physician, the components of the SOFA score for each system were collected and the SOFA score on day 1 following admission was computed. The patients were divided into the “death group” and “survival group”, according to their survival status at the 28-day follow-up. This study conformed to the Declaration of Helsinki and was approved by the Ethical Committee of Central Hospital of Jiangjin District, Chongqing (approval No. JJ2018017036). Written informed consent was obtained from either patients or their legal guardians.

### Inclusion and exclusion criteria

Study inclusion criteria consisted of: 1) meeting the Sepsis-3 classification criteria; 2) age  $\geq 18$  years and  $< 90$  years; and 3) completed medical and nursing data. Exclusion criteria included: 1) pulmonary embolism, acute myocardial infarction, cancer, trauma, and human immunodeficiency virus (HIV) infection; 2) breastfeeding or pregnancy; 3) recent major surgeries; and 4) patients lost to follow-up.

### Detection of miR-150 expression levels using quantitative real-time polymerase chain reaction

Peripheral blood samples were collected prior to therapeutic interventions, centrifuged at 2000 g for 10 min and then stored at  $-70^{\circ}\text{C}$  until the detection of miR-150. Total RNA was extracted with TRIzol (Invitrogen, Waltham, USA). The 1<sup>st</sup> strand of miR-150 was synthesized using 2  $\mu\text{g}$  total RNA through the miRNA First Strand cDNA Synthesis Tailing Reaction Kit (Sangon Biotech, Shanghai, China). Quantitative real-time polymerase chain reaction (qRT-PCR) was conducted with a 7500 Real-Time PCR System (Applied Biosystems, Waltham, USA), using iQ SYBR<sup>®</sup> Green Supermix (Bio-Rad, Hercules, USA). The *U6* was used as a reference gene. The miR-150 expression levels were evaluated using the  $2^{-\Delta\Delta\text{Ct}}$  method. The primers were synthesized by Sangon Biotech as follows: 5'-TCTCCCAACCCTTGTACCAGTG-3' for miR-150 forward, 5'-GCAAATTCGTGAAGCGTTCCATA-3' for *U6* forward and 5'-AACGAGACGACGACAGAC-3' for the universal miR primer.

### Statistical analyses

The normality of continuous variables was tested with the Kolmogorov–Smirnov test. Among them, the normally distributed variables were described using the mean  $\pm$  standard deviation (SD) and compared for intergroup differences with Student's t test. Non-normally distributed variables were described using the median (M) and interquartile range (IQR), and they were compared for intergroup differences using a Mann–Whitney U test.

Categorical variables were described with number and percentage (%) and compared for intergroup differences with a  $\chi^2$  test. Then, binary logistic regression analysis was performed for two-sided variables, and  $p < 0.10$  was used in univariate analysis to identify independent associations. Receiver operator characteristic (ROC) curve was employed to assess the values of the SOFA score, miR-150 and their combination in predicting 28-day mortality. The ROC curve of the combination of SOFA score and miR-150 was drawn using the probability derived from binary logistic regression analysis. The Z-test was used to compare the area under curve (AUC). The Youden index was computed to determine the optimal cutoff, providing the best sensitivity and specificity. Sensitivity, specificity, accuracy, false positive rate (FPR), false negative rate (FNR), positive predictive value (PPV), and negative predictive value (NPV) were also computed. Statistical analysis was performed with SPSS v. 17.0 (SPSS Inc., Chicago, USA), and statistical significance was set at  $p < 0.05$  for two-sided variables.

## Results

### Univariate analysis

Among the 487 sepsis patients, 29 (5.9%) were excluded due to incomplete medical and nursing data, 16 (3.2%) were excluded due to other serious disease or recent major surgeries, and 5 (1%) were excluded due to being lost to follow-up. Therefore, 437 patients were included and divided into the death group ( $n = 138$ , 31.6%) and survival group ( $n = 299$ , 68.4%).

Univariate analysis (Table 1) demonstrated that the differences in age, chronic renal failure, hypertension, serum creatinine (SCr), activated partial thromboplastin time (APTT), PCT, septic shock, miR-150, and the SOFA score were statistically significant between the death group and the survival group ( $p < 0.05$ ), and the differences in the remaining variables were not statistically significant. However, diabetes mellitus, blood urea nitrogen (BUN) and total bilirubin (TBil) had  $p$ -values of  $< 0.10$ .

### Multivariate analysis

Multivariate analysis was performed for the following variables: age, chronic renal failure, hypertension, SCr, APTT, PCT, septic shock, miR-150, the SOFA score, diabetes mellitus, BUN, and TBil (Table 2). These results demonstrated that miR-150 (odds ratio (OR) = 0.549, 95% confidence interval (95% CI) [0.372, 0.826],  $p < 0.001$ ), the SOFA score (OR = 1.216, 95% CI [1.039, 1.807],  $p = 0.008$ ), age, PCT, and septic shock were independently associated with the 28-day mortality of sepsis patients when the analysis is adjusted for chronic renal failure, hypertension, diabetes mellitus, APTT, SCr, BUN, and TBil.

## Predictive value

The AUC of miR-150 (Fig. 1), the SOFA score and their combination (Fig. 2) in predicting 28-day mortality of sepsis patients was 0.762 (standard error (SE) = 0.023, 95% CI [0.717, 0.808]), 0.735 (SE = 0.025, 95% CI [0.687, 0.784]) and 0.886 (SE = 0.015, 95% CI [0.857, 0.916]), respectively. The AUC of miR-150 (Fig. 1) was consistent with that of 1/miR-150 (Fig. 2). The predictive power of the AUC together with the SOFA score was significantly greater than independent predictions (0.886 compared to 0.762,  $Z = 4.516$ ,  $p < 0.001$ ; 0.886 compared to 0.735,  $Z = 5.179$ ,  $p < 0.001$ ). Clinical utility indexes of miR-150, the SOFA score and their combination in predicting 28-day mortality of sepsis patients are demonstrated in Table 3. The AUC for combination prediction of the quick SOFA score plus miR-150 was 0.806 (SE = 0.022, 95% CI [0.763, 0.848]) (Fig. 3).

## Discussion

The SOFA score, ranging from 0 to 24, is a well-known tool for evaluating patients with sepsis and septic shock. It collates the amount and severity of organ failures in 6 organs, including coagulative function, respiratory, cardiovascular, kidney, liver, and neurology systems. Higher scores are associated with higher probability of mortality. Vafaei et al. investigated the predictive values of the SOFA, Mortality in Emergency Department Sepsis (MEDS) and Predisposition, Infection, Response and Organ Dysfunction (PIRO) scores for 30-day mortality in sepsis patients.<sup>12</sup> Their results showed that the AUCs of the SOFA, MEDS and PIRO scores were 0.87, 0.94 and 0.83, respectively, and the MEDS score had the optimal performance in the prediction of 30-day mortality. Raith et al. found that an increase of 2 or more in the SOFA score had a higher prognostic accuracy for in-hospital mortality than the qSOFA score or the systemic inflammatory response syndrome (SIRS) criteria.<sup>13</sup> Liu et al. assessed the prognostic accuracy of the SOFA score, qSOFA score and lactate level on the mortality of sepsis patients through the public Medical Information Mart for Intensive Care III database (MIMIC III).<sup>14</sup> Their results showed that the AUCs of the SOFA score, qSOFA score and lactate level were 0.686, 0.664 and 0.547, respectively. Karakike et al. evaluated the performance of the early change of SOFA score in predicting 28-day mortality of sepsis patients.<sup>9</sup> Their results demonstrated that an early change of SOFA score was a more scalar, direct measurement tool for treatment effect of sepsis compared with traditional mortality endpoints. Iba et al. also demonstrated that the change of SOFA score was strongly associated with the 28-day sepsis mortality disseminated intravascular coagulation patients.<sup>15</sup> In our study, the AUC of the SOFA score for predicting 28-day mortality of sepsis patients was 0.735.

**Table 1.** Results of univariate analysis between death group and survival group

Variables	All patients (n = 437)	Death group (n = 138)	Survival group (n = 299)	$\chi^2/Z/t$	p-value
Male, n (%)	273 (62.5%)	91 (65.9%)	182 (60.9%)	1.036	0.309
Age [years], mean $\pm$ SD	68.40 $\pm$ 7.82	72.54 $\pm$ 7.53	66.49 $\pm$ 7.96	9.714	<0.001
Smoking, n (%)	191 (43.7%)	57 (41.3%)	134 (44.8%)	0.473	0.491
Drinking, n (%)	84 (19.2%)	23 (16.7%)	61 (20.4%)	0.848	0.357
BMI [kg/m <sup>2</sup> ], mean $\pm$ SD	23.82 $\pm$ 5.64	23.52 $\pm$ 5.75	23.96 $\pm$ 5.59	-1.279	0.201
Comorbidities, n (%)					
Diabetes mellitus	121 (27.7%)	46 (33.3%)	75 (25.1%)	3.210	0.073
Chronic renal failure	100 (22.9%)	43 (31.2%)	57 (19.1%)	7.828	0.005
Hypertension	187 (42.8%)	69 (50.0%)	118 (39.5%)	4.281	0.038
COPD	45 (10.3%)	16 (11.6%)	29 (9.7%)	0.367	0.545
Chronic liver disease	29 (6.6%)	11 (8.0%)	18 (6.0%)	0.580	0.446
Chronic coronary disease	92 (21.1%)	31 (22.5%)	61 (20.4%)	0.242	0.623
Laboratory examinations					
WBC [ $\times 10^9/L$ ], M (IQR)	11.53 (7.75)	10.74 (7.52)	11.82 (7.83)	-0.291	0.769
ALB [g/L], mean $\pm$ SD	29.70 $\pm$ 5.08	29.52 $\pm$ 4.03	29.78 $\pm$ 5.56	-1.176	0.249
PLT [ $\times 10^9/L$ ], M (IQR)	154.65 (116.72)	148.96 (104.87)	157.79 (122.35)	-0.174	0.875
LYM [ $\times 10^9/L$ ], M (IQR)	1.08 (7.98)	1.02 (5.86)	1.11 (8.97)	-0.647	0.526
NEU [ $\times 10^9/L$ ], M (IQR)	11.95 (11.26)	13.58 (11.47)	11.06 (11.15)	1.613	0.112
BUN [mmol/L], M (IQR)	9.02 (9.37)	11.17 (11.28)	7.98 (8.36)	1.814	0.069
TBil [ $\mu$ mol/L], M (IQR)	13.21 (9.98)	15.48 (10.77)	12.03 (9.62)	1.887	0.058
SCr [ $\mu$ mol/L], M (IQR)	86.91 (89.27)	108.81 (169.59)	75.89 (54.36)	2.485	0.019
APTT [s], M (IQR)	41.02 (11.87)	42.57 (17.96)	40.25 (8.78)	2.013	0.038
PT [s], M (IQR)	15.37 (2.79)	15.66 (2.52)	15.21 (2.93)	1.587	0.124
INR	1.23 (0.33)	1.28 (0.35)	1.21 (0.32)	1.136	0.143
PCT [ $\mu$ g/L], M (IQR)	1.21 (5.92)	3.08 (11.27)	0.32 (3.29)	3.479	<0.001
Site of infection, n (%)					
Abdominal/pelvic	103 (23.6%)	27 (19.6%)	76 (25.4%)	1.795	0.180
Respiratory	138 (31.6%)	46 (33.3%)	92 (30.8%)	0.287	0.592
Blood	49 (11.2%)	19 (13.8%)	30 (10.0%)	1.323	0.250
Urinary	69 (15.8%)	18 (13.0%)	51 (17.1%)	1.144	0.285
Skin and soft tissue	41 (9.4%)	15 (10.9%)	26 (8.7%)	0.525	0.469
Others	37 (8.5%)	13 (9.4%)	24 (8.0%)	0.237	0.627
Septic shock	219 (50.1%)	86 (62.3%)	133 (44.5%)	12.017	0.001
miR-150 (mean $\pm$ SD)	1.91 $\pm$ 1.11	1.56 $\pm$ 0.82	2.07 $\pm$ 1.25	-22.573	<0.001
SOFA score (mean $\pm$ SD)	7.91 $\pm$ 4.09	9.94 $\pm$ 4.86	6.97 $\pm$ 3.74	13.628	<0.001

SD – standard deviation; BMI – body mass index; COPD – chronic obstructive pulmonary disease; WBC – white blood cell; M – median; IQR – interquartile range; ALB – albumin; PLT – platelet count; LYM – lymphocyte count; NEU – neutrophils count; BUN – blood urea nitrogen; TBil – total bilirubin; SCr – serum creatinine; APTT – activated partial thromboplastin time; PT – prothrombin time; INR – international normalized ratio; PCT – procalcitonin; SOFA – sequential organ failure assessment; M – median; IQR – interquartile range.

Recent studies have shown that the combination of multiple biomarkers had a higher predictive value for 30-day mortality of sepsis patients compared to the SOFA score.<sup>16,17</sup> Moreover, when there is an additional set of biomarkers that can be added to the SOFA score, there were significant improvements in the prognostic accuracy for mortality of sepsis patients.<sup>18</sup> The miRs represent a new group of endogenous, small (from 19 to 23 nucleotides)

RNA molecules that do not encode proteins, but regulate gene expression based on sequence complementarity principles.<sup>19,20</sup> Studies indicate that miRs occupy only about 1% of the human genome, but modulate up to 60% of all protein-coding genes.<sup>21,22</sup> Thus, miRs are considered a part of complicated regulatory networks in the gene expression of both, pathophysiological and physiological processes.

**Table 2.** Results of multivariate analysis between the death group and the survival group

Variables	$\beta$	SE	Wald $\chi^2$	OR	95% CI	p-value
miR-150	-0.227	0.081	8.763	0.549	[0.372, 0.826]	<0.001
SOFA score	0.183	0.075	6.604	1.216	[1.039, 1.807]	0.008
Septic shock	0.312	0.119	5.718	2.153	[1.142, 4.219]	0.019
Age	0.135	0.068	4.237	1.194	[1.031, 1.463]	0.041
PCT	0.089	0.017	5.096	1.158	[1.022, 1.596]	0.032
Chronic renal failure	0.094	0.023	1.568	1.127	[0.904, 1.348]	0.208
Hypertension	-0.075	0.012	0.204	0.913	[0.857, 1.165]	0.645
Diabetes mellitus	0.101	0.020	2.538	1.148	[0.911, 1.438]	0.107
APTT	0.090	0.010	2.314	1.096	[0.897, 1.265]	0.132
SCr	0.116	0.021	3.409	1.152	[0.917, 1.494]	0.073
BUN	0.068	0.006	1.382	1.087	[0.826, 1.197]	0.254
TBil	0.073	0.009	1.494	1.089	[0.841, 1.206]	0.220

SE – standard error; OR – odds ratio; 95% CI – 95% confidence interval; SOFA – sequential organ failure assessment; PCT – procalcitonin; APTT – activated partial thromboplastin time; SCr – serum creatinine; BUN – blood urea nitrogen; TBil – total bilirubin.

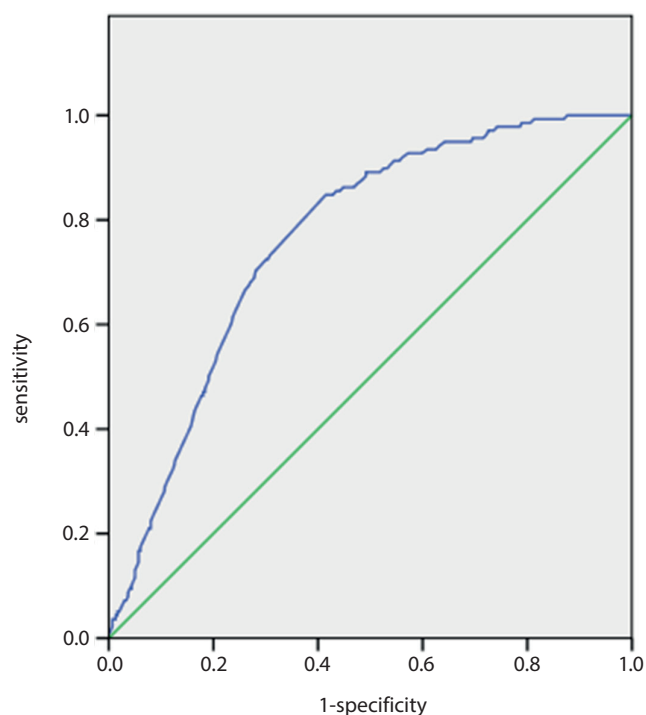


**Fig. 1.** Receiver operator characteristic (ROC) curve of miR-150 when predicting the 28-day mortality of sepsis patients

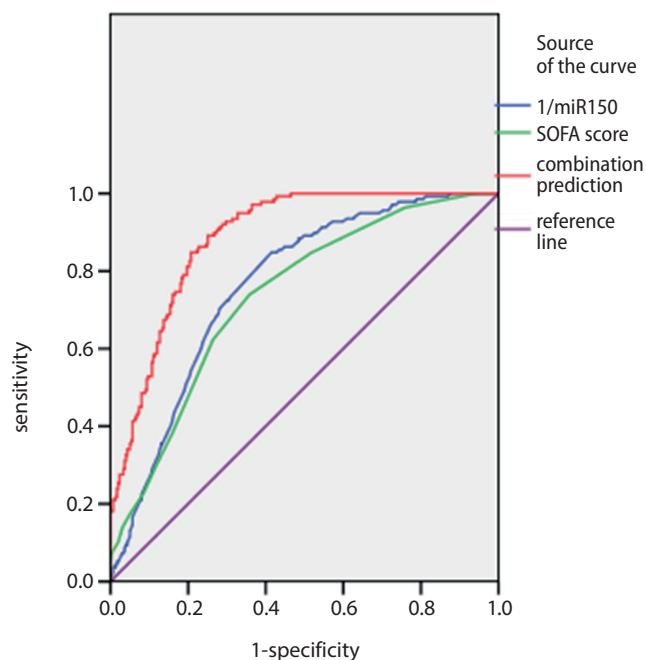


**Fig. 2.** Receiver operator characteristic (ROC) curves of 1/miR-150, sequential organ failure assessment (SOFA) score and combination of miR-150 and SOFA score in predicting the 28-day mortality of sepsis patients

Abnormal expression of miRs has been reported not only in highly modulated mechanisms such as cell death, aging and development,<sup>23</sup> but also in the initiation of complicated diseases such as sepsis, inflammation and infection,<sup>24–27</sup> partly because miRs can be detected in the blood and serve as biomarkers.<sup>28–30</sup> Circulating miRs are especially stable in the conditions that would generally degrade most of RNAs. Additionally, miRs are relatively small, generally possess a less complicated chemical structure and do not undergo post-processing modifications. Therefore, circulating miRs may be superior to other types of serum-based biomarkers.<sup>31</sup> The miR-150 belongs to part of a group of miRs including

miR-155, miR-223, miR-181, and the miR-17-92 cluster.<sup>32</sup> The upregulation of miR-150 expression in B-cells can lead to decreased c-Myb levels and prevent the transition from pro-B to pre-B cells. At a functional level, the downregulation of miR-150 expression is detected in cell lines, as well as in primary leukocytes derived from human volunteers upon the lipopolysaccharides administration.<sup>33</sup> Accordingly, mice with miR-150 knockout showed significant changes in their responses to different inflammatory stimuli,<sup>34</sup> implying a deep involvement of miR-150 in the activation process of immune cells during sepsis and inflammation. Several reports have identified miR-150 as a constituent of miRs panels,

**Table 3.** Clinical utility indices of miR-150, the SOFA score and their combination in predicting 28-day mortality of sepsis patients

Predictors	AUC	SE	p-value	95% CI		Best cut-off	Sensitivity	Specificity	Accuracy	FPR	FNR	PPV	NPV	Youden index
				lower bound	upper bound									
miR-150	0.762	0.023	<0.001	0.717	0.808	1.78	76.8%	62.2%	66.8%	51.6%	14.7%	48.4%	85.3%	0.39
SOFA score	0.735	0.025	<0.001	0.687	0.784	8.85	75.4%	60.5%	65.2%	53.2%	15.8%	46.8%	84.2%	0.36
Combination of miR-150 and SOFA score	0.886	0.015	<0.001	0.857	0.916	N/A	86.2%	80.6%	82.4%	32.8%	7.3%	67.2%	92.7%	0.67

SOFA – sequential organ failure assessment; AUC – area under curve; SE – standard error; 95% CI – 95% confidence interval; FPR – false positive rate; FNR – false negative rate; PPV – positive predictive value; NPV – negative predictive value; N/A – not applicable.

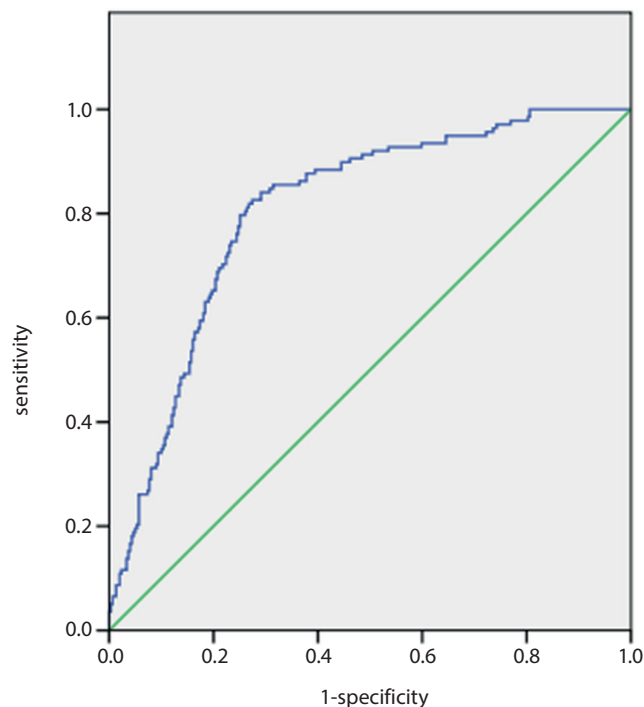


**Fig. 3.** Receiver operator characteristic (ROC) curve of the quick sequential organ failure assessment (SOFA) score plus miR-150 in predicting the 28-day mortality of sepsis patients

which are deregulated in peripheral blood mononuclear cells/leukocytes of sepsis patients compared with healthy controls through microarray-based gene expression analysis.<sup>35–37</sup> Vasilescu et al. demonstrated that miR-150 expression was significantly reduced in both plasma and leukocytes of patients with sepsis, which was associated with an elevated SOFA score, sepsis severity and elevated levels of proinflammatory cytokines.<sup>35</sup> Ma et al. found that miR-150 levels were lower in 2 independent cohorts of sepsis patients than in healthy controls or patients with noninfectious systemic inflammatory response syndrome (SIRS).<sup>38</sup> Roderburg et al. detected the levels of circulating miR-150 in healthy controls and a cohort of critically ill patients.<sup>11</sup> Their results demonstrated that miR-150 levels were decreased in patients with septic disease, but the difference was not statistically significant, suggesting that the potential of miR-150 levels was rather limited in differentiating between septic and non-septic disease. Nevertheless, they found a significant association between

decreased miR-150 levels and impaired prognosis of patients with critical illness, implying that miR-150 was more suitable to be a prognostic indicator than a diagnostic indicator. In addition, Huang et al. demonstrated that miR-150 might be correlated with the pathogenesis of neonatal sepsis through targeting BCL-11B, based on the analysis of the expression profile data of E-MTAB-4785.<sup>39</sup>

In our study, miR-150 expression levels were lower in non-survivors than in survivors, and the AUC of miR-150 expression levels applied in predicting mortality was 0.762. The combination of the SOFA score and miR-150 expression levels had a higher predictive value than the SOFA score or miR-150 expression levels. The AUC was up to 0.886 with a sensitivity of 86.2% and specificity of 80.6%. In addition, we evaluated the predictive value of the quick SOFA score plus miR-150 for the 28-day mortality of sepsis patients, and the AUC was 0.806. The data lend themselves to be utilized as a possible predictive bedside test for sepsis patients in emergency departments.

## Limitations

The limitations of this study mainly included a small sample size and a short follow-up time. Our next focus will be to evaluate the predictive value of the SOFA score combined with miR-150 for prognosis in sepsis patients on the basis of a large sample and a long follow-up time.

## Conclusions

The combination of the SOFA score and miR-150 could improve the prediction of prognosis in sepsis patients.

## ORCID iDs

Jun Yang <https://orcid.org/0000-0002-7032-919X>  
 Youxin Liao <https://orcid.org/0000-0003-2903-5728>  
 Yonghong Dai <https://orcid.org/0000-0002-1668-1141>  
 Ling Hu <https://orcid.org/0000-0001-8354-1707>  
 Yihong Cai <https://orcid.org/0000-0001-5720-0984>

## References

1. Singer M, Deutschman CS, Seymour CW, et al. The Third International Consensus Definitions for Sepsis and Septic Shock (Sepsis-3). *JAMA*. 2016;315(8):801–810. doi:10.1001/jama.2016.0287



2. De Backer D, Dorman T. Surviving sepsis guidelines: A continuous move toward better care of patients with sepsis. *JAMA*. 2017;317(8):807–808. doi:10.1001/jama.2017.0059
3. Yao YM, Luan Y. Precision evaluation of immune status and its significance in sepsis after burns or trauma [in Chinese]. *Zhonghua Shao Shang Za Zhi*. 2018;34(11):786–789. doi:10.3760/cma.j.issn.1009-2587.2018.11.013
4. Lago AF, de Oliveira AS, de Souza HCD, da Silva JS, Basile-Filho A, Clarice Gastaldi A. The effects of physical therapy with neuromuscular electrical stimulation in patients with septic shock: Study protocol for a randomized cross-over design. *Medicine (Baltimore)*. 2018;97(6):e9736. doi:10.1097/MD.00000000000009736
5. Venkatesh B, Finfer S, Cohen J, et al; ADRENAL Trial Investigators and the Australian–New Zealand Intensive Care Society Clinical Trials Group. Adjunctive glucocorticoid therapy in patients with septic shock. *N Engl J Med*. 2018;378(9):797–808. doi:10.1056/NEJMoa1705835
6. Leitgeb AM, Charunwatthana P, Rueangveerayut R, et al. Inhibition of merozoite invasion and transient de-sequestration by sevuparin in humans with *Plasmodium falciparum* malaria. *PLoS One*. 2017;12(12):e0188754. doi:10.1371/journal.pone.0188754
7. Balejo RDP, Cortelli JR, Costa FO, et al. Effects of chlorhexidine pre-procedural rinse on bacteremia in periodontal patients: A randomized clinical trial. *J Appl Oral Sci*. 2017;25(6):586–595. doi:10.1590/1678-7757-2017-0112
8. Vincent JL, Moreno R, Takala J, et al. The SOFA (Sepsis-related Organ Failure Assessment) score to describe organ dysfunction/failure. On behalf of the working group on Sepsis-related problems of the European Society of Intensive Care Medicine. *Intensive Care Med*. 1996;22(7):707–710. doi:10.1007/BF01709751
9. Karakike E, Kyriazopoulou E, Tsangaris I, Routsis C, Vincent JL, Giarellos-Bourboulis EJ. The early change of SOFA score as a prognostic marker of 28-day sepsis mortality: Analysis through a derivation and a validation cohort. *Crit Care*. 2019;23(1):387. doi:10.1186/s13054-019-2665-5
10. O'Connell RM, Rao DS, Baltimore D. MicroRNA regulation of inflammatory responses. *Annu Rev Immunol*. 2012;30:295–312. doi:10.1146/annurev-immunol-020711-075013
11. Roderburg C, Luedde M, Vargas Cardenas D, et al. Circulating microRNA-150 serum levels predict survival in patients with critical illness and sepsis. *PLoS One*. 2013;8(1):e54612. doi:10.1371/journal.pone.0054612
12. Vafaei A, Heydari K, Hashemi-Nazari SS, Izadi N, Zadeh HH. PIR0, SOFA and MEDS scores in predicting one-month mortality of sepsis patients: A diagnostic accuracy study. *Arch Acad Emerg Med*. 2019;7(1):e59. PMID:31875213
13. Raith EP, Udy AA, Bailey M, et al; Australian and New Zealand Intensive Care Society (ANZICS) Centre for Outcomes and Resource Evaluation (CORE). Prognostic accuracy of the SOFA score, SIRS criteria, and qSOFA score for in-hospital mortality among adults with suspected infection admitted to the intensive care unit. *JAMA*. 2017;317(3):290–300. doi:10.1001/jama.2016.20328
14. Liu Z, Meng Z, Li Y, et al. Prognostic accuracy of the serum lactate level, the SOFA score and the qSOFA score for mortality among adults with sepsis. *Scand J Trauma Resusc Emerg Med*. 2019;27(1):51. doi:10.1186/s13049-019-0609-3
15. Iba T, Arakawa M, Mochizuki K, Nishida O, Wada H, Levy JH. Usefulness of measuring changes in SOFA score for the prediction of 28-day mortality in patients with sepsis-associated disseminated intravascular coagulation. *Clin Appl Thromb Hemost*. 2019;25:1076029618824044. doi:10.1177/1076029618824044
16. Kim H, Hur M, Moon HW, Yun YM, Di Somma S; GREAT Network. Multi-marker approach using procalcitonin, presepsin, galectin-3, and soluble suppression of tumorigenicity 2 for the prediction of mortality in sepsis. *Ann Intensive Care*. 2017;7(1):27. doi:10.1186/s13613-017-0252-y
17. Shukeri WFWM, Ralib AM, Abdulah NZ, Mat-Nor MB. Sepsis mortality score for the prediction of mortality in septic patients. *J Crit Care*. 2018;43:163–168. doi:10.1016/j.jccr.2017.09.009
18. Song J, Moon S, Park DW, et al. Biomarker combination and SOFA score for the prediction of mortality in sepsis and septic shock: A prospective observational study according to the Sepsis-3 definitions. *Medicine (Baltimore)*. 2020;99(22):e20495. doi:10.1097/MD.00000000000020495
19. Wu J, Ding J, Yang J, Guo X, Zheng Y. MicroRNA roles in the nuclear factor kappa B signaling pathway in cancer. *Front Immunol*. 2018;9:546. doi:10.3389/fimmu.2018.00546
20. Vannini I, Fanini F, Fabbri M. Emerging roles of microRNAs in cancer. *Curr Opin Genet Dev*. 2018;48:128–133. doi:10.1016/j.gde.2018.01.001
21. Friedman RC, Farh KKH, Burge CB, Bartel DP. Most mammalian mRNAs are conserved targets of microRNAs. *Genome Res*. 2009;19(1):92–105. doi:10.1101/gr.082701.108
22. Krol J, Loedige I, Filipowicz W. The widespread regulation of microRNA biogenesis, function and decay. *Nat Rev Genet*. 2010;11(9):597–610. doi:10.1038/nrg2843
23. Bandiera S, Pfeffer S, Baumert TF, Zeisel MB. miR-122-A key factor and therapeutic target in liver disease. *J Hepatol*. 2015;62(2):448–457. doi:10.1016/j.jhep.2014.10.004
24. Cortez MA, Bueso-Ramos C, Ferdin J, Lopez-Berestein G, Sood AK, Calin GA. MicroRNAs in body fluids: The mix of hormones and biomarkers. *Nat Rev Clin Oncol*. 2011;8(8):467–477. doi:10.1038/nrclinonc.2011.76
25. Vasudevan S, Tong Y, Steitz JA. Switching from repression to activation: MicroRNAs can up-regulate translation. *Science*. 2007;318(5858):1931–1934. doi:10.1126/science.1149460
26. Wu S, Huang S, Ding J, et al. Multiple microRNAs modulate p21Cip1/Waf1 expression by directly targeting its 3' untranslated region. *Oncogene*. 2010;29(15):2302–2308. doi:10.1038/onc.2010.34
27. Roderburg C, Luedde T. Circulating microRNAs as markers of liver inflammation, fibrosis and cancer. *J Hepatol*. 2014;61(6):1434–1437. doi:10.1016/j.jhep.2014.07.017
28. Mitchell PS, Parkin RK, Kroh EM, et al. Circulating microRNAs as stable blood-based markers for cancer detection. *Proc Natl Acad Sci U S A*. 2008;105(30):10513–10518. doi:10.1073/pnas.0804549105
29. Lawrie CH, Gal S, Dunlop HM, et al. Detection of elevated levels of tumour-associated microRNAs in serum of patients with diffuse large B-cell lymphoma. *Br J Haematol*. 2008;141(5):672–675. doi:10.1111/j.1365-2141.2008.07077.x
30. Chen X, Ba Y, Ma L, et al. Characterization of microRNAs in serum: A novel class of biomarkers for diagnosis of cancer and other diseases. *Cell Res*. 2008;18(10):997–1006. doi:10.1038/cr.2008.282
31. Wang K, Zhang S, Marzolf B, et al. Circulating microRNAs, potential biomarkers for drug-induced liver injury. *Proc Natl Acad Sci U S A*. 2009;106(11):4402–4407. doi:10.1073/pnas.0813371106
32. Davidson-Moncada J, Papavasiliou FN, Tam W. MicroRNAs of the immune system: Roles in inflammation and cancer. *Ann NY Acad Sci*. 2010;1183:183–194. doi:10.1111/j.1749-6632.2009.05121.x
33. Schmidt WM, Spiel AO, Jilka B, Wolz M, Müller M. In vivo profile of the human leukocyte microRNA response to endotoxemia. *Biochem Biophys Res Commun*. 2009;380(3):437–441. doi:10.1016/j.bbrc.2008.12.190
34. Shapiro NI, Trzeciak S, Hollander JE, et al. A prospective, multicenter derivation of a biomarker panel to assess risk of organ dysfunction, shock, and death in emergency department patients with suspected sepsis. *Crit Care Med*. 2009;37(1):96–104. doi:10.1097/CCM.0b013e318192fd9d
35. Vasilescu C, Rossi S, Shimizu M, et al. MicroRNA fingerprints identify miR-150 as a plasma prognostic marker in patients with sepsis. *PLoS One*. 2009;4(10):e7405. doi:10.1371/journal.pone.0007405
36. How CK, Hou SK, Shih HC, et al. Expression profile of MicroRNAs in gram-negative bacterial sepsis. *Shock*. 2015;43(2):121–127. doi:10.1097/SHK.0000000000000282
37. Zhou J, Chaudhry H, Zhong Y, et al. Dysregulation in microRNA expression in peripheral blood mononuclear cells of sepsis patients is associated with immunopathology. *Cytokine*. 2015;71(1):89–100. doi:10.1016/j.cyto.2014.09.003
38. Ma Y, Vilanova D, Atalar K, et al. Genome-wide sequencing of cellular microRNAs identifies a combinatorial expression signature diagnostic of sepsis. *PLoS One*. 2013;8(10):e75918. doi:10.1371/journal.pone.0075918
39. Huang L, Qiao L, Zhu H, Jiang L, Yin L. Genomics of neonatal sepsis: Has-miR-150 targeting BCL11B functions in disease progression. *Ital J Pediatr*. 2018;44(1):145. doi:10.1186/s13052-018-0575-9



# Effect of infection after liver cancer interventional therapy on T lymphocyte subsets and Toll-like receptors in peripheral blood mononuclear cells and its mechanism

Conghui Zhu<sup>A,C-F</sup>, Guanfeng Chen<sup>B,C</sup>, Jiadi Yao<sup>B,C</sup>, Wenji Lin<sup>A,E,F</sup>

Department of Interventional Radiology, Quanzhou First Hospital Affiliated to Fujian Medical University, China

A – research concept and design; B – collection and/or assembly of data; C – data analysis and interpretation; D – writing the article; E – critical revision of the article; F – final approval of the article

Advances in Clinical and Experimental Medicine, ISSN 1899–5276 (print), ISSN 2451–2680 (online)

Adv Clin Exp Med. 2022;31(1):17–23

## Address for correspondence

Wenji Lin  
E-mail: linwenji6s8f@163.com

## Funding sources

None declared

## Conflict of interest

None declared

Received on May 27, 2021

Reviewed on July 4, 2021

Accepted on August 21, 2021

Published online on November 4, 2021

## Cite as

Zhu C, Chen G, Yao J, Lin W. Effect of infection after liver cancer interventional therapy on T lymphocyte subsets and Toll-like receptors in peripheral blood mononuclear cells and its mechanism. *Adv Clin Exp Med.* 2022;31(1):17–23. doi:10.17219/acem/141499

## DOI

10.17219/acem/141499

## Copyright

© 2022 by Wrocław Medical University  
This is an article distributed under the terms of the Creative Commons Attribution 3.0 Unported (CC BY 3.0) (<https://creativecommons.org/licenses/by/3.0/>)

## Abstract

**Background.** The T lymphocyte subset levels are an indicator used to evaluate the immune status of the body. In recent years, many studies have investigated the correlation between T lymphocyte subset levels and postoperative infection.

**Objectives.** To investigate the incidence of infection after liver cancer interventional therapy and its influence on T lymphocyte subset levels and toll-like receptors (TLRs).

**Materials and methods.** A total of 325 patients with primary liver cancer receiving interventional therapy were divided into an infection group (n = 37) and a non-infection group (n = 288). The infection site and the distribution of pathogenic bacteria in the infection group were observed. The serum T lymphocyte subset level and TLR2 and TLR4 levels in peripheral blood mononuclear cells were compared. The clinical value of the postoperative TLR2 and TLR4 levels in evaluating infection was analyzed using receiver operating characteristic (ROC) curves.

**Results.** Among 51 strains of pathogens isolated from the infected patients, strains of *Escherichia coli* (27.45%) and *Pseudomonas aeruginosa* (19.61%) were the most commonly observed. After surgery, the levels of CD3<sup>+</sup>, CD4<sup>+</sup> and CD4<sup>+</sup>/CD8<sup>+</sup> decreased, while the level of CD8<sup>+</sup> increased in both groups; the levels of TLR2 and TLR4 decreased in the non-infection group, while the levels of TLR2 and TLR4 increased in the infection group (all p < 0.05). Furthermore, the decreases and increases were more significant in the infection group than in the non-infection group (all p < 0.001). The area under the curve of postoperative TLR2 and TLR4 levels in evaluating infection were greater than 0.700 (p < 0.001).

**Conclusions.** Gram-negative bacteria account for the majority of infections in patients after liver cancer interventional therapy, and the main infection sites are the lung and abdomen. The infected patients show changes in T lymphocyte level and decreased immune function. The TLR2 and TLR4 can be used as auxiliary indicators to evaluate infection after surgery.

**Key words:** T lymphocytes, toll-like receptor, intervention, liver cancer, postoperative infection

## Introduction

Liver cancer is a common malignant tumor characterized by high morbidity and mortality.<sup>1–3</sup> For patients with early liver cancer, surgery is the most effective treatment. However, in most cases, the tumor has progressed to the middle or advanced stage at diagnosis, and patients have missed the best opportunity for surgery due to the insidious onset of symptoms.<sup>4–6</sup> Transhepatic arterial infusion chemotherapy, which is one of the important local treatments for liver cancer, has the advantages of minimal trauma and rapid postoperative recovery. For these reasons, it is widely used in the treatment of advanced liver cancer and shows significant effects.<sup>7</sup> Nevertheless, interventional therapy itself is invasive and the immune function of patients is often impacted, potentially resulting in postoperative infection. The rate of postoperative infection is reported to be about 10–15% in patients with liver cancer.<sup>8,9</sup> Therefore, further research on infection after liver cancer interventional therapy and biomarkers for predicting infection is clinically valuable for timely and effective prevention and control measures. Inflammatory response and immune dysfunction are the main mechanisms of postoperative infection. Infection can lead to a persistent inflammatory state, which can result in further immune dysfunction.

The T lymphocyte subset levels are an indicator used to evaluate the immune status of the body. In recent years, there have been many studies investigating the correlation between T lymphocyte subset levels and postoperative infection; however, there have been few reports on infection after interventional therapy for liver cancer. Toll-like receptors (TLRs), as a class of pathogen recognition receptors, can activate adaptive immunity by promoting the expression of inflammatory factors and participate in the inflammatory response of anti-infection.<sup>10</sup> A previous study confirmed that TLRs are closely linked to infection and that TLR levels in peripheral blood mononuclear cells (PBMCs) are increased in infected patients.<sup>10</sup> However, the role and mechanism of TLRs in postoperative infection of liver cancer remain unclear.

## Objectives

We aimed to explore the incidence of infection after liver cancer interventional therapy and the effect of infection on T lymphocytes and TLR levels in order to provide a reference for the prevention and treatment of infection in liver cancer patients.

## Materials and methods

### Study design

This prospective study included 325 patients with primary liver cancer who received interventional therapy in our hospital from July 2015 to July 2018. General data

were collected, including age, gender, body mass index (BMI), pathological type, Child–Pugh classification, site and size of lesion, clinical stage, fasting blood glucose level, and smoking and alcohol history. Each patient was assigned to the infection group ( $n = 37$ ) or non-infection group ( $n = 288$ ), according to their condition. The diagnostic criteria for infection were based on the Diagnostic Criteria for Nosocomial Infection.<sup>11</sup> This study was conducted in accordance with the Declaration of Helsinki and approved by the Medical Ethics Committee of our hospital.

### Inclusion and exclusion criteria

Patients were eligible for the study if they met the diagnostic and staging criteria of hepatocellular carcinoma<sup>12</sup>; had no infection and did not take anti-infection drugs within 3 months before the intervention; received no targeted drug therapy, radiotherapy, chemotherapy, or other drug therapy; had no other malignant tumors; were aged  $\geq 18$  years; and provided written informed consent or consent was provided by their families.

Patients were ineligible for the study if they had complications with infectious diseases before interventional surgery or had infection within 6 h after surgery; were administered immune agents or glucocorticoids within 3 months before surgery; had other underlying diseases; were not suitable for surgery; or had incomplete clinical data.

## Methods

### Transcatheter arterial chemoembolization

All patients were treated with transcatheter arterial chemoembolization (TACE). The chemotherapy regimens were as follows: 0.75–1.25 g of 5-fluorouracil (H31020593; Xudonghaipu Pharmaceutical Co. Ltd., Shanghai, China), 80–120 mg of cisplatin (H37021358; Qilu Pharmaceutical Co. Ltd., Jinan, China), 200 mg of oxaliplatin (H20093167; Qilu Pharmaceutical Co. Ltd.), and 80–120 mg of epirubicin (H20000496; Pfizer Pharmaceutical (Wuxi) Co. Ltd., Wuxi, China). A gelatin sponge (20193141731; ConvaTec Limited, Shanghai, China) was used as the embolic agent. The dosage of chemotherapeutic drugs and embolic agents depended on the tumor size and the extent of embolization.

### Diagnosis of infection and identification of pathogens

Biological samples from the sites of suspected infection (e.g., abdomen, lung, blood, intestine, surgical site, urinary system, skin) were collected, inoculated into culture media, and cultured at a constant temperature of 37°C for 2–3 days. Subsequently, the bacteria were isolated for strain identification (MicroScan WalkAway Plus 96; Beckman Coulter Inc., Brea, USA).

## Measurement of T lymphocyte subset levels

Fasting venous blood (3 mL) was drawn from each patient before treatment and within 6 h after treatment (before the occurrence of infection). The CD3<sup>+</sup>, CD4<sup>+</sup> and CD8<sup>+</sup> cells in whole blood were counted with flow cytometry (Beckman Coulter Inc.), and the changes in the CD4<sup>+</sup>/CD8<sup>+</sup> ratio before and after treatment were calculated. The cell counting kits were purchased from Beyotime Biotechnology Co., Ltd. (Shanghai, China).

## Measurement of TLR2 and TLR4 levels in PBMCs

Fasting venous blood (3 mL) was drawn from each patient before treatment and within 6 h after treatment (before the infection). Each blood sample was divided into 2 parts: 1 was mixed with monoclonal antibodies FitC-CD14 and PE-TLR2, and the other with phosphate-buffered saline (PBS) solution. The samples were fully mixed and maintained at 4°C for 30 min. Next, 2 mL of red blood cell lysate was added to both parts of the sample, which were mixed and allowed to stand in the dark for 20 min at room temperature. Then, the samples were washed twice with PBS and centrifuged to remove the supernatant. The PBS was added to adjust the concentration. The positive detection rate of TLR2 mononuclear cells was determined with flow cytometry (Beckman Coulter Inc.). The positive detection rate of TLR4 was similar to that of TLR2.

## Statistical analysis

Statistical analyses were performed using SPSS v. 22.0 software (IBM Corp., Armonk, USA). The  $\chi^2$  test was adopted for the comparison of enumeration data expressed as a ratio or percentage. The data were checked for a normal distribution using the Shapiro–Wilk test. Data that followed a normal distribution were expressed as the mean  $\pm$  standard deviation ( $\bar{x} \pm SD$ ), while data that did not meet the normal distribution were expressed as a percentile. The independent sample t-test was used for the comparisons between the 2 groups, and the paired sample t-test was applied for the comparison before and after intervention within the same group. Moreover, ROC curves were used to analyze the clinical value of postoperative TLR2 and TLR4 levels in evaluating postoperative infection. A value of  $p < 0.05$  was considered statistically significant.

## Results

### Comparison of general patient characteristics

Of the 325 patients, 37 developed postoperative infection (infection rate 11.38%). There was no significant difference

in gender, age, BMI, pathological type, Child–Pugh classification, site and size of lesion, clinical stage, fasting blood glucose level, and smoking and alcohol history between the 2 groups, suggesting that the 2 groups were comparable (all  $p > 0.05$ , Table 1).

### Site of infection and distribution of pathogenic bacteria

Among the 37 patients with infection, the main infection sites were the lung (24.32%), abdomen (21.62%), blood (16.22%), intestine (16.22%), surgical site (8.11%), urinary system (8.11%), skin (2.70%), and others (2.70%). A total of 51 strains of pathogenic bacteria were isolated from the infected patients. There were 38 strains of Gram-negative bacteria (74.51%), which were mainly *Escherichia coli* (27.45%) and *Pseudomonas aeruginosa* (19.61%), and 13 strains of Gram-positive bacteria (25.49%), which were mainly *Staphylococcus aureus* (11.76%) and coagulase-negative staphylococci (7.84%). See Fig. 1 and Table 2 for additional details.

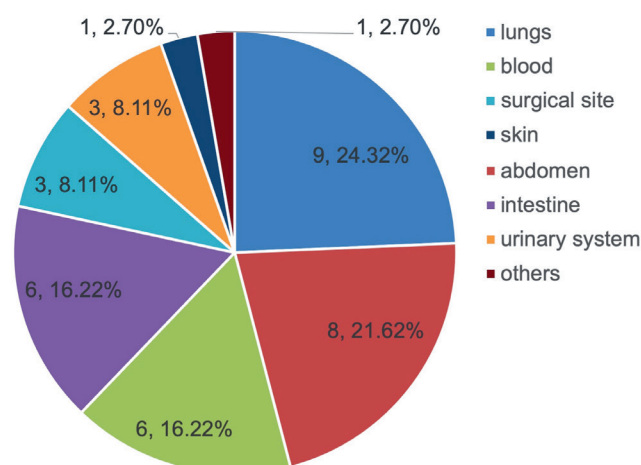


Fig. 1. Composition of postoperative infection sites in patients after liver cancer interventional therapy (%)

### Comparison of T lymphocyte subset levels before and after surgery

Before surgery, no significant differences were identified in CD3<sup>+</sup>, CD4<sup>+</sup>, CD8<sup>+</sup>, and CD4<sup>+</sup>/CD8<sup>+</sup> levels between the 2 groups (all  $p > 0.05$ ). After surgery, the CD3<sup>+</sup>, CD4<sup>+</sup> and CD4<sup>+</sup>/CD8<sup>+</sup> levels were significantly decreased, while the CD8<sup>+</sup> level was significantly increased in both groups (all  $p < 0.05$ ). The CD3<sup>+</sup>, CD4<sup>+</sup> and CD4<sup>+</sup>/CD8<sup>+</sup> levels were lower, and the CD8<sup>+</sup> level was higher in the infection group compared to the non-infection group (all  $p < 0.001$ ) (Table 3).

### Comparison of TLR2 and TLR4 levels in PBMCs before and after surgery

Before surgery, the TLR2 and TLR4 levels in PBMCs were  $53.86 \pm 19.97\%$  and  $51.96 \pm 18.83\%$  in the infection group, and  $54.12 \pm 18.36\%$  and  $52.23 \pm 17.92\%$  in the non-infection

**Table 1.** Comparison of general patient characteristics (n, x ± SD)

General data	Infection group (n = 37)	Non-infection group (n = 288)	$\chi^2/t$	p-value
Gender (n)				
Male	21	171	0.09 <sup>c</sup>	0.761
Female	16	117		
Age [years]	58.7 ± 5.4	58.4 ± 5.6	0.340 <sup>t</sup>	0.734
BMI [kg/m <sup>2</sup> ]	21.63 ± 1.44	21.59 ± 1.51	0.152 <sup>t</sup>	0.879
Pathological type (n)			0.465 <sup>c</sup>	0.793
Nodule type	14	102		
Massive type	16	117		
Diffused type	7	69		
Child–Pugh staging (n)			0.009 <sup>c</sup>	0.926
A	17	130		
B	20	158		
Lesion location (n)			0.002 <sup>c</sup>	0.965
Left	19	149		
Right	18	139		
Clinical stages (n)			0.352 <sup>c</sup>	0.553
IIb–III	30	221		
IV	7	67		
Fasting blood glucose [mmol/L]	4.73 ± 0.31	4.79 ± 0.33	1.048 <sup>t</sup>	0.259
Lesion size [cm]	7.13 ± 2.08	7.21 ± 2.11	0.217 <sup>t</sup>	0.828
Drinking history (n)			0.110 <sup>c</sup>	0.738
Yes	17	124		
No	20	164		
Smoking history (n)			0.260 <sup>c</sup>	0.601
Yes	19	135		
No	18	153		

SD – standard deviation; BMI – body mass index; <sup>t</sup> – using the independent sample t-test; <sup>c</sup> – using the  $\chi^2$  test.

**Table 2.** Composition of postoperative infection pathogens identified in patients after liver cancer interventional therapy (%)

Pathogens	Strain (s)	Constituent ratio (%)
Gram-negative bacteria	38	74.51
<i>Escherichia coli</i>	14	27.45
<i>Pseudomonas aeruginosa</i>	10	19.61
<i>Klebsiella pneumoniae</i>	4	7.84
<i>Acinetobacter baumannii</i>	3	5.88
<i>Proteus vulgaris</i>	3	5.88
Enterobacteriaceae	2	3.92
<i>Serratia</i>	1	1.96
<i>Enterobacter cloacae</i>	1	1.96
Gram-positive bacteria	13	25.49
<i>Staphylococcus aureus</i>	6	11.76
Coagulase-negative staphylococci	4	7.84
<i>Enterococcus</i>	2	3.92
Group A streptococcus	1	1.96

group, respectively. No significant differences were observed in the TLR2 and TLR4 levels in PBMCs between the 2 groups (both  $p > 0.05$ ). After surgery, the TLR2 and TLR4 levels in the infection group were increased ( $61.63 \pm 14.43\%$  and  $63.98 \pm 22.28\%$ , respectively; both  $p < 0.001$ ), while the levels in the non-infection group were

decreased ( $42.57 \pm 8.47\%$  and  $33.60 \pm 10.54\%$ , respectively; both  $p < 0.001$ ). The TLR2 and TLR4 levels in the infection group were significantly higher than those in the non-infection group (both  $p < 0.001$ , Table 4).

## ROC curves for TLR2 and TLR4 levels

When the area under the curve (AUC) of the postoperative TLR2 level for evaluating postoperative infection was 0.816, the cutoff value was 60.666%, with the sensitivity of 0.703 and the specificity of 0.965. When the AUC of the postoperative TLR4 level for evaluating postoperative infection was 0.865, the cutoff value was 53.679%, with the sensitivity of 0.757 and the specificity of 0.955. See Table 5 and Fig. 2 for additional details.

## Discussion

As medical technology develops, interventional therapy as a surgical treatment without laparotomy has become widely acknowledged by medical professionals for its clinical efficacy for middle-advanced liver cancer. However, cellular and humoral immune function is often impacted in patients who receive this treatment. Furthermore, the use of chemotherapeutics increases the risk of nosocomial infection. Our study showed that 37 out

**Table 3.** Comparison of T lymphocyte subset levels before and after surgery (x ± standard deviation (SD))

Group	Infection group (n = 37)	Non-infection group (n = 288)	t	p-value
CD3 <sup>+</sup>				
Before surgery	56.23 ±8.14	55.92 ±7.73	0.228	0.820
After surgery	41.26 ±9.24 <sup>a</sup>	51.38 ±8.19 <sup>a</sup>	6.971	<0.001
CD4 <sup>+</sup>				
Before surgery	34.33 ±3.95	34.24 ±4.21	0.126	0.901
After surgery	29.52 ±3.54 <sup>a</sup>	32.87 ±3.12 <sup>a</sup>	6.052	<0.001
CD8 <sup>+</sup>				
Before surgery	32.33 ±3.72	32.64 ±3.91	0.456	0.648
After surgery	38.24 ±4.83 <sup>a</sup>	35.01 ±4.18 <sup>a</sup>	4.401	<0.001
CD4 <sup>+</sup> /CD8 <sup>+</sup>				
Before surgery	1.06 ±0.21	1.07 ±0.18	0.312	0.755
After surgery	0.85 ±0.14 <sup>a</sup>	0.94 ±0.13 <sup>a</sup>	3.929	<0.001

Compared with before surgery, <sup>a</sup> p < 0.001. Independent sample t-tests were used for comparisons between the 2 groups; a paired t-test was used for comparisons before and after intervention within the same group.

**Table 4.** Comparison of TLR2 and TLR4 levels in PBMCs before and after surgery (x ± standard deviation (SD))

Group	TLR2 levels (%)		TLR4 levels (%)	
	before surgery	after surgery	before surgery	after surgery
Infection group (n = 37)	53.86 ±19.97	61.63 ±14.43 <sup>a</sup>	51.96 ±18.83	63.98 ±22.28 <sup>a</sup>
Non-infection group (n = 288)	54.12 ±18.36	42.57 ±8.47 <sup>a</sup>	52.23 ±17.92	33.60 ±10.54 <sup>a</sup>
t	0.080	11.701	0.086	14.018
p-value	0.936	<0.001	0.932	<0.001

Compared with before surgery, <sup>a</sup> p < 0.001. TLR – toll-like receptor; PBMCs – peripheral blood mononuclear cells. Independent sample t-tests were used for comparisons between 2 groups; a paired t-test was used for comparisons before and after intervention within the same group.

**Table 5.** Evaluation of the postoperative infection using ROC curves for TLR2 and TLR4 levels

Indicators	TLR2 levels (%)	TLR4 levels (%)
Cutoff value	60.666	53.679
AUC	0.816	0.865
95% CI	0.728, 0.911	0.782, 0.974
Sensitivity	0.703	0.757
Specificity	0.965	0.955
p-value	<0.001	<0.001

ROC – receiver operating characteristic; TLR – toll-like receptor; AUC – area under the curve; CI – confidence interval.

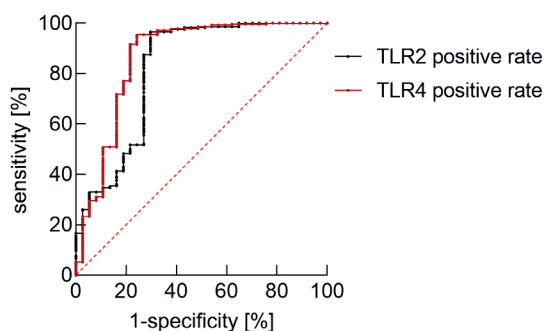


**Fig. 2.** Receiver operating characteristic (ROC) curves of postoperative TLR2 and TLR4 positive rates for evaluating infection

TLR – toll-like receptor.

of 325 patients had postoperative infections, indicating an infection rate of 11.38%. We isolated 51 strains of pathogenic bacteria from the infected patients (Gram-negative bacteria accounted for 74.51%). Notably, *Escherichia coli* (27.45%) and *Pseudomonas aeruginosa* (19.61%) were the most commonly observed bacteria. There are some differences in the proportion and species of strains between our findings and those of the prior research,<sup>13</sup> which may be due to the heterogeneity of the study patients and the composition of nosocomial pathogens. Pulmonary infection was identified as the main type of infection in the 37 infected patients. This is potentially because the function of respiratory muscles and ciliary movement, as well as the elasticity of the airway wall and lung tissue, weakened with age, resulting in difficulty excreting secretions. Generally, patients cannot forcefully cough and breathe deeply due to an increased pain after chemotherapy, which results in retention of pulmonary secretions and further increases the risk of infection.<sup>14</sup> This finding also highlights the need to actively take preventive measures in clinical practice in order to reduce the possibility of infection based on a patient's condition.

The T lymphocyte subset plays an important role in the immune mechanism. The CD4<sup>+</sup> cells can directly kill or damage tumor cells, while CD8<sup>+</sup> T cells function to suppress the immune response of the body.<sup>15</sup> Under normal physiological conditions, CD4<sup>+</sup> and CD8<sup>+</sup> cells

exist in a dynamic balance. A previous study found that the T lymphocyte subset level in patients infected after undergoing cesarean section was in a state of disorder, which suggests that the detection of T lymphocyte subsets plays a positive role in the prevention and treatment of postoperative infection.<sup>16</sup> To our knowledge, our study is the first to investigate the changes in T lymphocyte subset levels in patients with infection after liver cancer interventional surgery. We found that the CD3<sup>+</sup>, CD4<sup>+</sup> and CD4<sup>+</sup>/CD8<sup>+</sup> levels were significantly decreased while the CD8<sup>+</sup> level was greatly increased in the patients, indicating that immune function was decreased in both infected and non-infected groups. These changes may be due to the inhibition of immune function caused by surgical trauma and stress, or postoperative immune dysfunction resulting from abnormal anti-tumor function in patients with liver cancer.<sup>17–20</sup> Furthermore, the CD3<sup>+</sup>, CD4<sup>+</sup> and CD4<sup>+</sup>/CD8<sup>+</sup> levels were lower, and the CD8<sup>+</sup> level was higher in the infection group compared to the non-infection group. These results are consistent with those of the previous studies about changes in T lymphocyte subsets in patients with postoperative infection. We believe that this difference may occur due to the fact that the postoperative infections lead to more severe disturbance of the immune function. This result also suggests that medical professionals should pay attention to changes in T lymphocyte subsets in patients receiving liver cancer interventional therapy, so as to provide timely and effective prevention and control measures.

Toll-like receptors form the major family of pattern recognition receptors for innate immune responses. There are 11 subtypes found in humans, among which TLR2 and TLR4 are considered to be closely related to the development of liver cancer. It has been reported that TLR2 and TLR4 protein levels are significantly increased in liver cancer tissues compared with normal liver tissues.<sup>20,21</sup> Toll-like receptors are reported to be closely related to infection and inflammatory response. They are activated in response to infection or inflammation, which promotes the expression of their downstream pro-inflammatory factors and alters inflammatory signaling cascades.<sup>22</sup> There is also evidence suggesting that TLR2 mainly recognizes Gram-positive bacteria while TLR4 – Gram-negative bacteria.<sup>23</sup> Our study demonstrated that the expression levels of TLR2 and TLR4 in the non-infection group decreased after surgery, while the levels in the infection group increased compared to those before surgery. These results suggest that surgical treatment can improve TLR2 and TLR4 levels in patients. However, for patients with postoperative infection, the occurrence of infection results in a state of inflammatory response, which increases TLR2 and TLR4 levels. The results also suggest that changes in TLR2 and TLR4 levels are of great clinical significance to postoperative infection. The value of postoperative TLR2 and TLR4 levels for predicting postoperative infection was analyzed using ROC curves, and the results indicated that postoperative TLR2 and TLR4 levels have clinical value with high sensitivity

and specificity. Hence, we consider TLR2 and TLR4 levels after TACE to be useful biomarkers for evaluating postoperative infection in patients with liver cancer.

## Innovations

This study has the following innovations and advantages. Firstly, changes in the T lymphocyte subset level and positive rates of TLR2 and TLR4 in patients with infection after liver cancer interventional therapy were investigated for the first time. Secondly, we used patient blood samples for the analyses, which were easy to collect, involved simple procedures, and had high compliance.





## Limitations

This study is subject to several limitations. First, without further dynamic observation of each indicator, it is difficult to assess the relationship between the above indicators and patient prognosis. Second, this is a single-center study with a small sample size. Lastly, the constituent ratios of age, gender, age, BMI, pathological type, Child–Pugh classification, clinical stage, etc. differed among the enrolled patients, and we did not conduct further subgroup analyses of patients with different characteristics. Therefore, further studies are needed to address these issues.

## Conclusions

After interventional therapy for liver cancer, the main infection sites were identified as the lung and abdomen, with Gram-negative bacteria accounting for the majority of infections. Furthermore, the results indicated that the T lymphocyte subset level abnormally changed in patients with infection and that TLRs are closely related to the occurrence and development of postoperative infection. Postoperative TLR2 and TLR4 levels could be used as an auxiliary parameter to assess the postoperative infection risk.

## ORCID iDs

Conghui Zhu  <https://orcid.org/0000-0002-3564-4151>  
 Guanfeng Chen  <https://orcid.org/0000-0003-3017-731X>  
 Jiadi Yao  <https://orcid.org/0000-0002-8665-0906>  
 Wenji Lin  <https://orcid.org/0000-0002-9702-9824>

## References

- Salati U, Barry A, Chou FY, Ma R, Liu DM. State of the ablation nation: A review of ablative therapies for cure in the treatment of hepatocellular carcinoma. *Future Oncol.* 2017;13(16):1437–1448. doi:10.2217/fon-2017-0061
- Maharajan K, Hey HWD, Tham I, et al. Solitary vertebral metastasis of primary clear cell carcinoma of the liver: A case report and review of literature. *J Spine Surg.* 2017;3(2):287–293. doi:10.21037/jss.2017.06.06
- Titano J, Noor A, Kim E. Transarterial chemoembolization and radioembolization across Barcelona clinic liver cancer stages. *Semin Intervent Radiol.* 2017;34(2):109–115. doi:10.1055/s-0037-1602709



4. Ray CE, Battaglia C, Libby AM, et al. Interventional radiologic treatment of hepatocellular carcinoma: A cost analysis from the payer perspective. *J Vasc Interv Radiol.* 2012;23(3):306–314. doi:10.1016/j.jvir.2011.11.016
5. Nooron N, Ohba K, Takeda K, Shibahara S, Chiabchalard A. Dysregulated expression of MITF in subsets of hepatocellular carcinoma and cholangiocarcinoma. *Tohoku J Exp Med.* 2017;242(4):291–302. doi:10.1620/tjem.242.291
6. Pinato DJ, Howell J, Ramaswami R, Sharma R. Review article: Delivering precision oncology in intermediate-stage liver cancer. *Aliment Pharmacol Ther.* 2017;45(12):1514–1523. doi:10.1111/apt.14066
7. Kou PS, Zhang Y, Shao W, et al. Significant efficacy and well safety of apatinib in an advanced liver cancer patient: A case report and literature review. *Oncotarget.* 2017;8(12):20510–20515. doi:10.18632/oncotarget.14724
8. Correnti M, Raggi C. Stem-like plasticity and heterogeneity of circulating tumor cells: Current status and prospect challenges in liver cancer. *Oncotarget.* 2017;8(4):7094–7115. doi:10.18632/oncotarget.12569
9. Chen JB, Huang J, Chen MS, et al. Transcatheter arterial chemoembolization (TACE) versus hepatectomy in hepatocellular carcinoma with macrovascular invasion: A meta-analysis of 1683 patients. *J Cancer.* 2017;8(15):2984–2991. doi:10.7150/jca.20978
10. Novák K. Functional polymorphisms in Toll-like receptor genes for innate immunity in farm animals. *Vet Immunol Immunopathol.* 2014;157(1–2):1–11. doi:10.1016/j.vetimm.2013.10.016
11. Ministry of Health of the People's Republic of China. Diagnostic criteria for nosocomial infections (proposed). *Nat Med J Chin.* 2021;5:314. doi:10.3760/oma.j.issn.0376-2491.2001.05.027
12. Ministry of Health of the People's Republic of China. Primary liver cancer treatment specification (2011 edition). *Chin Clin Oncol.* 2011;10:929–946. [http://qikan.cqvip.com/Qikan/Article/Detail?id=39861125&from=Qikan\\_Search\\_Index](http://qikan.cqvip.com/Qikan/Article/Detail?id=39861125&from=Qikan_Search_Index). Accessed January 18, 2021.
13. Deng GL, Zeng S, Shen H. Chemotherapy and target therapy for hepatocellular carcinoma: New advances and challenges. *World J Hepatol.* 2015;7(5):787–798. doi:10.4254/wjh.v7.i5.787
14. Kim YJ, Goh PG, Moon HS, et al. Reactivation of tuberculosis in hepatocellular carcinoma treated with transcatheter arterial chemoembolization: A report of 3 cases. *World J Radiol.* 2012;4(5):236–240. doi:10.4329/wjr.v4.i5.236
15. Dong C. Helper T cells and cancer-associated inflammation: A new direction for immunotherapy? *J Interferon Cytokine Res.* 2017;37(9):383–385. doi:10.1089/jir.2017.0012
16. Liu CY, Deng LH. Related risk factors of postoperative infections after cesarean section and the changes of T lymphocyte subsets and interleukin clusters levels. *Chin J Fam Plan.* 2020;5:660–665. <http://qikan.cqvip.com/Qikan/Article/Detail?id=7102507581>. Accessed January 8, 2021.
17. Kwan SW, Harris WP, Gold LS, Hebert PL. Comparative effectiveness of transarterial embolization and sorafenib for hepatocellular carcinoma: A population-based study. *AJR Am J Roentgenol.* 2018;210(6):1359–1365. doi:10.2214/ajr.17.19094
18. Wu X, Chen R, Zheng WL, Hu H. Comprehensive analysis of factors affecting clinical response and short-term survival to drug-eluting bead transarterial chemoembolization for treatment in patients with liver cancer. *Technol Cancer Res Treat.* 2018;17:1533033818759878. doi:10.1177/1533033818759878
19. Wang H, Du PC, Wu MC, Cong WM. Postoperative adjuvant transarterial chemoembolization for multinodular hepatocellular carcinoma within the Barcelona Clinic Liver Cancer early stage and microvascular invasion. *Hepatobiliary Surg Nutr.* 2018;7(6):418–428. doi:10.21037/hbsn.2018.09.05
20. Lai JL, Liu YH, Liu C, et al. Indirubin inhibits LPS-induced inflammation via TLR4 abrogation mediated by the NF- $\kappa$ B and MAPK signaling pathways. *Inflammation.* 2017;40(1):1–12. doi:10.1007/s10753-016-0447-7
21. Mazur-Bialy AI, Pocheć E, Zarawski M. Anti-Inflammatory properties of irisin, mediator of physical activity, are connected with TLR4/MyD88 signaling pathway activation. *Int J Mol Sci.* 2017;18(4):701. doi:10.3390/ijms18040701
22. Alarcón MML, Ruocco JF, Ferreira F, et al. Toll-Like receptor 4 and NLRP3 caspase 1- interleukin-1 $\beta$ -axis are not involved in colon ascends stent peritonitis-associated heart disease. *Shock.* 2018;50(4):483–492. doi:10.1097/shk.0000000000001059
23. Li HM, Wang X, Xu AL. Effect of paclitaxel+hirudin on the TLR4-MyD88 signaling pathway during inflammatory activation of human coronary artery smooth muscle cells and mechanistic analysis. *Cell Physiol Biochem.* 2018;50(4):1301–1317. doi:10.1159/000494588



# Vitamin D status in Polish women with endocrine and osteoporotic disorders in relation to diet, supplement use and exposure to ultraviolet radiation

Małgorzata Godala<sup>1,A–F</sup>, Ewa Sewerynek<sup>2,A,F</sup>, Ewelina Gaszyńska<sup>1,A,E,F</sup>

<sup>1</sup> Department of Nutrition and Epidemiology, Medical University of Lodz, Poland

<sup>2</sup> Department of Endocrine Disorders and Bone Metabolism, Medical University of Lodz, Poland

A – research concept and design; B – collection and/or assembly of data; C – data analysis and interpretation;

D – writing the article; E – critical revision of the article; F – final approval of the article

Advances in Clinical and Experimental Medicine, ISSN 1899–5276 (print), ISSN 2451–2680 (online)

*Adv Clin Exp Med.* 2022;31(1):25–32

## Address for correspondence

Małgorzata Godala

E-mail: malgorzata.godala@umed.lodz.pl

## Funding sources

None declared

## Conflict of interest

None declared

Received on May 31, 2021

Reviewed on July 19, 2021

Accepted on August 25, 2021

Published online on October 12, 2021

## Cite as

Godala M, Sewerynek E, Gaszyńska E. Vitamin D status in Polish women with endocrine and osteoporotic disorders in relation to diet, supplement use and exposure to ultraviolet radiation. *Adv Clin Exp Med.* 2022;31(1):25–32. doi:10.17219/acem/141604

## DOI

10.17219/acem/141604

## Copyright

© 2022 by Wrocław Medical University

This is an article distributed under the terms of the Creative Commons Attribution 3.0 Unported (CC BY 3.0) (<https://creativecommons.org/licenses/by/3.0/>)

## Abstract

**Background.** In Europe, the rate of 25(OH)D deficiency is considered high. Thus, it seems necessary to conduct population-based studies to fully assess vitamin D deficiency in various groups of patients.

**Objectives.** To evaluate serum 25(OH)D levels and the frequency of deficiency in women in Poland with endocrine and osteoporotic disorders. The influences of diet, use of vitamin/mineral supplementation and exposure to ultraviolet (UVB) radiation on vitamin D status in women with metabolic disorders were also examined.

**Materials and methods.** The patient group consisted of 223 women aged 19–81 years diagnosed with endocrine and/or osteoporotic disorders. The control group consisted of 108 clinically healthy women aged 26–72 years. Serum 25(OH)D concentration was assessed using a chemiluminescent immunoassay (CLIA). An ad hoc questionnaire was used to assess the participants' exposure to UVB radiation. Food intake was assessed using a three-day 24-hour questionnaire interview.

**Results.** The following groups showed significantly higher 25(OH)D levels: women taking vitamin D supplements compared to women not taking vitamin D supplements ( $29.3 \pm 3.2$  compared to  $19.5 \pm 3.7$  ng/mL,  $p = 0.0024$ ); premenopausal women compared to postmenopausal women ( $28.9 \pm 5.2$  compared to  $21.5 \pm 4.5$  ng/mL,  $p = 0.0021$ ); women who visited sunny countries in the last 6 months compared to women who did not ( $28.1 \pm 3.1$  ng/mL compared to  $24.5 \pm 5.3$  ng/mL,  $p = 0.0031$ ); and normal weight or overweight women (according to body mass index (BMI)) compared to obese women ( $27.4 \pm 4.5$  ng/mL compared to  $22.3 \pm 4.7$  ng/mL,  $p = 0.0431$ ). In addition, 25(OH)D concentration correlated with total dietary vitamin D intake in the patient group ( $R = 0.17$ ,  $p = 0.0021$ ). Of all examined food groups, fish consumption affected serum 25(OH)D levels in patients ( $R = 0.20$ ,  $p = 0.0421$ ) and controls ( $R = 0.29$ ,  $p = 0.0002$ ). Consumption of fish products contributed to statistical differences between the patient group ( $R = 0.17$ ,  $p = 0.0072$ ) and healthy subjects ( $R = 0.19$ ,  $p = 0.0032$ ).

**Conclusions.** The most crucial factors influencing vitamin D status in the studied women were regular fish consumption, spending holidays in sunny destinations and regular intake of vitamin D preparations.

**Key words:** diet, metabolic disorders, ultraviolet radiation, 25(OH)D, vitamin D status

## Background

In light of recent research, vitamin D is recognized as more than just a factor preventing rickets and osteoporosis. An increasing number of studies have confirmed its role in the proper functioning of the cardiovascular system and prevention of neoplastic and autoimmune diseases.<sup>1–5</sup> The presence of vitamin D receptors (VDR) in tissues that are not involved in maintaining calcium-phosphate homeostasis proves the multidirectional activity of calcitriol.<sup>3,6,7</sup> Thus, vitamin D is thought to participate not only in bone metabolism, but also in cell proliferation and differentiation, as well as insulin secretion. Furthermore, it has pro- or anti-apoptogenic properties.<sup>8–10</sup> Until recently, vitamin D supplementation was recommended mainly for children. However, the need to introduce vitamin D supplementation in adults affected by various diseases, especially during the autumn-winter period, is increasingly discussed in the scientific literature.<sup>9,11</sup>

Both in Europe and worldwide, the rate of 25(OH)D deficiency is considered high.<sup>8,10,11</sup> This is caused by many factors including insufficient intake, insufficient exposure to sunlight, impaired cutaneous synthesis, and impaired formation of active metabolites in the liver and kidneys. Vitamin D regulates homeostasis of phosphate and calcium, and calcium intestinal absorption.<sup>3,7</sup> It also regulates blood pressure, and its concentration is inversely correlated with plasma renin activity.<sup>12,13</sup> Some studies have found that vitamin D may impact intracellular calcium concentration in pancreatic cells.<sup>14,15</sup> Since calcium stimulates insulin secretion, vitamin D deficiency may increase the risk of diabetes and other carbohydrate disorders. Vitamin D is also involved in lipid metabolism because its deficiency increases peripheral resistance to insulin, thereby worsening the lipid profile.<sup>10,13,14</sup> Moreover, studies have reported the decreased levels of 25(OH)D in obese patients resulting from sequestration of vitamin D in the overdeveloped adipose tissue.<sup>2,3,5</sup> Overall, vitamin D deficiency is associated with metabolic disorders and cardiovascular diseases, which are significant public health problems. However, whether vitamin D deficiency is a risk factor for cardiovascular and metabolic diseases, or if their existence predisposes an individual to deficiency, remains unclear. Thus, it seems necessary to conduct population-based studies in order to fully assess vitamin D deficiency in various groups of patients.

## Objectives

The aim of this study was to evaluate serum 25(OH)D levels and the frequency of deficiency in women with endocrine and osteoporotic disorders in Poland. Moreover, the influence of diet, use of vitamin/mineral supplementation and exposure to ultraviolet (UVB) radiation on vitamin D status in women with osteoporosis and endocrine disorders were examined.

## Materials and methods

### Patient and control groups

A total of 331 women living in the Łódź region of Poland participated in this study. The patient group consisted of 223 women aged 19–81 years (mean age: 64.6 ± 12.8 years) diagnosed with endocrine and/or osteoporotic disorders, recruited from the Department of Endocrine Disorders and Bone Metabolism, Chair of Endocrinology, Medical University of Lodz, between 2017 and 2019. The control group consisted of 108 clinically healthy women aged 26–72 years (mean age 61.4 ± 11.3 years) without the above disorders.

In the patient group, osteoporosis was found in 110 (49.3%) women, endocrine disorders (including hypothyroidism, Hashimoto inflammation and inactive nodules) were found in 53 (23.8%) women and both disorders were diagnosed in 60 (26.9%) women.

In the patient group, 26 (11.7%) women smoked cigarettes, and 173 (77.6%) took vitamin D supplements at a dose of 1000–2000 UI and a daily calcium dose of 500–600 mg for at least 3 months. In the control group, all women were non-smokers, and 31 (28.7%) took vitamin D at a dose of 1000–2000 UI without calcium for at least 3 months.

For both groups, women whose last menstrual period was at least 12 months prior to the commencement of the study were considered postmenopausal.

### Biochemical tests

Biochemical tests were performed by the hospital laboratory. Fasting blood was collected from the ulnar vein. The obtained blood samples were used to determine total 25(OH)D using a chemiluminescent immunoassay (CLIA). A serum 25(OH)D concentration of at least 30 ng/mL was considered normal, whereas a level below 30 ng/mL was considered insufficient (deficiency).<sup>9</sup> The 25(OH)D was assessed according to the season by dividing the year into quarters: I – January to March, II – April to June, III – July to September, and IV – October to December.

The collected blood samples were also used for the determination of total calcium concentration according to the Olympus Calcium Procedure (reaction of calcium ions Ca<sup>2+</sup> with Arsenazo III complex, corrected for albumin), and for the quantification of inorganic phosphorus using ultraviolet photometry.

### Assessment of exposure to UVB radiation

An ad hoc questionnaire developed by the authors of this study was used to assess participants' exposure to UVB radiation. The questionnaire estimated the time and the amount of sun exposure in all quarters of the year; the number of hours spent outdoors each week (8:00–16:00); and participants' preferences for being exclusively in the sun, both in the sun and shade, or only in the shade.

The questionnaire also assessed the frequency of solarium use (within the last 3 months), the frequency of visiting countries with high solar exposure (within the last 6 months), skin phototype (I – always burns, does not tan; II – burns easily, tans poorly; III – burns moderately, tans moderately; IV – burns minimally, tans easily; V – rarely burns, tans profusely; VI – never burns, never tans), and use of UVB protection agents (never, rarely, often, always).

## Anthropometry

All participants underwent standard anthropometric measurements. The waist-to-hip ratio (WHR) was determined by dividing the waist circumference by hip circumference. Body mass index (BMI) was determined by dividing participants' body weight (in kg) by height (in m<sup>2</sup>).

## Nutrition assessment

Before the tests, food intake was assessed using a 24-hour questionnaire interview administered 3 times (2 weekdays and 1 weekend day) for each participant by a trained dietician. The “Album of photographs of food products and dishes” by the National Food and Nutrition Institute in Warszawa, Poland was used to determine the normal size of the consumed portions. The average energy intake, as well as the intake of particular nutrients, was assessed using Diet v. 5.0 software (license No. 52/PD/2013; Instytut Żywności i Żywienia, Warszawa, Poland).<sup>16</sup>

In order to assess vitamin D intake over the last month, a questionnaire on the frequency of consumption of selected dietary products that are sources of vitamin D was used. The products were divided into 7 groups depending on the content of vitamin D in a standard portion size. The number of portions consumed per week and per month was determined. The assessed food groups were: fresh and smoked fish (3–10 µg of vitamin D), fish products (10–12 µg of vitamin D), milk and milk products (0.07–0.3 µg of vitamin D), eggs (0.85 µg of vitamin D), meat and meat products (0.09–0.75 µg of vitamin D), cereals (0.06–0.25 µg of vitamin D), and fats (0.03–0.31 µg of vitamin D). The amount and type of supplement intake were also taken into account.

## Statistical analyses

Statistical analyses were performed using STATISTICA v. 13 software (StatSoft Inc., Tulsa, USA). Results are reported using descriptive statistics, including mean and standard deviation (SD). For variables with nominal scales, the rate of occurrence was computed. The normality of the distribution of the variables was determined using the Shapiro–Wilk test. All analyzed variables deviated significantly from the normal distribution. The means of 2 independent groups were compared using the Mann–Whitney U test for continuous and dichotomous variables.

Spearman's rank order correlation was used to determine the correlation between variables. To assess the risk of vitamin D deficiency in patients with osteoporosis or endocrine disorders and in healthy subjects, receiver operating characteristic (ROC) classification models were used. A multivariate adaptive regression splines model was constructed to determine the relationship between the studied factors (vitamin D consumption, calcium and vitamin D supplement intake, consumption of fish, and normal weight/overweight/obese) and 25(OH)D concentrations. A value of  $p < 0.05$  was considered statistically significant.<sup>17</sup>

## Ethics approval

This study was performed according to the Declaration of Helsinki and approved by the Bioethics Committee of the Medical University of Lodz, Poland (approval No. RNN/556/10/KB). All participants provided written informed consent before participating in this study.

## Results

There were no statistically significant differences regarding age, weight, waist circumference, BMI, or WHR between the study and control groups. Similarly, there was no difference regarding UVB exposure. However, patients with osteoporotic and endocrine disorders used vitamin and mineral supplementation significantly more often than healthy women. In both groups, 1/5 of women had spent a holiday in a country with high solar exposure in the last 6 months, and 2/3 claimed to have spent more than 7 h per week outdoors in spring and summer. With regard to skin phototype, nearly 60% of women claimed that their skin burns rarely or moderately and tans moderately or easily. A small percentage of participants reported that they always use UVB protective agents (Table 1).

The concentration of 25(OH)D was significantly lower in the group of women with osteoporosis and endocrine disorders compared to the control group ( $25.9 \pm 11.8$  ng/mL compared to  $28.1 \pm 9.1$  ng/mL;  $Z = 2.1808$ ,  $p = 0.0029$ ). However, the prevalence of vitamin D deficiency was not significantly different between the 2 groups (Table 1). There were significantly higher 25(OH)D levels in the following groups: women taking vitamin D supplements compared to women not taking vitamin D supplements ( $29.3 \pm 3.2$  ng/mL compared to  $19.5 \pm 3.7$  ng/mL,  $Z = 3.2056$ ,  $p = 0.0024$ ); premenopausal women compared to postmenopausal women ( $28.9 \pm 5.2$  ng/mL compared to  $21.5 \pm 4.5$  ng/mL,  $Z = 2.9634$ ,  $p = 0.0021$ ); women who visited sunny countries in the last 6 months compared to women who did not ( $28.1 \pm 3.1$  ng/mL compared to  $24.5 \pm 5.3$  ng/mL,  $Z = 2.9583$ ,  $p = 0.0031$ ); and normal-weight or overweight women (based on BMI) compared to obese women ( $27.4 \pm 4.5$  ng/mL compared to  $22.3 \pm 4.7$  ng/mL,  $Z = 3.2845$ ,  $p = 0.0431$ ). In the control

Table 1. Characteristics of the study participants

Characteristics	Patient group n = 223	Control group n = 108	Z, p-value Mann–Whitney test
	mean ±SD/n (%)	mean ±SD/n (%)	
Age [years]	64.6 ±12.8	61.4 ±11.3	4.2306, 0.4673
Weight [kg]	71.5 ±14.7	73.5 ±7.9	1.1365, 0.6233
Body mass index (BMI) [kg/m <sup>2</sup> ]	27.8 ±5.5	26.1 ±5.8	1.4817, 0.7671
Waist circumference [cm]	88.8 ±12.9	87.2 ±7.2	1.1463, 0.5659
Pre-menopausal women, n (%)	84 (37.67)	41 (37.96)	1.0453, 0.7352
Regular vitamin D supplements users, n (%)	173 (77.6)	31 (28.7)	4.5638, <0.0001
UVB exposure			
Sunny vacation during the previous 6 months, n (%)	44 (19.73)	20 (18.52)	1.3482, 0.8671
Outside during daylight >7 h/week, n (%)	151 (67.71)	79 (73.15)	0.9834, 0.9654
Summer	136 (60.99)	72 (66.67)	1.7384, 0.7694
Winter	62 (27.80)	25 (23.15)	0.9954, 0.4739
Preference, n (%)			
Sun avoiders	49 (21.97)	22 (20.37)	1.2376, 0.9674
Some exposure	155 (69.51)	74 (68.52)	1.0674, 0.7698
Frequent exposure	19 (8.52)	12 (11.11)	1.1054, 0.8033
Sunbathing during previous 3 months, n (%)	5 (2.24)	4 (3.70)	0.8725, 0.6713
Skin phototype, n (%)			
I–II	39 (17.49)	19 (17.59)	1.1358, 0.7474
III–IV	132 (59.19)	62 (57.41)	1.0386, 0.6704
V–VI	52 (23.32)	27 (25)	1.1079, 0.8552
Sun-protection products, n (%)			
Never	70 (31.39)	34 (31.48)	1.1637, 0.8452
Rarely	59 (26.46)	28 (25.93)	0.9427, 0.7752
Often	65 (29.15)	30 (27.78)	1.0926, 0.8047
Always	29 (13.00)	16 (14.81)	0.9963, 0.9172
Dietary intake			
Energy [kcal/day]	1415.7 ±447.4	2127.2 ±1182.3	4.2349, <0.0001
Fats [g/day]	53.4 ±24.3	79.3 ±57.7	3.9465, <0.0001
Proteins [g/day]	57.9 ±19.5	99.6 ±45.8	2.9836, <0.0001
Carbohydrates [g/day]	189.0 ±61.0	268.8 ±139.8	6.4326, <0.0001
Vitamin D (without supplements) [µg/day]	3.7 ±2.3	7.4 ±5.6	2.9987, <0.0001
Total vitamin D (including supplements) [µg/day]	38.2 ±15.0	21.1 ±13.6	3.9075, 0.0028
Calcium (without supplements) [mg/day]	512.5 ±278.1	690.1 ±486.0	2.9967, <0.0001
Total calcium (including supplements) [mg/day]	713.4 ±419.3	690.1 ±486.0	3.0784, <0.0001
Phosphorus [mg/day]	921.3 ±318.7	1579.6 ±764.3	4.0237, <0.0001
Groups of products			
Fresh and smoked fish [portions/week]	1.2 ±0.7	2.4 ±1.1	4.2271, <0.0001
Fresh and smoked fish [µg vitamin D/week]	10.7 ±3.3	21.3 ±6.8	3.9566, <0.0001
Fish products [portions/week]	1.3 ±0.5	2.7 ±0.9	3.2874, <0.0001
Fish products [µg vitamin D/week]	13.8 ±2.9	26.8 ±5.6	4.0376, <0.0001
Serum concentration			
25(OH)D total [ng/mL]	25.9 ±11.8	28.1 ±9.1	2.1808, 0.0029
25(OH)D deficiency, n (%)	149 (66.8)	68 (62.9)	0.8725, 0.8043
Parathormone [pg/mL]	54.4 ±19.1	84.4 ±12.5	2.4381, 0.0068
Calcium [mmol/L]	2.4 ±0.6	2.4 ±0.2	0.5683, 0.9269
Phosphorus [mmol/L]	1.1 ±0.5	1.3 ±0.5	0.7856, 0.4738

UVB – ultraviolet radiation; SD – standard deviation.

group, higher 25(OH)D levels were observed in women taking vitamin D supplements compared to those who were not ( $32.58 \pm 3.2$  ng/mL compared to  $26.7 \pm 4.6$  ng/mL,  $Z = 2.9743$ ,  $p = 0.0492$ ) and in normal-weight or overweight women (based on BMI) compared to obese women ( $35.3 \pm 4.7$  ng/mL compared to  $27.8 \pm 3.7$  ng/mL,  $Z = 3.3124$ ,  $p = 0.0476$ ). The use of personal UVB protective agents, skin phototype, and time spent outdoors did not differentiate between 25(OH)D concentrations in the 2 groups. There was no seasonal variation in 25(OH)D concentration in the group of women with endocrine and osteoporotic disturbances or in the control group.

In the patient group, Spearman's rank order correlation analysis indicated significant correlations between 25(OH)D concentration and serum Ca ( $R = 0.50$ ,  $p < 0.0001$ ), phosphorus ( $R = 0.47$ ,  $p < 0.0001$ ), and parathormone ( $R = -0.65$ ,  $p < 0.0001$ ) levels. In the control group, the 25(OH)D concentration was only significantly correlated with the level of parathormone ( $R = -0.29$ ,  $p < 0.0001$ ).

In addition, Spearman's rank order correlation analysis detected a correlation between serum 25(OH)D concentration and the occurrence of osteoporosis ( $R = 0.21$ ,  $p < 0.0001$ ). Such a correlation was not found for thyroid diseases. Moreover, there was a correlation between serum 25(OH)D level and BMI in women with osteoporotic and endocrine disorders ( $R = -0.31$ ,  $p = 0.0027$ ) and in healthy women ( $R = -0.42$ ,  $p < 0.0001$ ). An inverse correlation between vitamin D level and waist circumference in the patient group ( $R = -0.27$ ,  $p = 0.0413$ ), an observation that was not confirmed in the control group, was also noted. Participants' age and vitamin D concentration were not correlated (Table 2).

According to Spearman's rank order correlation, 25(OH)D concentration correlated with the total dietary vitamin D intake in the patient group ( $R = 0.17$ ,  $p = 0.0021$ ) and in the control group ( $R = 0.43$ ,  $p = 0.0000$ ). Furthermore, 25(OH)D concentration positively correlated with total dietary calcium intake in the patient group ( $R = 0.22$ ,  $p = 0.0041$ ) and in the control group ( $R = 0.34$ ,  $p < 0.0001$ ). Of all food groups, fish consumption was correlated with serum 25(OH)D levels in the patient ( $R = 0.20$ ,  $p = 0.0421$ ) and control groups ( $R = 0.29$ ,  $p = 0.0002$ ). Consumption of fish products was also correlated with serum 25(OH)D levels in the patient ( $R = 0.17$ ,  $p = 0.0072$ ) and control groups ( $R = 0.19$ ,  $p = 0.0032$ ). No relationship was found between the intake of food from other groups and serum vitamin D levels in patient group or control group.

The multivariate adaptive regression splines model showed that there was a relationship between vitamin 25(OH)D serum level in all studied women and dietary intake, including intake of vitamin D and calcium supplements, consumption of 1 portion of fish per week, and a normal body weight, as measured with BMI (correlation coefficient  $R = 0.386$ ,  $p < 0.0001$ ; Fig. 1). Moreover, the risk of vitamin D deficiency in the 2 groups was determined.

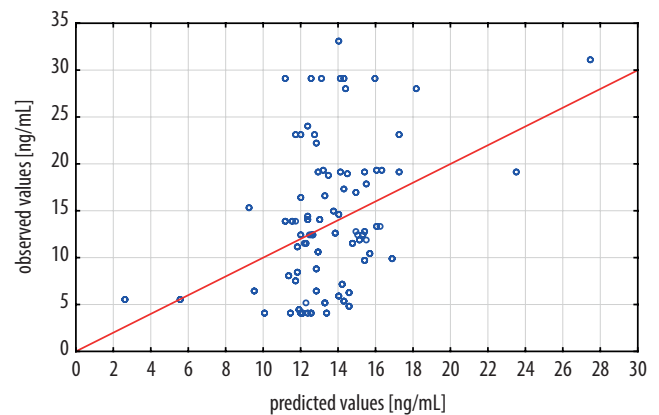


Fig. 1. Multivariate adaptive regression model for the serum level of 25(OH)D and its consumption with diet, accounting for intake of vitamin D and calcium supplements, consumption of fish, and normal body weight

The highest predictive quality was obtained for women with thyroid diseases and the lowest was obtained for healthy women (Fig. 2).

## Discussion

In our study, we found significantly lower serum 25(OH)D concentrations in women with metabolic disorders compared to healthy women. The prevalence of vitamin D deficiency in both groups was similar; more than 60% of studied women failed to demonstrate the recommended serum vitamin D concentration, despite the fact that about 77% of patients and nearly 30% of healthy women regularly took vitamin D supplements. In 2013, recommendations for supplemental prophylactic and therapeutic doses of vitamin D changed. Adults with normal 25(OH)D levels should take 800–2000 IU per day, while those with vitamin D deficiency should take up to 10,000 IU per day, but not more than 50,000 IU per week.<sup>9</sup> Compensation of vitamin D deficiency is particularly important among patients with bone metabolism disorders, and failure to achieve optimal 25(OH)D concentrations can make the anti-osteoporotic therapy less effective. Cutaneous synthesis is the main source of vitamin D. However, it is often insufficient to provide optimal concentrations of the vitamin even in spring and summer months, as confirmed in prior studies.<sup>18–21</sup> Thus, it is suggested that people over 65, obese people, and people who avoid the sun or use UV filters should also take vitamin D preparations in summer.<sup>9</sup> Such a high recommended dosage may raise doubts in patients, pharmacists and even doctors who are accustomed to the earlier recommendations. In our study, patients took low daily doses of supplementation, not exceeding 2000 IU. It was shown that in most cases, the recommended levels were achieved in neither sick nor healthy women. Similar results were obtained in other studies, in which supplementation used in different groups

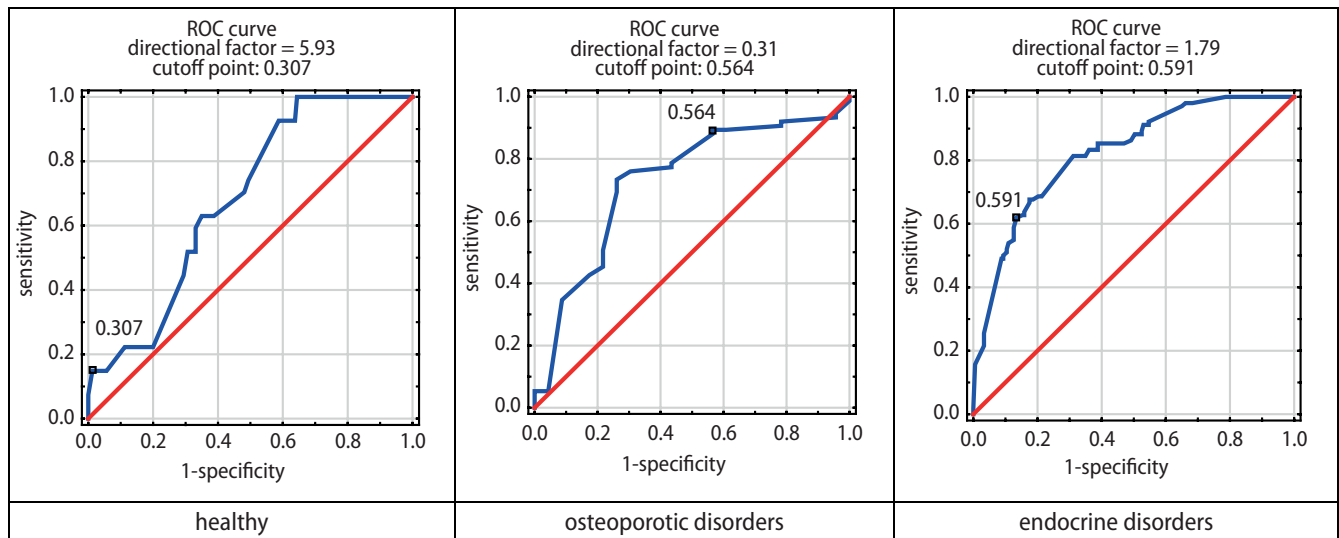


Fig. 2. Predicted prevalence of 25(OH)D deficiency in patients with different metabolic disorders

ROC – receiver operating characteristic.

Table 2. Multivariate adaptive regression model for the serum level of 25(OH)D and its consumption with diet, accounting for the intake of vitamin D and calcium supplements, consumption of fish, and normal body mass index (BMI)

Vitamin D [ng/dL]	correlation coefficient	F-test	df	Standard error of estimate	p-value
	0.386	10.883	3.186	7.234	<0.0001
Vitamin D and Ca supplements intake			0.334		<0.0001
Consumption of fish [1 portion/week]			0.21		<0.0001
Normal body weight [BMI < 25 kg/m <sup>2</sup> ]			0.11		<0.0001

df – degrees of freedom.

of patients proved to be insufficient in normalizing serum 25(OH)D levels.<sup>19,22,23</sup>

This study demonstrated a significant effect of dietary vitamin D and calcium intake on serum 25(OH)D levels. Vitamin D intake without supplements in the patient group was  $3.7 \pm 2.3 \mu\text{g}$  and in the control group was  $7.4 \pm 5.6 \mu\text{g}$ , whereas the recommended intake is  $15 \mu\text{g}$ . Low intake of vitamin D is common in European countries and ranges between  $4 \mu\text{g}$  and  $10 \mu\text{g}$  per day.<sup>24–28</sup> Hence, recommendations not just on possible need for supplementation, but concerning various doses of vitamin D administered to different age groups of patients with different disorders, are currently widely discussed. Insufficient intake of vitamin D may result from the fact that high doses of this vitamin can be found only in a few alimentary products. In countries where there is an obligation to fortify low-fat dairy products and margarines with vitamin D (Scandinavian countries), and in countries with a high intake of marine fish (Scandinavian and Mediterranean countries), vitamin D intake is higher than in central Europe.<sup>29–32</sup> In our study, we showed a significant increase in 25(OH)D concentrations in women consuming fish and fish products. These alimentary products are essential dietary components as they are the greatest source of vitamin D.

Cutaneous synthesis provides 90% of the body supply of vitamin D.<sup>33,34</sup> Due to a low exposure to sunlight in autumn and winter, supplementation is necessary to maintain optimal serum 25(OH)D concentrations. Thus, we also evaluated participants' exposure to ultraviolet radiation. We found that 25(OH)D concentrations did not show seasonal variation. Furthermore, factors such as time spent outdoors, use of UV protective agents and preference regarding exposure intensity did not significantly affect serum levels of 25(OH)D. In contrast, significantly higher 25(OH)D concentrations were observed in women who had spent holidays in countries with high solar exposure within the 6 months prior to the commencement of the study.

It is possible that brief but intense exposure of a large skin area to sunlight is a more effective method of supplying the body with vitamin D than supplementation. This possibility has been discussed in clinical studies evaluating the effects of sun exposure on vitamin D synthesis in the skin. However, the results were often contradictory. Some authors' results were consistent with ours, as they noted a significant increase in 25(OH)D concentration after strong exposure to sunlight during holidays.<sup>33,35</sup> Other studies failed to confirm this relationship.<sup>8,11,36</sup> Clinical studies on the efficiency of cutaneous vitamin D synthesis



showed that a single erythemal dose leads to a large increase in 25(OH)D concentrations due to the release of about 30 µg D3 from 1 m<sup>2</sup> of body surface per day. The standard pre-exposure vitamin D concentration in healthy subjects was restored after several days. However, in patients with 25(OH)D deficiency, the increase in 25(OH)D concentration after sun exposure was observed for much longer,<sup>37,38</sup> which is consistent with the results of our study.

The effect of vitamin D concentration on calcium-phosphate metabolism is often discussed, as it is of particular importance for osteoporotic patients. This study revealed an inverse relationship between 25(OH)D and parathormone levels, and a positive relationship between calcium and phosphorus levels. Increased parathormone levels and decreased vitamin D blood levels result in rapid bone turnover and decreased bone mass, which promotes the development of osteomalacia and reduces muscle strength. Vitamin D, which contributes to the reabsorption of calcium from the gastrointestinal tract, enables maintenance of the calcium and phosphate balance. In addition, the gut is reported to be highly adaptive depending on the amount of dietary calcium intake.<sup>8,9,11</sup> When dietary calcium is low, the gut produces more calcium-binding protein, so calcium absorption is increased. Hypocalcemia in turn stimulates parathyroid gland production of parathormone, which stimulates renal 1 $\alpha$ -hydroxylase to increase synthesis of 1,25(OH)<sub>2</sub>D. Once serum calcium levels are normalized, parathormone synthesis and calcium absorption in the gastrointestinal tract decrease. Despite insufficient dietary calcium intake, we observed normal mean concentrations in the patient and control groups, which confirms the mechanisms described above.

The factors influencing vitamin D nutritional status in patients with metabolic disorders are complex and require further research. Undoubtedly, the nutritional status and age of participants are variables that may influence the effect of sun exposure on cutaneous vitamin D synthesis. Many studies have reported lower 25(OH)D concentrations in obese subjects,<sup>39–42</sup> which were also demonstrated in this study. Other authors reported a decrease in 25(OH)D concentration that occurred with age,<sup>20,21,25</sup> which was not confirmed in our study. However, our study revealed an influence of menopause on vitamin D level, with a significantly lower concentration of 25(OH)D in postmenopausal women. Although similar relationships have been reported in other studies,<sup>20,21</sup> it is worth mentioning that this may be a result of less efficient dermal synthesis in older people and not necessarily a result of menopause.

Despite great knowledge about the factors influencing 25(OH)D concentration, the results of the present study and studies conducted by other authors confirm that the suggested amount and type of sun exposure, the amount of supplement intake and the need of vitamin D food fortification require further research, especially regarding patients with metabolic disorders.

## Limitations


Our study is subject to several limitations. Firstly, we could not evaluate the impact of cigarette smoking on 25(OH)D level due to the limited number of participants who were current smokers. Secondly, it was not possible to confirm the impact of calcium supplementation on 25(OH)D concentration in the control group, which may be important. Lastly, we were not able to assess seasonal changes in 25(OH)D because participants' blood samples were only taken once.


## Conclusions

The group of women with osteoporotic and endocrine disorders demonstrated vitamin D deficiency despite the intake, however insufficient, of supplements. The crucial factors determining vitamin D status in the patient group included regular fish consumption, spending holidays in sunny destinations and regular intake of vitamin D supplements.

### ORCID iDs

Małgorzata Godala  <https://orcid.org/0000-0003-3579-8537>

Ewa Sewerynek  <https://orcid.org/0000-0001-9705-4264>

Ewelina Gaszyńska  <https://orcid.org/0000-0001-7568-3502>

### References

- Al Mheid I, Quyyumi AA. Vitamin D and cardiovascular disease. *J Am Coll Cardiol*. 2017;70(1):89–100. doi:10.1016/j.jacc.2017.05.031
- Manson JE, Cook NR, Lee IM, et al. Vitamin D supplements and prevention of cancer and cardiovascular disease. *N Engl J Med*. 2019; 380(1):33–44. doi:10.1056/NEJMoa1809944
- Christakos S, Dhawan P, Verstuyf A, Verlinden L, Carmeliet G. Vitamin D: Metabolism, molecular mechanism of action, and pleiotropic effects. *Physiol Rev*. 2016;96(1):365–408. doi:10.1152/physrev.00014.2015
- Daffara V, Verdoia M, Rolla R, et al. Impact of polymorphism rs7041 and rs4588 of vitamin D binding protein on the extent of coronary artery disease. *Nutr Metab Cardiovasc Dis*. 2017;27(9):775–783. doi:10.1016/j.numecd.2017.06.002
- Almesri N, Das NS, Ali ME, Gumaa K, Giha HA. Independent associations of polymorphisms in vitamin D binding protein (GC) and vitamin D receptor (VD) genes with obesity and plasma 25OHD3 levels demonstrate sex dimorphism. *Appl Physiol Nutr Metab*. 2016;41(4): 345–353. doi:10.1139/apnm-2015-0284
- Fleet JC. The role of vitamin D in the endocrinology controlling calcium homeostasis. *Mol Cell Endocrinol*. 2017;453:36–45. doi:10.1016/j.mce.2017.04.008
- Battault S, Whiting SJ, Peltier SL, Sadrin S, Gerber G, Maixent JM. Vitamin D metabolism, functions and needs: From science to health claims. *Eur J Nutr*. 2013;52(2):429–441. doi:10.1007/s00394-012-0430-5
- Pludowski P, Ducki C, Konstantynowicz J, Jaworski M. Vitamin D status in Poland. *Pol Arch Med Wewn*. 2016;126(7–8):530–539. doi:10.20452/pamw.3479
- Pludowski P, Holick MF, Grant WB, et al. Vitamin D supplementation guidelines. *J Steroid Biochem Mol Biol*. 2018;175:125–135. doi:10.1016/j.jsbmb.2017.01.021
- Wimalawansa SJ. Associations of vitamin D with insulin resistance, obesity, type 2 diabetes, and metabolic syndrome. *J Steroid Biochem Mol Biol*. 2018;175:177–189. doi:10.1016/j.jsbmb.2016.09.017
- O'Neill CM, Kazantzidis A, Ryan MJ, et al. Seasonal changes in vitamin D-effective UVB availability in Europe and associations with population serum 25-hydroxyvitamin D. *Nutrients*. 2016;8(9):533. doi:10.3390/nu8090533

12. Beveridge LA, Struthers AD, Khan F, et al. Effect of vitamin D supplementation on blood pressure: A systematic review and meta-analysis incorporating individual patient data. *JAMA Int Med.* 2015;175(5):745–754. doi:10.1001/jamainternmed.2015.0237
13. Pilz S, Gaksch M, Kienreich K, et al. Effects of vitamin D on blood pressure and cardiovascular risk factors: A randomized controlled trial. *Hypertension.* 2015;65(6):1195–1201. doi:10.1161/HYPERTENSIONAHA.115.05319
14. Yoon HK. Gestational diabetes mellitus, fetal growth and vitamin D. *J Bone Metab.* 2017;24(33):155–159. doi:10.11005/jbm.2017.24.3.155
15. Li X, Liu Y, Zheng Y, Wang P, Zhang Y. The effect of vitamin D supplementation on glycemic control in type 2 diabetes patients: A systematic review and meta-analysis. *Nutrients.* 2018;10(3):375. doi:10.3390/nu10030375
16. Jarosz M. *Normy żywienia dla populacji polskiej.* Warszawa, Poland: Instytut Żywności i Żywienia; 2012.
17. Przybyłek M, Jeliński T, Słabuszewska J, Ziółkowska D, Mroczyńska K, Cysewski P. Application of multivariate adaptive regression splines (MARSplines) methodology for screening of dicarboxylic acids cocrystal using 1D and 2D molecular descriptors. *Cryst Growth Des.* 2019;19(7):3876–3887. doi:10.1021/acs.cgd.9b00318
18. Kamińska S, Pikala M, Dziankowska-Zaborszczyk E, et al. Vitamin D: Dietary intake, supplementation and metabolic status of Polish adults. *Int J Occup Med Environ Health.* 2020;33(1):107–118. doi:10.13075/ijom.1896.01400
19. Grant WB, Bhattoa HP, Boucher BJ. Seasonal variations of U.S. mortality rates: Roles of solar ultraviolet-B doses, vitamin D, gene expression, and infections. *J Steroid Biochem Mol Biol.* 2017;173:5–12. doi:10.1016/j.jsbmb.2017.01.003
20. Kocka K, Ślusarska B, Nowicki G, et al. Level of vitamin 25 (OH) D and B group vitamins and functional efficiency among the chronically ill elderly in domiciliary care: A pilot study. *Ann Agric Environ Med.* 2019;26(3):489–495. doi:10.26444/aaem/105801
21. Stolarczyk A, Horvath A, Szczechura M, Kamińska M, Dziechciarz P. High prevalence of vitamin D insufficiency in community-dwelling postmenopausal Polish women. *Prz Menopauzalny.* 2014;13(5):289–292. doi:10.5114/pm.2014.46471
22. Cashman KD, van den Heuvel EG, Schoemaker RJ, Preveraud DP, Macdonald HM, Arcot J. 25-hydroxyvitamin D as a biomarker of vitamin D status and its modeling to inform strategies for prevention of vitamin D deficiency within the population. *Adv Nutr.* 2017;8(6):947–957. doi:10.3945/an.117.015578
23. Brouwer-Brolsma EM, Vaes AMM, van der Zwaluw NL, et al. Relative importance of summer sun exposure, vitamin D intake, and genes to vitamin D status in Dutch older adults: The B-PROOF study. *J Steroid Biochem Mol Biol.* 2016;164:168–176. doi:10.1016/j.jsbmb.2015.08.008
24. Cashman KD, Dowling KG, Skrabakova Z, et al. Vitamin D deficiency in Europe-Pandemic? *Am J Clin Nutr.* 2016;103(4):1033–1044. doi:10.3945/ajcn.115.120873
25. Hilger J, Friedel A, Herr R, et al. A systematic review of vitamin D status in populations worldwide. *Br J Nutr.* 2014;111(1):23–45. doi:10.1017/S0007114513001840
26. Didriksen A, Burild A, Jakobsen J, Fuskevåg OM, Jorde R. Vitamin D3 increases in abdominal subcutaneous fat tissue after supplementation with vitamin D3. *Eur J Endocrinol.* 2015;172(3):235–241. doi:10.1530/EJE-14-0870
27. Yasein N, Shroukh W, Hijjawi R. Serum vitamin D and the metabolic syndrome among osteoporotic postmenopausal female patients of a family practice clinic in Jordan. *Adv Clin Exp Med.* 2015;24(2):245–250. doi:10.17219/acem/41375
28. Belen E, Aykan AC, Kalaycioglu E, Sungur MA, Sungur A, Cetin M. Low-level vitamin D is associated with atrial fibrillation in patients with chronic heart failure. *Adv Clin Exp Med.* 2016;25(1):51–57. doi:10.17219/acem/34690
29. Macdonald HM, Mavroei A, Fraser WD, et al. Sunlight and dietary contributions to the seasonal vitamin D status of cohorts of healthy postmenopausal women living at northerly latitudes: A major cause for concern? *Osteoporos Int.* 2011;22(9):2461–2472. doi:10.1007/s00198-010-1467-z
30. Cashman KD. Food-based strategies for prevention of vitamin D deficiency as informed by vitamin D dietary guidelines, and consideration of minimal-risk UVB radiation exposure in future guidelines. *Photochem Photobiol Sci.* 2020;19(6):800–809. doi:10.1039/c9pp00462a
31. Chandran M, Chan Maung A, Mithal A, Parameswaran R. Vitamin D in COVID-19: Dousing the fire or averting the storm? A perspective from the Asia-Pacific. *Osteoporos Sarcopenia.* 2020;6(3):97–105. doi:10.1016/j.afos.2020.07.003
32. Kiely M, Cashman KD. The ODIN project: Development of food-based approaches for prevention of vitamin D deficiency throughout life. *Nutr Bull.* 2015;40:235–246. doi:10.1111/nbu.12159
33. O'Sullivan F, Laird E, Kelly D, et al. Ambient UVB dose and sun enjoyment are important predictors of vitamin D status in an older population. *J Nutr.* 2017;147(5):858–868. doi:10.3945/jn.116.244079
34. Neville JJ, Palmieri T, Young AR. Physical determinants of vitamin D photosynthesis: A review. *JBM R Plus.* 2021;5(1):e10460. doi:10.1002/jbm4.10460
35. Sieniawska J, Lesiak A, Segerbäck D, Young AR, Woźniacka A, Narbutt J. Holiday sun exposure increases level of vitamin D and thymine dimers in children. *Forum Dermatol.* 2016;2(2):73–80. [https://journals.viamedica.pl/forum\\_dermatologicum/article/view/47992/37333](https://journals.viamedica.pl/forum_dermatologicum/article/view/47992/37333). Accessed September 15, 2021.
36. Hribar M, Hristov H, Gregorič M, et al. Nutrihealth study: Seasonal variation in vitamin D status among the Slovenian adult and elderly population. *Nutrients.* 2020;12(6):1838. doi:10.3390/nu12061838
37. Cashman KD, Kazantzidis A, Webb AR, Kiely M. An integrated predictive model of population serum 25-hydroxyvitamin D for application in strategy development for vitamin D deficiency prevention. *J Nutr.* 2015;145(10):2419–2425. doi:10.3945/jn.115.217968
38. Makris K, Bhattoa HP, Cavalier E, et al. Recommendations on the measurement and the clinical use of vitamin D metabolites and vitamin D binding protein: A position paper from the IFCC Committee on bone metabolism. *Clin Chim Acta.* 2021;517:171–197. doi:10.1016/j.cca.2021.03.002
39. Pannu PK, Zhao Y, Soares MJ. Reductions in body weight and percent fat mass increase the vitamin D status of obese subjects: A systematic review and metaregression analysis. *Nutr Res.* 2016;36(3):201–213. doi:10.1016/j.nutres.2015.11.013
40. Ganji V, Tangpricha V, Zhang X. Serum vitamin D concentration  $\geq 75$  nmol/L is related to decreased cardiometabolic and inflammatory biomarkers, metabolic syndrome, and diabetes, and increased cardiorespiratory fitness in US adults. *Nutrients.* 2020;12(3):E730. doi:10.3390/nu12030730
41. Zhang R, Li B, Gao X, et al. Serum 25-hydroxyvitamin D and the risk of cardiovascular disease: Dose-response meta-analysis of prospective studies. *Am J Clin Nutr.* 2017;105(4):810–819. doi:10.3945/ajcn.116.140392
42. Žmitek K, Hribar M, Hristov H, Pravst I. Efficiency of vitamin D supplementation in healthy adults is associated with Body Mass Index and baseline serum 25-hydroxyvitamin D level. *Nutrients.* 2020;12(5):1268. doi:10.3390/nu12051268

# Clinical anatomy of the spatial structure of the right ventricular outflow tract

Agata Ewa Kaczyńska<sup>1,A,C,D</sup>, Adam Kosiński<sup>1,E</sup>, Katarzyna Bobkowska<sup>2,C</sup>, Miłosz Andrzej Zajczkowski<sup>1,C</sup>, Rafał Kamiński<sup>1,E</sup>, Grzegorz Marek Piwko<sup>1,E</sup>, Marta Gleinert-Rożek<sup>1,B</sup>, Tomasz Gos<sup>3,B</sup>, Karol Karnecki<sup>3,B</sup>, Dariusz Kozłowski<sup>4,F</sup>

<sup>1</sup> Department of Clinical Anatomy, Medical University of Gdańsk, Poland

<sup>2</sup> Faculty of Civil and Environmental Engineering, Gdańsk University of Technology, Poland

<sup>3</sup> Department of Forensic Medicine, Medical University of Gdańsk, Poland

<sup>4</sup> Department of Cardiology and Electrotherapy, Medical University of Gdańsk, Poland

A – research concept and design; B – collection and/or assembly of data; C – data analysis and interpretation;

D – writing the article; E – critical revision of the article; F – final approval of the article

Advances in Clinical and Experimental Medicine, ISSN 1899–5276 (print), ISSN 2451–2680 (online)

*Adv Clin Exp Med.* 2022;31(1):33–40

## Address for correspondence

Adam Kosiński  
adam.kosinski@gumed.edu.pl

## Funding sources

This work was supported by the National Science Centre, grant No. MN-01-0412/08/212 (<http://www.nauka.gov.pl/en/>).

## Conflict of interest

None declared

Received on October 27, 2020

Reviewed on November 11, 2020

Accepted on December 17, 2020

Published online on November 5, 2021

## Abstract

**Background.** The right ventricular outflow tract (RVOT) is located above the supraventricular crest and reaches the level of the pulmonary valve. Detailed knowledge of the RVOT spatial structure and its morphology is extremely important for cardiac invasive therapeutic procedures.

**Objectives.** To examine the spatial structure of the RVOT using virtual models of the right ventricle (RV) interior obtained post mortem.

**Materials and methods.** The study was carried out using 40 adult hearts from both sexes fixed in formalin. Donors had a negative history of cardiovascular diseases. Silicone models of the interior of the RV were made and then subjected to a digital modelling procedure using the photogrammetry technique. For each 3D model of the RV, the RVOT was extracted and measurements were performed.

**Results.** Statistical analysis demonstrated that the dimensions of the transverse ( $p < 0.001$ ) and sagittal ( $p = 0.002$ ) axis at the level of the upper and lower border of the RVOT differed significantly. There was also a significant difference between the right and left height of the RVOT ( $p = 0.009$ ). A clear correlation was found between the volume of the RVOT and the volume of the entire RV ( $r = 0.718$ ,  $p < 0.001$ ).

**Conclusions.** The obtained 3D models of the RVOT can help standardize the data related to RVOT architecture. Furthermore, they can extend knowledge about the RVOT in the field of cardiology and improve the procedures in cardiac surgery.

**Key words:** photogrammetry, RVOT, right ventricle, cardiac imaging, 3D modelling

## Cite as

Kaczyńska AE, Kosiński A, Bobkowska K, et al. Clinical anatomy of the spatial structure of the right ventricular outflow tract. *Adv Clin Exp Med.* 2022;31(1):33–40. doi:10.17219/acem/131752

## DOI

10.17219/acem/131752

## Copyright

© 2022 by Wrocław Medical University

This is an article distributed under the terms of the Creative Commons Attribution 3.0 Unported (CC BY 3.0) (<https://creativecommons.org/licenses/by/3.0/>)

## Background

The right ventricle (RV) and structures located in its area are gradually gaining more interest among researchers. The relationship between anatomical components of the RV and various heart diseases is being increasingly recognized. There are reports in the scientific literature related to the analysis of the structure and function of the RV, both for healthy hearts and those with pathological changes.<sup>1,2</sup> There are also many papers that present the spatial architecture of the RV and its components. One notable study is that by Ho and Nihoyannopoulos, who comprehensively described the RV and its internal structures in terms of echocardiography.<sup>1</sup> Unfortunately, much of the available data about the context of the nomenclature of the structures within the RV are still ambiguous.

One component of the RV sparking serious controversies is the right ventricular outflow tract (RVOT), which is the outflow path of the blood flowing through the RV during the cardiac cycle. The RVOT area is located between the pulmonary valve and the level of the upper part of the supraventricular crest.<sup>1,2</sup>

Due to its clinical significance, the RVOT is an important region for morphological studies. It has been shown that the knowledge of the shape of this area is of great importance in the context of the implantation of cardiac stimulating systems.<sup>3</sup> Furthermore, the source of idiopathic ventricular arrhythmias is often located within the RVOT.<sup>4</sup> Therefore, thorough knowledge of this area and the structures located in its cavity is the basis for optimizing ablation procedures for arrhythmogenic foci presented by Pytkowski et al.<sup>5</sup>

From a practical perspective, the spatial structure of the RVOT seems to be particularly important. Information obtained from 3D modelling can serve as a source of valuable and abundant data, especially in clinical aspects. Due to modern developments in imaging techniques, cardiac visualization is becoming an essential component of the diagnostic and therapeutic process in cardiology and cardiac surgery.

Photogrammetry, which has been used in medicine for many years, is a technique that enables imaging of anatomical structures post mortem. In the context of the heart, photogrammetric methods are primarily aimed at understanding the shape and size of this organ. Due to the ability to make silicone models of the heart cavities, it has also become possible to analyze these spaces. An additional application and major advantage of photogrammetric techniques is the ability to obtain a durable 3D model that can be processed and analyzed many times. Photogrammetry is most often associated with the use of the visible electromagnetic radiation range (which was used for the purpose of image registration in this study), although other ranges of radiation are also used, e.g. x-rays, near and mid-infrared radiation, etc.

The importance of photogrammetry in medicine has significantly increased and it is now associated with the computerization and digitization of many medical analysis processes.

For example, it can be used to model the requirements for 3D printing of missing or replacement structures<sup>6</sup> or for the collection of objective data about the dimensions and shapes of given organs (as in the present study). A dataset collected using photogrammetry can be used for many years.

## Objectives

The aim of this study was to perform manual measurements of RVOT dimensions and volumes based on virtual models of the RV interior obtained post mortem in order to analyze RVOT morphology.

## Materials and methods

### Model preparation

Observations were carried out for 40 hearts from adults aged 18–85 years (average age: 44 years) of both sexes (13 women, 27 men). All donors had a negative history of cardiovascular diseases. The hearts were fixed in formalin solution. In order to obtain the RVOT model, 40 silicone internal models of the RV were first made according to the procedure described in Kaczyńska et al.<sup>7</sup> (Fig. 1).

This study was approved by the Independent Bioethics Committee for Scientific Research at Medical University of Gdańsk, Poland (approval No. 407/2015 granted on September 15, 2015).

### Digital modelling

The obtained models were subjected to a digital modelling procedure using photogrammetry techniques. This method uses serial photos of the physical model to transform it into a virtual model. For this purpose, a Sony Alpha DSLR-A300 (Sony Corp., Tokyo, Japan) camera was used with a Sony 3.5–5.6/18–70 lens (Sony Corp.), and 50 continuous photos were taken of each model. Next, the photos were imported into Autodesk ReCap Photo (Autodesk Inc., San Rafael, USA), transformed into a virtual model, and then scaled. In addition, digital processing and manual RVOT measurements were made (Fig. 2).

### Right ventricular outflow tract boundary determination

Before manual processing of the 3D models, macroscopic analyses of the obtained silicone models and specimens of the interior of the RV were carried out to determine the characteristic points that would be used to evaluate the RVOT boundaries. During the process of extracting the RVOT from the 3D model of the entire RV, a virtual vertical cut was first made, starting from the location of the supraventricular crest – the largest indentation on the model

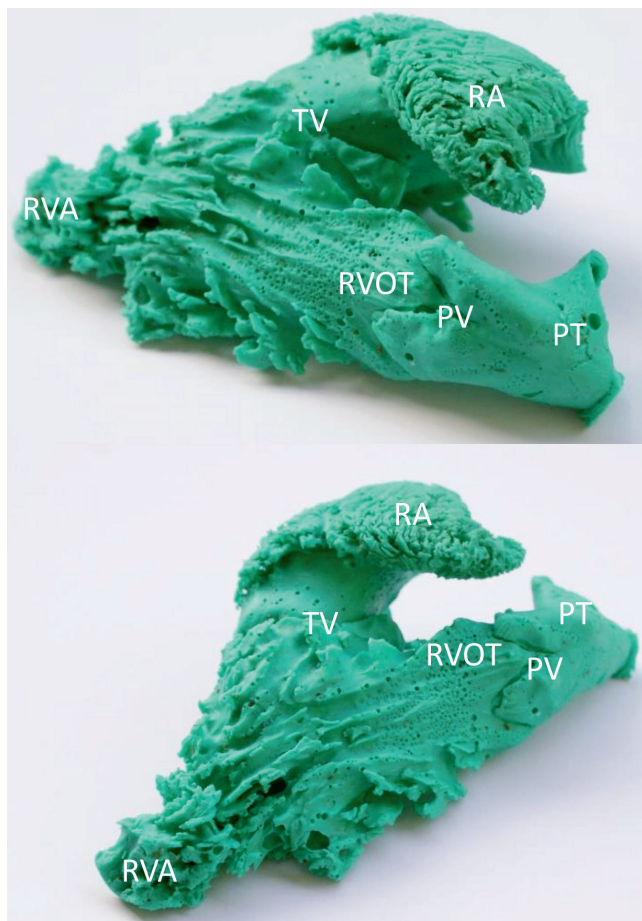


Fig. 1. Silicone model of the interior

RA – right atrium; TV – tricuspid valve; RVA – right ventricle apex; RVOT – right ventricle outflow tract; PT – pulmonary trunk; PV – pulmonary valve.

– to the apex of the RV. Next, from the first of these points, another cut was made to the left edge of the RV, where the free wall meets the septal wall. On this edge, the location of the first characteristic indentation on the model (from the pulmonary valve to the apex of the RV) was determined, which defines the lower border of the RVOT. Hearts were grouped according to the presence of indentation or no visible indentation. The upper border of the RVOT was defined as the ring connecting the attachment points (commissural points) of the pulmonary valve cusps (Fig. 3A).

### Manual measurements

For the obtained 40 models of the RVOT, the following measurements of the spatial structures were performed: the largest dimension in the transverse axis, at the level of the upper (a) and lower (a') border of the RVOT; the largest dimension in the sagittal axis, at the level of the upper (b) and lower (b') border of the RVOT and the right (c) and left (c') height of the RVOT, connecting the furthest points at the upper and lower border of the RVOT (Fig. 4). The RVOT volume and the volume of the entire RV were also measured prior to extracting the RVOT.

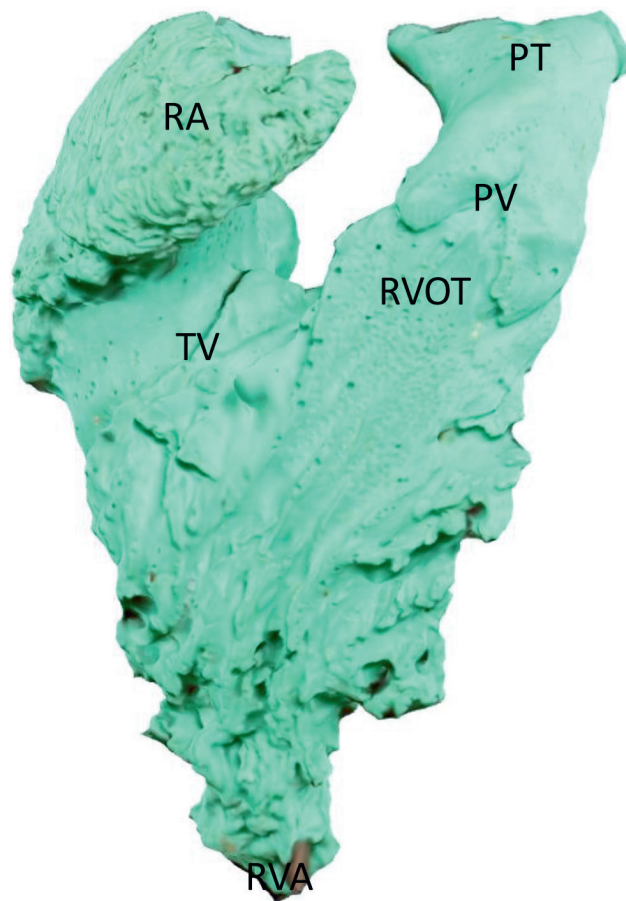


Fig. 2. Digitized silicone model

RA – right atrium; TV – tricuspid valve; RVA – right ventricle apex; RVOT – right ventricle outflow tract; PT – pulmonary trunk; PV – pulmonary valve.

### Statistical analysis

Statistical analysis was performed using Statistica Software v. 13.1 for Windows (StatSoft Inc., Tulsa, USA). The D'Agostino's and Pearson's tests were used to check the normality of the distribution. The data had a normal distribution. Student's t-test for independent samples was used to compare the RVOT measurements. This test was chosen because of the small sample size (40 hearts) and for comparing 2 groups. Pearson's correlation analysis was performed to assess the relationship between the entire RV volume and the RVOT volume. Results with  $p < 0.05$  were considered statistically significant.

## Results

### Macroscopic analysis

The RVOT was extracted from each of the forty 3D models of the RV. During the determination of the RVOT boundaries, 2 characteristic indentations were observed on the virtual models. The 1<sup>st</sup> indentation was

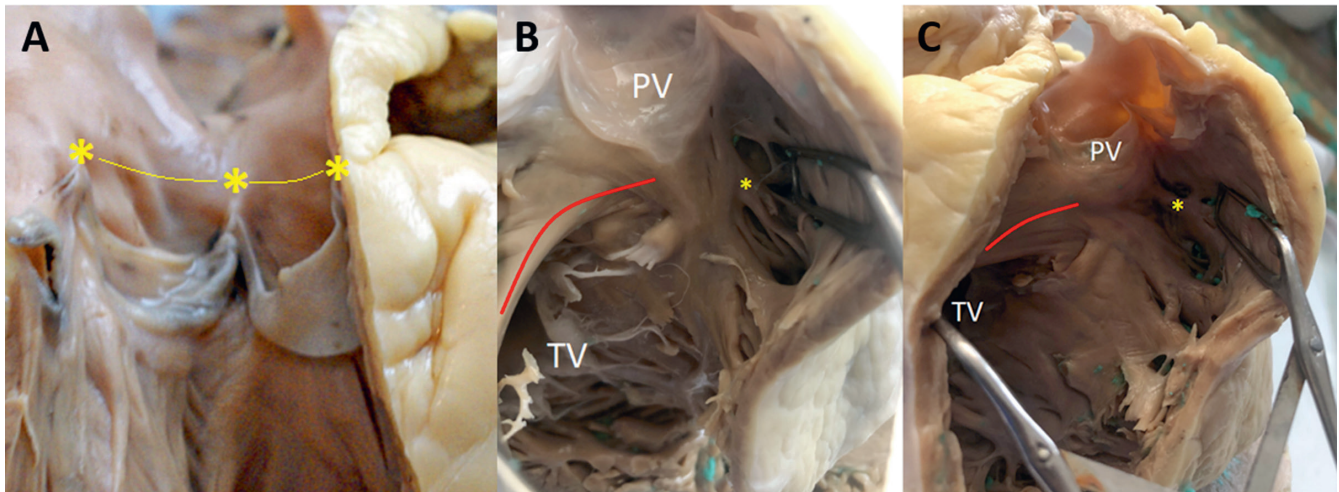


**Fig. 3.** A. Setting the upper border of the right ventricle outflow tract (RVOT). The yellow asterisk indicates the attachments of the pulmonary valve cusps to the internal surface of the vessel. The line marks are the assumed upper border of the RVOT; B and C. The view of the RVOT from the perspective of the free wall. The yellow asterisk indicates the extension of the supraventricular crest that causes characteristic indentation on the 3D model. The red line marks the supraventricular crest that separates the inflow from outflow tract in the right ventricle (RV)

TV – tricuspid valve; PV – pulmonary valve.

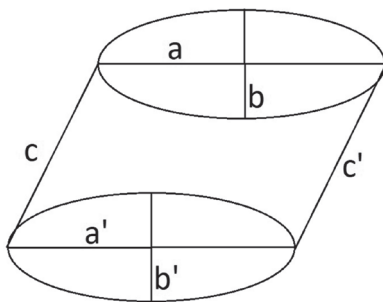


**Fig. 4.** Scheme of the measurements performed for the right ventricle outflow tract (RVOT)

a – dimension in the transverse axis at the level of the upper border of the RVOT; a' – dimension in the transverse axis at the level of the lower border of the RVOT; b – dimension in the sagittal axis at the level of the upper border of the RVOT; b' – dimension in the sagittal axis at the level of the lower border of the RVOT; c – right border of RVOT; c' – left border of RVOT.

the equivalent of the supraventricular crest that separated the RVOT on the model from the right atrioventricular orifice. The lowest point lying on this indentation was used to determine the virtual cut towards the apex and left margin of the RV. The 2<sup>nd</sup> indentation was on the left margin of the RV and was located as the highest point towards the pulmonary valve. It was used to set the 2<sup>nd</sup> point in order to determine the lower border of the RVOT (Fig. 5).

A characteristic indentation was not present only on 4 RVOT models or it was not possible to identify it (Fig. 5A). The rest 36 RVOT models had a noticeable indentation (Fig. 5B,C). After indentation analysis of the 3D models, macroscopic assessment of this structure was carried out on the specimens fixed in formalin. It was found that the structure that created the characteristic indentation on the 3D model during the process of silicone modelling is a muscular element, that connects the septal wall with

the free wall of the RV (Fig. 3B). This structure emerges below the pulmonary valve cusps, at the level of the supraventricular crest, and then goes downwards overlapping the free wall of the RV. Above this element, the trabeculation is less intense compared to the RV architecture below this structure. The macroscopic examination also revealed that the protruding element does not reach the point where the septal wall connects directly with the free wall of the RV. The structure appeared as a free bundle of muscles connecting both walls. Deriving a line along the supraventricular crest and the examined structure, it was found that the line along the examined element is an extension of the supraventricular crest, and both marked lines form an arch that curves below the pulmonary valve (Fig. 3C).

### Right ventricular outflow tract dimensions and volume

The mean dimension in the transverse axis of the RVOT at the level of the upper border (a) was 23.51 mm (standard deviation (SD) = 4.81 mm); the same mean dimension at the level of the lower border (a') was 28.18 mm (SD = 6.36 mm). Statistical analysis showed that the dimension in the transverse axis differed significantly at the level of the upper and lower RVOT (Student's t-test,  $p < 0.001$ ; Fig. 6).

The obtained data indicated that this dimension, starting from the lower border to the upper one, became smaller. The mean dimension in the sagittal axis at the level of the upper border of the structure (b) was 18.24 mm (SD = 4.85 mm), while that at the level of the lower border (b') was 14.95 mm (SD = 4.56 mm). This difference was statistically significant (Student's t-test,  $p = 0.002$ ), indicating that the anteroposterior dimension of the RVOT becomes larger towards the pulmonary valve (Fig. 7).

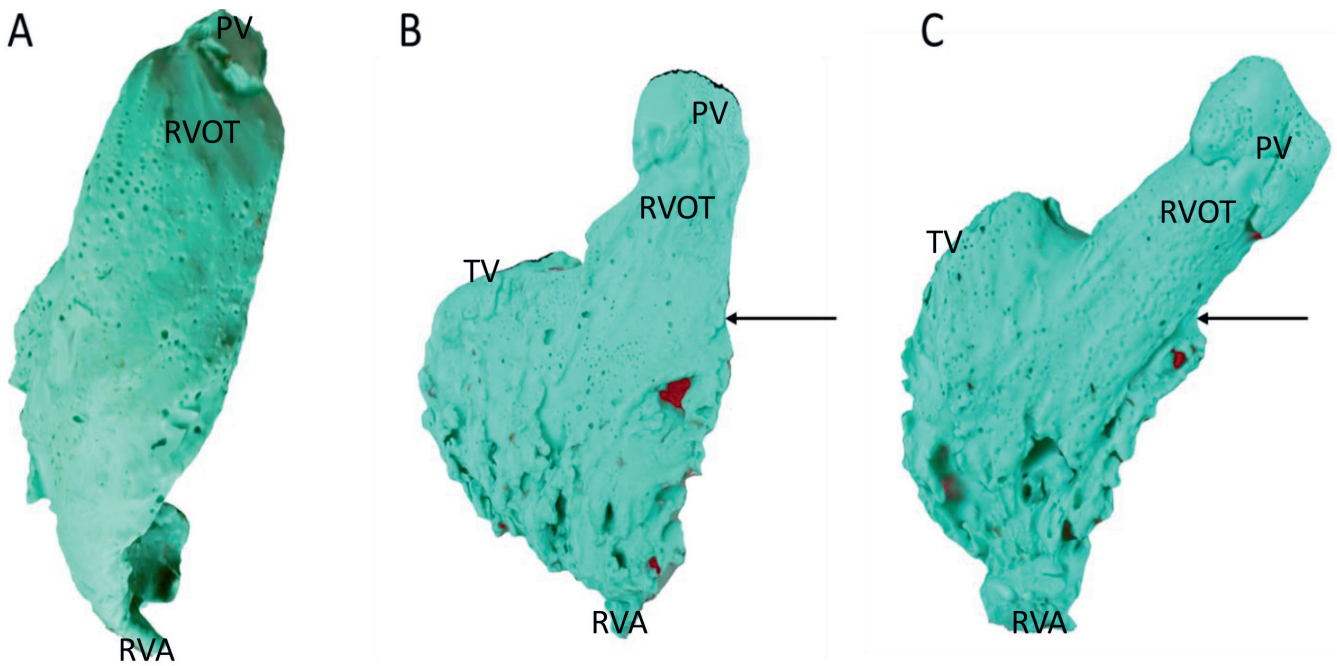


Fig. 5. A view of the 3D model of the right ventricle (RV). A. No visible indentation; B and C. Visible indentation (marked with an arrow)  
 TV – tricuspid valve; RVA – right ventricle apex; RVOT – right ventricle outflow tract; PV – pulmonary valve.

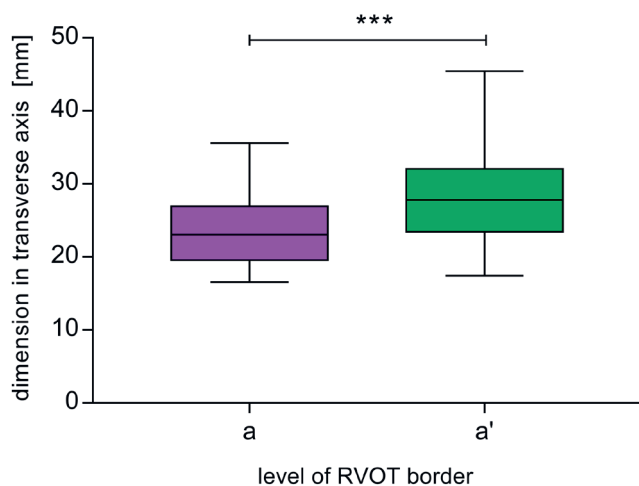


Fig. 6. Comparison of the dimension in the transverse axis at the level of the upper (a) and lower (a') border of the right ventricle outflow tract (RVOT). The values are given in millimeters [mm]

a – M = 23.51, standard deviation (SD) = 4.81; a' – M = 28.18, SD = 6.36.

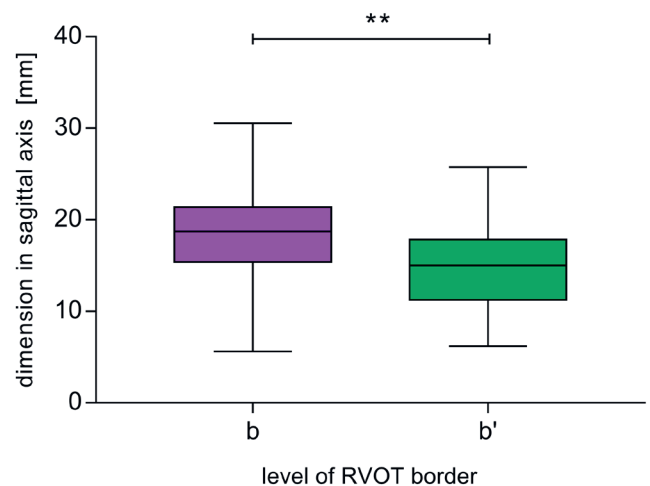


Fig. 7. Comparison of the dimension in the sagittal axis at the level of the upper (b) and lower (b') border of the right ventricle outflow tract (RVOT). The values are given in millimeters [mm]

b – M = 18.24, standard deviation (SD) = 4.85; b' – M = 14.95, SD = 4.56.

The obtained data also allowed us to assess the right (c) and left (c') mean height of the RVOT structure, which was 35.96 mm (SD = 6.02 mm) and 39.45 mm (SD = 5.63 mm), respectively. The difference between these measurements was statistically significant (Student's t-test,  $p = 0.009$ ) (Fig. 8). The left height (c') of the RVOT was significantly greater than the right height (c).

The mean volume of the RVOT was 11.98 mL, which comprised 24% of the volume of the entire RV. There was a strong positive correlation between the volume of the RVOT and the volume of the entire RV ( $r = 0.718$ ,  $p < 0.001$ ). The obtained data clearly show that

as the volume of the entire RV increases, the RVOT volume also increases (Fig. 9).

## Discussion

At present, the interior of the RV is divided into 3 parts: inflow tract, trabeculated apex and outflow tract. However, the existing data lack the definition of the exact border between the RVOT and the trabeculated apex of the RV. Due to conflicting data, knowledge about this area is inconsistent.

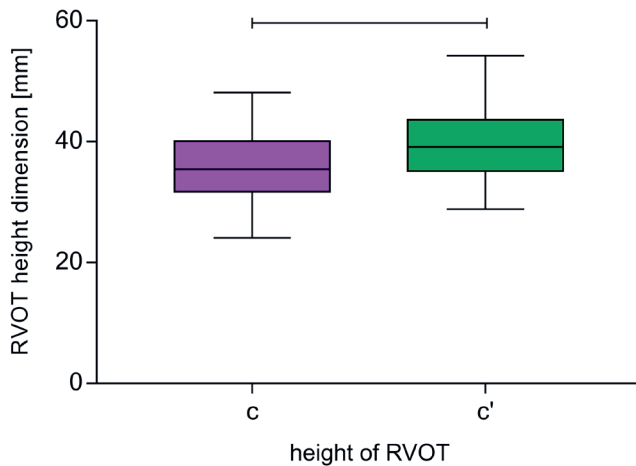


Fig. 8. Comparison of the right (c) and left (c') border of the right ventricle outflow tract (RVOT). The values are given in millimeters [mm]

c – M = 35.96, standard deviation (SD) = 6.02; c' – M = 39.45, SD = 5.63.

The supraventricular crest, which separates the inflow tract from outflow tract of the RV, forms a noticeable boundary structure between the 2 components of the RV. This structure penetrates the interventricular septum between the anterior and posterior limb of the septomarginal trabecula.

The pulmonary infundibulum, which is part of the RVOT, has the form of a smooth and muscular sleeve. Along that structure extends the anterior limb of the septomarginal trabecula, which supports the cusps of the pulmonary valve by lifting the entire valve apparatus above the base of the heart. This is possible because the fragments of the infundibulum are built into the 3 pulmonary sinuses. The locations of the attachments of the pulmonary valve cusps determine the sinotubular junction, while the anatomical border between the RV and the pulmonary trunk is defined as the line to which the infundibular musculature reaches within the base of the cusps sinuses.<sup>1,8,9</sup> Despite large variation in length, size and angle of the curvature of the pulmonary infundibulum, its dimensions do not depend on the dimensions of the RV itself.<sup>10</sup>

In the present study, the place of attachment of the pulmonary valve cusps to the inner surface of the vessel wall was assumed to be the upper border of the RVOT. The connected attachment points of the pulmonary valve formed a ring that was easy to locate on the 3D models of the RV. Determining the lower RVOT border was unfortunately not as easy, due to the lack of a clear border between the trabecular apex and the infundibulum.<sup>8,11–13</sup>

Based on our observations, the structure most suitable for determining the lower border seems to be the element of the RV that causes the characteristic indentation on the 3D model in the area of contact between the free and septal wall. This indentation occurred in up to 90% of the examined hearts, and may thus serve as a determinant of the lower border of the RVOT. Macroscopic analysis of the specimens revealed that the indentation

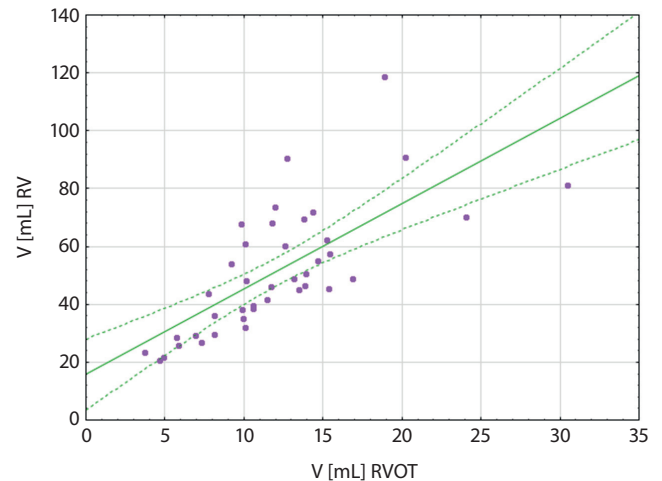


Fig. 9. Correlation between the volume of the entire right ventricle (V RV) and the volume of the right ventricle outflow tract (V RVOT). The values are given in milliliters [mL]

is caused by a muscle structure that passes from the septal wall to the free wall, directly from the pulmonary trunk to the apex of the RV (Fig. 9). Notably, this element is the last protrusion towards the infundibulum that has a smooth wall. Moreover, this structure appears as a free muscle bundle that attaches to the septal wall. Due to its connection with the free and septal walls, it can be determined that this element is not a typical part of the septoparietal trabeculation that lies on the internal surface of the walls of the RV. This structure is also not a free part of the septomarginal trabecula, as evidenced by its too high location in the ventricular space. Based on macroscopic analysis of this structure, it seems to be an extension of the supraventricular crest on the free wall of the RV. In a study by Kosiński et al., the trabecular element was described as a component of the RV.<sup>14</sup> It was an extension of the ventricular septal muscle bundle and was indicated as the lower part of the supraventricular crest. Reaching the base of the heart, this element separated the inflow tract from the RVOT, which was visible in our macroscopic analysis of the specimens. It seems that the macroscopic characteristics of the structure that causes the protrusion on the 3D models corresponds to the extended part of the supraventricular crest.

Assuming that this structure is a part of the supraventricular crest, it seems justified to use it as a determinant of the lower border of RVOT, because it occurs in the vast majority of cases. Importantly, its location within the RV is permanent, compared to the variable trabeculation. In addition, the supraventricular crest has an analogous embryological origin to the RVOT.<sup>15,16</sup>

Previous scientific reports have attempted to establish the lower border of RVOT, which was typically determined in the context of the implantation of cardiac pacing or ablation of arrhythmogenic foci. In a study by Mond et al.,<sup>17</sup> the trabecular part was included in the RVOT area and the lower border of the RVOT was designated as the line



from the highest point of the tricuspid valve towards the left edge of the heart. Based on its different electrophysiological properties, the RVOT was divided into 4 wall segments: anterior, posterior, free wall part, and ventricular septum.

In order to define the optimal pacing sites in the RVOT, Lieberman et al. similarly marked the lower border of this area.<sup>3</sup> The placement of an electrode in a specific segment of the RVOT is characterized by a different morphology of the QRS complex in electrocardiography. Thus, unifying the definition of the RVOT anatomical boundaries is crucial for various cardiac procedures.

In contrast to the findings of Saremi et al.<sup>8</sup> that the size of the infundibulum, which is an element of the RVOT, is not dependent on the size of the entire RV, our results showed that the volume of the RVOT is dependent on the volume of the entire RV. Thus, it can be concluded that as the RV volume of the examined hearts increases, the RVOT volume also increases. However, the specific dimensions, angles and spatial structures of the RVOT and RV may differ significantly and they require further research.

In a study by Izumo et al. using 3D transesophageal echocardiography (3D TEE), it was shown that the RVOT cross-sectional geometry is more oval than round, as previously thought.<sup>18</sup> The fact that we set the lines connecting the points placed furthest apart from each other in the sagittal and transverse axis, at the level of the upper and lower RVOT border, also supports this view. In addition, we showed that the transverse dimension becomes smaller towards the upper border of the RVOT while the sagittal dimension increases. The different values of these dimensions certainly reflect the change in the shape of the RVOT cross section. For this reason, it is necessary to carefully examine these dimensions at different levels of the RVOT sections. In addition, differences in the left and right height of the RVOT structure indicate a change in the position of its subsequent sections and their certain displacement, which may be associated with RVOT rotation.

A study by Bobkowska et al. reported that differences in measurements between physical and virtual models are negligible.<sup>19</sup> The developed modelling procedure is characterized by intuitiveness, ease of implementation by people less experienced in photogrammetry, and good quality results. The experiments carried out by the authors indicate the possibility of obtaining better quality models than those obtained using optical scanners.<sup>19</sup> Manual photo recording allows any orientation and adjustment of the camera distance to the object. The significant advantages of this method justified its choice to digitize silicone models of the RV interior in the present study.

## Clinical implications

Extension of knowledge about the anatomy of the RVOT using imaging and modelling techniques may contribute

to the optimization of pacemaker implantation procedures, resulting in more effective cardiac stimulation, better fixation of the stimulating lead, and less frequent mechanical interaction of the device with the valvular apparatus. In patients with arrhythmias within the RVOT area, better understanding of RVOT morphology may help to more accurately localize the arrhythmogenic foci, thereby increasing the effectiveness of ablation treatment. Moreover, it may be helpful in avoiding ablation-related damage to structures located in close proximity to the RVOT.

## Limitations

This research, however, is subject to several limitations. First, the study was carried out on relatively small number of hearts and thus the RVOTs, which is related to the availability of specimens.

Another limitation is the disproportion between the number of hearts of both sexes, with male hearts being the majority.









Additionally, the density of the silicone used in the models preparation may be insufficient for modeling the smallest structures inside RV.

## Conclusions

Post mortem 3D modelling of the RV interior allows for a comprehensive analysis of RVOT anatomy. We demonstrated that the RVOT diameter narrows towards the pulmonary trunk; RVOT height is not symmetrical, which may be associated with RVOT rotation; and RVOT volume is proportionate to total RV volume.

Further studies are needed to collect more data on morphological variants of the RVOT, especially studies based on the analysis of cross sections.

## ORCID iDs

Agata Ewa Kaczyńska  <https://orcid.org/0000-0002-7509-5839>  
 Adam Kosiński  <https://orcid.org/0000-0001-7507-2285>  
 Katarzyna Bobkowska  <https://orcid.org/0000-0003-4968-3407>  
 Miłosz Andrzej Zajączkowski  <https://orcid.org/0000-0002-5981-336X>  
 Rafał Kamiński  <https://orcid.org/0000-0003-3632-0340>  
 Grzegorz Marek Piwko  <https://orcid.org/0000-0003-2301-6075>  
 Marta Gleinert-Rożek  <https://orcid.org/0000-0001-7807-4323>  
 Tomasz Gos  <https://orcid.org/0000-0003-0161-9270>  
 Karol Karnecki  <https://orcid.org/0000-0001-8386-4207>  
 Dariusz Kozłowski  <https://orcid.org/0000-0003-2089-0656>

## References

1. Ho SY, Nihoyannopoulos P. Anatomy, echocardiography, and normal right ventricular dimensions. *Heart*. 2006;92(Suppl 1):i2–13. doi:10.1136/hrt.2005.077875
2. Sanz J, Sánchez-Quintana D, Bossone E, Bogaard HJ, Naeije R. Anatomy, function, and dysfunction of the right ventricle: JACC state-of-the-art review. *J Am Coll Cardiol*. 2019;73(12):1463–1482. doi:10.1016/j.jacc.2018.12.076
3. Lieberman R, Grenz D, Mond HG, Gammage MD. Selective site pacing: Defining and reaching the selected site. *Pacing Clin Electrophysiol*. 2004;27(6 Pt 2):883–886. doi:10.1111/j.1540-8159.2004.00551.x

4. Kukla P, Sławuta A, Jastrzębski M, Gajek J, Stec S. Unusual changes in ventricular repolarization before right ventricular outflow tract arrhythmias. *Am J Med Sci.* 2017;353(3):311–312. doi:10.1016/j.amjms.2016.11.009
5. Pytkowski M, Maciąg A, Sterliński M, et al. Lokalizacja ogniska arytmii u chorych z zaburzeniami rytmu serca pochodzącymi z drogi odpływu prawej komory. *Folia Cardiol Excerpta.* 2006;1(4):211–220. [https://journals.viamedica.pl/fovia\\_cardiologica/article/view/24007](https://journals.viamedica.pl/fovia_cardiologica/article/view/24007). Accessed September 7, 2021.
6. Liaw CY, Guvendiren M. Current and emerging applications of 3D printing in medicine. *Biofabrication.* 2017;9(2):024102. doi:10.1088/1758-5090/aa7279
7. Kaczyńska A, Kosiński A, Kamiński R, Zajączkowski M, Nowicka E, Gleinert-Rożek M. A novel approach to visualization of the right ventricular outflow tract. *Eur J Transl Clin Med.* 2019;1(2):36–40. doi:10.31373/ejtcmm/100603
8. Saremi F, Ho SY, Cabrera JA, Sánchez-Quintana D. Right ventricular outflow tract imaging with CT and MRI: Part 1, morphology. *Am J Roentgenol.* 2013;200(1):W39–W50. doi:10.2214/AJR.12.9333
9. Loukas M, Shane Tubbs R, Louis RG, et al. An endoscopic and anatomical approach to the septal papillary muscle of the conus. *Surg Radiol Anat.* 2009;31(9):701–706. doi:10.1007/s00276-009-0510-2
10. Geva T, Powell AJ, Crawford EC, Chung T, Colan SD. Evaluation of regional differences in right ventricular systolic function by acoustic quantification echocardiography and cine magnetic resonance imaging. *Circulation.* 1998;98(4):339–345. doi:10.1161/01.cir.98.4.339
11. Keren A, Billingham ME, Popp RL. Echocardiographic recognition of paraseptal structures. *J Am Coll Cardiol.* 1985;6(4):913–919. doi:10.1016/s0735-1097(85)80505-2
12. Merrick AF, Yacoub MH, Ho SY, Anderson RH. Anatomy of the muscular subpulmonary infundibulum with regard to the Ross procedure. *Ann Thorac Surg.* 2000;69(2):556–561. doi:10.1016/s0003-4975(99)01300-4
13. Hasdemir C, Aktas S, Govsa F, et al. Demonstration of ventricular myocardial extensions into the pulmonary artery and aorta beyond the ventriculo-arterial junction. *Pacing Clin Electrophysiol.* 2007;30(4):534–539. doi:10.1111/j.1540-8159.2007.00704.x
14. Kosiński A, Nowiński J, Kozłowski D, Pivko G, Kuta W, Grzybiak M. The crista supraventricularis in the human heart and its role in the morphogenesis of the septomarginal trabecula. *Ann Anat.* 2007;189(5):447–456. doi:10.1016/j.aanat.2007.01.008
15. Anderson RH, Webb S, Brown NA, Lamers W, Moorman A. Development of the heart: (3) Formation of the ventricular outflow tracts, arterial valves, and intrapericardial arterial trunks. *Heart.* 2003;89(9):1110–1118. doi:10.1136/heart.89.9.1110
16. Poelmann RE, Mikawa T, Gittenberger-De Groot AC. Neural crest cells in outflow tract septation of the embryonic chicken heart: Differentiation and apoptosis. *Dev Dyn.* 1998;212(3):373–384. doi:10.1002/(SICI)1097-0177(199807)212:3<373::AID-AJA5>3.0.CO;2-E
17. Mond HG, Hillock RJ, Stevenson IH, McGavigan AD. The right ventricular outflow tract: The road to septal pacing. *Pacing Clin Electrophysiol.* 2007;30(4):482–491. doi:10.1111/j.1540-8159.2007.00697.x
18. Izumo M, Shiota M, Saitoh T, et al. Non-circular shape of right ventricular outflow tract a real-time 3-dimensional transesophageal echocardiography study. *Circ Cardiovasc Imaging.* 2012;5(5):621–627. doi:10.1161/CIRCIMAGING.112.974287
19. Bobkowska K, Przyborski M, Kaczyńska A, Kosiński A. Digital photogrammetry in the analysis of the ventricles' shape and size. Paper presented at: 2017 Baltic Geodetic Congress (BGC Geomatics); 2017; Gdańsk, Poland.

# Impact of selected risk factors on uterine healing after cesarean section in women with single-layer uterine closure: A prospective study using two- and three-dimensional transvaginal ultrasonography

Joanna Budny-Wińska<sup>A–D</sup>, Aleksandra Zimmer-Stelmach<sup>B,C</sup>, Michał Pomorski<sup>D–F</sup>

2<sup>nd</sup> Department of Gynecology and Obstetrics, Wrocław Medical University, Poland

A – research concept and design; B – collection and/or assembly of data; C – data analysis and interpretation; D – writing the article; E – critical revision of the article; F – final approval of the article

Advances in Clinical and Experimental Medicine, ISSN 1899–5276 (print), ISSN 2451–2680 (online)

*Adv Clin Exp Med.* 2022;31(1):41–48

## Address for correspondence

Joanna Budny-Wińska  
E-mail: joanna.budny-winska@umed.wroc.pl

## Funding sources

None declared

## Conflict of interest

None declared

Received on June 20, 2021  
Reviewed on August 11, 2021  
Accepted on September 22, 2021

Published online on November 4, 2021

## Cite as

Budny-Wińska J, Zimmer-Stelmach A, Pomorski M. Impact of selected risk factors on uterine healing after cesarean section in women with single-layer uterine closure: A prospective study using two- and three-dimensional transvaginal ultrasonography. *Adv Clin Exp Med.* 2022;31(1):41–48. doi:10.17219/acem/142519

## DOI

10.17219/acem/142519

## Copyright

© 2022 by Wrocław Medical University  
This is an article distributed under the terms of the Creative Commons Attribution 3.0 Unported (CC BY 3.0) (<https://creativecommons.org/licenses/by/3.0/>)

## Abstract

**Background.** Modern obstetrics must meet many challenges, including long-term complications resulting from the presence of a uterine niche after cesarean section.

**Objectives.** To assess the impact of selected risk factors on the uterine healing process after cesarean section. The uterus was closed with a single-layer continuous suture covering the entire thickness of the myometrium, excluding the decidua.

**Materials and methods.** A prospective, case-controlled study was carried out at 2<sup>nd</sup> Department of Gynecology and Obstetrics, Wrocław Medical University, Poland. Women who delivered by cesarean section at our Department were invited to undergo an ultrasonographic assessment of the cesarean section scar from 6 to 9 weeks after the procedure. In all cases, the uterus was closed with a single-layer continuous suture. The ultrasound examination of the niche was performed according to the modified Delphi protocol. The volume of the niche was calculated and a 3D model was created. The obtained data were analyzed with clinical information from the maternal medical history and the course of the pregnancy.

**Results.** A total of 204 patients participated in the study. Five patients had a residual myometrial thickness (RMT) <2.2 mm and 35 had a residual myometrial thickness to adjacent myometrial thickness ratio (RMT/AMT) ≤0.5. In 45% of women, pregnancy course was complicated by gestational diabetes mellitus (GDM), gestational hypertension and hypothyroidism. The cervical canal was colonized with pathogenic flora in 22% of women. No correlation between maternal and gestational age at delivery, presence of medical complications during pregnancy, colonization of the cervical canal, and presence of niche and its parameters were found.

**Conclusions.** Our study revealed that the selected risk factors, such as systemic diseases during pregnancy and in the maternal medical history, as well as the colonization of the cervical canal, have no impact on uterine scar healing in women undergoing single-layer uterine closure spanning the entire thickness of the myometrium, excluding the decidua.

**Key words:** 3D ultrasonography, cesarean scar niche, risk factors of cesarean scar niche, systemic diseases during pregnancy, single-layer suture

## Background

Modern obstetrics must meet many challenges, including the increased frequency of cesarean sections and long-term complications resulting from the presence of a uterine niche after cesarean section. Additionally, worldwide, there has been an increased incidence and prevalence of systemic diseases appearing in pregnancy, such as gestational hypertension and gestational diabetes mellitus (GDM).<sup>1,2</sup> The another challenge for obstetricians is the increased rate of pregnancy among older women<sup>3,4</sup> due to the sociocultural changes in family planning that leads to the postponement of maternal plans, as well as the improved availability and effectiveness of assisted reproductive methods.

The consequence of cesarean section is a scar formation within the uterine muscle. In recent years, the rate of deliveries by cesarean section has increased all over the world. In Poland, the rate of cesarean section is 44.8% (data from Statistics Poland for 2019). The World Health Organization (WHO) recommends an ideal cesarean section rate of 10–15% of all births. This percentage is associated with a decrease in maternal and neonatal mortality. Above this level, the increased incidence of cesarean delivery is no longer associated with reduced mortality.<sup>5</sup>

With rising cesarean rates, the incidence of cesarean-related iatrogenic complications is also on the rise. In cases of incomplete healing, a niche can develop within the scar.

Various imaging methods including two- and three-dimensional ultrasonography, sonohysterography, hysterothography, hysteroscopy, and magnetic resonance imaging (MRI) can be used to assess the anterior uterine wall and to diagnose a cesarean scar niche.<sup>6–8</sup> Despite the availability of various diagnostic methods, there are no clear diagnostic criteria for uterine niches after cesarean section. In 2019, the European Niche Taskforce defined a uterine niche as an indentation of at least 2 mm in the uterine myometrium at the site of the cesarean scar, assessed using transvaginal ultrasound.<sup>9</sup> The incidence of uterine niches varies widely in the literature, ranging from 24% to 84%.<sup>10–13</sup>

Differences in the frequency of uterine niches result from the use of different diagnostic criteria, the time elapsed after the cesarean procedure and the diagnostic method used. The incidence is often underestimated because many women are asymptomatic and clinicians may not consider a niche as a cause of a patient's symptoms, due to lack of awareness.<sup>8</sup>

Most of the small uterine niches after cesarean section are asymptomatic and do not pose a threat to the health or life of the patient. However, the consequences of the presence of the large and symptomatic cesarean scar niche include uterine bleeding, chronic pelvic pain, reduced fertility, complications in subsequent pregnancies (morbidity adherent placenta, placenta previa), as well

as directly life-threatening conditions (uterine rupture, cesarean scar pregnancy).<sup>6,14–17</sup> Additionally, cesarean scar niches may increase the risk of complications in gynecological procedures such as embryo transfer and intrauterine device placement and removal.<sup>18,19</sup>

Due to the potentially dangerous consequences resulting from the presence of a uterine niche after cesarean section, it is necessary to develop preventive strategies aimed at reducing the risk of isthmocele formation, and thus preventing adverse outcomes. To achieve this, it is essential to identify related risk factors for the formation of a uterine niche after cesarean section, and to develop appropriate diagnostic and therapeutic protocols. Therefore, in the past several years, numerous studies have been published concerning the uterine scar niche, but most of them have been performed using selected populations of symptomatic women.

## Objectives

This study aimed to assess the impact of the most common risk factors in obstetrics on the uterine healing process after cesarean section, using a prospectively collected and unselected population, in which the uterus was closed with a single-layer continuous suture covering the entire thickness of the myometrium, excluding the decidua.

## Materials and methods

### Study design

This prospective descriptive study was designed to assess the prevalence and risk factors for improper uterine healing after cesarean delivery and niche formation. This study is a continuation of our previous research, in which we assessed the impact of mode and number of previous cesarean sections, type of uterine incision expansion, operator's experience, uterine flexion, and stage of labor at the time of cesarean section on uterine healing.<sup>20</sup>

### Setting and participants

The study was carried out at 2<sup>nd</sup> Department of Gynecology and Obstetrics, Wrocław Medical University, Poland. The study protocol was accepted by the ethics committee (approval No. KB 221/2016 and No. KB 153/2020) and all participants signed an informed consent form before participating in the study. The study was conducted in accordance with the 1964 Declaration of Helsinki and its later amendments.

Women who delivered by cesarean section at our Department from 2017 to 2019 were invited to undergo an ultrasonographic assessment of the cesarean section

scar. They were recruited either before the cesarean delivery (elective surgery) or within 2 days after the operation (emergency cesarean delivery). Patients who agreed to participate in the study were scheduled for the ultrasound examination from 6 to 9 weeks after the cesarean section.

## Surgical technique

The cesarean section procedures were performed by various obstetricians working in our Department using a standardized manner, i.e., low transverse uterine incision with a single-layer continuous suture covering the entire thickness of the myometrium, excluding the decidua. All physicians used the same suture material (Surgicryl® 910 polyglactine-braided synthetic absorbable suture; SMI AG, St. Vith, Belgium).

## Ultrasound examination

The examinations were conducted using a Voluson V8 Expert ultrasound machine (General Electric Medical Systems, Chicago, USA) with a 4–9 MHz transvaginal 3D probe. All transvaginal ultrasound examinations were performed by the first author, who was blinded to clinical information. During the examination, the parameters of the niche were assessed and a 3D model was created. All data were saved on the internal hard drive of the ultrasound machine. According to the international definition, a niche was defined as an indentation in the myometrium of at least 2 mm.<sup>9</sup> All measurements were obtained on a sagittal view of the uterus. To standardize the ultrasound evaluation, all examinations were performed using the modified Delphi protocol, and the exams performed prior to the publication of the modified Delphi protocol were reloaded and recalculated in accordance with the guidelines.<sup>9</sup>

The following niche parameters were assessed according to the modified Delphi protocol: width (W [mm]), height (D [mm]), volume of the anechoic triangle, residual myometrial thickness (RMT [mm]), and adjacent myometrial thickness (AMT [mm]). Additionally, the following parameters were calculated: the RMT/AMT ratio, the RMT/W ratio and the RMT/D ratio.

The VOCAL program was used to create 3D models and calculate the volume of the niche. The following settings were used: manual trace and rotation angle of 15°. The boundaries of the anechoic niche were manually outlined on the touch screen of the Voluson V8 Expert ultrasound machine.

## Clinical data analysis

Clinical information, such as laboratory results, maternal medical history pregnancy, and cesarean section course, was collected from the medical record and analyzed after ultrasonographic assessment of the cesarean section scar.

## Inclusion and exclusion criteria

The inclusion criteria were low transverse uterine incision, single-layer continuous full thickness uterine closure, uneventful postoperative course and singleton pregnancy. The exclusion criteria included a vertical or inverted “T” uterine incision, congenital uterine malformations and the use of more than 3 additional hemostatic uterine sutures.

## Statistical analyses

Data were collected and recorded using an Excel spreadsheet. Statistical analyses were performed using the STATISTICA v. 13.3 PL package (StatSoft Inc., Tulsa, USA). For quantitative variables, basic descriptive statistics were calculated (for all patients and taking into account the assumed division into groups), while the frequency of occurrence of their individual variants was calculated for qualitative variables (also taking into account the assumed division). The Mann–Whitney U test, post hoc comparisons for the Kruskal–Wallis analysis of variance (ANOVA) test and non-parametric Spearman’s rank correlation test were used in the analysis of non-parametric data. The Pearson’s  $\chi^2$  test and Fisher’s exact test were used to evaluate the differences in the distributions of qualitative variables. The criterion for statistical significance was set at a p-value <0.05.

## Results

A total of 204 patients participated in the study. The mean age was 32.25 years (standard deviation (SD)  $\pm 4.156$ ) and the mean gestational age was 37.863 weeks (SD  $\pm 2.43$ ). A total of 117 (57%) participants had no previous deliveries. Of the 204 patients, 56 (27%) had at least 1 cesarean section in the past, while 32 (16%) had at least 1 previous vaginal delivery. Eighty-two (40%) patients underwent emergency cesarean delivery and 122 (60%) underwent elective cesarean delivery. The most common reasons for elective cesarean delivery were previous cesarean delivery (40%) and breech presentation (9%). The most common reasons for emergency cesarean delivery were impending fetal asphyxia (40%) and prolonged labor (17%).

Out of all examined women, 153 were diagnosed with a niche after cesarean section (75%). Five of those patients had a RMT < 2.2 mm and 35 patients had an RMT/AMT ratio of 0.5 or less. The mean RMT value in the study group was 8.3 mm (SD  $\pm 3.37$ ).

The course of pregnancy was uncomplicated by pregnancy-related systemic diseases in 55% (n = 112) of women. In this group, uterine scar niches were diagnosed after cesarean section in 71% (n = 79) of patients. In contrast, in 21 patients (10%) with GDM, a uterine niche was diagnosed after cesarean section in 91% of these women. In 11% of respondents, their pregnancy was complicated

**Table 1.** Comparison of the analyzed variables and the occurrence of uterine niche after the cesarean section

Variable	Chronic diseases in pregnancy		Gestational diabetes		Gestational hypertension		Culture of cervical canal	
	yes	no	yes	no	yes	no	negative	positive
Niche, n (%)	75 (49)	78 (51)	18 (12)	135 (88)	14 (9)	139 (91)	92 (79)	24 (21)
Non-niche, n (%)	17 (33)	34 (67)	3 (6)	48 (94)	9 (18)	42 (82)	32 (76)	10 (24)
p-value*	0.0536		0.2949		0.1236		0.6665	

\*Fisher's exact test.

**Table 2.** Characteristics of the parameters of the cesarean scar niche depending on the occurrence of systemic diseases during pregnancy and cervical colonization (Mann-Whitney U test)

Variable	Chronic diseases in pregnancy		Gestational diabetes		Gestational hypertension		Hypothyroidism in pregnancy		Culture of cervical canal	
	yes	no	yes	no	yes	no	yes	no	positive	negative
Height [cm]										
Mean (SD)	0.50 (0.24)	0.49 (0.20)	0.54 (0.24)	0.49 (0.22)	0.51 (0.33)	0.49 (0.21)	0.49 (0.21)	0.51 (0.23)	0.49 (0.18)	0.52 (0.23)
p-value	0.7150		0.5091		0.5491		0.7047		0.5346	
Width [cm]										
Mean (SD)	0.80 (0.36)	0.83 (0.37)	0.80 (0.33)	0.82 (0.37)	0.79 (0.43)	0.82 (0.35)	0.80 (0.34)	0.83 (0.37)	0.76 (0.24)	0.84 (0.40)
p-value	0.4332		0.9848		0.4332		0.6807		0.5435	
Residual myometrial thickness [cm]										
Mean (SD)	0.84 (0.35)	0.82 (0.33)	0.84 (0.30)	0.83 (0.34)	0.87 (0.32)	0.82 (0.34)	0.82 (0.35)	0.83 (0.33)	0.81 (0.29)	0.82 (0.35)
p-value	0.3905		0.9487		0.3905		0.8058		0.8590	
Adjacent myometrial thickness [cm]										
Mean (SD)	1.25 (0.38)	1.17 (0.38)	1.32 (0.41)	1.19 (0.38)	1.21 (0.32)	1.21 (0.39)	1.23 (0.38)	1.20 (0.39)	1.16 (0.28)	1.22 (0.41)
p-value	0.6636		0.4952		0.9373		0.6962		0.7239	
Residual myometrial thickness/adjacent myometrial thickness										
Mean (SD)	0.67 (0.21)	0.71 (0.22)	0.64 (0.16)	0.70 (0.22)	0.74 (0.24)	0.69 (0.21)	0.66 (0.21)	0.71 (0.22)	0.71 (0.22)	0.68 (0.23)
p-value	0.7392		0.9782		0.5172		0.8663		0.5840	
Residual myometrial thickness/width										
Mean (SD)	1.24 (0.88)	1.05 (0.57)	1.18 (0.62)	1.14 (0.76)	1.24 (0.73)	1.14 (0.74)	1.18 (0.76)	1.13 (0.73)	1.04 (0.49)	1.16 (0.81)
p-value	0.4332		0.6176		0.4332		0.9496		0.7950	
Residual myometrial thickness/height										
Mean (SD)	1.96 (1.40)	1.81 (1.19)	1.76 (0.90)	1.89 (1.34)	1.98 (1.15)	1.87 (1.31)	1.94 (1.49)	1.86 (1.20)	1.65 (0.74)	1.82 (1.30)
p-value	0.5153		0.9782		0.5153		0.8663		0.8740	
Niche volume [cm <sup>3</sup> ]										
Mean (SD)	0.15 (0.20)	0.15 (0.25)	0.12 (0.10)	0.15 (0.24)	0.18 (0.28)	0.14 (0.22)	0.14 (0.20)	0.15 (0.24)	0.09 (0.14)	0.17 (0.27)
p-value	0.9850		0.7231		0.9850		0.8728		0.0362	

SD – standard deviation.

by gestational hypertension (n = 28), and among them, 65% were diagnosed with a niche of the uterus after cesarean section. Out of the 59 (29%) patients who developed hypothyroidism during their pregnancy, 85% were diagnosed with a uterine niche after cesarean section. There was no statistical correlation between the prevalence or parameters of a uterine niche after cesarean section and the abovementioned medical complications of pregnancy.

In our study, there were no cases of postoperative, symptomatic infections. However, the influence of cervical canal colonization by microbes on the healing of uterine scars was evaluated. Swabs from the cervical canal were taken

from 158 pregnant women on admission to the hospital. In 78% (n = 124) of pregnant women, a negative culture was reported. In 22% (n = 34) of women, the culture was positive for pathogenic flora such as *Staphylococcus agalactiae* spp (n = 8, 24%), *Candida* (including *C. albicans* spp, *C. glabrata* spp; n = 10.29%), *Enterococcus* (including *E. faecalis* spp; n = 4.12%), *Escherichia coli* spp (n = 6.18%), *Klebsiella pneumoniae* spp (n = 4.12%), and *Pseudomonas putida* spp (n = 1.3%). The percentage of identified niches in women with negative culture was 74% (n = 92). The same percentage of niches was found in the group of women with positive cultures from the cervical canal

**Table 3.** Comparison of the maternal age and the occurrence of uterine niche after cesarean section

Variable	≤25 years	25–30 years	31–35 years	36–40 years	>40 years
Niche, n (%)	8 (5)	45 (29)	73 (48)	21 (14)	6 (4)
Non-niche, n (%)	4 (8)	13 (25)	23 (45)	10 (20)	1 (2)
p-value	0.7346*				

\*Pearson’s  $\chi^2$  test, degrees of freedom (df) = 4.

**Table 4.** Comparison of the parameters of the cesarean scar niche depending on maternal age

Variable	≤25 years	25–30 years	31–35 years	36–40 years	>40 years	p-value*
H [cm], mean (SD)	0.49 (0.29)	0.47 (0.19)	0.50 (0.22)	0.52 (0.27)	0.47 (0.23)	0.8210
W [cm], mean (SD)	0.84 (0.21)	0.83 (0.42)	0.83 (0.37)	0.73 (0.24)	0.84 (0.22)	0.6992
RMT [cm], mean (SD)	0.9 (0.33)	0.87 (0.35)	0.81 (0.34)	0.80 (0.33)	0.80 (0.31)	0.6749
AMT [cm], mean (SD)	1.30 (0.40)	1.24 (0.39)	1.20 (0.38)	1.15 (0.41)	1.21 (0.45)	0.8959
RMT/AMT	0.72 (0.25)	0.70 (0.21)	0.68 (0.22)	0.71 (0.23)	0.68 (0.17)	0.8408
RMT/W	0.92 (0.40)	1.21 (0.69)	1.13 (0.80)	1.17 (0.79)	1.02 (0.57)	0.7671
RMT/H	1.61 (0.86)	2.06 (1.31)	1.83 (1.31)	1.81 (1.47)	1.90 (1.00)	0.5102
Niche volume [cm <sup>3</sup> ], mean (SD)	0.20 (0.21)	0.16 (0.30)	0.14 (0.20)	0.12 (0.11)	0.16 (0.25)	0.8994

H – height; W – width; RMT – residual myometrial thickness; AMT – adjacent myometrial thickness; SD – standard deviation; \*Kruskal–Wallis analysis of variance (ANOVA) test.

**Table 5.** Comparison of the occurrence of uterine scar niche by gestational age and history of miscarriages

Variable	Preterm delivery		Miscarriage in the past	
	yes	no	yes	no
Niche, n (%)	11 (22)	40 (78)	10 (20)	41 (80)
Non-niche, n (%)	22 (14)	131 (86)	33 (22)	120 (78)
p-value*	0.2720		0.8448	

\*Fisher’s exact test.

(n = 25, 74%). In this study, no statistically significant correlation was found between the prevalence and parameters of the uterine scar niche and the colonization of the cervix by pathogens. Table 1 and Table 2 present the comparison data between the incidence and parameters of cesarean scar niche and systemic diseases appearing in pregnancy, and the colonization of the cervix by pathogenic bacteria.

The study group was divided into subgroups by age. Table 3 presents the detailed characteristics of each subgroup.

Also, the impact of gestational age at the time of cesarean section was assessed. In 16% of patients (n = 33), cesarean section was performed on a preterm pregnancy in which 67% (n = 22) of these resulted in a uterine niche. In women undergoing cesarean section at term (n = 171, 84% of patients), the percentage of uterine scar niches after cesarean section was 77% (n = 132). For women with a history of miscarriages (n = 43, 21% of patients), a niche was diagnosed in 33 (77%) of these patients. There was no statistical correlation between the prevalence or parameters of the niche after cesarean section and maternal age during cesarean section, preterm delivery and history of miscarriages (Table 4,5,6).

## Discussion

Currently, there are no guidelines concerning the optimal timing for cesarean section scar assessment.

Most of the research concerning uterine niches after cesarean section have focused on examining women with symptoms related to its presence. The interval between cesarean section and evaluation of the cesarean scar varied in different publications. Most publications assessed the uterine scar from 6 to 8 weeks, 6 months,<sup>21</sup> 1 year,<sup>22</sup> or more than 5 years<sup>23,24</sup> after performing the cesarean section. This study aimed to evaluate the influence of individual factors and systemic diseases appearing during pregnancy on the process of uterine healing after cesarean section. In this study, every woman who had cesarean section with a single-layer, full thickness uterine closure excluding the decidua, was invited for a uterine scar examination. The examination was performed from 6 to 9 weeks after the operation, during which the uterine scar was still healing and no clinical symptoms are present. Van der Voet et al. found that the prevalence of niches did not change with time (niches found during an examination at 6–12 weeks after the cesarean section were also

**Table 6.** Comparison of analyzed parameters of cesarean scar niche depending on the history of miscarriages and gestational age

Variable	History of miscarriages			Gestational age		
	no	yes	p-value*	preterm delivery	term delivery	p-value*
H [cm], mean (SD)	0.50 (0.23)	0.50 (0.18)	0.4301	0.48 (0.24)	0.52 (0.22)	0.3757
W [cm], mean (SD)	0.80 (0.32)	0.90 (0.48)	0.3868	0.81 (0.48)	0.82 (0.34)	0.3081
RMT [cm], mean (SD)	0.84 (0.34)	0.79 (0.34)	0.2912	0.89 (0.36)	0.82 (0.33)	0.2423
AMT [cm], mean (SD)	1.22 (0.39)	1.17 (0.35)	0.5697	1.23 (0.41)	1.21 (0.38)	0.8455
RMT/AMT	0.70 (0.21)	0.67 (0.87)	0.3472	0.73 (0.22)	0.69 (0.21)	0.3672
RMT/W	1.15 (0.65)	1.12 (1.01)	0.2202	1.16 (0.61)	1.14 (0.76)	0.5342
RMT/H	1.91 (1.27)	1.77 (1.40)	0.1832	2.03 (1.41)	1.86 (1.28)	0.7800
Niche volume [cm <sup>3</sup> ], mean (SD)	0.13 (0.17)	0.20 (0.37)	0.9947	0.23 (0.43)	0.13 (0.17)	0.9588

H – height; W – width; RMT – residual myometrial thickness; AMT – adjacent myometrial thickness; SD – standard deviation; \*Mann–Whitney U test.

present on an examination performed 1 year after cesarean section).<sup>25</sup>

Transvaginal ultrasound examination at 6–9 weeks after cesarean section allows for the identification of patients with a potential risk of abnormal uterine healing after cesarean section, due to a large niche that may threaten the next pregnancy or be the cause of cesarean scar syndrome. Patients with a large niche and low RMT, as well as physicians treating them need to be aware of the risk of possible complications as soon as possible. Currently, in our clinical practice, we found many women with abnormal uterine bleeding related to the niche, who are unnecessarily treated by other doctors with oral contraceptives or invasive procedures such as dilatation and curettage. Moreover, women with extremely low RMT face life-threatening complications in subsequent pregnancies due to the risk of scar rupture at 21 weeks of gestation.<sup>26</sup> Taking into consideration the above problems and the limited knowledge gynecologists have of niche-related complications, we suggest cesarean section scar assessment be routinely performed in all women who have undergone cesarean section at the end of puerperium.

In this study, all niches, whether classified as small or large, were assessed using two and three-dimensional ultrasound.<sup>7</sup> Even though 2 meta-analyses have concluded single-layer closure to be associated with decreased RMT in comparison to double-layer sutures, in our study group, only 2.4% of women had a RMT < 2.2 mm. An RMT < 2.2 mm is considered a risk factor for severe scar complications in subsequent pregnancies.<sup>9</sup> Both of these meta-analyses have shown no differences in the risk of maternal morbidity or long-term outcomes between single-compared to double-layer uterine closure.<sup>27,28</sup>

This study is a continuation of our previous research in which we proved there was no correlation between an operator's experience and the prevalence and parameters of uterine niches after cesarean section.<sup>20</sup> The lack of a relationship between the operator's experience and the formation of a uterine niche after cesarean section is supported in the literature.<sup>11</sup> It should be emphasized that all cesarean sections were performed in a standardized manner, i.e., low

transverse uterine incision with single-layer full thickness uterine closure using the same suture material.

There was also no correlation between the parameters of the niche, incidence of niches and a woman's age at the time of cesarean section, which is in line with other studies.<sup>29</sup> In the study by Pomorski et al., a positive correlation was found between the height of the niche and the mother's age.<sup>30</sup> In another publication, the presence of a niche was significantly associated with younger maternal age at the time of cesarean section. In this study, younger patients had cesarean section performed during the active phase of labor.<sup>31</sup> According to some studies, performing cesarean section during the active phase of labor or phase II of labor increases the risk of a large niche formation.<sup>11,33</sup> In our study, only 6 patients were in the active phase of labor (dilation >4 cm to full dilation of cervix) and 10 patients were in phase II of labor at the time of cesarean section. Therefore, due to the low numbers, we did not use these variables in the statistical analysis of the subgroups of maternal age.

There are conflicting reports in the literature regarding the impact of gestational age on niche formation. In our study, no relationship was found between gestational age at the time of delivery and the prevalence and parameters of the niche. This finding is supported by other studies.<sup>29,30,32</sup> On the other hand, Vikhareva and Valentin found that delivery before 37 weeks gestation was a predictor of large niches.<sup>33</sup> The study by Hayakawa et al. demonstrated a positive link between the gestational age of 37–41 weeks at delivery and the presence of wedge niches.<sup>34</sup>

The influence of medical conditions associated with pregnancy on uterine niche development was analyzed. No correlation was found between GDM and the prevalence and parameters of niches. However, Antila-Långsjö et al. found GDM and higher body mass index (BMI) to be positively correlated with the incidence of uterine niche after cesarean section.<sup>11</sup> Interestingly, such a correlation has not been found for pregestational diabetes. In our study, the mean prepregnancy BMI in women diagnosed with cesarean scar niche was 27.1 (±6.1) kg/m<sup>2</sup> compared to 25.1 (±5.3) kg/m<sup>2</sup> in women without a niche. Consequently,



it means that most of the women in this study were overweight. In other studies, no correlation was found between BMI and the presence of a uterine niche.<sup>33,34</sup>

Our study also evaluated the influence of gestational hypertension on uterine healing. No statistically significant correlation was found between the frequency of occurrence or parameters of a niche and the presence of gestational hypertension. To our knowledge, only 1 other study evaluated the effect gestational hypertension has on the incidence of uterine scar defect – and failed to show any correlation.<sup>35</sup> Considering the influence of pregnancy-related systemic diseases, it is impossible to ignore the influence of hypothyroidism on tissue metabolism. The correlation between hypothyroidism and a higher risk of perioperative complications has been known for a long time.<sup>36</sup> To date, no other studies have been performed to assess the effect of hypothyroidism on uterine healing after cesarean section. In our study, no relationship was found between hypothyroidism and uterine scar niche parameters. When assessing the impact of individual diseases on uterus healing and comparing conflicting reports in the literature, it should be remembered that each population has its own individual characteristics and the incidences of GDM, gestational hypertension and hypothyroidism vary worldwide.

In our study, the effect cervical colonization by microorganisms has on the prevalence and parameters of a uterine niche was evaluated, because previous studies have correlated the bacterial load of the cervix with the bacterial load within the uterine cavity.<sup>37,38</sup> This suggests that cervical microbiota may be a source of microbes for colonization of the uterine cavity and may influence the healing process of the cesarean section scar. However, our study showed no correlation between the cervical colonization and the prevalence and parameters of uterine niches after cesarean section. This may be due to the use of perioperative antibiotics for surgical prophylaxis. Although, further research is needed to confirm this hypothesis.

In other studies, the influence of inflammatory processes such as postpartum fever,<sup>33,35</sup> the application of antibiotics during childbirth,<sup>39</sup> perinatal and puerperal infection in the form of chorioamnionitis, postoperative wound infection, urinary tract infection, and endometritis<sup>34</sup> were analyzed, but no correlation between the abovementioned variables and the prevalence of niches after cesarean section was found.

## Limitations

The main limitation of our study is the lack of comparison between a single-layer continuous uterine suture and a double-layer uterine suture closure, due to the single-layer continuous uterine suture being the standard of care at our Department. The other limitation is that we were checking the colonization of the cervical canal without uterine cavity colonization.

The etiology of a uterine niche after cesarean section is multifactorial. In our study, we evaluated a few potential factors that could disturb the proper healing process of the uterus. The effect of other important individual risk factors such as BMI, corticosteroid use, previous myomectomy and smoking status on the prevalence and parameters of cesarean section niche was not investigated in our study, which is a limitation.

## Conclusions

Two- and three-dimensional ultrasonographic cesarean scar assessment revealed that the selected risk factors concerning systemic diseases during pregnancy, maternal medical history and colonization of the cervical canal have no impact on uterine scar healing in women with single-layer uterine closure covering the entire thickness of the myometrium, excluding the decidua.

## ORCID iDs

Joanna Budny-Wińska  <https://orcid.org/0000-0002-3094-2213>  
 Aleksandra Zimmer-Stelmach  <https://orcid.org/0000-0003-1114-6980>  
 Michał Pomorski  <https://orcid.org/0000-0002-4501-353X>

## References

1. Anna V, van der Ploeg HP, Cheung NW, Huxley RR, Bauman AE. Socio-demographic correlates of the increasing trend in prevalence of gestational diabetes mellitus in a large population of women between 1995 and 2005. *Diabetes Care*. 2008;31(12):2288–2293. doi:10.2337/dc08-1038
2. Guariguata L, Linnenkamp U, Beagley J, Whiting DR, Cho NH. Global estimates of the prevalence of hyperglycaemia in pregnancy. *Diabetes Res Clin Pract*. 2014;103(2):176–185. doi:10.1016/j.diabres.2013.11.003
3. Johnson JA, Tough S; SOGC GENETICS COMMITTEE. Delayed childbearing. *J Obstet Gynaecol Can*. 2012;34(1):80–93. doi:10.1016/S1701-2163(16)35138-6
4. Rendtorff R, Hinkson L, Kiver V, Dröge LA, Henrich W. Pregnancies in women aged 45 years and older: A 10-year retrospective analysis in Berlin. *Geburtshilfe Frauenheilkd*. 2017;77(3):268–275. doi:10.1055/s-0043-100105
5. Betran AP, Torloni MR, Zhang J, et al. What is the optimal rate of caesarean section at population level? A systematic review of ecologic studies. *Reprod Health*. 2015;12:57. doi:10.1186/s12978-015-0043-6
6. Pomorski M, Fuchs T, Zimmer M. Prediction of uterine dehiscence using ultrasonographic parameters of cesarean section scar in the nonpregnant uterus: A prospective observational study. *BMC Pregnancy Childbirth*. 2014;14:365. doi:10.1186/s12884-014-0365-3
7. Ludwin A, Martins WP, Ludwin I. Evaluation of uterine niche by three-dimensional sonohysterography and volumetric quantification: Techniques and scoring classification system. *Ultrasound Obstet Gynecol*. 2019;53(1):139–143. doi:10.1002/uog.19181
8. Setubal A, Alves J, Osório F, et al. Treatment for uterine isthmocele, a pouchlike defect at the site of a cesarean section scar. *J Minim Invasive Gynecol*. 2018;25(1):38–46. doi:10.1016/j.jmig.2017.09.022
9. Jordans IPM, de Leeuw RA, Stegwee SI, et al. Sonographic examination of uterine niche in non-pregnant women: A modified Delphi procedure. *Ultrasound Obstet Gynecol*. 2019;53(1):107–115. doi:10.1002/uog.19049
10. van der Voet LF, Bij de Vaate AM, Veersema S, Brölmann HA, Huirne JA. Long-term complications of caesarean section: The niche in the scar. A prospective cohort study on niche prevalence and its relation to abnormal uterine bleeding. *BJOG*. 2014;121(2):236–244. doi:10.1111/1471-0528.12542
11. Antila-Längsjö RM, Mäenpää JU, Huhtala HS, Tomás EI, Staff SM. Cesarean scar defect: A prospective study on risk factors. *Am J Obstet Gynecol*. 2018;219(5):458.e1–458.e8. doi:10.1016/j.ajog.2018.09.004

12. Vikhareva O, Rickle GS, Lavesson T, Nedopekina E, Brandell K, Salvesen KÅ. Hysterotomy level at Cesarean section and occurrence of large scar defects: A randomized single-blind trial. *Ultrasound Obstet Gynecol.* 2019;53(4):438–442. doi:10.1002/uog.20184
13. Bij de Vaate AJ, van der Voet LF, Naji O, et al. Prevalence, potential risk factors for development and symptoms related to the presence of uterine niches following Cesarean section: Systematic review. *Ultrasound Obstet Gynecol.* 2014;43(4):372–382. doi:10.1002/uog.13199
14. Vikhareva O, Valentin L. Clinical importance of appearance of cesarean hysterotomy scar at transvaginal ultrasonography in non-pregnant women. *Obstet Gynecol.* 2011;117(3):525–532. doi:10.1097/AOG.0b013e318209abf0
15. Kaelin Agten A, Cali G, Monteagudo A, Oviedo J, Ramos J, Timor-Tritsch I. The clinical outcome of cesarean scar pregnancies implanted “on the scar” versus “in the niche”. *Am J Obstet Gynecol.* 2017; 216(5):510.e1–510.e6. doi:10.1016/j.ajog.2017.01.019
16. Vervoort A, Vissers J, Hehenkamp W, Brölmann H, Huirne J. The effect of laparoscopic resection of large niches in the uterine cesarean scar on symptoms, ultrasound findings and quality of life: A prospective cohort study. *BJOG.* 2018;125(3):317–325. doi:10.1111/1471-0528.14822
17. Pomorski M, Fuchs T, Rosner-Tenerowicz A, Zimmer M. Sonographic evaluation of surgical repair of uterine cesarean scar defects. *J Clin Ultrasound.* 2017;45(8):455–460. doi:10.1002/jcu.22449
18. Tower AM, Frishman GN. Cesarean scar defects: An underrecognized cause of abnormal uterine bleeding and other gynecologic complications. *J Minim Invasive Gynecol.* 2013;20(5):562–572. doi:10.1016/j.jmig.2013.03.008
19. Patounakis G, Ozcan MC, Chason RJ, et al. Impact of a prior cesarean delivery on embryo transfer: A prospective study. *Fertil Steril.* 2016;106(2):311–316. doi:10.1016/j.fertnstert.2016.03.045
20. Budny-Winska J, Zimmer-Stelmach A, Pomorski M. Two- and three-dimensional transvaginal ultrasound in assessment of the impact of selected obstetric risk factors on cesarean scar niche formation: The case-controlled study. *Ginekol Pol.* 2021;92(5):378–382. doi:10.5603/GPa2021.0024
21. Osser OV, Jokubkiene L, Valentin L. High prevalence of defects in Cesarean section scars at transvaginal ultrasound examination. *Ultrasound Obstet Gynecol.* 2009;34(1):90–97. doi:10.1002/uog.6395
22. Bij de Vaate AJ, Brölmann HA, van der Voet LF, van der Slikke JW, Veersema S, Huirne JA. Ultrasound evaluation of the Cesarean scar: Relation between a niche and postmenstrual spotting. *Ultrasound Obstet Gynecol.* 2011;37(1):93–99. doi:10.1002/uog.8864
23. Armstrong V, Hansen WF, Van Voorhis BJ, Syrop CH. Detection of cesarean scars by transvaginal ultrasound. *Obstet Gynecol.* 2003; 101(1):61–65. doi:10.1016/s0029-7844(02)02450-x
24. Chen HY, Chen SJ, Hsieh FJ. Observation of cesarean section scar by transvaginal ultrasonography. *Ultrasound Med Biol.* 1990;16(5): 443–447. doi:10.1016/0301-5629(90)90166-a
25. van der Voet LF, Jordans IPM, Brölmann HAM, Veersema S, Huirne JAF. Changes in the uterine scar during the first year after a cesarean section: A prospective longitudinal study. *Gynecol Obstet Invest.* 2018;83(2):164–170. doi:10.1159/000478046
26. Pomorski M, Fuchs T, Budny-Winska J, Zimmer A, Zimmer M. Natural history of cesarean scar pregnancy. *Ginekol Pol.* 2019;90(6):351–352. doi:10.5603/GPa2019.0054
27. Di Spiezio Sardo A, Saccone G, McCurdy R, Bujold E, Bifulco G, Berghella V. Risk of Cesarean scar defect following single- vs double-layer uterine closure: Systematic review and meta-analysis of randomized controlled trials. *Ultrasound Obstet Gynecol.* 2017;50(5):578–583. doi:10.1002/uog.17401
28. Roberge S, Demers S, Berghella V, Chaillet N, Moore L, Bujold E. Impact of single- vs double-layer closure on adverse outcomes and uterine scar defect: A systematic review and meta-analysis. *Am J Obstet Gynecol.* 2014;211(5):453–460. doi:10.1016/j.ajog.2014.06.014
29. Ofili-Yebovi D, Ben-Nagi J, Sawyer E, et al. Deficient lower-segment Cesarean section scars: Prevalence and risk factors. *Ultrasound Obstet Gynecol.* 2008;31(1):72–77. doi:10.1002/uog.5200
30. Pomorski M, Fuchs T, Rosner-Tenerowicz A, Zimmer M. Morphology of the cesarean section scar in the non-pregnant uterus after one elective cesarean section. *Ginekol Pol.* 2017;88(4):174–179. doi:10.5603/GPa2017.0034
31. Pomorski M, Fuchs T, Rosner-Tenerowicz A, Zimmer M. Standardized ultrasonographic approach for the assessment of risk factors of incomplete healing of the cesarean section scar in the uterus. *Eur J Obstet Gynecol Reprod Biol.* 2016;205:141–145. doi:10.1016/j.ejogrb.2016.08.032
32. Yazicioglu F, Gökdogan A, Kelekci S, Aygün M, Savan K. Incomplete healing of the uterine incision after cesarean section: Is it preventable? *Eur J Obstet Gynecol Reprod Biol.* 2006;124(1):32–36. doi:10.1016/j.ejogrb.2005.03.023
33. Vikhareva O, Valentin L. Risk factors for incomplete healing of the uterine incision after cesarean section. *BJOG.* 2010;117(9):1119–1126. doi:10.1111/j.1471-0528.2010.02631.x
34. Hayakawa H, Itakura A, Mitsui T, et al. Methods for myometrium closure and other factors impacting effects on cesarean section scars of the uterine segment detected by the ultrasonography. *Acta Obstet Gynecol Scand.* 2006;85(4):429–434. doi:10.1080/00016340500430436
35. Pan H, Zeng M, Xu T, et al. The prevalence and risk predictors of cesarean scar defect at 6 weeks postpartum in Shanghai, China: A prospective cohort study. *Acta Obstet Gynecol Scand.* 2019;98(4):413–422. doi:10.1111/aogs.13505
36. Chen HY, Chen SJ, Hsieh FJ. Observation of cesarean section scar by transvaginal ultrasonography. *Ultrasound Med Biol.* 1990;16(5):443–447. doi:10.1016/0301-5629(90)90166-a
37. Chen C, Song X, Wei W, et al. The microbiota continuum along the female reproductive tract and its relation to uterine-related diseases. *Nat Commun.* 2017;8(1):875. doi:10.1038/s41467-017-00901-0
38. Winters AD, Romero R, Gervasi MT, et al. Does the endometrial cavity have a molecular microbial signature? *Sci Rep.* 2019;9(1):9905. doi:10.1038/s41598-019-46173-0
39. Voet LLFV, Vaate AMJB, Heymans MW, Brölmann HAM, Veersema S, Huirne JAF. Prognostic factors for niche development in the uterine cesarean section scar. *Eur J Obstet Gynecol Reprod Biol.* 2017;213:31–32. doi:10.1016/j.ejogrb.2017.03.039

# Isoastilbin inhibits neuronal apoptosis and oxidative stress in a rat model of ischemia-reperfusion injury in the brain: Involvement of SIRT1/3/6

Lifeng An<sup>1,B,D</sup>, Dandan Zhu<sup>2,B</sup>, Xin Zhang<sup>2,C</sup>, Jingwen Huang<sup>1,C</sup>, Guangbao Lu<sup>1,A,F</sup>

<sup>1</sup> Jiamusi College, Heilongjiang University of Chinese Medicine, China

<sup>2</sup> Graduate School, Heilongjiang University of Chinese Medicine, Jiamusi, China

A – research concept and design; B – collection and/or assembly of data; C – data analysis and interpretation;

D – writing the article; E – critical revision of the article; F – final approval of the article

Advances in Clinical and Experimental Medicine, ISSN 1899–5276 (print), ISSN 2451–2680 (online)

*Adv Clin Exp Med.* 2022;31(1):49–57

## Address for correspondence

Guangbao Lu  
E-mail: lujm65@126.com

## Funding sources

None declared

## Conflict of interest

None declared

Received on April 28, 2021

Reviewed on August 12, 2021

Accepted on September 12, 2021

Published online on October 14, 2021

## Abstract

**Background.** Isoastilbin (IAB) has been shown to have antioxidative and anti-apoptotic functions. A recent study found that IAB can reduce oxidative stress in Alzheimer's disease. However, whether the antioxidative function of IAB is also protective in other brain diseases remains unknown.

**Objectives.** To investigate the roles and underlying mechanisms of IAB in middle cerebral artery occlusion-reperfusion (MCAO/R) in rats.

**Materials and methods.** Male Wistar rats were randomly divided into 5 groups: sham group, MCAO/R group, and 3 MCAO/R groups administered IAB (20 mg/kg, 40 mg/kg or 80 mg/kg) once a day for 3 days. Infarction size, modified Neurological Severity Score (mNSS), oxidative stress markers, and neuronal apoptosis markers were used to assay the function of IAB.

**Results.** Compared with the MCAO/R group, administration of IAB reduced the infarction size and mNSS scores in MCAO/R rats. Isoastilbin also decreased the level of malondialdehyde (MDA) and enhanced the activity of catalase (CAT), superoxide dismutase (SOD) and glutathione peroxidase (GSH-PX). Isoastilbin treatment attenuated MCAO/R-induced neuronal apoptosis compared with the MCAO/R group, as indicated by the results of terminal deoxynucleotide transferase-mediated X-dUTP nick end (TUNEL) and western blot assays. Isoastilbin also reversed MCAO/R-induced downregulation of SIRT1/3/6 protein expression.

**Conclusions.** These observations suggest that IAB protects against oxidative stress and neuronal apoptosis in rats following cerebral ischemia-reperfusion (I/R) injury through the upregulation of SIRT1/3/6, indicating that IAB might be a promising therapeutic agent for cerebral I/R injury.

**Key words:** apoptosis, oxidative stress, isoastilbin, focal cerebral ischemia-reperfusion injury

## Cite as

An L, Zhu D, Zhang X, Huang J, Lu G. Isoastilbin inhibits neuronal apoptosis and oxidative stress in a rat model of ischemia-reperfusion injury in the brain: Involvement of SIRT1/3/6. *Adv Clin Exp Med.* 2022;31(1):49–57. doi:10.17219/acem/142164

## DOI

10.17219/acem/142164

## Copyright

© 2022 by Wrocław Medical University

This is an article distributed under the terms of the Creative Commons Attribution 3.0 Unported (CC BY 3.0) (<https://creativecommons.org/licenses/by/3.0/>)

## Background

Ischemic and hemorrhagic stroke are among the leading causes of disability and death throughout the world.<sup>1,2</sup> Ischemic stroke is caused by obstructions in blood vessels, thereby putting target organs at risk of cell death.<sup>3</sup> Although the most effective treatment for cerebral ischemia is to rapidly reinstate blood supply, thrombolytic therapy may increase the infarction size and aggravate ischemia-reperfusion (I/R) injury within the brain.<sup>1,4</sup> Therefore, there is an urgent need to develop new drugs for the treatment of cerebral I/R injury.

Ischemia-reperfusion injury in the brain involves complex pathophysiology, including the occurrence of oxidative stress, apoptosis and adenosine triphosphate (ATP) depletion, all of which can lead to neuronal injury.<sup>5</sup> Reactive oxygen species (ROS) are produced during ischemia, leading to neuronal apoptosis and neurological dysfunction.<sup>6</sup> Specifically, NADPH oxidases generate ROS during I/R injury, which causes oxidative stress. This stress is marked by increased lipid peroxidation, decreased catalase (CAT) and superoxide dismutase (SOD) activity, and a decreased glutathione (GSH) level.<sup>7–11</sup> High levels of ROS and oxidative stress will, in turn, trigger cell death through the mitochondrial apoptotic pathway following cerebral I/R injury.<sup>12</sup> Mitochondrial permeability transition pores may open as a consequence of superfluous accumulation of ROS, resulting in lower mitochondrial transmembrane potential and increased production of caspase activators such as cytochrome c, ultimately initiating the caspase cascade and resulting in cell death.<sup>12</sup> Geng et al. proposed that the apoptosis of neuronal cells is at least partially mediated by the mitochondrial apoptosis pathway in cerebral I/R injury.<sup>13</sup> Consequently, the inhibition or reversal of oxidative stress and neuronal apoptosis are a promising new method to attenuate cerebral I/R injury.

Isoastilbin (IAB) is a dihydroflavonol glycoside compound (Fig. 1A) that is widely distributed in *Sparassis crispa* and *Armillaria mellea*.<sup>14,15</sup> As an anti-oxidative molecule, the extraction and purification of IAB from herbal preparations is well established.<sup>14,16</sup> However, if and how IAB may reduce oxidative stress in clinical diseases, remains unknown. Recently, Yu et al. investigated the protective effects of IAB on Alzheimer's disease (AD) in vivo, and found that IAB reduces oxidative stress through regulating the level of ROS induced by apoptosis.<sup>15</sup> This protective effect of IAB in the nervous system suggests that it may serve as a treatment for I/R injury. Therefore, we established an in vivo model of middle cerebral artery occlusion-reperfusion (MCAO/R) to examine whether IAB exerts protective effects against apoptosis and oxidative stress in the nervous system. Here, we demonstrate that IAB decreases cerebral I/R injury in rats by inhibiting apoptosis and reducing oxidative stress.

To explore the mechanism through which IAB attenuates I/R-induced damages, we focused on the SIRT

signaling cascade. Recent studies have shown a protective role of SIRT1/3/6 in various diseases, including neural degeneration in the brain, blood vessel inflammation and fat body accumulation. Indeed, we found that IAB treatment increases the SIRT expression level during I/R injury, indicating that IAB may protect against cell apoptosis by upregulating SIRT expression. Taken together, our results suggest that IAB is a potentially useful treatment for clinical cerebral I/R injury.

## Objectives

Our overall aim was to examine the effects and underlying mechanisms of IAB in I/R injury using MCAO/R animal model.

## Materials and methods

### Animals

Male Wistar rats were acquired from the Shanghai Laboratory Animal Company (Shanghai, China). Rats aged 60–90 days with normal body weight (200–250 g) were fed ad libitum food and water and maintained under a consistent environment (25 ± 2°C, 40 ± 10% relative humidity, and 12 h light/dark cycle). Animals were handled as per the guidelines for the care and use of laboratory animals of Jiamusi College, Heilongjiang University of Traditional Chinese Medicine, China. The Institutional Animal Care and Use Committee of Jiamusi College, Heilongjiang University of Chinese Medicine approved animal procedures (approval No. 20190815).

### Establishment of MCAO/R injury and IAB treatment

The toxicity of IAB was determined as previously described.<sup>15</sup> Isoastilbin (Chengdu Purechem-Standard Co., Ltd., Chengdu, China) was diluted to final concentrations of 20 mg/kg, 40 mg/kg and 80 mg/kg in phosphate-buffered solution (PBS). Animals were randomized into 5 groups: 1. sham; 2. MCAO/R; 3. MCAO/R followed by 20 mg/kg IAB; 4. MCAO/R followed by 40 mg/kg IAB; and 5. MCAO/R followed by 80 mg/kg IAB.

Rats were anesthetized using intraperitoneal (ip.) injection of 50 mg/kg sodium pentobarbital (Sino-pharm Chemical Reagent, Beijing, China). To introduce MCAO/R, we exposed the carotid arteries, namely the external carotid artery (ECA), right common carotid artery (CCA) and internal carotid artery (ICA). The ECA and CCA were proximally ligated. The ICA was ligated using a 0.285 mm monofilament suture, inserted into the lumen of the ICA for about 18 mm through the ECA stump to obstruct the middle cerebral artery (MCA). A Laser

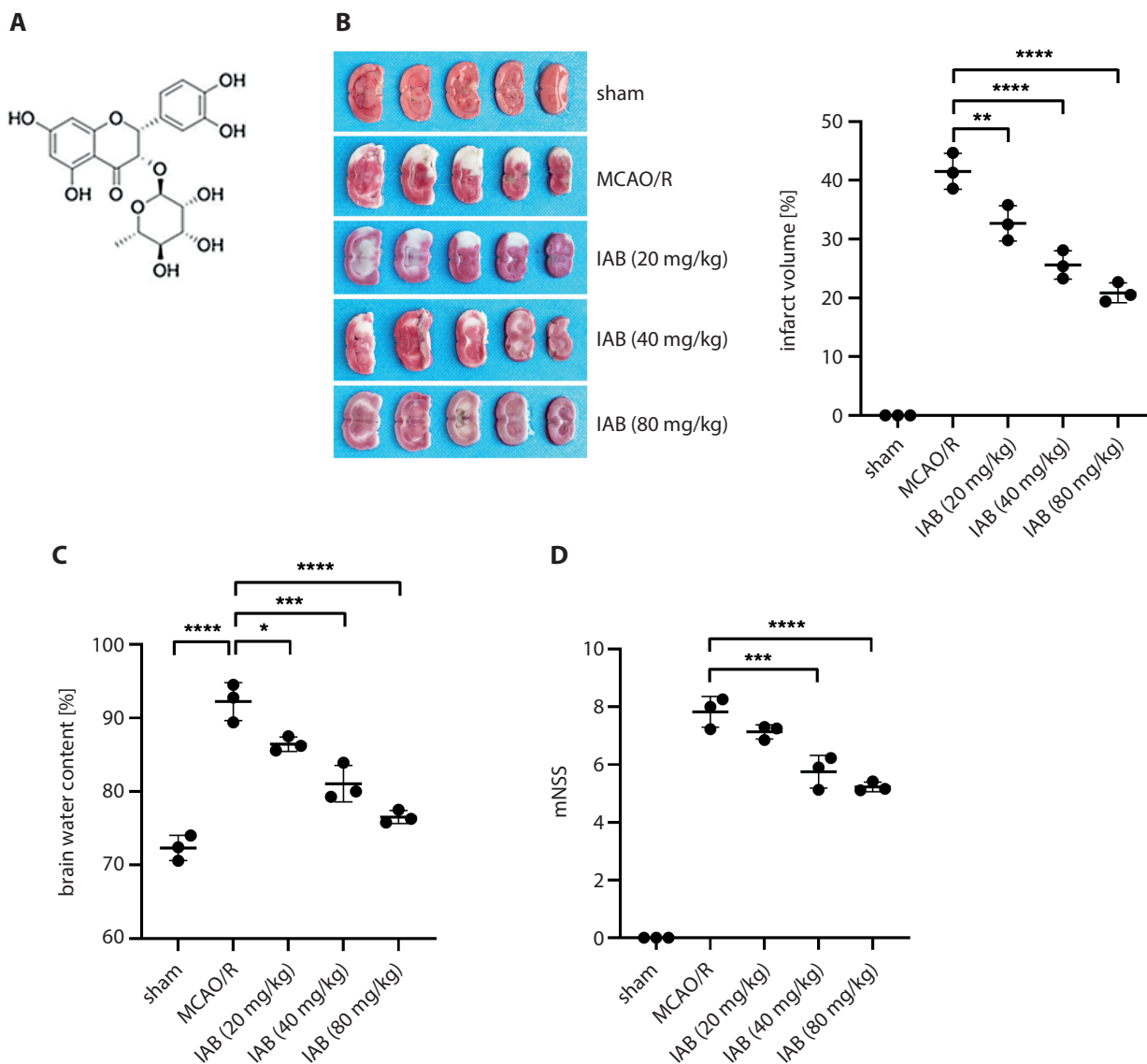


**Fig. 1.** Isoastilbin (IAB) reduced the volume of brain infarct size, brain edema and neurological deficits in rats subjected to middle cerebral artery occlusion-reperfusion (MCAO/R). **A.** Chemical structure of IAB; **B.** Left: Representative images of brains subjected to MCAO/R injury. Right: Quantification of brain infarct size in different treatments. Note that IAB attenuated MCAO/R-induced brain infarction; **C.** Quantification of brain water concentration in different treatments; **D.** Quantification of neurological deficits in different treatments using modified Neurological Severity Score (mNSS). Note the significant reduction in infarction size, water concentration and mNSS after IAB treatment. Comparisons were made using one-way analysis of variance (ANOVA). \*  $p < 0.05$ , \*\*  $p < 0.01$ , \*\*\*  $p < 0.001$  and \*\*\*\*  $p < 0.0001$

Doppler (USCN KIT INC., Wuhan, China) was used to confirm that blood flow was reduced to less than 20% of normal level. The sham group underwent the same operation; however, the arteries were not ligated. After 2 h of occlusion, the ligated arteries were reperfed and the rats were then gavaged with IAB (20 mg/kg, 40 mg/kg or 80 mg/kg) or PBS daily for 3 consecutive days. Lastly, 72 h after MCAO/R, the neurological capacity of the rats was assessed.

### Evaluating rat brain infarct volume

Seventy-two hours after MCAO surgery, rats were euthanized by cervical dislocation. The brains were quickly isolated and cut into 2-mm slices. The brain slices were

incubated with 2% 2,3,5-triphenyltetrazolium chloride (TTC; Sigma-Aldrich, St. Louis, USA) solution for 30 min at 37°C and then fixed in 10% formalin overnight. Uninjured tissues were stained with red, while infarcted tissues were stained with white. A digital camera was used to acquire images of the slices and ImageJ software (National Institutes of Health (NIH), Bethesda, USA) was used to quantify the infarct volume. The infarct volume is reported as the percentage of total brain volume.

### Water concentration in the brain

After IAB treatment, brains were quickly weighed to measure their wet weight. Subsequently, brains were dehydrated at 100°C for 24 h to assess their dry weight.

The concentration of water in the brain was calculated as:  $(\text{wet weight} - \text{dry weight})/\text{wet weight} \times 100\%$ .

### Modified neurological severity score (mNSS)

Sensory, motor, balance and reflex neurological functions were assessed 72 h after MCAO surgery using mNSS.<sup>17</sup> The severity of neurological deficits was ranked on a scale from 0 to 10, with a higher score indicating more severe damage to the nervous system.

### Measurement of superoxide dismutase (SOD), malondialdehyde (MDA), catalase (CAT), and glutathione peroxidase (GSH-PX)

After IAB treatment, protein content was determined from brain tissues. Protein concentration of cortical homogenates was determined using BCA kits (Beyotime, Shanghai, China). The SOD, MDA, CAT, and GSH-PX were detected using the corresponding kits (catalog No. A003-1, A001-3, A007, and A005; Nanjing Jiancheng Bio-engineering Institute, Nanjing, China). Briefly, the supernatant of cortical homogenate was collected. For SOD, samples were incubated with WST-8/enzyme working solution at 37°C for 30 min. The absorption was measured at a wavelength of 450 nm. One SOD enzymatic activity unit (U) was defined as the amount of sample needed to achieve a 50% inhibition rate of WST-8 formazan dye. For MDA, samples were mixed with working solution and then heated at 100°C for 15 min. The absorption of supernatant was measured at a wavelength of 532 nm. For CAT, samples were mixed with CAT detection buffer and hydrogen peroxide solution and then incubated at 25°C for 5 min. The absorption was detected at a wavelength of 520 nm. For GSH-PX, samples were mixed with GSH at 37°C for 5 min. The absorption of supernatant was measured at a wavelength of 412 nm. One unit (U) of enzyme activity was defined as the amount of GSH-PX in 1 mg of protein that catalyzed the consumption of 1 μmol/L GSH, while deducting the effect of the non-enzyme reaction.

### Terminal deoxynucleotidyl transferase dUTP nick end labeling (TUNEL) staining

Ipsilateral hemisphere brain tissues were isolated, fixed in 4% paraformaldehyde and embedded in paraffin. Tissues were then cut into 5-μm slices and antigen exposed after 10 min of microwave heating in citrate buffer. Neuronal apoptosis was assessed using the TUNEL assay (In Situ Cell Death Detection Kit; Roche, Penzberg, Germany), according to the manufacturer's instructions. In brief, brain slices were placed in ice-cold 4% paraformaldehyde for 30 min and then, were incubated in the dark with the TUNEL reaction mixture at 37°C for 1 h. Subsequently, the nuclei were stained with 6-diamidino-2-phenylindole (DAPI;

Sigma-Aldrich). Samples were imaged and the apoptosis index was calculated as the number of TUNEL-positive cells divided by the total number of cells.

### Western blot

Rat brain tissues were lysed using radio-immunoprecipitation assay (RIPA) buffer (Beyotime, Dalian, China). Proteins were subjected to 12–15% sodium dodecyl sulfate polyacrylamide gel electrophoresis (SDS-PAGE) and then transferred onto polyvinylidene fluoride (PVDF) membranes (Millipore, Billerica, USA). Membranes were blocked using 5% fat-free milk and incubated with primary antibodies at 4°C overnight. Horseradish peroxidase (HRP)-conjugated secondary antibodies were subsequently incubated at room temperature for 2 h. Specific signals of labeled proteins were detected using a chemiluminescence system. The β-actin was used to normalize the protein expression levels of Bcl-2, Bax and Sirtuin (SIRT1/3/6). Images were analyzed using ImageJ software.

### Statistical analyses

Data are presented as the mean ± standard deviation (SD) from 3 independent experiments. Data from each group were confirmed to follow a normal distribution using the Shapiro–Wilk test. The differences between groups were analyzed using one-way analysis of variance (ANOVA), followed by Tukey's post hoc test using Prism v. 8 software (GraphPad Software, San Diego, USA). A value of  $p < 0.05$  indicated statistical significance. A post hoc power analysis was performed using G\*Power 3.1.9.7 software (Heinrich Heine University, Düsseldorf, Germany).

## Results

### Isoastilbin protects neurons from MCAO/R-induced injury

To explore if IAB protected neurons subjected to cerebral I/R, the concentration of water in the brain and infarct volume were analyzed. In control animals, there was no infarction and the water concentration was relatively low (Fig. 1B,C; sham group). After MCAO/R surgery, we observed significant increases in the infarct size and water concentration (Fig. 1B,C). Infarction and ischemic edema indicate that our approach successfully generated I/R model in rats. Interestingly, when we applied different concentrations of IAB (20 mg/kg, 40 mg/kg and 80 mg/kg) immediately after injury, we observed dose-dependent recovery of infarction and ischemic cerebral edema (Fig. 1B,C). This result suggests that IAB protects against ischemia-induced brain damage. Next, we examined cell apoptosis using the mNSS assay. As shown in Fig. 1D, sham-operated rats exhibited no obvious neurological

deficits, whereas MCAO/R rats showed significantly increased mNSS scores. Consistent with the morphological changes shown in Fig. 1B and Fig. 1C, IAB treatment significantly decreased the mNSS score of MCAO/R rats (Fig. 1D). Taken together, these results provide evidence that IAB has a neuroprotective function in an in vivo rodent model of cerebral I/R injury. Given that a higher IAB concentration had better protective effects without obvious side effects, we used 80 mg/kg for the following experiments.

### Isoastilbin attenuates oxidative stress in MCAO/R rats

To assess the influence of IAB on oxidative stress, the GSH-PX, MDA, SOD, and CAT levels were assessed after IAB treatment. Due to the increase in oxidative stress, rats subjected to MCAO/R had higher levels of MDA compared with sham rats. This effect was attenuated by IAB treatment (Fig. 2A). Furthermore, CAT, SOD and GSH-PX levels decreased in MCAO/R rats compared to sham rats (Fig. 2B,D). Treatment with IAB elevated the levels of CAT, SOD and GSH-PX in MCAO/R rats (Fig. 2B,D), suggesting that IAB protected against cerebral I/R injury by attenuating oxidative stress.

### Isoastilbin inhibits neuronal apoptosis in MCAO/R rats

Next, we utilized the TUNEL assay to assess neuronal apoptosis after cerebral I/R injury. As depicted in Fig. 3A, there was an increased number of TUNEL-positive cells in MCAO/R rats, which was reduced by IAB treatment (Fig. 3A). To explore the underlying mechanisms of IAB protection, we examined the expression of the apoptosis proteins Bax and Bcl-2 using western blot. In rats subjected to MCAO/R, the expression of Bax (pro-apoptotic marker) was upregulated, while that of Bcl-2 (anti-apoptotic marker) was downregulated, compared with the sham group (Fig. 3B,C). However, IAB treatment prevented MCAO/R-induced changes (Fig. 3B,C). These results suggest that IAB inhibited neuronal apoptosis in MCAO/R rats.

### Isoastilbin upregulates SIRT expression

Next, we sought to examine how IAB protects neurons from oxidative stress. The SIRT, a NAD<sup>+</sup>-dependent deacetylase mainly localized in mitochondria, has been found to be associated with cell survival and apoptosis, cell metabolism, and response to stress. The SIRT may activate mitochondrial signals and pathways to promote mitochondria proliferation and ATP generation. It also participates in inflammation, in a way that the reduction in SIRT leads to the increases in chronic inflammation factors, like NFκB and RelA/p65 activity.<sup>18–20</sup> Interestingly, several studies have found that SIRT exerts a neural protective

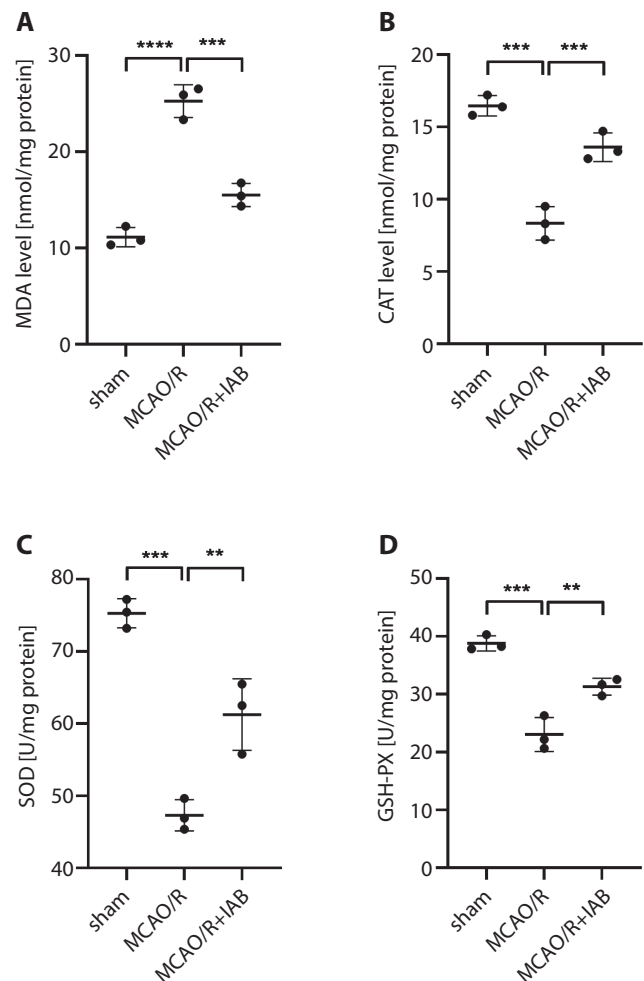
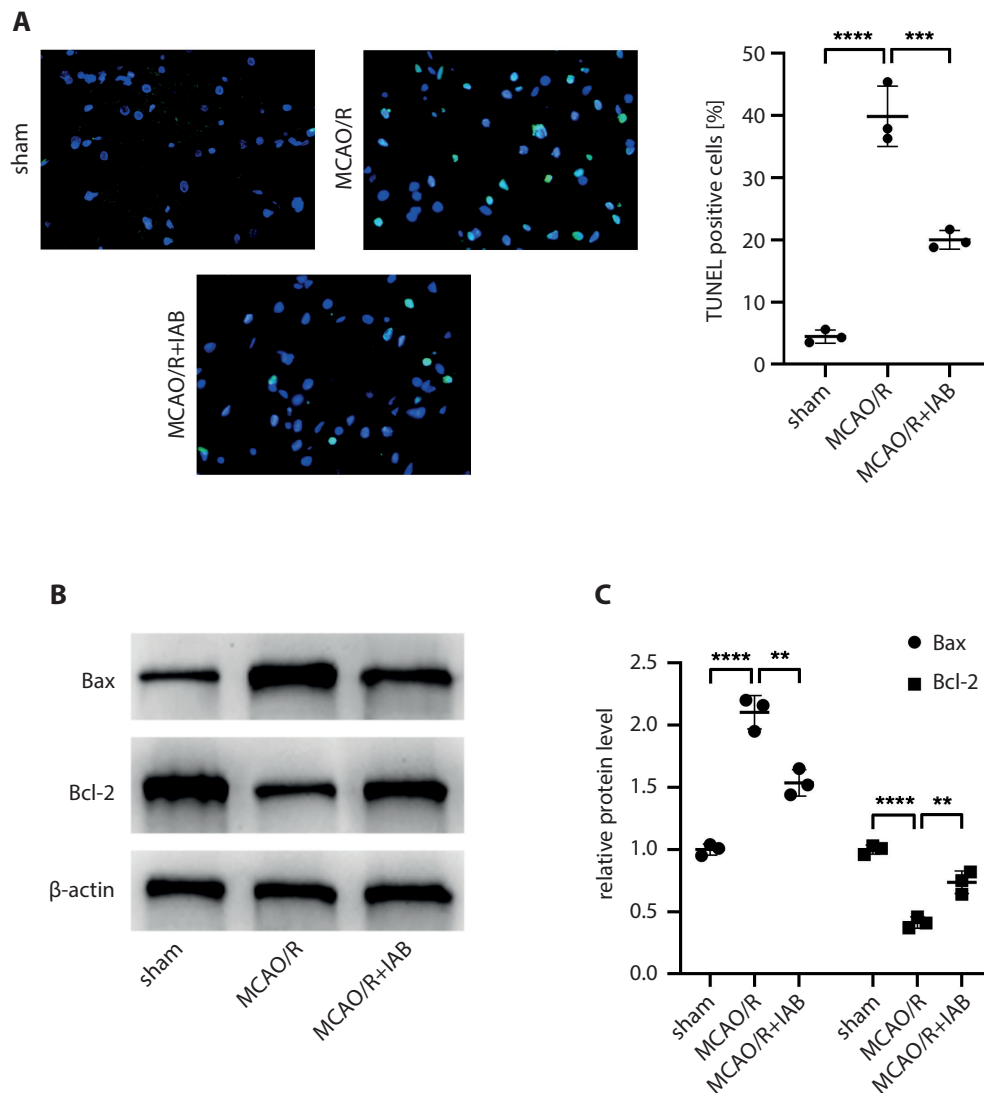


Fig. 2. Isoastilbin (IAB) mitigated oxidative stress in rats subjected to middle cerebral artery occlusion-reperfusion (MCAO/R). Rats were administered IAB (80 mg/kg) after MCAO/R surgery. A. Quantification of malondialdehyde (MDA) level in different treatments. Note that IAB treatment attenuated the MCAO/R-induced MDA increase; B. Quantification of catalase (CAT) level in different treatments; C. Quantification of superoxide dismutase (SOD) activity in different treatments; D. Quantification of glutathione peroxidase (GSH-PX) activity in different treatments. Note that CAT level, SOD activity and GSH-PX activity increased after IAB treatment. Comparisons were made using one-way analysis of variance (ANOVA). \*\*  $p < 0.01$ , \*\*\*  $p < 0.001$  and \*\*\*\*  $p < 0.0001$

effect and attenuates oxidative stress in the pathophysiology of cerebral I/R injury.<sup>21</sup> Here, we investigated brain expression of SIRT1/3/6 in rats subjected to MCAO/R. We found that MCAO/R injury decreased the protein levels of SIRT1/3/6, while IAB treatment attenuated these effects (Fig. 4A–D). These data suggest that IAB might be protective in MCAO/R rats by upregulating SIRT1/3/6 expression in protection against oxidative stress.

## Discussion

Previous research has established that I/R induces apoptosis and oxidative stress, resulting in neurologic disorders or even death.<sup>22–24</sup> Oxidative stress is an important cause of brain reperfusion injury because during reperfusion,



**Fig. 3. Isoastilbin (IAB) inhibits neuronal apoptosis in rats subjected to middle cerebral artery occlusion-reperfusion (MCAO/R).** A. Left: Representative images of brain tissue using TUNEL staining. Right: Quantification of TUNEL-positive cells in different treatments. MCAO/R induced cell apoptosis, which was reversed by IAB treatment; B. Western blots showed increased Bax and decreased Bcl-2 protein expression after MCAO/R, which was reversed by IAB treatment; C. Quantification of the protein levels of Bcl-2 and Bax in different treatments. Comparisons were made using one-way analysis of variance (ANOVA). \*\*  $p < 0.01$ , \*\*\*  $p < 0.001$  and \*\*\*\*  $p < 0.0001$

ROS concentration rises to a peak, which may potentially induce apoptosis or cell necrosis.<sup>25–28</sup> There are several well-established markers of oxidative stress. For example, MDA, a cytotoxic compound produced by lipid peroxidation,<sup>29</sup> is increased in rat cardiomyocytes after I/R damage.<sup>30</sup> The antioxidant enzymes SOD, CAT and GSH-PX play important roles in scavenging superoxides and preventing oxidative damage.<sup>31,32</sup> Moreover, changes in the activity of these enzymes are also related to oxidative stress. Attenuating oxidative stress is a potential way of protecting tissues from I/R injury.

A recent study demonstrated that the neuroprotective effect of IAB might be due to the modulation of oxidative stress. Specifically, the study found that IAB inhibited ROS generation and induced SOD and GSH-PX to ameliorate oxidative damage in a mouse AD model.<sup>15</sup> However, if and how IAB protects against I/R injury in brain, is not yet known. In the present study, we demonstrated that IAB successfully attenuates cerebral I/R injury by reducing the infarct volume and neurological deficits after MCAO/R injury. To test whether the effects of IAB are due to attenuation of ROS species, we measured several markers

of oxidative stress. Isoastilbin treatment after MCAO/R was found to decrease MDA levels, but increase CAT, SOD, and GSH-PX activity. These results suggest that the underlying mechanism of IAB-mediated neuroprotection against I/R injury is through the reduction of oxidative stress.

Indeed, cerebral I/R is able to induce apoptosis of neurons.<sup>33,34</sup> The activation of pro-apoptotic proteins (Bax and Bak) and parallel inactivation of anti-apoptotic proteins (such as Bcl-2) occurred during cerebral I/R injury. Both, Bcl-2 and Bax are found in the exterior part of the mitochondrial membrane, and participate in the modulation of cell apoptosis.<sup>35–37</sup> Previous studies have shown that Bcl-2 overexpression blocks neuronal death in vitro and in vivo.<sup>38</sup> Erfani et al. found that the Bax/Bcl-2 ratio was increased during cerebral I/R injury, contributing to neuronal apoptosis.<sup>39</sup> Moreover, Bax upregulation and Bcl-2 downregulation were found in mice brains subjected to MCAO/R.<sup>40</sup> In addition, IAB has been found to modulate the protein expression levels of both Bcl-2 and Bax to improve the redox system in mice with AD, indicating the anti-apoptotic role of IAB in this condition.<sup>15</sup> In the present study, we showed



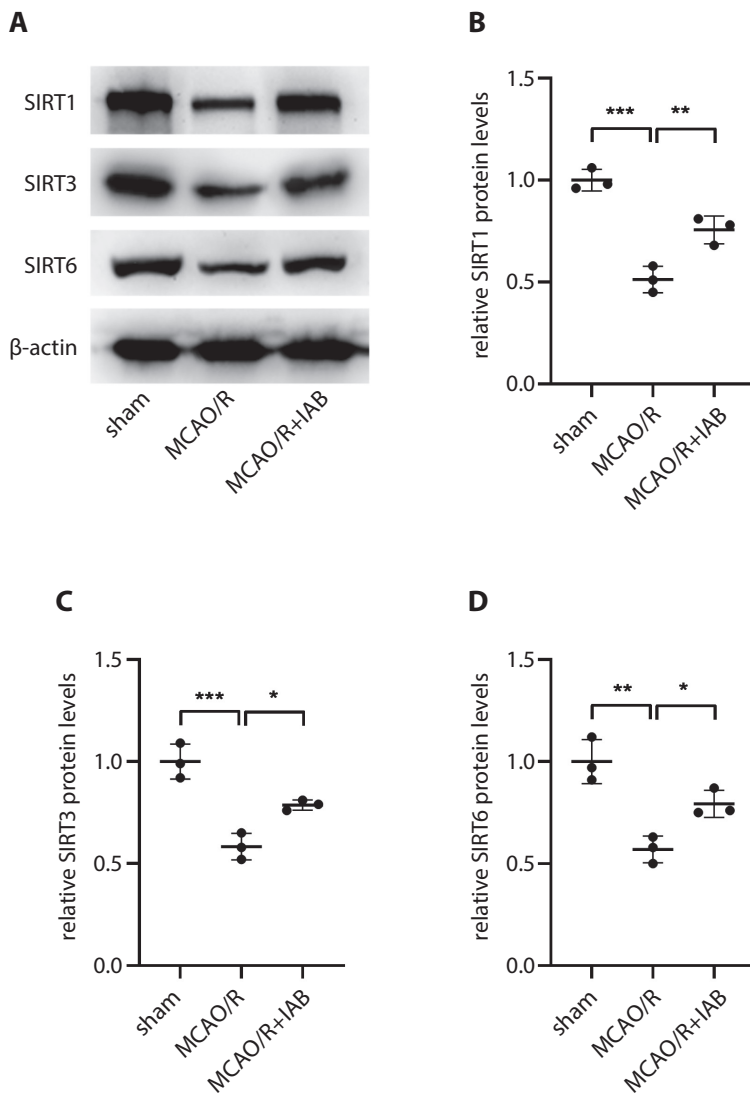


**Fig. 4.** Isoastilbin (IAB) regulated the expression of SIRT1/3/6 in rats subjected to middle cerebral artery occlusion-reperfusion (MCAO/R). A. Western blots showed decreased SIRT1, SIRT3 and SIRT6 expression after MCAO/R, which was reversed by IAB treatment; B–D. Quantification of the protein levels of SIRT1, SIRT3 and SIRT6 in different treatments. Comparisons were made using one-way analysis of variance (ANOVA). \*  $p < 0.05$ , \*\*  $p < 0.01$  and \*\*\*  $p < 0.001$

that the administration of IAB reduced I/R-induced neuronal apoptosis *in vivo* by downregulating Bax and upregulating Bcl-2. These findings imply that the neuroprotective capability of IAB is dependent on its anti-apoptotic activity in rats. However, I/R may also lead to necrosis, which is not mediated by oxidative stress.<sup>25–28</sup> It is of great interest to examine whether IAB may also function by inhibiting necrosis to attenuate I/R injury.

To examine the mechanism through which IAB attenuates oxidative stress, we focused on SIRT proteins. A previous report has found that overexpression of SIRT3 inhibited mitochondrial fission to protect against cerebral I/R injury.<sup>41</sup> Moreover, SIRT6 can protect the brain against I/R damage through the suppression of oxidative stress.<sup>42</sup> Herein, we discovered that SIRT1/3/6 was significantly downregulated in MCAO/R rats, whereas administration of IAB increased the expression of SIRT1/3/6. To the best of our knowledge, this study is the first to demonstrate that IAB may increase SIRT1/3/6 protein expression to attenuate oxidative stress and neuronal apoptosis induced by cerebral I/R injury.

## Limitations

There are many different protective pathways against oxidative stress. Here, we demonstrated that the signaling mechanism of IAB protection is through SIRT 1/3/6. However, other mechanisms against oxidative stress or cerebral I/R injury should be further elucidated. During I/R injury, both apoptosis and necrosis are involved; however, we only focused on apoptosis. Thus, further research on the role of IAB in necrosis will be necessary to fully explain the protective function of IAB during I/R injury.

## Conclusions

Here, we demonstrated that IAB can alleviate oxidative stress and apoptosis of neurons in rats subjected to cerebral I/R. Moreover, the antioxidative stress and anti-apoptotic functions of IAB might arise through the regulation of the SIRT1/3/6 expression. Taken together, our data suggest that IAB is a candidate treatment for cerebral I/R injury.

## ORCID iDs

Lifeng An  <https://orcid.org/0000-0002-4835-1817>  
 Dandan Zhu  <https://orcid.org/0000-0001-9119-9956>  
 Xin Zhang  <https://orcid.org/0000-0002-9496-1691>  
 Jingwen Huang  <https://orcid.org/0000-0001-6449-5362>  
 Guangbao Lu  <https://orcid.org/0000-0002-2465-8996>

## References

- Rossi DJ, Brady JD, Mohr C. Astrocyte metabolism and signaling during brain ischemia. *Nat Neurosci.* 2007;10(11):1377–1386. doi:10.1038/nn2004
- Ribeiro PW, Cola PC, Gatto AR, et al. Relationship between dysphagia, National Institutes Of Health Stroke Scale score, and predictors of pneumonia after ischemic stroke. *J Stroke Cerebrovasc Dis.* 2015;24(9):2088–2094. doi:10.1016/j.jstrokecerebrovasdis.2015.05.009
- Hu X, De Silva TM, Chen J, Faraci FM. Cerebral vascular disease and neurovascular injury in ischemic stroke. *Circ Res.* 2017;120(3):449–471. doi:10.1161/circresaha.116.308427
- Tabassum R, Vaibhav K, Shrivastava P, et al. Perillyl alcohol improves functional and histological outcomes against ischemia-reperfusion injury by attenuation of oxidative stress and repression of COX-2, NOS-2 and NF- $\kappa$ B in middle cerebral artery occlusion rats. *Eur J Pharmacol.* 2015;747:190–199. doi:10.1016/j.ejphar.2014.09.015
- Woodruff TM, Thundyil J, Tang SC, Sobey CG, Taylor SM, Arumugam TV. Pathophysiology, treatment, and animal and cellular models of human ischemic stroke. *Mol Neurodegener.* 2011;6(1):11. doi:10.1186/1750-1326-6-11
- Gonzalez-Rodriguez PJ, Xiong F, Li Y, Zhou J, Zhang L. Fetal hypoxia increases vulnerability of hypoxic-ischemic brain injury in neonatal rats: Role of glucocorticoid receptors. *Neurobiol Dis.* 2014;65:172–179. doi:10.1016/j.nbd.2014.01.020
- Rodrigo R, Fernández-Gajardo R, Gutiérrez R, et al. Oxidative stress and pathophysiology of ischemic stroke: Novel therapeutic opportunities. *CNS Neurol Disord Drug Targets.* 2013;12(5):698–714. doi:10.2174/1871527311312050015
- Zhang C, Ling CL, Pang L, et al. Direct macromolecular drug delivery to cerebral ischemia area using neutrophil-mediated nanoparticles. *Theranostics.* 2017;7(13):3260–3275. doi:10.7150/thno.19979
- Kahles T, Luedike P, Endres M, et al. NADPH oxidase plays a central role in blood–brain barrier damage in experimental stroke. *Stroke.* 2007;38(11):3000–3006. doi:10.1161/strokeaha.107.489765
- Chen H, Song YS, Chan PH. Inhibition of NADPH oxidase is neuroprotective after ischemia-reperfusion. *J Cereb Blood Flow Metab.* 2009;29(7):1262–1272. doi:10.1038/jcbfm.2009.47
- Kapoor M, Sharma N, Sandhir R, Nehru B. Effect of the NADPH oxidase inhibitor apocynin on ischemia-reperfusion hippocampus injury in rat brain. *Biomed Pharmacother.* 2018;97:458–472. doi:10.1016/j.biopha.2017.10.123
- Yu S, Wang C, Cheng Q, et al. An active component of *Achyranthes bidentata* polypeptides provides neuroprotection through inhibition of mitochondrial-dependent apoptotic pathway in cultured neurons and in animal models of cerebral ischemia. *PLoS One.* 2014;9(10):e109923. doi:10.1371/journal.pone.0109923
- Geng HX, Li RP, Li YG, et al. 14,15-EET suppresses neuronal apoptosis in ischemia-reperfusion through the mitochondrial pathway. *Neurochem Res.* 2017;42(10):2841–2849. doi:10.1007/s11064-017-2297-6
- Du Q, Li L, Jerz G. Purification of astilbin and isoastilbin in the extract of *Smilax glabra* rhizome by high-speed counter-current chromatography. *J Chromatogr A.* 2005;1077(1):98–101. doi:10.1016/j.chroma.2005.04.072
- Yu H, Yuan B, Chu Q, Wang C, Bi H. Protective roles of isoastilbin against Alzheimer's disease via Nrf2-mediated antioxidation and anti-apoptosis. *Int J Mol Med.* 2019;43(3):1406–1416. doi:10.3892/ijmm.2019.4058
- Zhou X, Xu Q, Li JX, Chen T. Structural revision of two flavanone glycosides from *Smilax glabra*. *Planta Med.* 2009;75(6):654–655. doi:10.1055/s-0029-1185360
- Morimoto J, Yasuhara T, Kameda M, et al. Electrical stimulation enhances migratory ability of transplanted bone marrow stromal cells in a rodent ischemic stroke model. *Cell Physiol Biochem.* 2018;46(1):57–68. doi:10.1159/000488409
- Torrens-Mas M, Pons DG, Sastre-Serra J, Oliver J, Roca P. SIRT3 silencing sensitizes breast cancer cells to cytotoxic treatments through an increment in ROS production. *J Cell Biochem.* 2017;118(2):397–406. doi:10.1002/jcb.25653
- Nassir F, Arndt JJ, Johnson SA, Ibdah JA. Regulation of mitochondrial trifunctional protein modulates nonalcoholic fatty liver disease in mice. *J Lipid Res.* 2018;59(6):967–973. doi:10.1194/jlr.M080952
- Torrens-Mas M, Hernández-López R, Oliver J, Roca P, Sastre-Serra J. Sirtuin 3 silencing improves oxaliplatin efficacy through acetylation of MnSOD in colon cancer. *J Cell Physiol.* 2018;233(8):6067–6076. doi:10.1002/jcp.26443
- Hernández-Jiménez M, Hurtado O, Cuartero MI, et al. Silent information regulator 1 protects the brain against cerebral ischemic damage. *Stroke.* 2013;44(8):2333–2337. doi:10.1161/strokeaha.113.001715
- Chen GY, Nuñez G. Sterile inflammation: Sensing and reacting to damage. *Nat Rev Immunol.* 2010;10(12):826–837. doi:10.1038/nri2873
- Eltzschig HK, Eckle T. Ischemia and reperfusion: From mechanism to translation. *Nat Med.* 2011;17(11):1391–1401. doi:10.1038/nm.2507
- Dziedzic T. Systemic inflammation as a therapeutic target in acute ischemic stroke. *Expert Rev Neurother.* 2015;15(5):523–531. doi:10.1586/14737175.2015.1035712
- Yemisci M, Gursoy-Ozdemir Y, Vural A, Can A, Topalkara K, Dalkara T. Pericyte contraction induced by oxidative-nitrative stress impairs capillary reflow despite successful opening of an occluded cerebral artery. *Nat Med.* 2009;15(9):1031–1037. doi:10.1038/nm.2022
- Chen H, Yoshioka H, Kim GS, et al. Oxidative stress in ischemic brain damage: Mechanisms of cell death and potential molecular targets for neuroprotection. *Antioxid Redox Signal.* 2011;14(8):1505–1517. doi:10.1089/ars.2010.3576
- Olmez I, Ozyurt H. Reactive oxygen species and ischemic cerebrovascular disease. *Neurochem Int.* 2012;60(2):208–212. doi:10.1016/j.neuint.2011.11.009
- Guo J, Cheng C, Chen CS, et al. Overexpression of Fibulin-5 attenuates ischemia/reperfusion injury after middle cerebral artery occlusion in rats. *Mol Neurobiol.* 2016;53(5):3154–3167. doi:10.1007/s12035-015-9222-2
- Qiang M, Xu Y, Lu Y, et al. Autofluorescence of MDA-modified proteins as an in vitro and in vivo probe in oxidative stress analysis. *Protein Cell.* 2014;5(6):484–487. doi:10.1007/s13238-014-0052-1
- Hou S, Zhao MM, Shen PP, et al. Neuroprotective effect of salvianolic acids against cerebral ischemia/reperfusion injury. *Int J Mol Sci.* 2016;17(7). doi:10.3390/ijms17071190
- Adibhatla RM, Hatcher JF. Lipid oxidation and peroxidation in CNS health and disease: From molecular mechanisms to therapeutic opportunities. *Antioxid Redox Signal.* 2010;12(1):125–169. doi:10.1089/ars.2009.2668
- Staroń A, Mąkosa G, Koter-Michalak M. Oxidative stress in erythrocytes from patients with rheumatoid arthritis. *Rheumatol Int.* 2012;32(2):331–334. doi:10.1007/s00296-010-1611-2
- Aşci S, Demirci S, Aşci H, Doğuç DK, Onaran İ. Neuroprotective effects of pregabalin on cerebral ischemia and reperfusion. *Balkan Med J.* 2016;33(2):221–227. doi:10.5152/balkanmedj.2015.15742
- Tao T, Li CL, Yang WC, et al. Protective effects of propofol against whole cerebral ischemia/reperfusion injury in rats through the inhibition of the apoptosis-inducing factor pathway. *Brain Res.* 2016;1644:9–14. doi:10.1016/j.brainres.2016.05.006
- Martinou JC, Youle RJ. Mitochondria in apoptosis: Bcl-2 family members and mitochondrial dynamics. *Dev Cell.* 2011;21(1):92–101. doi:10.1016/j.devcel.2011.06.017
- Borner C, Andrews DW. The apoptotic pore on mitochondria: Are we breaking through or still stuck? *Cell Death Differ.* 2014;21(2):187–191. doi:10.1038/cdd.2013.169
- Siddiqui WA, Ahad A, Ahsan H. The mystery of BCL2 family: Bcl-2 proteins and apoptosis. An update. *Arch Toxicol.* 2015;89(3):289–317. doi:10.1007/s00204-014-1448-7
- Maes ME, Schlamp CL, Nickells RW. BAX to basics: How the BCL2 gene family controls the death of retinal ganglion cells. *Prog Retin Eye Res.* 2017;57:1–25. doi:10.1016/j.preteyeres.2017.01.002
- Erfani S, Khaksari M, Oryan S, Shamsaei N, Aboutaleb N, Nikbakht F. Namp1/PBEF/visfatin exerts neuroprotective effects against ischemia/reperfusion injury via modulation of Bax/Bcl-2 ratio and prevention of caspase-3 activation. *J Mol Neurosci.* 2015;56(1):237–243. doi:10.1007/s12031-014-0486-1

40. Chen L, Cao J, Cao D, et al. Protective effect of dexmedetomidine against diabetic hyperglycemia-exacerbated cerebral ischemia/reperfusion injury: An in vivo and in vitro study. *Life Sci.* 2019;235:116553. doi:10.1016/j.lfs.2019.116553
41. Zhao H, Luo Y, Chen L, et al. Sirt3 inhibits cerebral ischemia-reperfusion injury through normalizing Wnt/ $\beta$ -catenin pathway and blocking mitochondrial fission. *Cell Stress Chaperones.* 2018;23(5):1079–1092. doi:10.1007/s12192-018-0917-y
42. Zhang W, Wei R, Zhang L, Tan Y, Qian C. Sirtuin 6 protects the brain from cerebral ischemia/reperfusion injury through NRF2 activation. *Neuroscience.* 2017;366:95–104. doi:10.1016/j.neuroscience.2017.09.035



# Metformin protects against abdominal aortic aneurysm by Atg7-induced autophagy

Jingjing Guo<sup>1,A,D,F</sup>, Zhu Wang<sup>2,A,D,F</sup>, Ming Xue<sup>3,A,D,F</sup>, Lei Mi<sup>4,B,C,E,F</sup>,  
Mengpeng Zhao<sup>2,B,C,E,F</sup>, Chao Ma<sup>2,B,C,E,F</sup>, Jian Wu<sup>2,B,C,E,F</sup>, Xinqiang Han<sup>2,A,D,F</sup>

<sup>1</sup> Department of Obstetrics and Gynecology, Binzhou Medical University Hospital, China

<sup>2</sup> Department of Interventional Medicine and Vascular Surgery, Binzhou Medical University Hospital, China

<sup>3</sup> Department of Interventional Radiology, Weihai Municipal Hospital, China

<sup>4</sup> Department of General Surgery, Tai'an City Central Hospital, China

A – research concept and design; B – collection and/or assembly of data; C – data analysis and interpretation;  
D – writing the article; E – critical revision of the article; F – final approval of the article

Advances in Clinical and Experimental Medicine, ISSN 1899–5276 (print), ISSN 2451–2680 (online)

*Adv Clin Exp Med.* 2022;31(1):59–69

## Address for correspondence

Xinqiang Han  
E-mail: CHQPeng17hp@yeah.net

## Funding sources

None declared

## Conflict of interest

None declared

Received on July 27, 2021

Reviewed on August 28, 2021

Accepted on September 8, 2021

Published online on October 29, 2021

## Abstract

**Background.** Abdominal aortic aneurysm (AAA) is a pathological dilation of the abdominal aorta. It is often asymptomatic, yet it has a high susceptibility to rupture. Our previous study showed that metformin protected against the pathophysiology of AAA by reducing the activation of the PI3K/AKT/mTOR pathway.

**Objectives.** To investigate the potential involvement of the autophagy-related pathways in AAA and the ability of metformin to modulate these effects.

**Materials and methods.** The expression of autophagy-related proteins was detected with western blot in patients with AAA. Angiotensin II (Ang-II) was also used to construct an AAA model in mice and in vascular smooth muscle cells (VSMCs). The expression of Atg7 and Atg4 was determined using western blot assay. The Atg7 expression was regulated by overexpressed plasmid, siRNA (small interfering RNA), or metformin, and cell proliferation, migration, apoptosis and autophagy caused by Ang-II were examined.

**Results.** Autophagy-related proteins were increased in patients with AAA. The Ang-II also induced the expression of Atg7, and metformin reversed this effect both in vivo and in vitro. The suppression of Atg7 inhibited cell proliferation and cell migration, and reduced cell apoptosis and autophagy, while the overexpression of Atg7 enhanced cell proliferation and migration, and induced cell apoptosis and autophagy. Furthermore, Atg7 regulated the expression of the autophagy-related protein in Ang-II treated VSMCs. The Atg7-mediated autophagy was also attenuated by metformin.

**Conclusions.** Metformin reduced autophagy in AAA and this effect was mediated by Atg7, suggesting that Atg7 is a potential downstream effector of metformin in protecting against the pathophysiology of AAA.

**Key words:** metformin, abdominal aortic aneurysm, autophagy, Ang-II, Atg7

## Cite as

Guo J, Wang Z, Xue M, et al. Metformin protects against abdominal aortic aneurysm by Atg7-induced autophagy. *Adv Clin Exp Med.* 2022;31(1):59–69. doi:10.17219/acem/142026

## DOI

10.17219/acem/142026

## Copyright

© 2022 by Wrocław Medical University

This is an article distributed under the terms of the Creative Commons Attribution 3.0 Unported (CC BY 3.0) (<https://creativecommons.org/licenses/by/3.0/>)

## Background

Abdominal aortic aneurysm (AAA), a degenerative vascular disease, is a pathological dilation that can lead to a potentially fatal aortic rupture.<sup>1</sup> Although the incidence of AAA has recently decreased,<sup>2</sup> the worldwide mortality rate due to this condition has remained stable.<sup>3</sup> Aneurysms are characterized by a decrease in the number of medial smooth muscle cells (SMCs) in the aortic wall.<sup>1</sup> An increasing number of studies have reported that the development of AAA is associated with a reduction in the structural integrity of the vessel wall, which is caused by cell apoptosis and senescence in SMCs.<sup>4,5</sup> While the histopathological features of AAA are well documented, the cellular and molecular mechanisms underlying the pathogenesis of AAA remain unclear, and no effective pharmacological therapy has been identified to prevent AAA. Therefore, the search for a novel therapeutic approach remains a challenge.

Autophagy is a highly regulated process that includes the delivery of damaged organelles and cytoplasmic constituents to the lysosome for clearance.<sup>6</sup> Autophagy-related genes (Atgs) play a critical role in the regulation of this process.<sup>7</sup> The Atg7 is a central regulator of autophagy and serves as an E1-like enzyme for the ubiquitin-like proteins Atg12 and Atg8.<sup>8</sup> The *ApoE*<sup>-/-</sup> mice with SMC-specific Atg7 deficiency exhibit increased plaque sizes and accelerated SMC senescence in the fibrous cap.<sup>9</sup> Moreover, the SMC-specific deletion of Atg7 results in reduced serum-induced cell growth, increased cell death and a decreased cell proliferation rate.<sup>10</sup> Furthermore, the loss of Atg7 in SMCs exacerbates angiotensin II (Ang-II)-associated aortic remodeling.<sup>11</sup> The disruption of autophagic flux caused by vascular SMC (VSMC)-specific deletion of Atg7 results in defective mitophagy, an exacerbation of VSMC apoptosis and, in turn, plaque vulnerability.<sup>12</sup> This latter observation reveals the important role of autophagy in the pathogenesis of AAA. Others have reported that metformin suppresses Ang-II-induced AAA progression by inhibiting the activation of the NF- $\kappa$ B and STAT3 signaling pathways.<sup>13–15</sup> The levels of the autophagy factors Beclin and LC3 have also been shown to be elevated in human and mouse AAA tissues.<sup>16</sup> As the primary cellular constituent of the aorta, the loss of VSMCs through apoptosis or necroptosis is a significant distinguishing characteristic of AAA.<sup>17</sup> Moreover, a recent study showed that autophagy plays a key role in regulating VSMC death and aortic wall homeostasis and repair.<sup>18</sup>

## Objectives

This study aimed to investigate the potential involvement of autophagy-related signaling pathways in AAA and the ability of metformin to modulate these effects.

## Materials and methods

### Clinical samples

Clinical samples were obtained from patients and controls at the Shandong Provincial Hospital (Jinan, China). Detailed information on patients and sample collection has been provided in our previous study.<sup>15</sup> The aneurysmal wall tissues of AAA and aortic tissues from the control group were lysed in RIPA buffer (ab156034; Abcam, Cambridge, UK) for western blot assays. This study was approved by the Human Research Committee of Shandong Provincial Hospital (Approval No. SZRJ:NO.2021-160), affiliated with Shandong University. The procedures followed the Declaration of Helsinki and informed consent was obtained before conducting the experiments on human subjects.

### Animal model

As previously described,<sup>15</sup> a mouse model of Ang-II-induced AAA was developed. All procedures with animals were approved by the Animal Care and Use Committee at Shandong Provincial Hospital and were conducted following institutional guidelines. A total of 30 mice (male, 8 weeks old) were randomly assigned to one of the 3 groups: AAA group (n = 10), sham group (n = 10) and AAA + metformin (Met) group (n = 10). In the AAA group, mice were infused with Ang-II (1.44 mg/kg/day, ab120183; Abcam, Cambridge, UK) for 7 or 28 days using implanted micro-osmotic pumps. Mice in the sham group received an equal volume of saline. In the AAA+Met group, mice were injected with Ang-II (1.44 mg/kg/day) by implanted micro-osmotic pumps, and were fed water containing metformin (100 mg/kg/day) for 7 or 28 days.

### Cell culture and treatment

The VSMCs were isolated from the normal arteries of healthy rats as described previously<sup>19</sup> and cultured in Dulbecco's modified Eagle medium (DMEM) (10313039; Thermo Fisher Scientific, Shanghai, China), supplemented with 10% fetal bovine serum (FBS) at 37°C with 5% CO<sub>2</sub>. These VSMCs were then treated with Ang-II (1  $\mu$ M), metformin (10 mM), or a combination of siRNA or plasmid with Ang-II.

### Transfection with plasmid or siRNA

The pcDNA3.1-Atg7 overexpression vector was constructed and validated using restriction enzyme digestion and DNA sequencing analysis. The polymerase chain reaction (PCR) primers for amplification of Atg7 (NM\_006395) were Atg7-F (5'-CGCAAATGGGCGGTAGGCGTG-3') and Atg7-R (5'-TAGAAGGCACAGTCCGAGG-3').

Verification of the correct cloning of the sequence in the pcDNA3.1-Atg7 overexpression vector is shown in Fig. 1. Negative control (NC) or Atg7 siRNA was purchased from GenePharma (Shanghai, China). The plasmid or siRNA was transfected into VSMCs using Lipofectamine 2000 (Invitrogen, Waltham, USA) according to the manufacturer's instructions.

## Immunofluorescence

The Ang-II-treated VSMCs were transfected with NC siRNA, Atg7 siRNA, control plasmid, or overexpressed Atg7 plasmid for 48 h. Cells were fixed and blocked with 1% bovine serum albumin (BSA) for 30 min at room temperature. The cells were then incubated with anti-Atg7 antibodies overnight at 4°C. After washing with phosphate buffered saline (PBS) 3 times, fluorescein isothiocyanate (FITC)-conjugated secondary antibodies were used. The DAPI was used to stain the cell nuclei. The images of these cells were taken with an Olympus CX71 microscope (Olympus Corp., Tokyo, Japan).

## Cell apoptosis

Cells were harvested and stained with Annexin V and propidium iodide (PI), using an Annexin V-FITC apoptosis detection kit (Becton Dickinson Biosciences, Franklin Lakes, USA) according to the manufacturer's instructions. Cell samples were analyzed using CellQuest software on a FACSCalibur™ instrument (Becton Dickinson Biosciences).

## 5-ethynyl-2'-deoxyuridine (EdU) staining

Cell permeabilization and staining were performed using a Click-iT EdU Imaging Kit (Invitrogen). Cells were fixed in 4% formaldehyde for 15 min and then were incubated with 0.1% Triton X-100 for 10 min. Thereafter, cells were treated with 0.5 mL of Click-iT reaction cocktail in the dark for 30 min. After removing the reaction cocktail, cells were washed with 3% BSA in PBS, and their nuclei were stained with 1 µg/mL DAPI for 5 min in the dark. Cells were then washed with PBS, and Olympus CX71 microscope was used to capture the images.

## Transwell assay

After overnight starvation, cells were reseeded in the upper chamber of a transwell plate ( $1 \times 10^5$  in 100 µL of medium) that was pretreated with 1% Matrigel (Becton Dickinson Biosciences) in PBS. The bottom chambers were also filled with 500 µL cell culture medium. After 24 h, the nonmigrated cells were removed and the migrated cells were fixed and stained with crystal violet. Images of these cells were captured using Olympus CX71 microscope.

## Western blotting

Cells were lysed in ice-cold RIPA lysis buffer and protein concentrations were determined using a BCA protein kit (ab102536; Abcam). A total of 30 µg of protein was separated using 12% sodium dodecyl sulphate-polyacrylamide gel electrophoresis (SDS-PAGE) gel. After transfer to polyvinylidene difluoride (PVDF) membranes and blocking with 5% fat free milk for 1 h at room temperature, the membranes were incubated overnight at 4°C with primary antibodies against Atg7, p62, Beclin 1, LC3B, or GAPDH. The membranes were washed 3 times with Tris-buffered saline with Tween (TBST) and incubated for 2 h at room temperature with horseradish peroxidase (HRP)-conjugated secondary antibody. Enhanced chemiluminescence (ECL) was used to view the protein bands.

## Transmission electron microscopy (TEM)

Cells were fixed with 2.5% glutaraldehyde and washed 4 times with PBS. The cells were then fixed with 1% osmic acid. After washing, the cells were dehydrated using 50% acetone, 70% acetone, 90% acetone, and 100% acetone. Cells were infiltrated, embedded, sliced, and stained using uranium acetate lead citrate. The cell morphology was examined using a Hitachi-7500 transmission electron microscope (Hitachi, Tokyo, Japan).

## Statistical analyses

Data were analyzed using GraphPad Prism software v. 9.0.1 (GraphPad Software, San Diego, USA). All experiments were repeated at least 3 times. The corresponding data are expressed as mean  $\pm$  standard deviation (SD). Unpaired Student's t-tests were used to determine statistical differences between 2 groups and one-way analysis of variance (ANOVA) was used to determine statistical differences between multiple groups, followed by Tukey's post hoc test. The Shapiro–Wilk test was used to assess normality. Statistical significance was defined as a p-value less than 0.05.

## Results

### The expression of Atg7 is induced in patients with AAA and in an AAA mouse model

Our previous study found that metformin protected against the pathophysiology of AAA by inhibiting autophagy in vivo and in vitro. To understand the mechanism behind these effects, the expression of the autophagy-related proteins Atg4 and Atg7 was evaluated in patients with AAA. It was found that Atg7 expression was increased in patients with AAA compared to controls,

whereas the expression of Atg4 remained unchanged (Fig. 2A). Furthermore, the expression of Beclin 1 and LC3B II/I was increased and the expression of p62 was decreased (Fig. 2A), suggesting that the autophagy is triggered in AAA. The Ang-II was also used to construct a mouse AAA model, and it was discovered that Ang-II induced the expression levels of Atg7, Beclin 1 and LC3B II/I, and reduced the expression of p62 (Fig. 2B). On the other hand, metformin reversed the induction of Atg7, Beclin 1 and LC3B II/I (Fig. 2B). Given that Atg7 is an essential factor for the induction of autophagy, the increased level of Atg7 might contribute to the induction of autophagy in AAA.

### Metformin attenuates Ang-II-induced Atg7 expression

The Ang-II was used to construct an AAA model in VSMCs and the expression of autophagy-related proteins was examined. It was found that Ang-II induced the protein expression level of Atg7 (Fig. 3A) but not of Atg4. Moreover, metformin reversed the induction of Atg7 (Fig. 3A). To assess the functional role of Atg7 in the AAA in vitro model (Ang-II treated VSMCs), Atg7 was overexpressed or suppressed using a plasmid or siRNA, and immunofluorescence (IF) was used to determine the transfection efficiency. As shown in Fig. 3B,C, the expression of Atg7 was increased or decreased by transfection.

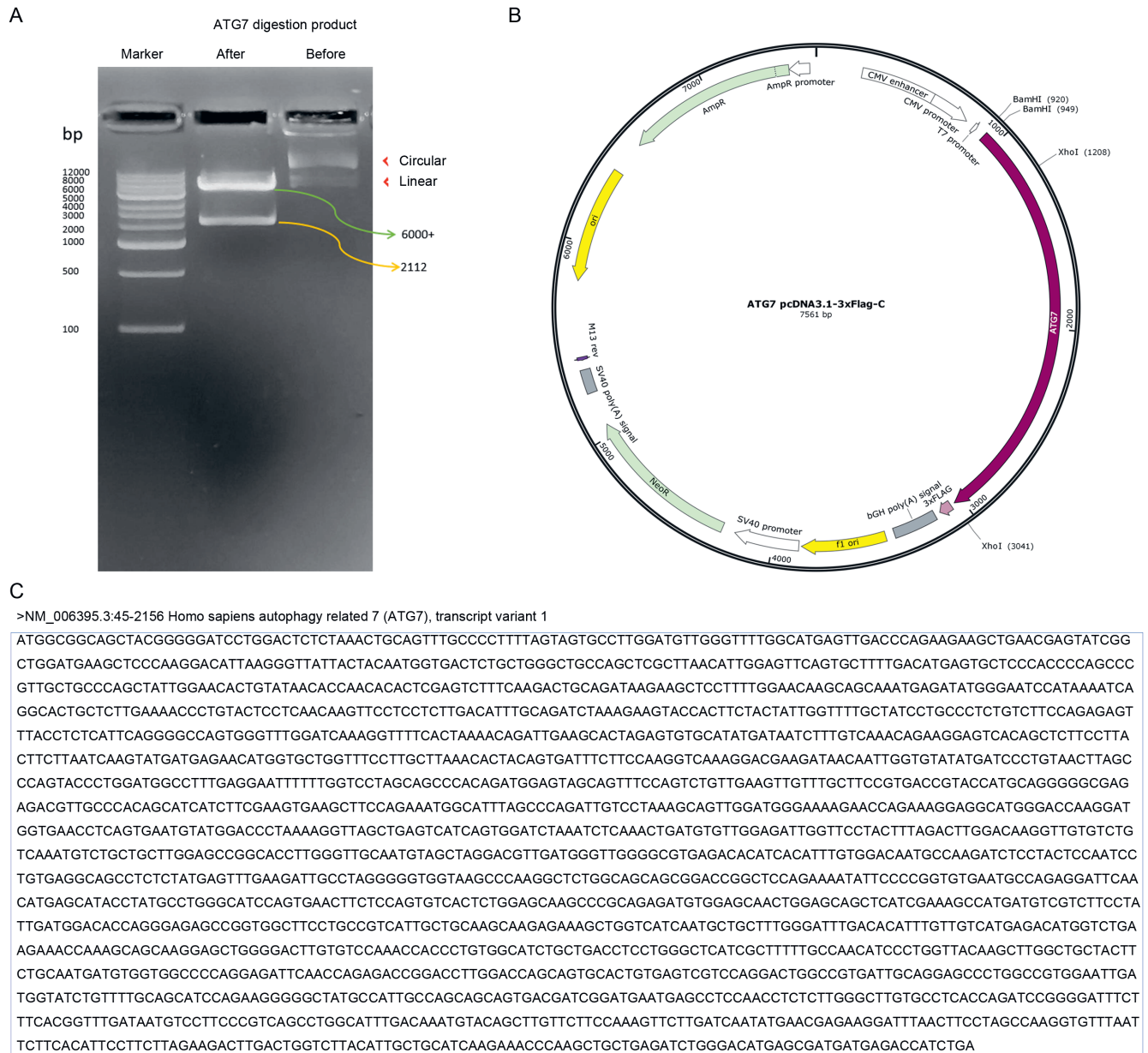
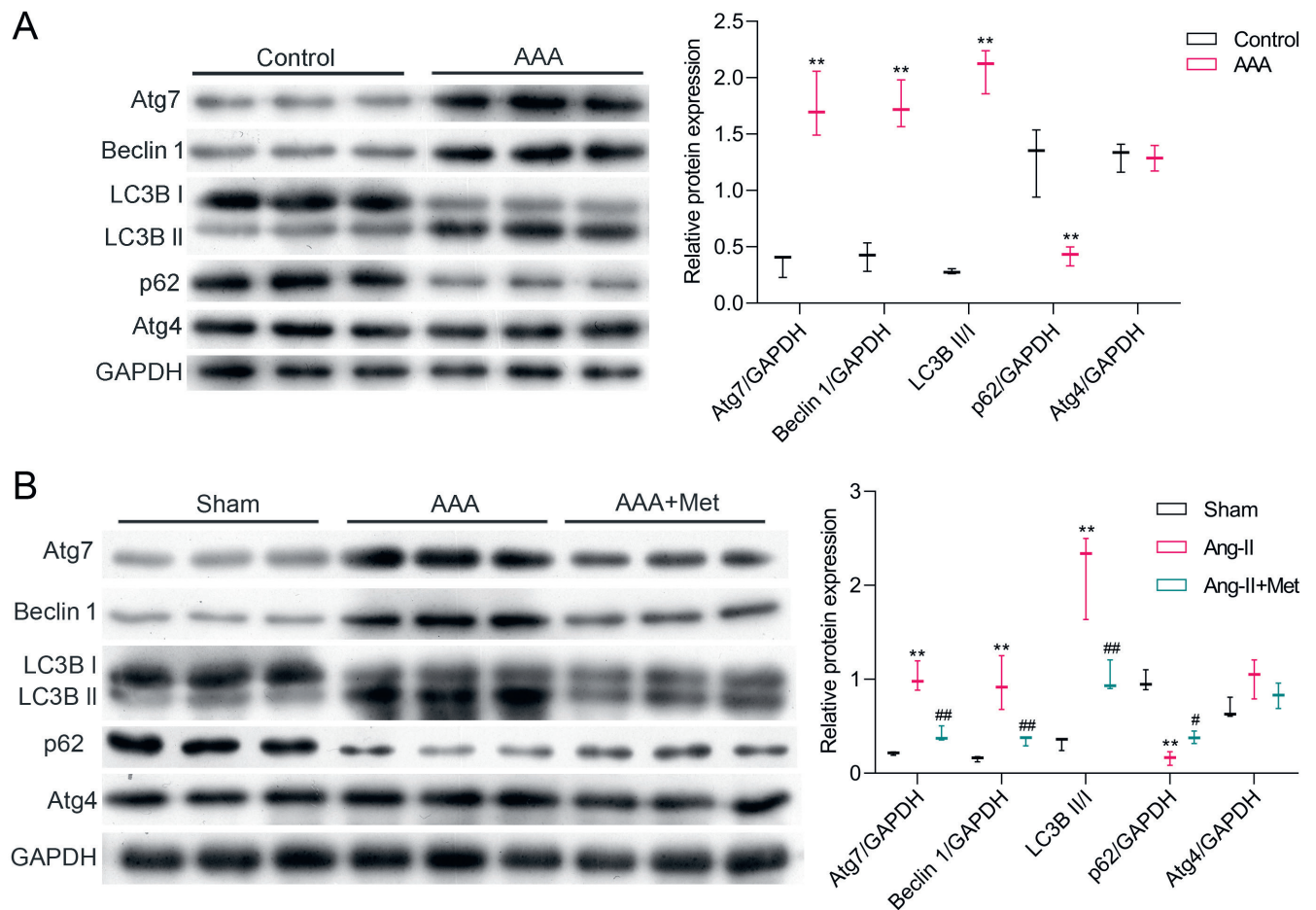


Fig. 1. Cloning of Atg7. A. The electrophoresis results of Atg7 polymerase chain reaction (PCR) product before and after restriction endonuclease digestion; B. The vector map of pcDNA3.1-Atg7; C. The cDNA sequence of Atg7





**Fig. 2.** The expression of Atg7 is induced in patients with abdominal aortic aneurysm (AAA) and in an AAA mouse model. **A.** Clinical samples from patients (n = 3) and controls (n = 3) were collected and lysed for western blot assays. The GAPDH was used as a loading control. Image J software was used to determine relative protein expression. \*\*p < 0.01 compared to the control group. Results were statistically analyzed using an unpaired Student's t-test; **B.** Mice were infused with Ang-II (1.44 mg/kg/day) by implanting micro-osmotic pumps (AAA group) or infused with Ang-II and fed water containing metformin (AAA + metformin (Met) group). The aneurysmal wall tissues were collected and lysed for western blot assays. The GAPDH was used as a loading control. Relative protein expression was evaluated using Image J software. \*\*p < 0.01 compared to the sham group, #p < 0.05, ##p < 0.01 compared to the Ang-II group. Results were statistically analyzed using one-way analysis of variance (ANOVA) followed by Tukey's post hoc test

### Atg7 mediates the proliferation and migration of VSMCs under Ang-II treatment

To demonstrate the effects of Atg7 on the proliferation and migration of VSMCs, an Atg7-expressing vector was constructed (Fig. 1). The EdU staining was used to determine the cell proliferation rate and it was found that the overexpression of Atg7 significantly increased the rate of cell proliferation. The Atg7 overexpression occurred in an average of 82% of treated cells compared to 38% of controls. The reduction of Atg7 using siRNA reduced cell proliferation from 37% to 8% (Fig. 4A,C). Moreover, cell migration was induced by Atg7 and reduced by inhibiting Atg7 (Fig. 4B,D). These findings indicate that Atg7 regulates cell proliferation and migration in the AAA in vitro cell model.

### Inhibition of Atg7 reduces cell apoptosis and autophagy in Ang-II-treated VSMCs

To determine the apoptotic effects of Atg7 on VSMCs, an Annexin V assay was performed to assess the early and late stages of cell apoptosis. As shown in Fig. 5A, silencing Atg7 reduced early cell apoptosis (22% compared to 13%), while the overexpression of Atg7 enhanced early cell apoptosis (19% compared to 30%). Moreover, the Atg7 overexpression increased autophagic vacuole formation, whereas the Atg7 suppression decreased autophagic vacuole formation (Fig. 5B). The expression of the autophagy-related proteins was further evaluated and it was found that Atg7 overexpression increased the expression of LC3B II/I and Beclin 1, whereas the level of p62 was decreased (Fig. 5C). Furthermore, the suppression of Atg7 by siRNA inhibited LC3B II/I and Beclin 1 but increased p62 expression (Fig. 5C). These results suggest that Atg7 mediates both, Ang-II-induced cell apoptosis and autophagy.

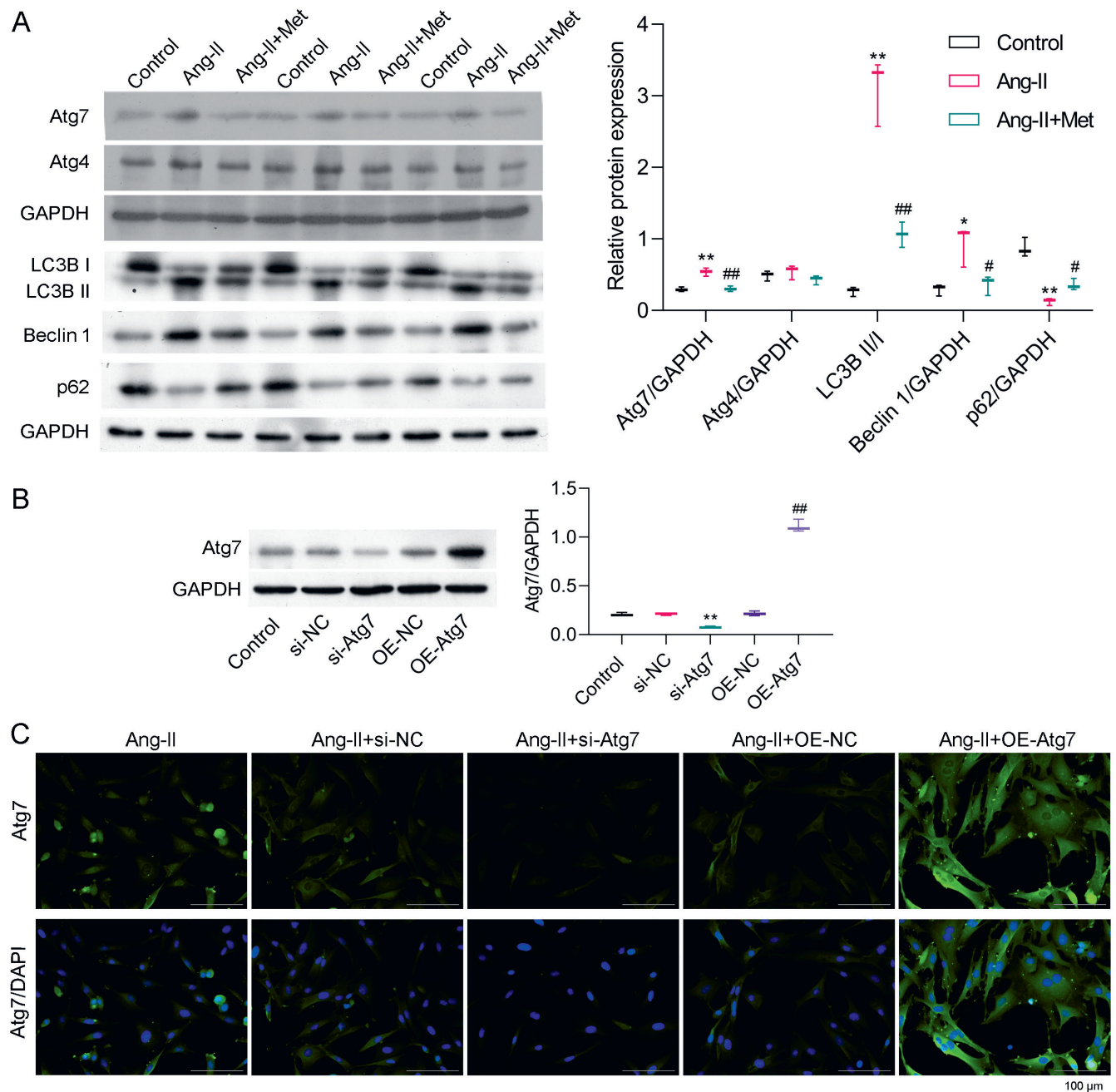


**Fig. 3.** Metformin attenuates Ang-II-induced Atg7 expression. **A.** The vascular smooth muscle cells (VSMCs) were treated with Ang-II alone or a combination of Ang-II (1  $\mu$ M) and metformin (Met, 10 mM) for 48 h. Cells were collected and lysed for western blotting. The GAPDH was used as a loading control. Relative protein expression was assessed using Image J software. \* $p < 0.05$ , \*\* $p < 0.01$  compared to control group, # $p < 0.05$ , ## $p < 0.01$  compared to the Ang-II group. Results were statistically analyzed using one-way analysis of variance (ANOVA) followed by Tukey's post hoc test; **B.** The VSMCs were treated with Ang-II (1  $\mu$ M) and transfected with negative control (NC) siRNA (si-NC), Atg7 siRNA (si-Atg7), a control plasmid (OE-NC) or an overexpressed Atg7 (OE-Atg7) plasmid for 48 h. Western blot analysis was performed to determine the expression of Atg7. \*\* $p < 0.01$  compared to the si-NC group, ## $p < 0.01$  compared to the OE-NC group. Results were statistically analyzed using ANOVA followed by Tukey's post hoc test; **C.** Cells were fixed and stained using an Atg7 antibody

### Reduction of autophagy by metformin in AAA is mediated by Atg7

To determine whether Atg7 regulated metformin-induced suppression of autophagy in Ang-II-treated VSMCs, the Atg7 was overexpressed in both metformin- and Ang-II-treated VSMCs (Fig. 6A), and it was found that metformin reversed the autophagic vacuole formation induced by Atg7 (Fig. 6A,B). Similarly, metformin reversed the increased expression

of LC3B II/I and Beclin 1, and the decreased p62 levels induced by Atg7 overexpression (Fig. 6C). Therefore, our results suggest that metformin inhibits autophagy by suppressing Atg7.

### Discussion

The AAA is a pathologic dilation of the abdominal aorta that is often asymptomatic, yet has a high susceptibility

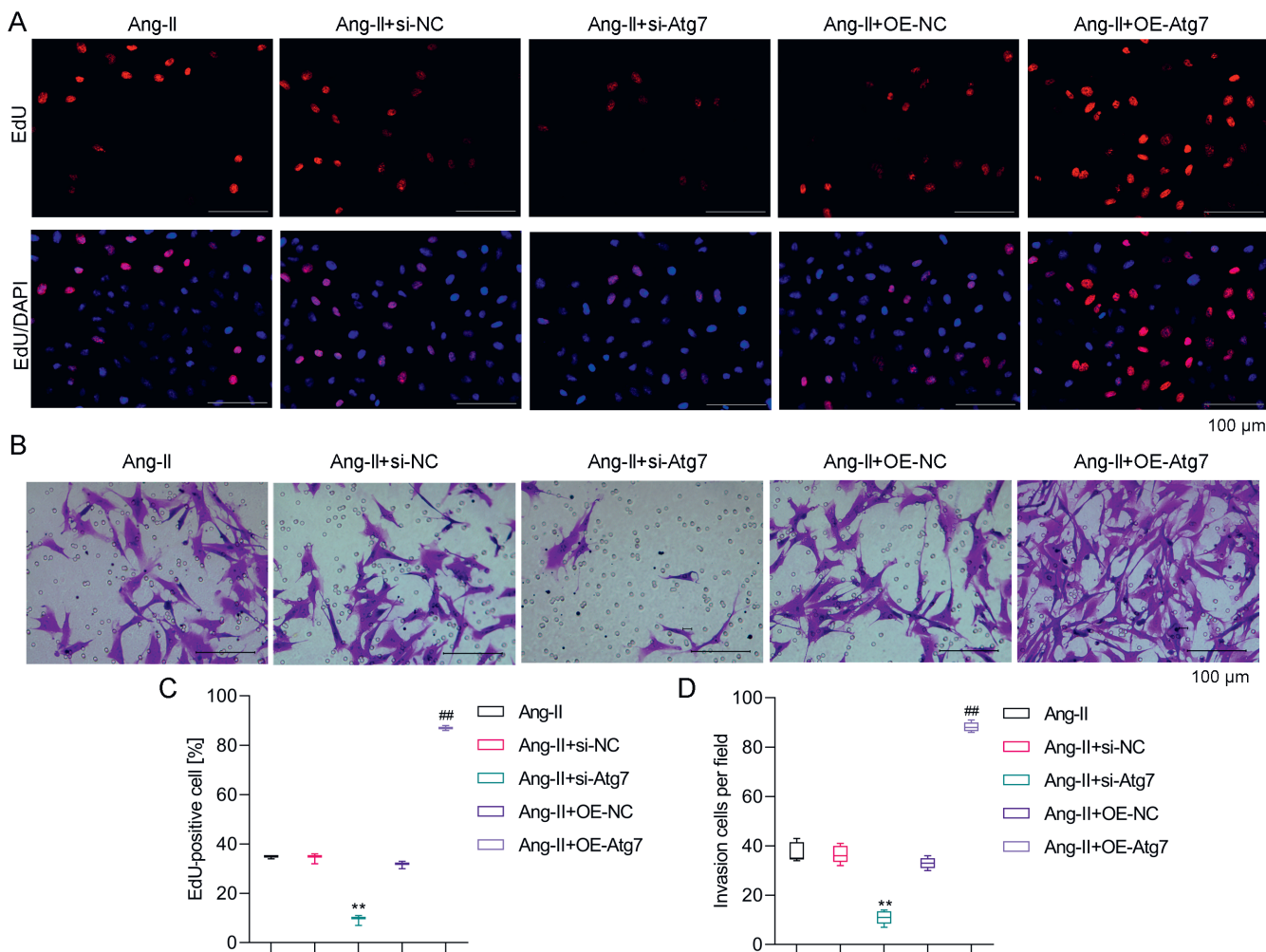


**Fig. 4.** The Atg7 mediates the cell proliferation and migration of vascular smooth muscle cells (VSMCs) following Ang-II treatment. The VSMCs were treated with Ang-II (1  $\mu$ M) and transfected with NC siRNA (si-NC), Atg7 siRNA (si-Atg7), a control plasmid (OE-NC) or an overexpressed Atg7 (OE-Atg7) plasmid for 48 h. A. Cells were fixed and stained for EdU; B. Transwell assay was performed; C and D. A summary of the EdU and transwell assays. The respective images are shown. \*\* $p < 0.01$  compared to the Ang-II+si-NC group, ## $p < 0.01$  compared to the Ang-II+OE-NC group. Results were statistically analyzed using one-way analysis of variance (ANOVA) followed by Tukey's post hoc test

to rupture. In this study, it was found that the expression of the autophagy-related protein Atg7 is increased in patients with AAA, and in vitro and in vivo models of the condition. More importantly, metformin reversed the induced expression of Atg7. Furthermore, cell proliferation, migration, apoptosis, and autophagy in an in vitro AAA cell model were regulated by Atg7. However, these Atg7-induced effects were reversed by metformin. Taken together, these findings suggest that Atg7 is a potential downstream effector of metformin that is involved in protecting against the pathophysiology of AAA.

The upregulation of LC3, Atg5 and Atg7 has been found in dissected AAA tissues from Ang-II-treated *ApoE*<sup>-/-</sup> mice, and Ang-II-challenged SMC Atg7-specific knockout mice exhibit severe cardiac dysfunction and larger suprarenal aortic diameters.<sup>11</sup> As a major component of the vessel wall, VSMCs control blood flow and arterial pressure by changing the lumen diameter in resistance vessels in response to Ang-II.<sup>20</sup> The Ang-II induces autophagy in cells by increasing Beclin 1, Vps34, Atg12-Atg5,

Atg4 and Atg7 protein levels, Beclin 1 phosphorylation, and the number of autophagic vesicles.<sup>21</sup> In the current study, it was observed that Atg7 was upregulated not only in patients with AAA, but also in Ang-II-treated mice or VSMCs. Our previous study demonstrated that metformin suppressed the pathophysiology of AAA by inhibiting the autophagy pathway.<sup>15</sup> Furthermore, in this study, it was found that the induced expression of Atg7 in AAA was reversed by metformin. No previous studies have evaluated whether metformin regulates Atg7 in Ang-II-induced VSMCs. Our findings indicate that Atg7 might be involved in metformin-reduced autophagy in AAA, which is evidenced by a decrease in autophagy-related proteins.

The AAA is caused by changes in the aortic wall structure, including the loss of VSMCs and the degradation of the extracellular matrix, which results in thinning of the media and adventitia.<sup>22</sup> The proliferation and apoptosis of VSMCs are associated with the progression of AAA.<sup>18</sup> Furthermore, the loss of autophagy in VSMCs promotes VSMC death and endoplasmic reticulum stress-dependent

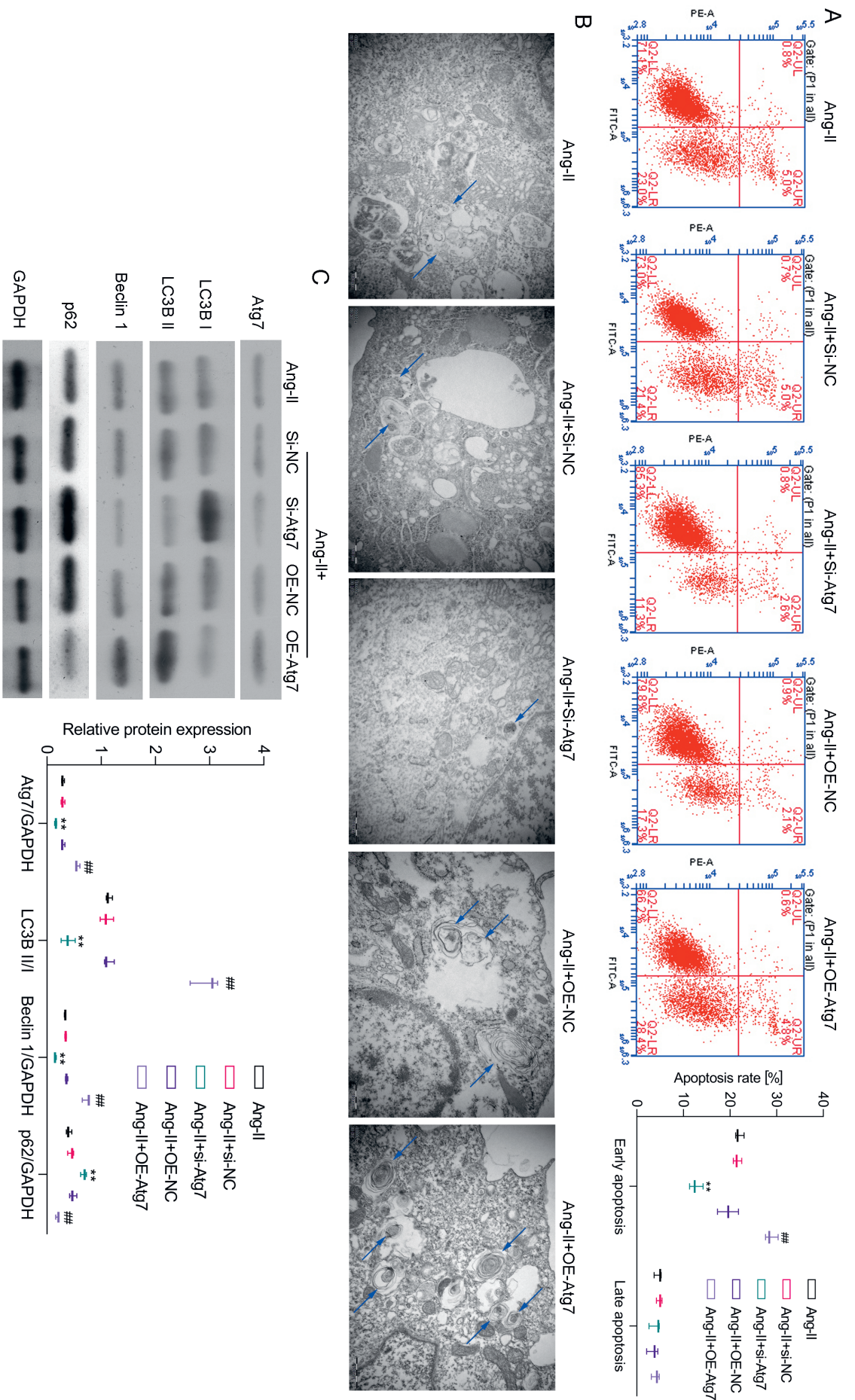


**Fig. 5.** Inhibition of Atg7 reduces cell apoptosis and autophagy in Ang-II treated vascular smooth muscle cells (VSMCs). The VSMCs were treated with Ang-II (1  $\mu$ M) and transfected with negative control (NC) siRNA (si-NC), Atg7 siRNA (si-Atg7), a control plasmid (OE-NC), or an overexpressed Atg7 (OE-Atg7) plasmid for 48 h. **A.** Annexin V staining. **\*\*** $p < 0.01$  compared to the Ang-II+si-NC group, **##** $p < 0.01$  compared to the Ang-II+OE-NC group. **B.** Transmission electron microscopy (TEM) (the blue arrow indicates autophagic vacuoles). **C.** Western blot with the indicated antibodies. **\*\*** $p < 0.01$  compared to the Ang-II+si-NC group, **##** $p < 0.01$  compared to the Ang-II+OE-NC group. Results were statistically analyzed using one-way analysis of variance (ANOVA) followed by Tukey's post hoc test

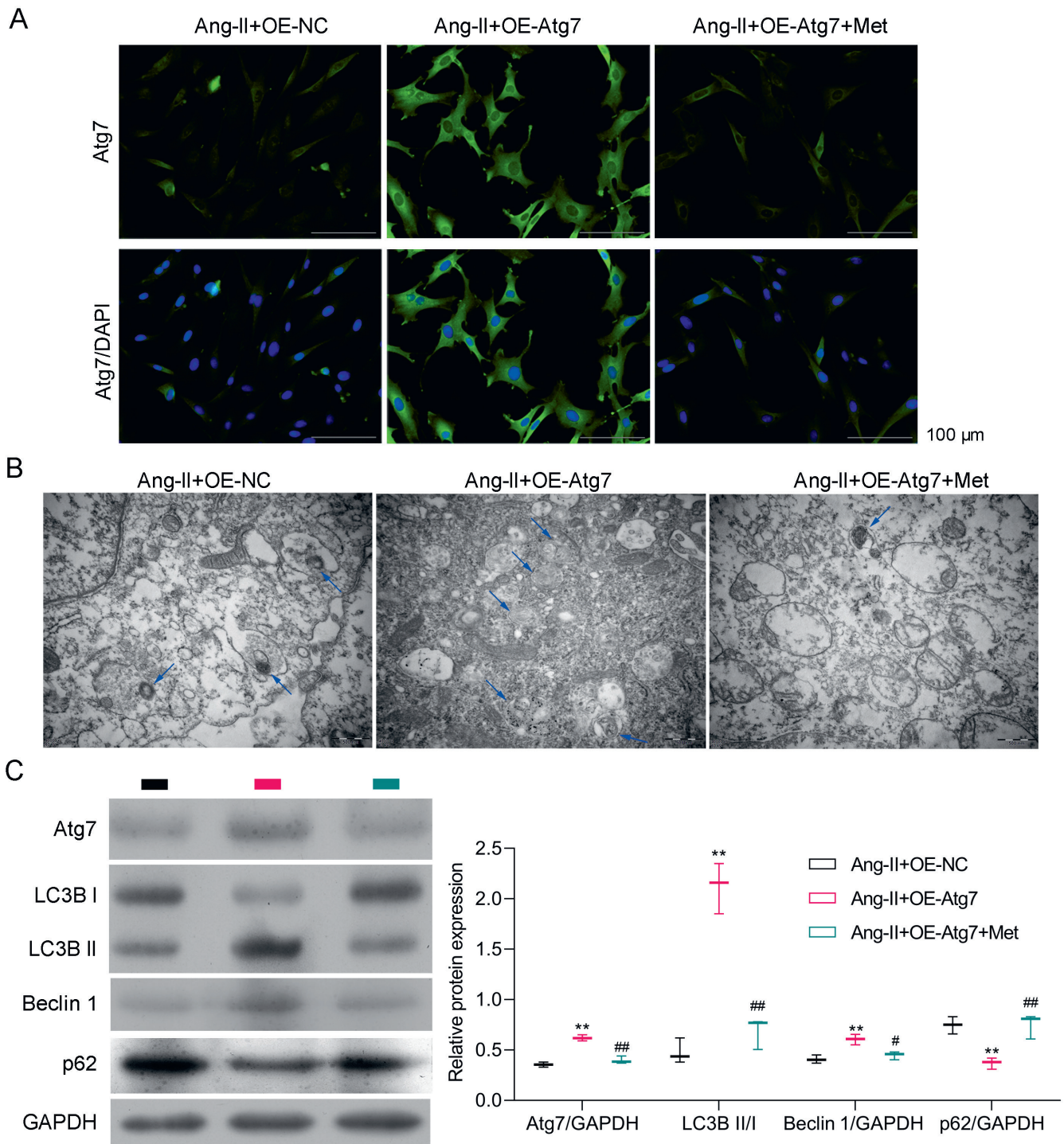


**Fig. 6.** The Atg7 mediates the inhibition of autophagy by metformin in abdominal aortic aneurysm (AAA). The vascular smooth muscle cells (VSMCs) were treated with a combination of Ang-II and metformin, and transfected with control (OE-NC) or Atg7 (OE-Atg7) overexpressed plasmids. **A.** The expression of Atg7 was evaluated using immunofluorescence (IF); **B.** Autophagic bodies and vesicles were identified using transmission electron microscopy (TEM) (the blue arrow indicates autophagic vacuoles); **C.** The expression of autophagy-related proteins was determined using western blotting. \*\* $p < 0.01$  compared to the Ang-II+OE-NC group, # $p < 0.05$ , ## $p < 0.01$  compared to the Ang-II+OE-Atg7 group. Results were statistically analyzed using one-way analysis of variance (ANOVA) followed by Tukey's post hoc test

vascular inflammation, thus aggravating AAA.<sup>11</sup> Autophagy is a multistep process that is mediated by Beclin 1, Vps34 and 2 ubiquitin-like systems, LC3 and the autophagy-related proteins.<sup>23</sup> The Atg7 functions as the E1 enzyme of the ubiquitin-proteasome system to mediate the formation of an Atg12-Atg5-Atg16 complex, which

is required for the elongation of the autophagosome.<sup>24</sup> Recent studies have revealed that atherosclerotic lesions in *ApoE*<sup>-/-</sup> mice with deleted Atg7 in VSMCs display enhanced apoptosis.<sup>12</sup> The current study provides evidence that inhibition of Atg7 suppresses cell proliferation, migration, apoptosis, and autophagy, whereas the overexpression

of Atg7 increases cell proliferation, migration, apoptosis, and autophagy. Therefore, Atg7 is an important regulator of proliferation, migration, apoptosis, and autophagy in Ang-II-treated VSMCs.

Metformin is a well-known drug that affects both metabolism and the inflammatory response, which makes it a potential therapeutic drug for several cardiovascular diseases.<sup>25</sup> Multiple studies have found that metformin significantly slows the growth of AAA<sup>13,14,26</sup> and inhibits cell growth and proliferation, leading to cell apoptosis.<sup>27</sup> Furthermore, metformin administration may be associated with a lower risk of AAA.<sup>28</sup> Recently, we demonstrated that metformin protects against Ang-II-induced AAA by activating the PI3K/AKT/mTOR/autophagy pathway.<sup>15</sup> However, the molecular mechanisms involved in these effects remained unclear. In this study, using an in vitro AAA model, it was shown that metformin reverses autophagy induced by Atg7, suggesting that metformin reduces autophagy by suppressing Atg7.

## Limitations

A relatively low number of clinical samples were examined in the current study. Clinical samples continue to be collected and will be examined for further verification. In addition, we plan to identify the molecular mechanisms of Atg7-induced autophagy in in vivo rat models and in clinical samples in future studies.


## Conclusions

In this study, it was found that Ang-II induced the expression of Atg7 and that metformin reversed this effect. The expression of Atg7 regulated cell proliferation, migration, apoptosis, and autophagy. Furthermore, Atg7 mediated the expression of autophagy-related proteins in Ang-II treated VSMCs. It was also found that metformin inhibited Atg7-induced autophagy. In conclusion, the current results revealed that the suppression of autophagy in AAA by metformin was mediated by an Atg7 central autophagy regulator. This suggests that Atg7 is a potential downstream effector of metformin in protecting against the pathophysiology of AAA.


Metformin reduces autophagy in AAA and Atg7 mediates this effect. These findings suggest that Atg7 acts as a downstream effector of metformin in suppressing the pathophysiology of AAA (Fig. 7).


## ORCID iDs


Jingjing Guo  <https://orcid.org/0000-0003-2412-8546>


Zhu Wang  <https://orcid.org/0000-0002-1753-5015>


Ming Xue  <https://orcid.org/0000-0001-6389-9314>

Lei Mi  <https://orcid.org/0000-0001-9072-3154>

Mengpeng Zhao  <https://orcid.org/0000-0001-5355-4806>

Chao Ma  <https://orcid.org/0000-0002-1602-0327>

Jian Wu  <https://orcid.org/0000-0002-2819-4498>

Xinqiang Han  <https://orcid.org/0000-0002-6224-6554>

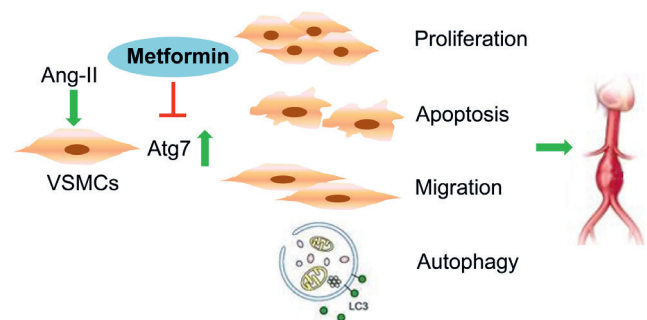


Fig. 7. Schematic diagram of the suppression of Atg7-induced cell proliferation, cell migration, cell apoptosis, and autophagy by metformin in an in vitro abdominal aortic aneurysm (AAA) model

## References

- Davis FM, Rateri DL, Daugherty A. Abdominal aortic aneurysm: Novel mechanisms and therapies. *Curr Opin Cardiol*. 2015;30(6):566–573. doi:10.1097/HCO.0000000000000216
- Anjum A, Powell JT. Is the incidence of abdominal aortic aneurysm declining in the 21<sup>st</sup> century? Mortality and hospital admissions for England & Wales and Scotland. *Eur J Vasc Endovasc Surg*. 2012;43(2):161–166. doi:10.1016/j.ejvs.2011.11.014
- Sidloff D, Stather P, Dattani N, et al. Aneurysm global epidemiology study: Public health measures can further reduce abdominal aortic aneurysm mortality. *Circulation*. 2014;129(7):747–753. doi:10.1161/CIRCULATIONAHA.113.005457
- Rowe VL, Stevens SL, Reddick TT, et al. Vascular smooth muscle cell apoptosis in aneurysmal, occlusive, and normal human aortas. *J Vasc Surg*. 2000;31(3):567–576. PMID:10709071
- Riches K, Angelini TG, Mudhar GS, et al. Exploring smooth muscle phenotype and function in a bioreactor model of abdominal aortic aneurysm. *J Transl Med*. 2013;11:208. doi:10.1186/1479-5876-11-208
- Mandhair HK, Arambasic M, Novak U, Radpour R. Molecular modulation of autophagy: New venture to target resistant cancer stem cells. *World J Stem Cells*. 2020;12(5):303–322. doi:10.4252/wjsc.v12.i5.303
- Choi AM, Ryter SW, Levine B. Autophagy in human health and disease. *N Engl J Med*. 2013;368(7):651–662. doi:10.1056/NEJMr1205406
- Shimizu S. Biological roles of alternative autophagy. *Mol Cells*. 2018;41(1):50–54. doi:10.14348/molcells.2018.2215
- Grootaert MO, da Costa Martins PA, Bitsch N, et al. Defective autophagy in vascular smooth muscle cells accelerates senescence and promotes neointima formation and atherogenesis. *Autophagy*. 2015;11(11):2014–2032. doi:10.1080/15548627.2015.1096485
- Osonoi Y, Mita T, Azuma K, et al. Defective autophagy in vascular smooth muscle cells enhances cell death and atherosclerosis. *Autophagy*. 2018;14(11):1991–2006. doi:10.1080/15548627.2018.1501132
- Ramadan A, Singh KK, Quan A, et al. Loss of vascular smooth muscle cell autophagy exacerbates angiotensin II-associated aortic remodeling. *J Vasc Surg*. 2018;68(3):859–871. doi:10.1016/j.jvs.2017.08.086
- Nahapetyan H, Moulis M, Grousset E, et al. Altered mitochondrial quality control in Atg7-deficient VSMCs promotes enhanced apoptosis and is linked to unstable atherosclerotic plaque phenotype. *Cell Death Dis*. 2019;10(2):119. doi:10.1038/s41419-019-1400-0
- Fujimura N, Xiong J, Kettler EB, et al. Metformin treatment status and abdominal aortic aneurysm disease progression. *J Vasc Surg*. 2016;64(1):46–54.e8. doi:10.1016/j.jvs.2016.02.020
- Itoga NK, Rothenberg KA, Suarez P, et al. Metformin prescription status and abdominal aortic aneurysm disease progression in the U.S. veteran population. *J Vasc Surg*. 2019;69(3):710–716.e3. doi:10.1016/j.jvs.2018.06.194
- Wang Z, Guo J, Han X, et al. Metformin represses the pathophysiology of AAA by suppressing the activation of PI3K/AKT/mTOR/autophagy pathway in ApoE(–/–) mice. *Cell Biosci*. 2019;9:68. doi:10.1186/s13578-019-0332-9
- Salmon M, Spinosa M, Zehner ZE, Upchurch GR, Ailawadi G. Klf4, Klf2, and Zfp148 activate autophagy-related genes in smooth muscle cells during aortic aneurysm formation. *Physiol Rep*. 2019;7(8):e14058. doi:10.14814/phy2.14058

17. Quintana RA, Taylor WR. Cellular mechanisms of aortic aneurysm formation. *Circ Res*. 2019;124(4):607–618. doi:10.1161/CIRCRESAHA.118.313187
18. Clement M, Chappell J, Raffort J, et al. Vascular smooth muscle cell plasticity and autophagy in dissecting aortic aneurysms. *Arterioscler Thromb Vasc Biol*. 2019;39(6):1149–1159. doi:10.1161/ATVBAHA.118.311727
19. Wang M, Li W, Chang GQ, et al. MicroRNA-21 regulates vascular smooth muscle cell function via targeting tropomyosin 1 in arteriosclerosis obliterans of lower extremities. *Arterioscler Thromb Vasc Biol*. 2011;31(9):2044–2053. doi:10.1161/ATVBAHA.111.229559
20. Gomez D, Owens GK. Smooth muscle cell phenotypic switching in atherosclerosis. *Cardiovasc Res*. 2012;95(2):156–164. doi:10.1093/cvr/cvs115
21. Mondaca-Ruff D, Riquelme JA, Quiroga C, et al. Angiotensin II-regulated autophagy is required for vascular smooth muscle cell hypertrophy. *Front Pharmacol*. 2019;9:1553. doi:10.3389/fphar.2018.01553
22. Sakalihasan N, Michel JB, Katsargyris A, et al. Abdominal aortic aneurysms. *Nat Rev Dis Primers*. 2018;4(1):34. doi:10.1038/s41572-018-0030-7
23. Yin Z, Pascual C, Klionsky DJ. Autophagy: Machinery and regulation. *Microb Cell*. 2016;3(12):588–596. doi:10.15698/mic2016.12.546
24. Mizushima N, Noda T, Yoshimori T, et al. A protein conjugation system essential for autophagy. *Nature*. 1998;395(6700):395–398. doi:10.1038/26506
25. Rena G, Lang CC. Repurposing metformin for cardiovascular disease. *Circulation*. 2018;137(5):422–424. doi:10.1161/CIRCULATIONAHA.117.031735
26. Golledge J, Moxon J, Pinchbeck J, et al. Association between metformin prescription and growth rates of abdominal aortic aneurysms. *Br J Surg*. 2017;104(11):1486–1493. doi:10.1002/bjs.10587
27. Ben Sahra I, Regazzetti C, Robert G, et al. Metformin, independent of AMPK, induces mTOR inhibition and cell-cycle arrest through REDD1. *Cancer Res*. 2011;71(13):4366–4372. doi:10.1158/0008-5472.CAN-10-1769
28. Yu X, Jiang D, Wang J, et al. Metformin prescription and aortic aneurysm: Systematic review and meta-analysis. *Heart*. 2019;105(17):1351–1357. doi:10.1136/heartjnl-2018-314639





# Molecular epidemiological analysis of integron gene cassettes and *tetA/tetB/tetD* gene associations in *Escherichia coli* strains producing extended-spectrum $\beta$ -lactamase (ESBL) in urine cultures

Ayşegül Çopur Çiçek<sup>1,A,B,D,F</sup>, Vicdan Şemen<sup>2,B,C</sup>, Nebahat Aydoğan Ejder<sup>1,C</sup>, Deniz Zehra Ulusan Gündoğdu<sup>4,B,D,E</sup>, Sema Koçyiğit Kalcan<sup>3,A,D,E</sup>, Fatma Tufan Köse<sup>4,B,C</sup>, Osman Birol Özgümüş<sup>1,D,E</sup>

<sup>1</sup> Department of Medical Microbiology, Faculty of Medicine, Recep Tayyip Erdoğan University, Rize, Turkey

<sup>2</sup> Microbiology Laboratory, Sakarya Yenikent State Hospital, Turkey

<sup>3</sup> Laboratory of Microbiology, Rize State Hospital, Turkey

<sup>4</sup> Department of Microbiology, Rize Education and Research Hospital, Turkey

A – research concept and design; B – collection and/or assembly of data; C – data analysis and interpretation;

D – writing the article; E – critical revision of the article; F – final approval of the article

Advances in Clinical and Experimental Medicine, ISSN 1899–5276 (print), ISSN 2451–2680 (online)

Adv Clin Exp Med. 2022;31(1):71–79

## Address for correspondence

Ayşegül Çopur Çiçek  
E-mail: acopurcicek@gmail.com

## Funding sources

None declared

## Conflict of interest

None declared

## Acknowledgements

We thank Prof. Dr. Barış Ötlü for his contribution to dendrogram analyses.

Received on May 10, 2021

Reviewed on August 10, 2021

Accepted on September 16, 2021

Published online on October 27, 2021

## Cite as

Çopur Çiçek A, Şemen V, Aydoğan Ejder N, et al. Molecular epidemiological analysis of integron gene cassettes and *tetA/tetB/tetD* gene associations in *Escherichia coli* strains producing extended-spectrum  $\beta$ -lactamase (ESBL) in urine cultures. *Adv Clin Exp Med*. 2022;31(1):71–79. doi:10.17219/acem/142333

## DOI

10.17219/acem/142333

## Copyright

© 2022 by Wrocław Medical University

This is an article distributed under the terms of the Creative Commons Attribution 3.0 Unported (CC BY 3.0) (<https://creativecommons.org/licenses/by/3.0/>)

## Abstract

**Background.** Epidemiological studies of tetracycline (TE) resistance genes and integron gene cassettes, particularly in urine samples, are limited in Turkey.

**Objectives.** To investigate antibiotic susceptibility profiles, extended-spectrum beta-lactamase (ESBL) positivity, *tet* gene types, class-I/II integron gene cassettes, and clonal relationships among *tet*-resistant isolates of *Escherichia coli* from urine cultures of outpatients.

**Materials and methods.** Isolates were identified using conventional methods and the automated Vitek® 2 Compact system. Antimicrobial susceptibility was performed for 19 antibiotics. The ESBL production was performed using the Kirby–Bauer disk diffusion test. The double disk synergy test was used for confirmatory testing. Polymerase chain reaction (PCR) was used to determine the presence of class-I/II integron gene cassettes and *tetA*, *tetB* and *tetD* resistance genes. The pulsed-field gel electrophoresis typing was performed to identify clonal relations.

**Results.** A total of 121 isolates were obtained and found to be resistant or sensitive to ampicillin and amikacin/imipenem. Resistance to ceftazidime, cefotaxime and ceftriaxone was determined to be 31.3%, 77.6% and 83.1%, respectively. Tetracycline resistance was detected in 82 isolates, mostly caused by the *tetB* gene. No *tet* gene was detected in the remaining 39 isolates. Although 64 out of 82 isolates carried a class-I integron, only 4 had a class-II integron (with sizes of 800–2900 base pairs). Furthermore, *tet* genes were identified with different size class-I integron gene cassettes. However, *tet* genes were not detected in any isolate identified with integron gene cassette II. Clonally, the isolates were found to be related in subgroups because they were community-acquired.

**Conclusions.** This study showed that the *tetB* gene is most commonly found in *E. coli* isolates grown in urine samples from the Turkish population.

**Key words:** *E. coli*, PFGE, tetracycline resistance, ESBL, integron gene cassettes

## Background

Urinary tract infections (UTIs) are usually caused by Gram-negative Enterobacteriales, with the most common pathogens being *Escherichia coli* and *Klebsiella pneumoniae* spp.<sup>1,2</sup> Antimicrobial resistance is increasing among uropathogens and the production of  $\beta$ -lactamases is a major resistance mechanism.<sup>3</sup>

Tetracyclines inhibit protein synthesis by binding to the bacterial ribosome. At present, the prevalence of tetracycline (TE) resistance is increasing in bacteria isolated from both, human patients<sup>4,5</sup> and animals.<sup>6</sup> Resistance is widely disseminated in *E. coli* through TE resistance genes, such as *tetA*.<sup>7</sup> A previous study found that the prevalence of TE resistance in *E. coli* isolates from humans increased by 0.45% per year from 1950 to 2001.<sup>5</sup> Because of the spread of TE resistance, the use of tetracyclines in humans has gradually decreased. However, tetracyclines remain among the most used antibiotics in livestock production worldwide.<sup>8</sup>

Different TE resistance determinants have been demonstrated. They have been classified as A–E classes, being the most frequently detected genes among the Enterobacteriales family.<sup>9</sup> Tetracycline resistance genes (*tet* genes) are divided into 11 classes that comprise more than 40 genes.<sup>10–12</sup> Studies from the USA have shown that *tetA* is the 2<sup>nd</sup> most frequent TE resistance efflux pump in both, human and animal isolates.<sup>13</sup> In Denmark, *tetA* is also the most common TE efflux pump type found in clinical isolates of *E. coli*.<sup>14</sup>

Integrons are genetic elements that encode antibiotic resistance determinants and have the ability to integrate or transport certain genes. They can also be transferred from one bacterium to another, as they are carried by plasmids or transposons. This causes a strong antibiotic selective pressure resulting from the transfer and spread of antibiotic resistance elements.<sup>15,16</sup>

The rapid spread of TE resistance among bacteria is due to the localization of *tet* genes on movable genetic structures such as plasmids, transposons and integrons. However, there are scarcely any studies showing the relationships between the main *tet* genes and integrons.

## Objectives

The present study aimed to screen the *tetA*, *B* and *D* genes together with class 1 and 2 integron gene cassettes from 121 extended-spectrum  $\beta$ -lactamase (ESBL)-positive *E. coli* isolates, obtained from the urine cultures of adults. Additional aims were to determine the molecular sizes and classes of the detected integrons and the clonal relationship with pulsed-field gel electrophoresis (PFGE) among the TE resistance isolates. Studying integron gene cassettes and related resistance phenotypes will provide

important information about the mechanisms of the acquisition of multiple antibiotic resistance genes in clinical isolates, which then can be used to effectively guide clinical treatment.

## Materials and methods

### Ethical approval

The study protocol was approved by the Faculty of Medicine Non-invasive Studies Ethics Committee, Recep Tayyip Erdoğan University, Turkey (approval No. 40465587-050.01.04-14 and No. 2021/13), and the Rize Provincial Health Directorate (Ref. No. 64247179-799).

### Sample collection and bacterial isolation/identification

*Escherichia coli* isolates were obtained from urine samples collected at 7 different clinics (infectious diseases, urology, internal medicine, emergency service, nephrology, neurology, and gynecology) between June 2017 and June 2018. All urine samples were obtained from outpatient adults aged 18–83 years. Since TE is not used in pediatric patients, the pediatric age group was not included in this study. The clinical data of the patients were retrospectively obtained from medical records and medical tables.

Samples were sent to a microbiology laboratory (Rize State Hospital, Rize, Turkey) for analysis. Clinical specimens were plated on eosin methylene blue (EMB)/MacConkey agar for isolation. The isolates were identified using conventional methods and the automated Vitek® 2 Compact system (BioMérieux, Marcy-l'Étoile, France).

### Antimicrobial susceptibility testing

Antimicrobial susceptibility experiments were performed in accordance with the Clinical and Laboratory Standards Institute (CLSI) criteria<sup>17</sup> using both the Kirby–Bauer disk diffusion method and the automated Vitek® 2 Compact system (BioMérieux). Sensitivity to the following antibiotics was tested: ampicillin (AMP), ampicillin/sulbactam (AMP/SAM), amoxicillin/clavulanic acid (AMC), cefazolin (KZ), cefotaxime (CTX), cefuroxime (CXM), cefixime (CFM), ceftriaxone (CRO), ceftazidime (CAZ), amikacin (AK), gentamicin (CN), tobramycin (TOB), ciprofloxacin (CIP), norfloxacin (NOR), imipenem (IPM), aztreonam (ATM), nitrofurantoin (F), trimethoprim/sulfamethoxazole (TMP/SXT), and tetracycline (TE). The *E. coli* ATCC 25922 (American Type Cell Culture (ATCC), Manassas, USA) was used as the quality control strain.<sup>18</sup> Categorical variables are expressed in terms of frequency (n) and percentage (%).

## Screening of extended-spectrum $\beta$ -lactamase production

All isolates were screened for extended-spectrum  $\beta$ -lactamase (ESBL) production with the Kirby–Bauer disk diffusion test using 3 indicator cephalosporins, namely ceftazidime (30  $\mu$ g), cefotaxime (30  $\mu$ g), and ceftriaxone (30  $\mu$ g). The test was performed by inoculation on a Mueller–Hinton agar plate (Merck, Darmstadt, Germany) with a sample of the tested strain. The isolates were considered to be resistant if the diameter of the inhibition zone for ceftazidime, cefotaxime or ceftriaxone was  $\leq 22$  mm,  $\leq 27$  mm or  $\leq 25$  mm, respectively, after 18-h incubation at 37°C.<sup>18,19</sup>

## Confirmation of ESBL-producing isolates

All *E. coli* isolates showing resistance to any of the 3 cephalosporins were then subjected to confirmatory testing using the double disk synergy test (DDST), according to the 2019 CLSI guidelines.<sup>18</sup> Ceftazidime (30  $\mu$ g), cefotaxime (30  $\mu$ g), ceftriaxone (30  $\mu$ g), and amoxicillin-clavulanic acid (20/10  $\mu$ g) were used for ESBL detection. Amoxicillin/clavulanic acid and cephalosporin disks were placed at a distance of 20 mm from the center on lawn cultures on Muller–Hinton agar plates. The plates were incubated at 37°C overnight for 24 h. The zone of inhibition of cephalosporins towards the amoxicillin/clavulanic acid disk was considered to be a positive result and the isolates were interpreted as ESBL producers. *Escherichia coli* ATCC 25922 was used as the control.<sup>18–20</sup>

## Detection of integron gene cassettes and *tet* genes

The presence of integron gene cassettes and *tet* genes was investigated with polymerase chain reaction (PCR) method (Table 1). To obtain template DNA, single colony bacterial strains were inoculated in 3 mL of Luria–Bertani (LB) broth medium (1% tryptone, 0.5% yeast extract, 0.5% NaCl, pH 7.4) at 37°C for 16 h at 200 rpm. Next, 1.5 mL

of the grown culture was used to obtain total genomic DNA using the boiling method. For PCR testing, 3  $\mu$ L of the supernatant was used as the template DNA. The PCR was performed using the compositions and cycling parameters detailed in Table 1. The amplification products were then run in 1.2% agarose gel with a 100 base pair (bp) molecular marker (Thermo Fisher Scientific, Waltham, USA) and visualized with UV light. The oligonucleotides used in PCR testing are listed in Table 1.

## Molecular typing of *tetA*-, *tetB*-, and *tetD*-positive isolates

The PFGE typing was performed to identify the clonal relations among 46 isolates coding *tetA*, *tetB* and *tetD*. Isolation and deproteinization of genomic DNA were performed following a previously reported protocol with minor modifications.<sup>25</sup> Briefly, *E. coli* colonies on Mueller–Hinton agar were suspended in 1 mL of cell suspension solution (CSS) (100 mL of Tris-HCl, 100 mL of ethylenediaminetetraacetic acid (EDTA) pH 8.0) and optical density (OD) was adjusted to 0.8 (590 nm). The cells were embedded in low (2%) melting agarose. Molds were prepared with the help of agarose and refrigerated at 4°C for 10 min. The prepared strain molds were mixed with cell lysis solution-1 (CLS-1) (50 mm Tris-HCl, 50 mm EDTA, pH 8.0, 2.5 mg/mL lysozyme, 1.5 mg/mL proteinase K) and incubated at 37°C for 1 h in a water bath. At the end of the period, CLS-1 was removed. The cell lysis solution-2 (CLS-2; 0.5 M EDTA, 1% sarcosyl, 400  $\mu$ g/mL proteinase K) was placed on molds and incubated in a water bath at 55°C for 2 h. After the lysis step, the molds were washed 3 times, each with dH<sub>2</sub>O and 1  $\times$  TE (Tris-EDTA). After digestion of the cells and washing of the plugs, genomic DNA in the agarose plugs was restricted with 10 U of XbaI (Thermo Fisher Scientific) for 3 h at 37°C in an incubator. The DNA fragments were separated on 1% pulse-field certified agarose (Bio-Rad Laboratories, Nazareth, Belgium) gels run in 0.5  $\times$  Tris-borate-EDTA buffer (44.5 mM/L Tris, 44.5 mM/L boric acid, 1 mM/L EDTA (pH 8.0)) using a CHEF-DR II system (Bio-Rad Laboratories). The electrophoresis conditions

Table 1. Primers used in the amplification of *tet* genes and integron gene cassettes

Primer name	Target gene	Primer sequence (5'→3')	Amplicon size [bp]
<i>tet</i> (A)-1 <i>tet</i> (A)-2	<i>tetA</i>	5'-GTAATTCTGAGCACTGTCCG-3' 5'-CTGCCTGGACAACATTGCTT-3'	917 <sup>21</sup>
<i>tet</i> (B)-1 <i>tet</i> (B)-2	<i>tetB</i>	5'-CTCAGTATTCCAAGCCTTTG-3' 5'-ACTCCCCGTGAGCTTGAGGGG-3'	396 <sup>21</sup>
<i>tet</i> (D)-1 <i>tet</i> (D)-2	<i>tetD</i>	5'-AAACCATTACGGCATTCTGC-3' 5'-GACCGGATACCCATCCATC-3'	787 <sup>22</sup>
5'-CS 3'-CS	class-I integron	5'-GGCATCCAAGCAGCAAG-3' 5'-AAGCAGACTTGACCTGA-3'	variable <sup>23</sup>
hep51 hep74	class-II integron	5'-GATGCCATCGCAAGTACGAG-3' 5'-CGGGATCCCGGACGGATGCACGATTTGTA-3'	variable <sup>24</sup>

were 14°C at 6 V/cm<sup>2</sup> for 18 h. The initial and final switch times were 5 s and 20 s, respectively. The gel was stained with ethidium bromide (5 mg/mL) for 30 min and photographed under ultraviolet (UV) light. The DNA band profiles were analyzed using GelCompar software v. 3.0 (Applied Maths, Sint-Martens-Latem, Belgium). According to the interpretative criteria of Tenover et al., the clinical isolates were aligned according to the PFGE profiles, with profiles sharing 100% similarity grouped in clusters.<sup>26</sup>

## Results

A total of 121 ESBL-positive *E. coli* isolates were obtained from the outpatients' urine samples. These strains were biochemically characterized using an automated system, and subjected to antibiotic susceptibility testing, ESBL screening and phenotype confirmation tests. All isolates were tested for susceptibility to 19 antimicrobials. The frequency of resistance to each of the tested antibiotics is shown in Table 2.

Antibiograms showed that 121 (100%) isolates were resistant and sensitive to ampicillin and amikacin/imipenem, respectively. Although there was 100% resistance to ampicillin, ampicillin/sulbactam resistance was found to be 33.8%. This showed the rate of resistance against inhibitors in the isolates. Similarly, for the amoxicillin/clavulanic acid combination, the rate of resistance to the inhibitor was 12.2%. In the ESBL screening test, resistance to ceftazidime,

**Table 2.** Antimicrobial susceptibility ratio (%) of clinical *Escherichia coli* isolates (n = 121)

Antibiotic	R	I	S
Ampicillin	100	0	0
Ampicillin/sulbactam	33.8	27.7	38.5
Amoxicillin/clavulanic acid	12.2	59.2	28.6
Cefazolin	87.7	1.5	10.8
Cefotaxime	77.6	0	22.4
Cefuroxime	87.5	0	12.5
Cefixim	87.5	6.3	6.3
Ceftriaxone	83.1	0	16.9
Ceftazidime	31.3	18.8	50
Amikacin	0	0	100
Gentamicin	44.6	0	55.4
Tobramycin	46.9	10.2	42.9
Ciprofloxacin	56.9	0	43.1
Imipenem	0	0	100
Norfloxacin	56.9	0	43.1
Aztreonam	61.5	6.2	32.3
Nitrofurantoin	7.7	4.6	87.7
Trimethoprim/sulfamethoxazole	70.8	0	29.2
Tetracycline	67.7	0	32.3

R – resistant; I – medium sensitive; S – sensitive.

cefotaxime and ceftriaxone was determined to be 31.3%, 77.6% and 83.1%, respectively. All ESBL-producing strains were determined to be susceptible to amikacin and imipenem. This result is important in terms of showing that there is no resistance to these antibiotics in outpatients. After amikacin and imipenem, the highest sensitivity was observed for nitrofurantoin. Tetracycline resistance was determined in 82 isolates (67.7%).

Among ESBL-producing *E. coli* isolates, those with TE resistance were selected and the presence of *tet* genes responsible for resistance and class-I/-II gene cassettes responsible for transferable resistance was investigated (Table 3). Among these samples (n = 46), *tetA*, *tetD* and *tetB*, which are responsible for TE resistance, were detected in 12, 4 and 30 isolates, respectively. This result showed that TE resistance in clinical *E. coli* samples was mostly caused by the *tetB* resistance gene. No *tet* genes were detected in the remaining 36 isolates. The integron gene cassettes were isolated in a total of 68 samples (class-I integron: n = 64; class-II integron: n = 4). The largest integron gene cassette was determined as approx. 2900 bp, while the smallest integron gene cassette was determined as 800 bp. The average integron gene cassette size was around 1600 bp. The *tet* genes were identified together with different size class-I gene cassettes. However, the same was not true for the integron class-II gene cassettes: they were detected in 4 samples, but none of the *tetA*, *tetB* and *tetD* genes were detected. This result showed that TE resistance developed in isolates carrying class-II gene cassettes by a mechanism different from these 3 genes. The dendrogram was basically divided into 2 different clades. One clade consisted of 1 *tetD*-positive and 12 *tetB*-positive isolates. In the other clade, *tetA*, *tetB* and *tetD* were located together in different arms (Fig. 1).

## Discussion

*Escherichia coli* isolates are present in normal human fecal flora, and some strains are the most common cause of UTIs. Antimicrobial therapy is very important in the treatment of UTIs. However, the drug resistance generated specifically by ESBL-producing microorganisms results in failure in the treatment of UTIs. In the present study, ESBL production was observed to be high in *E. coli* isolates obtained from outpatients with symptomatic UTI and 121 of them exhibited resistance to at least 1 of the 3 indicator cephalosporins and identified as ESBL producers. Furthermore, 82 of the ESBL-positive isolates were TE-resistant and *tet* genes (A, B and D types) were determined in 46 of these isolates. These 3 *tet* genes are associated with TE efflux in Gram-negative bacilli and have been previously detected in TE-resistant *E. coli* isolates.<sup>27</sup> In addition, in UTIs, the *tetD* gene was present at the lowest rate while the *tetB* gene was present at the highest rate; notably, they did not occur together in any strain. We failed to detect

**Table 3.** Antimicrobial resistance patterns and integron gene cassettes of tetracycline-positive *Escherichia coli* clinical isolates (n = 82)

Strain No.	Unit	R type	Integron [~bp]	tet type
1	NP	CRO, CXM, CFM, KZ, SAM, AMP, SXT	900	A
2	NR	CRO, CXM, CFM, KZ, CIP, NOR, AMP, SXT	1600	A
3	NG	CRO, CXM, CFM, KZ, CIP, NOR, AMP, SXT	1600	A
4	IM	CRO, CXM, CFM, KZ, CIP, SAM, NOR, AMP, SXT	1600	–
5	UC	CRO, CXM, CFM, KZ, CN, CIP, NOR, AMP, SXT	1700	–
6	NG	CXM, CN, CIP, SAM, NOR, AMP	1700	B
7	NG	AMP	800	A
8	IM	CXM, AMP	800	B
9	UC	CXM, KZ, CIP, NOR, AMP, SXT	1700	A
10	IM	ATM, CRO, CXM, CFM, KZ, CN, CIP, SAM, NOR, AMP, SXT	1700	A
11	IDS	ATM, CTX, CRO, AMP, SXT	2100	B
12	UC	CN, CIP, NOR, AMP, SXT	1800	–
13	NG	ATM, CXM, CFM, KZ, CIP, SAM, NOR, AMP, SXT	2900	A
14	NG	ATM, CTX, CRO, SAM, AMP, SXT	1200	–
15	UC	ATM, CTX, CRO, CN, SAM, AMP, SXT	1000	–
16	IM	CRO, CXM, CN, CIP, NOR, AMP, SXT	800	B
17	NG	CIP, SAM, NOR, AMP, SXT	1600	B
18	IM	CIP, NOR, AMP, SXT	1600	B
19	IM	CRO, CXM, AMP, SXT	1500	B
20	UC	CRO, CXM, CFM, KZ, CIP, SAM, NOR, AMP, SXT	1500	A
21	UC	ATM, CAZ, CRO, CXM, CFM, KZ, CN, CIP, SAM, NOR, AMP, SXT	1500	–
22	NG	CXM, CFM, KZ, CIP, SAM, NOR, AMP, SXT	1500	A
23	NG	CTX, CRO, AMC, AMP, SXT	2100	A
25	IM	CRO, CXM, CFM, KZ, CIP, NOR, AMP, SXT	1600	D
26	IM	CTX, CRO, AMC, AMP	1200	–
27	IM	CRO, CXM, AMP, SXT	900	–
28	IM	CN, CIP, NOR, AMP, SXT	1600	A
29	IM	ATM, CRO, CXM, CFM, KZ, CN, CIP, NOR, AMP, SXT	1600	A
30	UC	CTX, CRO, AMC, SAM, AMP, SXT	1600	–
30	ES	ATM, CRO, CXM, CFM, KZ, CIP, SAM, NOR, AMP, SXT	1600	B
31	UC	ATM, CAZ, CRO, CXM, CFM, KZ, CN, CIP, SAM, NOR, AMP, SXT	1600	–
32	IM	ATM, CAZ, CRO, CXM, CFM, KZ, CN, CIP, SAM, NOR, SXT, AMP	1600	B
33	ES	ATM, CAZ, CRO, CXM, CFM, KZ, CN, CIP, SAM, NOR, SXT, AMP	1600	B
34	UC	ATM, CAZ, CRO, CXM, CFM, KZ, CIP, SAM, NOR, AMP, SXT	1100	B
35	UC	ATM, CAZ, CRO, KZ, CIP, SAM, NOR, AMP	1500	B
36	UC	ATM, CAZ, CRO, CXM, KZ, CN, SAM, AMP, SXT	1600	B
37	IM	ATM, CAZ, CRO, CXM, CFM, KZ, CN, SAM, AMP, SXT	1600	B
38	IDS	CTX, CRO, AMC, KZ, SAM, AMP, SXT	1600	B
39	IDS	KZ, CIP, SAM, NOR, AMP, SXT	1600	–
40	ES	CTX, CRO, AMC, ATM, CAZ, AMP	1000	–
41	UC	CTX, CRO, AMC, KZ, SAM, AMP	1000	D
42	UC	AMP, SXT	2200	–
43	IDS	CTX, CRO, AMC, AMP, SXT	2000	–
44	IM	ATM, CTX, CRO, AMP, SXT	2200	–
45	IM	CRO, CXM, AMP, SXT	1000	–
46	IM	ATM, CTX, CRO, AMP, SXT	1000	–
47	IDS	CTX, CRO, AMC, AMP, SXT	1600	–

**Table 3.** Antimicrobial resistance patterns and integron gene cassettes of tetracycline-positive *Escherichia coli* clinical isolates (n = 82) – cont.

Strain No.	Unit	R type	Integron [~bp]	<i>tet</i> type
48	NG	CIP, SAM, NOR, AMP	2000	B
49	IDS	ATM, CAZ, CRO, CXM, CFM, KZ, CN, CIP, SAM, NOR, AMP, SXT	1600	–
50	IM	CRO, CXM, CFM, KZ, SAM, AMP, SXT	2200	D
51	NG	ATM, CRO, CXM, CFM, KZ, AMP, SXT	1600	–
52	NG	CN, CIP, SAM, NOR, AMP, SXT	2000	B
53	IDS	ATM, CTX, CRO, AMP, SXT	1800	B
54	NG	ATM, CAZ, CRO, CXM, CFM, KZ, CN, CIP, SAM, NOR, AMP, SXT	1800	–
55	NG	ATM, CAZ, CRO, CXM, CFM, KZ, CN, CIP, NOR, AMP, SXT	1900	B
56	IM	ATM, CAZ, CRO, CXM, CFM, KZ, CN, CIP, SAM, NOR, AMP, SXT	1800	B
57	NP	ATM, CAZ, AMP	1800	B
58	NP	ATM, CAZ, CRO, CN, AMP, SXT	1800	–
59	IDS	ATM, CAZ, CRO, CXM, CFM, KZ, CN, CIP, SAM, NOR, AMP, SXT	1800	–
60	UC	CTX, CRO, AMC, CN, AMP, SXT	1600	B
61	IM	CN, CIP, NOR, AMP, SXT	1600	–
62	UC	CRO, CXM, CFM, KZ, CIP, SAM, NOR, AMP, SXT	2000	–
63	IM	CRO, CXM, CFM, KZ, SAM, AMP, SXT	2200	D
64	UC	ATM, CAZ, CRO, CXM, CFM, KZ, CN, CIP, SAM, NOR, AMP, SXT	1800	–
65	IM	ATM, CAZ, CRO, CXM, CFM, KZ, CN, CIP, NOR, AMP, SXT,	1800	B
66	NP	ATM, CAZ, CRO, CXM, CFM, KZ, CN, CIP, SAM, NOR, AMP, SXT	1900	B
67	NP	AMP, SXT	1900	B
68	IDS	ATM, CAZ, CN, AMP, SXT	2000p	B
69	NG	AMP, SXT	–	B
70	IDS	KZ, CIP, SAM, NOR, F, AMP, SXT	–	–
71	NG	ATM, CRO, CXM, CFM, KZ, CN, CIP, NOR, F, AMP, SXT	–	B
72	NG	AMP, SXT	–	B
73	IM	ATM, CAZ, AMP, SXT	–	–
74	UC	ATM, CAZ, AMP, SXT	–	–
75	IM	CIP, NOR, AMP	–	B
76	ES	ATM, CRO, CXM, CFM, KZ, CN, CIP, NOR, AMP, SXT	–	–
77	IM	CIP, NOR, AMP, SXT	–	–
78	UC	KZ, SAM, AMP	–	–
79	ES	ATM, CAZ, CRO, CXM, CFM, KZ, CN, AMP, SXT	–	–
80	ES	SAM, AMP, SXT	–	–
81	IDS	CRO, CXM, CFM, AMP, SXT	–	–
82	IM	AMP, SXT	–	–

IDS – Infectious Diseases Service; UC – urology clinic; IM – internal medicine; ES – emergency service; NP – nephrology; NR – neurology; NG – gynecology; AMP – ampicillin; SAM – sulbactam; KZ – ceftazidime; CTX – cefotaxime; CXM – cefuroxime; CFM – cefixime; CRO – ceftazidime; CAZ – ceftazidime; CIP – ciprofloxacin; NOR – norfloxacin; ATM – aztreonam; SXT – sulfamethoxazole; CN – gentamicin.

\* tetracycline (TE) is not shown in the table because all isolates were TE-resistant. While isolates 26, 44, 46, and 47 harbored class-II integron gene cassettes, class-I gene cassettes were found in the rest of the isolates.

the *tet* gene in the remaining 39 TE-resistant isolates. However, these isolates may have harbored another resistance mechanism, i.e., different *tet* genes besides *tetA*, *tetB* and *tetD*, or enzymatic alteration or ribosomal protection.<sup>28</sup> Ribosomal protection has been demonstrated as another mechanism of resistance to TE in the Enterobacteriales family that is mediated by different *tet* genes.<sup>29</sup> Both *tetA*

and *tetB* genes encode efflux mechanisms to confer resistance to tetracyclines, and have been previously identified as the most common TE resistance genes in *E. coli* of both, human and animal origin.<sup>30</sup> It has also been reported that *tetB* provides additional resistance against doxycycline, in contrast to *tetA* which confers resistance against TE, oxytetracycline and chlortetracycline.<sup>9</sup>

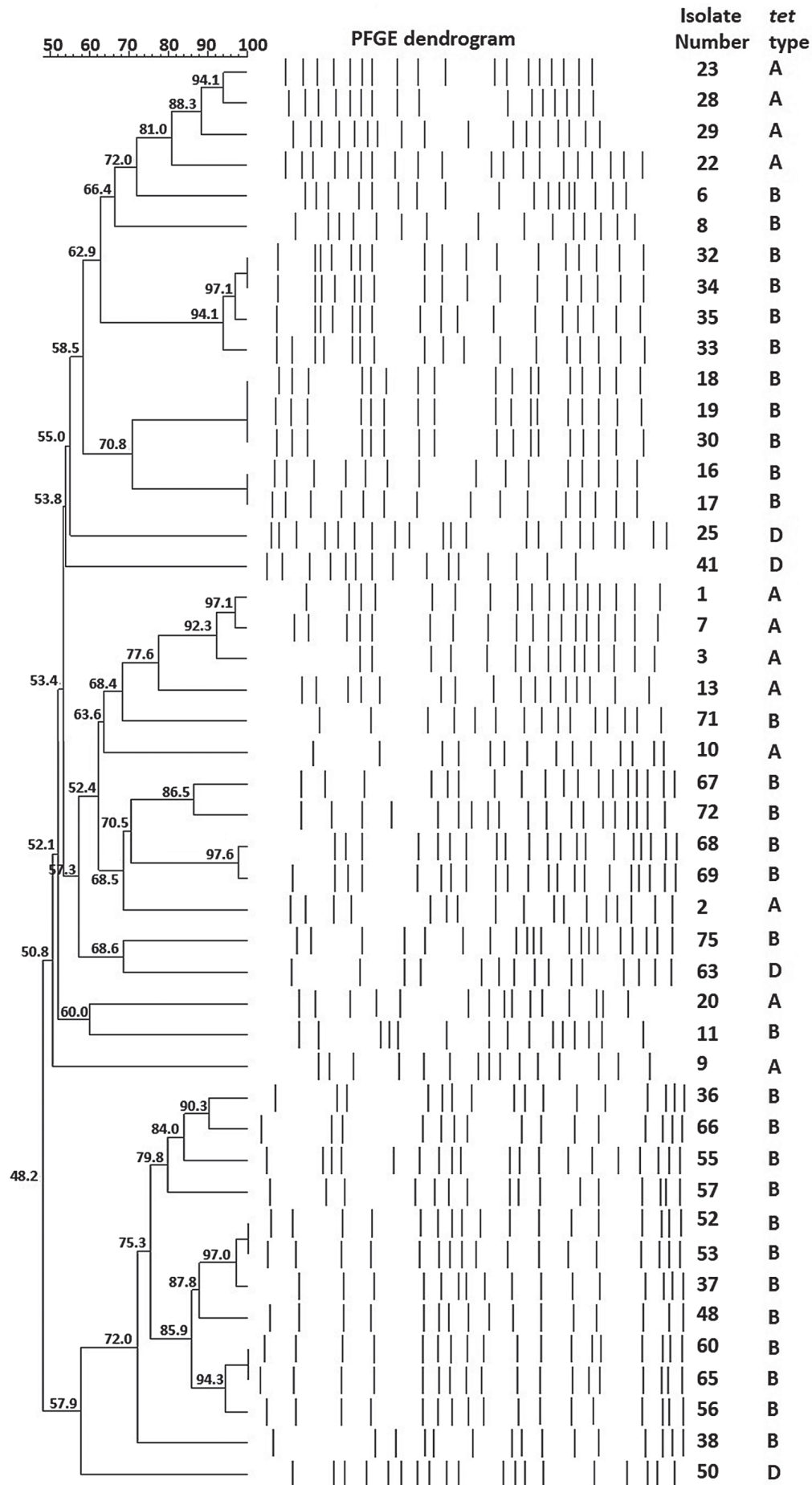


Fig. 1. Pulsed-field gel electrophoresis (PFGE) analysis of *Escherichia coli* isolates generated 3 major clusters (A, B and C) based on tetracycline (TE) resistance coding genes

The majority of ESBL positivity and *tet* resistance is associated with conjugative or mobilizable elements, which partially explains their wide distribution in bacterial species. Gram-negative efflux determinants are normally found in transposons inserted into a diverse group of plasmids from a variety of incompatibility groups. These plasmids may carry multiple antibiotic resistance genes, which confer resistance to various antibiotic families.<sup>27</sup> Integrons cause the spread of antimicrobial drug resistance. Although the transport of ESBL and TE resistance on integrons was not investigated in this study, the high rate of integron gene cassette carriers has made us consider the possibility of transferring genes responsible for ESBL resistance. Tetracycline resistance genes may also be carried together with other antibiotic resistance genes by plasmids harbored integron gene cassettes. A selective advantage for resistance genes carried on the plasmid may enhance the persistence of plasmid-bearing strains in an environment contaminated with antimicrobial compounds. Effective expression of *tet* genes in the Enterobacteriaceae family could result in high levels of resistance to TE. We are of the opinion that this may be an important risk factor in the treatment of human infectious diseases caused by these microorganisms.

In our study, since *E. coli* isolates are community-acquired samples, they were not expected to be highly similar clonally. The PFGE was found to be effective for distinguishing isolates from each other only in subgroups according to *tet* type. Furthermore, it has been observed that PFGE grouped the isolates according to other genomic factors, rather than by the antibiotic resistance profile of isolates. For example, *tetD*-positive strains were co-resistant to CRO but they grouped in the different clades. Besides this, isolates No. 50 and 63 have exactly the same antibiotic profile but they were located on different branches, which also supports the notion that PFGE is independent of the resistance profile.

## Limitations








Our study has 2 main limitations. Firstly, it is not a multi-institutional study. Secondly, base sequence analysis of integrons could not be performed due to limited funding.

## Conclusions

In summary, this is one of limited studies investigating the coexistence of *tet* genes and integron gene cassettes of *E. coli* isolates, obtained from urine samples in Turkey. The results provide data on the coexistence of integrons and *tet* genes in *E. coli* strains isolated from the outpatients. Studying integron gene cassettes and related resistance phenotypes can provide important information about the mechanisms of acquisition of multiple antibiotic resistance genes in clinical isolates. It can be argued that uncontrolled broad-spectrum antibiotic use may be

the main reason for the development and increase of resistance. Furthermore, high rates of resistance may lead to a trend towards new alternatives or antibiotics that were used extensively in the past, but their use has decreased in recent years. Comprehensive studies are needed to better examine the relationship between antibiotic resistance and integron gene cassettes together with epidemiological data.

## ORCID iDs

Ayşegül Çopur Çiçek  <https://orcid.org/0000-0002-3673-9670>  
 Vicdan Şemen  <https://orcid.org/0000-0002-1540-7968>  
 Nebahat Aydoğan Ejder  <https://orcid.org/0000-0001-9557-2033>  
 Deniz Zehra Uluşan Gündoğdu  <https://orcid.org/0000-0003-1839-3060>  
 Sema Koçyiğit Kalcan  <https://orcid.org/0000-0003-2933-4197>  
 Fatma Tufan Köse  <https://orcid.org/0000-0001-5598-5589>  
 Osman Birol Özgümüş  <https://orcid.org/0000-0002-9550-1646>

## References

1. Stultz JS, Doern CD, Godbout E. Antibiotic resistance in pediatric urinary tract infections. *Curr Infect Dis Rep.* 2016;18(2):40. doi:10.1007/s11908-016-0555-4
2. Han SB, Lee SC, Lee SY, Jeong DC, Kang JH. Aminoglycoside therapy for childhood urinary tract infection due to extended-spectrum  $\beta$ -lactamase-producing *Escherichia coli* or *Klebsiella pneumoniae*. *BMC Infect Dis.* 2015;15:414. doi:10.1186/s12879-015-1153-z
3. Khoshnood S, Heidary M, Mirnejad R, Bahramian A, Sedighi M, Mirzaei H. Drug resistant gram-negative uropathogens: A review. *Biomed Pharmacother.* 2017;94:982–994. doi:10.1016/j.biopha.2017.08.006
4. Lanata CF, Fischer-Walker CL, Olascoaga AC, et al. Global causes of diarrheal disease mortality in children <5 years of age: A systematic review. *PLoS One.* 2013;8(9):72788. doi:10.1371/journal.pone.0072788
5. Liu L, Johnson HL, Cousens S, et al. Global, regional, and national causes of child mortality: An updated systematic analysis for 2010 with time trends since 2000. *Lancet.* 2012;379(9832):2151–2161. doi:10.1016/S0140-6736(12)60560-1
6. Huicho L, Trelles M, Gonzales F. National and sub-national under-five mortality profiles in Peru: A basis for informed policy decisions. *BMC Public Health.* 2006;6:173. doi:10.1186/1471-2458-6-173
7. Møller TSB, Overgaard M, Nielsen SS, et al. Relation between *tetR* and *tetA* expression in tetracycline resistant *Escherichia coli*. *BMC Microbiol.* 2016;16:39. doi:10.1186/s12866-016-0649-z
8. Qadri F, Svennerholm AM, Faruque ASG, Sack RB. Enterotoxigenic *Escherichia coli* in developing countries: Epidemiology, microbiology, clinical features, treatment, and prevention. *Clin Microbiol Rev.* 2005;18(3):465–483. doi:10.1128/CMR.18.3.465-483.2005
9. Chopra I, Roberts M. Tetracycline antibiotics: Mode of action, applications, molecular biology, and epidemiology of bacterial resistance. *Microbiol Mol Biol Rev.* 2001;65(2):232–260. doi:10.1128/MMBR.65.2.232-260.2001
10. Becker SL, Vogt J, Knopp S, et al. Persistent digestive disorders in the tropics: Causative infectious pathogens and reference diagnostic tests. *BMC Infect Dis.* 2013;13:37. doi:10.1186/1471-2334-13-37
11. O’Ryan GM, Ashkenazi-Hoffnung L, O’Ryan-Soriano MA, Ashkenazi S. Management of acute infectious diarrhea for children living in resource-limited settings. *Expert Rev Anti Infect Ther.* 2014;12(5):621–632. doi:10.1586/14787210.2014.901168
12. Ochoa TJ, Ruiz J, Molina M, et al. High frequency of antimicrobial drug resistance of diarrheagenic *Escherichia coli* in infants in Peru. *Am J Trop Med Hyg.* 2009;81(2):296–301. PMID:19635887
13. Wellington EM, Boxall AB, Cross P, et al. The role of the natural environment in the emergence of antibiotic resistance in gram-negative bacteria. *Lancet Infect Dis.* 2013;13(2):155–165. doi:10.1016/S1473-3099(12)70317-1
14. Sengelov G, Halling-Sorensen B, Aarestrup FM. Susceptibility of *Escherichia coli* and *Enterococcus faecium* isolated from pigs and broiler chickens to tetracycline degradation products and distribution of tetracycline resistance determinants in *E. coli* from food animals. *Vet Microbiol.* 2003;95(1–2):91–101. doi:10.1016/s0378-1135(03)00123-8



15. Deng Y, Bao X, Ji L, et al. Resistance integrons: Class 1, 2 and 3 integrons. *Ann Clin Microbiol Antimicrob*. 2015;14:45. doi:10.1186/s12941-015-0100-6
16. Bennett PM. Integrons and gene cassettes: A genetic construction kit for bacteria. *J Antimicrob Chemother*. 1999;43(1):1–4. PMID:10381094
17. Clinical and Laboratory Standards Institute (CLSI). Performance standards for antimicrobial susceptibility testing. 18<sup>th</sup> informational supplement, M 100. Wayne, USA: CLSI; 2008.
18. Clinical and Laboratory Standards Institute (CLSI). Performance standards for antimicrobial susceptibility testing. 28<sup>th</sup> ed. Wayne, USA: CLSI; 2019.
19. Harwalkar A, Sataraddi J, Gupta S, Yoganand R, Rao A, Srinivasa H. The detection of ESBL-producing *Escherichia coli* in patients with symptomatic urinary tract infections using different diffusion methods in a rural setting. *J Infect Public Health*. 2013;6(2):108–114. doi:10.1016/j.jiph.2012.10.004
20. Falagas ME, Karageorgopoulos DE. Extended-spectrum beta-lactamase-producing organisms. *J Hosp Infect*. 2009;73(4):345–354. doi:10.1016/j.jhin.2009.02.021
21. Guardabassi L, Dijkshoorn L, Collard JM, Dalsgaard A. Distribution and in vitro transfer of tetracycline resistance determinants in clinical and aquatic *Acinetobacter* strains. *J Med Microbiol*. 2000;49(10):929–936. doi:10.1099/0022-1317-49-10-929
22. Marshall B, Tachibana C, Levy SB. Frequency of tetracycline resistance determinant classes among lactose fermenting coliforms. *Antimicrob Agents Chemother*. 1983;24(6):835–840. doi:10.1128/aac.24.6.835
23. Lévesque C, Piche L, Larose C, Roy PH. PCR mapping of integrons reveals several novel combinations of resistance genes. *Antimicrob Agents Chemother*. 1995;39(1):185–191. doi:10.1128/aac.39.1.185
24. White PA, Mclver CJ, Rawlinson WD. Integrons and gene cassettes in the Enterobacteriaceae. *Antimicrob Agents Chemother*. 2001;45(9):2658–2661. doi:10.1128/AAC.45.9.2658-2661.2001
25. Durmaz R, Otlu B, Koksall F, et al. The optimization of a rapid pulsed-field gel electrophoresis protocol for the typing of *Acinetobacter baumannii*, *Escherichia coli* and *Klebsiella* spp. *Jpn J Infect Dis*. 2009;62(5):372–377. PMID:19762987
26. Tenover FC, Arbeit RD, Goering RV, et al. Interpreting chromosomal DNA restriction patterns produced by pulsed-field gel electrophoresis: Criteria for bacterial strain typing. *J Clin Microbiol*. 1995;33(9):2233–2239. doi:10.1128/JCM.33.9.2233-2239.1995
27. Roberts MC. Tetracycline resistance determinants: Mechanisms of action, regulation of expression, genetic mobility, and distribution. *FEMS Microbiol Rev*. 1996;19(1):1–24. doi:10.1111/j.1574-6976.1996.tb00251.x
28. Rice LB, Bonono RA. Genetic and biochemical mechanisms of bacterial resistance to antimicrobial agents. In: Lorian V, ed. *Antibiotics in Laboratory Medicine*. Baltimore, USA: Williams & Wilkins; 1996:502–578.
29. Taylor DE, Chau A. Tetracycline resistance mediated by ribosomal protection. *Antimicrob Agents Chemother*. 1996;40(1):1–5. doi:10.1128/AAC.40.1.1
30. Dominguez E, Zarazaga M, Saenz Y, Brinas L, Torres C. Mechanisms of antibiotic resistance in *Escherichia coli* isolates obtained from healthy children in Spain. *Microb Drug Resist*. 2002;8(4):321–327. doi:10.1089/10766290260469589



# Gene capsules as functional pharmaceutical formulations for delivery of DNA as an active substance

Edyta Banaczowska-Duda<sup>A–D</sup>, Alicja Bieńkowska-Tokarczyk<sup>B–D</sup>, Maciej Małecki<sup>A,D–F</sup>

Department of Applied Pharmacy, Faculty of Pharmacy, Medical University of Warsaw, Poland

A – research concept and design; B – collection and/or assembly of data; C – data analysis and interpretation; D – writing the article; E – critical revision of the article; F – final approval of the article

Advances in Clinical and Experimental Medicine, ISSN 1899–5276 (print), ISSN 2451–2680 (online)

*Adv Clin Exp Med.* 2022;31(1):81–93

## Address for correspondence

Alicja Bieńkowska-Tokarczyk  
E-mail: alicja.bienkowska-tokarczyk@wum.edu.pl

## Funding sources

The present study was partially supported by the National Centre for Research and Development (grant No. Strategmed1/233264/4/NCBR/2014; acronym: MentorEYE) and Medical University of Warsaw (grant No. FW29/N/20).

## Conflict of interest

None declared

Received on November 25, 2020

Reviewed on July 6, 2021

Accepted on September 2, 2021

Published online on October 14, 2021

## Abstract

**Background.** Capsules are solid drug forms that are well accepted by patients. Capsules usually consist of a medicinal substance with therapeutic benefits plus excipients. From a pharmaceutical point of view, DNA coding sequences can be treated as active substances.

**Objectives.** To develop and assess gelatin capsules containing DNA based on the methods included in the Polish Pharmacopoeia XI, as well as non-pharmacopoeial methods.

**Materials and methods.** The mass uniformity of the obtained capsules was estimated. The stability of the DNA was verified using polymerase chain reaction (PCR) method. A study of the disintegration time of the gene capsules containing DNA mixed with lactose, and placebo capsules with lactose only was also performed. A dissolution test under conditions similar to the nature and specificity of the active substance (DNA) was performed. The transduction activity of the obtained capsules was assessed in cell culture conditions.

**Results.** The DNA and lactose-based gene capsules were obtained. The capsules were characterized by mass uniformity and stability over time. Efficient transduction of B16-F10 cancer cells with the gene product from the capsule was observed using fluorescence microscopy. Groups of green fluorescent protein-positive cells were observed in the microscope field of view.

**Conclusions.** The findings showed that it is possible to obtain a solid pharmaceutical form of the drug, i.e., a capsule containing DNA as an active substance. The gene capsules enabled the introduction of DNA into cells. This method may have valuable implications for increasing the availability of gene-based drugs for patients.

**Key words:** drug delivery, gene therapy, gene capsules, applied pharmacy

## Cite as

Banaczowska-Duda E, Bieńkowska-Tokarczyk A, Małecki M. Gene capsules as functional pharmaceutical formulations for delivery of DNA as an active substance. *Adv Clin Exp Med.* 2022;31(1):81–93. doi:10.17219/acem/141898

## DOI

10.17219/acem/141898

## Copyright

© 2022 by Wrocław Medical University  
This is an article distributed under the terms of the Creative Commons Attribution 3.0 Unported (CC BY 3.0) (<https://creativecommons.org/licenses/by/3.0/>)

## Background

Capsules are a well-known solid dosage form of drug administration. According to the definition of Polish Pharmacopoeia XI (Ph Pol XI), capsules are solid formulations that have the form of a reservoir of various shapes and sizes, usually containing a single dose of active ingredient(s).<sup>1</sup> Solid oral dosage forms, such as tablets and capsules, are generally the preferred method of drug delivery due to their comfort of use, low cost and high patient acceptability.<sup>2</sup> Capsules are used to administer drugs to patients suffering from various diseases, and therefore they play an important role in delivering diverse drugs.<sup>3</sup> Studies of patients' preferred dosage form found that more than half of patients (52.9%) prefer a capsule, 28.4% prefer a coated tablet, 12.7% prefer an uncoated tablet, and 3.5% prefer a soft-gel capsule. Preferences regarding capsules were significantly associated with the easiest way of swallowing this drug form.<sup>4</sup> One of the many advantages of capsules over tablets is the ability to deliver medicinal substances not only in a solid form, but also in nonaqueous liquid and semi-solid substance forms.<sup>5,6</sup>

Capsules are a form of a drug formed not only in industrial settings, but also directly in pharmacies. Pharmacists' knowledge about the physicochemical properties of drugs and medicinal products is necessary for the preparation of the drug form.<sup>7</sup> Drug prescribing is useful for practical pharmacy, since physicians do not have to be limited to the available industrial preparations. Then, the capsules can be prepared in a pharmacy, based on the physician's prescription for an individual patient.<sup>3</sup> Therefore, this form of drug delivery may be applicable for personalized therapy.<sup>8</sup> Pharmacies have an educated personnel and specialized equipment for drug production. Consequently, they may play an important role in clinical trials.<sup>9</sup> Capsules containing various active substances can be prepared at a pharmacy. Compared with tablets, capsules usually contain less excipients.<sup>10</sup> It is well-documented that the composition can be limited to 1 excipient without its own pharmacological and adverse effects.<sup>1,11</sup> An example of a known excipient is lactose (saccharum lactis,  $\beta$ -D-galactopyranosyl-(1-4)-D-glucopyranose), which is often used in industry and in pharmaceutical formulations. It shows a tendency to crystallize when stored at a high relative humidity; however, it is stable and nontoxic. Moreover, lactose does not interact pharmaceutically and pharmacodynamically with other drug components and improves taste.<sup>12</sup> Although preparation of capsules is well-established, the preparation of capsules containing genes is of great interest due to their potential use in gene therapy.

Gene therapy is a treatment method based on the use of nucleic acids as active substances. The proteins encoded by the selected gene sequences cause a therapeutic

effect.<sup>13</sup> Currently, gene preparations are administered to patients mainly in liquid form as an injection or infusion of solutions or suspensions. These preparations are then administered to patients intravenously, intramuscularly, intratumorally, intradermally, or subretinally (in ophthalmology).<sup>14</sup> The literature has reported many experimental studies in the field of gene therapy for cancer, metabolic and infectious diseases, and correction of congenital disorders.<sup>15</sup> Patients' expectations are raised by gene preparations registered for treatment. Glybera, Luxturna and Zolgensma are used in the treatment of metabolic diseases, ophthalmic diseases and neurodegenerative disorder, respectively, and belong to the parenteral drugs.<sup>16</sup> Glybera is a solution for intramuscular injection that contains the following excipients: disodium phosphate anhydrous, potassium chloride, potassium dihydrogen phosphate, sodium chloride, sucrose, and water for injection.<sup>17</sup> Luxturna is a solution for subretinal injection. Before administration, it is prepared by diluting the concentrate with a solvent. Both solutions contain the same excipients: sodium chloride, sodium dihydrogen phosphate monohydrate and dihydrate, poloxamer 188, and water for injection.<sup>18</sup> Zolgensma is intended for intravenous infusion and, in addition to the medicinal substance, contains tromethamine, magnesium chloride, sodium chloride, poloxamer 188, hydrochloric acid, and water for injection.<sup>19</sup> Concepts of gene therapy based on oral drug forms are detailed in experimental studies. The literature describes the attempts to use microspheres, forms based on chitosan, modified silica, and modified micelles.<sup>20-23</sup> The plasmid encoding interleukin 10 (IL-10) incorporated in microspheres has been used for the treatment of inflammatory bowel disease.<sup>20</sup> Chitosan microparticles containing plasmid DNA have been developed.<sup>21</sup> Oral gene delivery using poly-L-lysine modified silica nanoparticles has been attempted, and the ability of poly (allylamine) amphiphilic polymer micelles to deliver small interfering RNA (siRNA) through the gastrointestinal tract has been assessed.<sup>22,23</sup> The described examples of oral gene preparations emphasize the importance of this method in experimental studies in search for a new route of delivering gene therapy products. Achieving the therapeutic potential of DNA requires the development of new pharmaceutical formulations to enable a safe and effective administration of gene drugs.

## Objectives

The aim of this study was to design gene capsules containing plasmid DNA (pDNA) or recombinant adeno-associated virus (rAAV). The capsule formulations were then characterized by appropriate pharmaceutical and biological tests to verify their stability and activity.

## Materials and methods

### Formulation and preparation of gene capsules

Hard gelatin capsules (Eprus, Bielsko-Biała, Poland) containing genes were prepared. In accordance with the manufacturer's recommendations for capsule capacity, each capsule contained 0.18 g of lactose (pure lactose monohydrate; Chempur, Piekary Śląskie, Poland) and 50 µg of the pAAV/LacZ plasmid (LacZ – β-galactosidase; Cat. No. 240071; Agilent, Santa Clara, USA) or  $4 \times 10^4$  genome copies (gc) rAAV/GFP (rAAV/DJ-CAG-GFP; Cat. No.7078; Vector Biolabs, Malvern, USA). Placebo hard gelatin capsules containing only 0.18 g of lactose were also produced. The capsules with plasmid and placebo were made with a manual capsule filling machine (Eprus), while capsules with the viral vector were prepared by hand.

Size 3 hard gelatin capsules were prepared. For the placebo capsules, using an analytical balance, 18.0 g of lactose was weighed and then the powder was thoroughly ground in a mortar. The empty capsules were placed in the manual capsule filling machine using a positioner. The capsules were opened using the top plate of the capsule machine and the prepared powder mass was placed on the plate

of the capsule machine. The powder mass was gently spread into the capsules. The capsules were then closed and removed from the capsule filling machine. Next, the gene capsules were prepared (Fig. 1). On an analytical balance, 18.0 g of lactose was weighed and 1000 µL of 5 µg/µL pAAV/LacZ solution (50 µg of pDNA per capsule) was added and mixed gently. A larger amount of solution leads to over-wetting of the excipient and to softening and deformation of the capsule, consequently reducing its stability. The 2<sup>nd</sup> group of gene capsules contained the rAAV vector encoding the green fluorescent protein (*GFP*) reporter gene. For this purpose, 0.18 g of lactose was weighed into each capsule and  $4 \times 10^4$  gc of rAAV in 10 µL of water for injection was added.

The obtained capsules were then tested using the following pharmacopeial methods<sup>1</sup>: uniformity of single-dose preparations, examination of disintegration time, dissolution and stability tests, and transduction activity tests.

### Mass uniformity of single-dose preparations

The study was performed in 5 groups of 20 gene (Table 1) and 5 groups of 20 placebo capsules (Table 2), based on the Ph Pol XI.<sup>1</sup> The capsules were weighed on an analytical balance.

Table 1. Mass uniformity of gene capsules

No.of capsule	Capsule mass [g]	Shell mass [g]	Lactose mass [g]	Deviation [g]	Deviation [%]
1	0.234	0.047	0.187	0.007	1.1
2	0.234	0.049	0.185	0.005	5.6
3	0.224	0.048	0.176	-0.004	-2.2
4	0.229	0.046	0.183	0.003	2.8
5	0.226	0.048	0.178	-0.002	-1.1
6	0.234	0.048	0.186	0.006	3.3
7	0.236	0.047	0.189	0.009	5.0
8	0.225	0.048	0.177	-0.003	-1.7
9	0.210	0.047	0.163	-0.017	0.6
10	0.219	0.049	0.170	-0.010	-8.4
11	0.229	0.047	0.182	0.002	2.3
12	0.237	0.048	0.189	0.009	1.1
13	0.225	0.050	0.175	-0.005	-2.8
14	0.246	0.048	0.198	0.018	<b>11.2</b>
15	0.229	0.050	0.179	-0.001	-0.6
16	0.210	0.048	0.162	-0.018	-9.5
17	0.234	0.049	0.185	0.005	2.3
18	0.227	0.048	0.179	-0.001	-0.6
19	0.238	0.048	0.190	0.010	7.3
20	0.209	0.048	0.161	-0.019	<b>-10.1</b>
X = 0.180					

A total of 20 capsules were tested (numbered 1–20); the 14<sup>th</sup> and 20<sup>th</sup> capsules exceeded the allowable deviation. X – average weight of lactose with pAAV/LacZ solution; deviation [%] – deviation expressed as a percentage of the difference from the average mass of capsules. Values in bold slightly exceeded the allowable deviation, according to Polish Pharmacopoeia XI (Ph Pol XI)<sup>1</sup>.

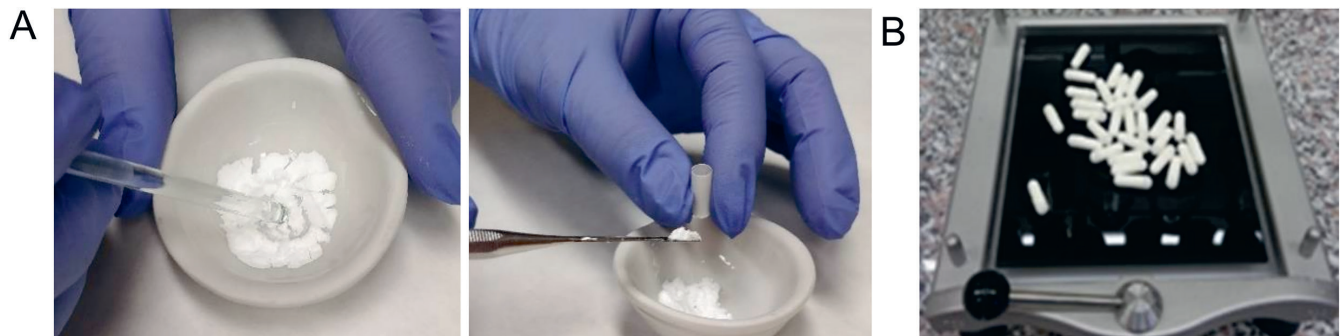


Fig. 1. Preparation of gene and placebo capsules. A. Manual preparation of gene capsules (containing the recombinant adeno-associated virus (rAAV)/ green fluorescent protein (GFP) vector); B. Gene capsules (containing the pAAV/LacZ plasmid) prepared using a capsule filling machine. The placebo capsules were prepared in the same manner

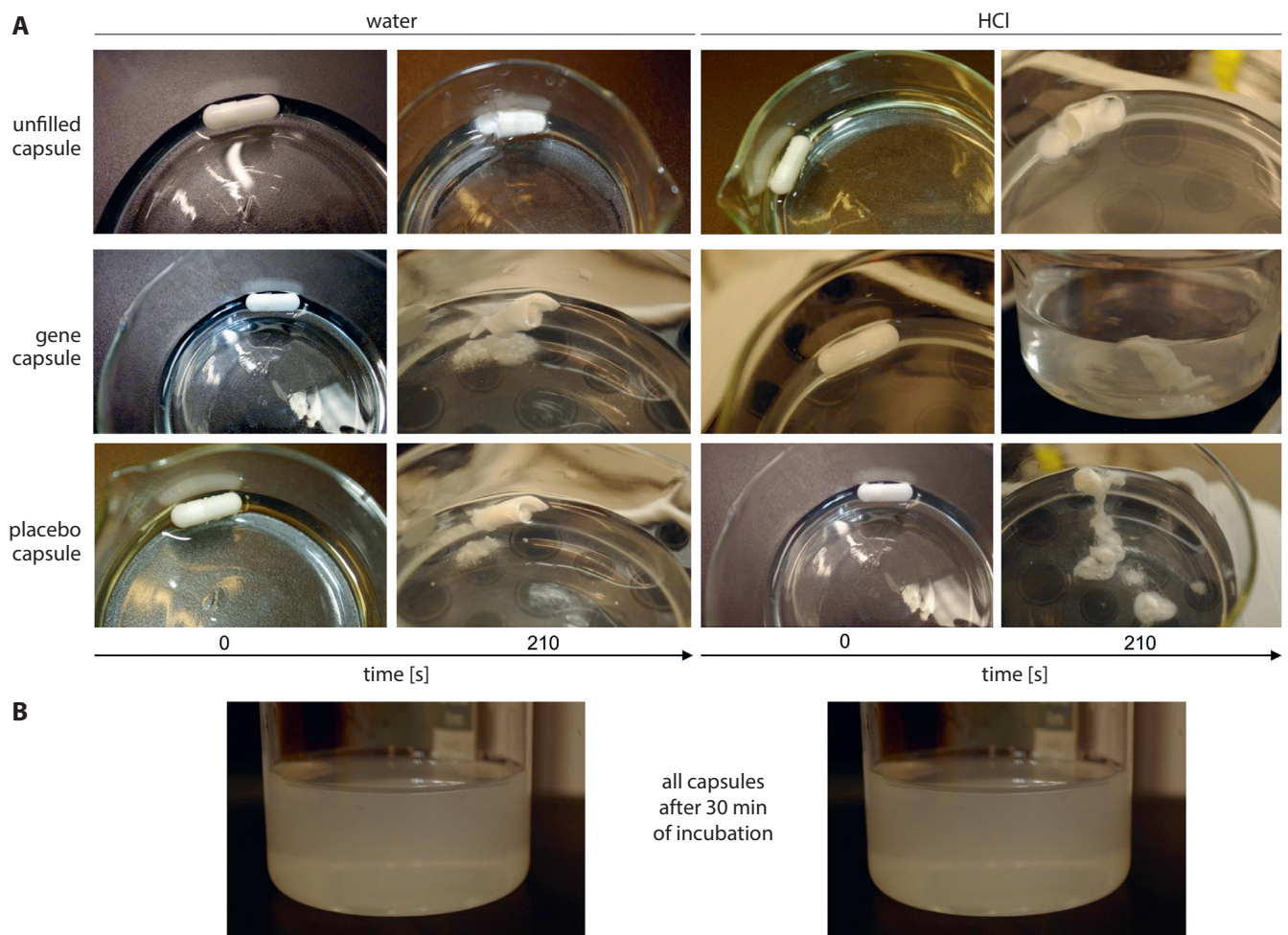


Fig. 2. The disintegration time of empty, gene and placebo capsules in water or HCl solution (pH 1.5) at 35°C. A. Capsules placed in solution (1<sup>st</sup> column) and at 210 s (2<sup>nd</sup> column) of the test in water or HCl; B. A solution of water or HCl after 30 min of testing. All of the capsules disintegrated

Each capsule was first weighed. Next, the capsule was opened without losing any part of the casing, the contents were emptied as completely as possible and the casing was weighed. The weight of the contents is the difference between the weight of the filled and emptied capsule. According to Ph Pol XI,<sup>1</sup> for capsules weighing less than 300 mg, the permissible deviation is  $\pm 10\%$ . For 20 tested capsules, 2 may exceed the acceptable deviation, but not more than twice.

### Capsule disintegration time

The disintegration time study was based on Ph Pol XI<sup>1</sup> with some modifications due to the physicochemical properties of the active substance (DNA). According to the definition in Ph Pol XI, a complete disintegration is defined as the state where all remainders of the capsule are a soft mass without a compact, non-wetted core, except for fragments of undissolved capsule shell.

Table 2. Mass uniformity of placebo capsules

No. of capsule	Capsule mass [g]	Shell mass [g]	Lactose mass [g]	Deviation [g]	Deviation [%]
1	0.231	0.048	0.183	0.004	2.2
2	0.237	0.049	0.188	0.009	5.0
3	0.225	0.049	0.176	-0.003	-1.7
4	0.231	0.046	0.185	0.006	3.5
5	0.228	0.048	0.180	0.001	0.6
6	0.223	0.047	0.176	-0.003	-1.7
7	0.236	0.047	0.189	0.010	5.6
8	0.218	0.048	0.170	-0.009	-5.0
9	0.225	0.048	0.177	-0.002	-1.1
10	0.210	0.047	0.163	-0.016	-8.9
11	0.229	0.047	0.182	0.003	1.7
12	0.230	0.048	0.182	0.003	1.7
13	0.222	0.049	0.173	-0.006	-3.4
14	0.214	0.048	0.166	-0.013	-7.2
15	0.249	0.050	0.199	0.020	<b>11.2</b>
16	0.209	0.048	0.161	-0.018	<b>-10.0</b>
17	0.238	0.049	0.189	0.010	5.6
18	0.228	0.047	0.181	0.002	1.1
19	0.239	0.048	0.191	0.012	6.7
20	0.224	0.048	0.176	-0.003	-1.7
X = 0.179					

A total of 20 capsules were tested (numbered from 1–20); the 15<sup>th</sup> capsule exceeded the allowable deviation and the 16<sup>th</sup> capsule was at the limit of the allowable deviation. X – the average weight of lactose; deviation [%] – deviation expressed as a percentage of the difference from the average mass of capsules. Values in bold slightly exceeded or were at the limit of the allowable deviation, according to Polish Pharmacopoeia XI (Ph Pol XI).

According to the indications of the Ph Pol XI,<sup>1</sup> 6 capsules were tested at one time. The temperature of the liquid was maintained at 37°C ±0.2°C (water or 0.1 M hydrochloric acid solution) and the test time did not exceed 30 min. The capsules were placed in 250 mL beakers containing 100 mL of water or hydrochloric acid solution (pH 1.5) in a shaking incubator (Jeio Tech, Daejeon, South Korea) at 37°C and 100 rpm. The capsules were observed and the appearance of the capsules and the time needed for disintegration were assessed (Fig. 2). Additionally, the disintegration time experiment was carried out at a temperature 2°C lower than that recommended by the Ph Pol XI. This variant of the study at 35°C allowed for more accurate tracking of capsule disintegration and the preparation of appropriate photographic documentation (Fig. 2).

## DNA release from gene capsules

Test conditions similar to the nature and specificity of the active substance, i.e., plasmid DNA, were created. Water was used as the dissolution medium for the polymerase chain reaction (PCR) method of DNA detection. The level of HCl, phosphate buffer or NaOH recommended in the Ph Pol XI would disrupt the PCR process. Capsules were prepared as described in the “Formulation

and preparation of gene capsules” section. Single capsules were placed in 250 mL beakers containing 100 mL water and placed in a shaking incubator (Jeio Tech) at 37°C and 100 rpm. Samples (8 µL) were collected every 30 s for 10 min and after 30 min (Fig. 3).

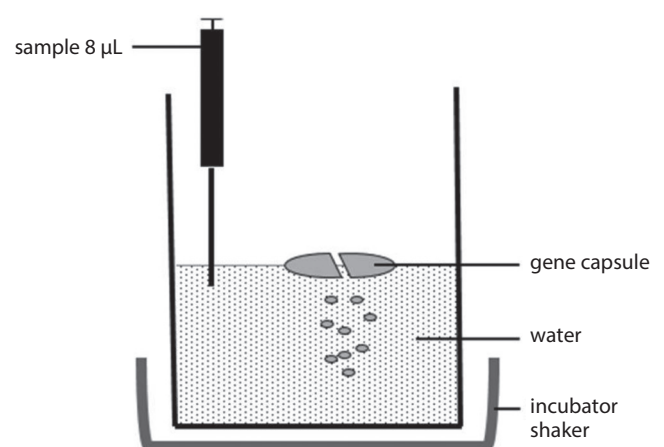
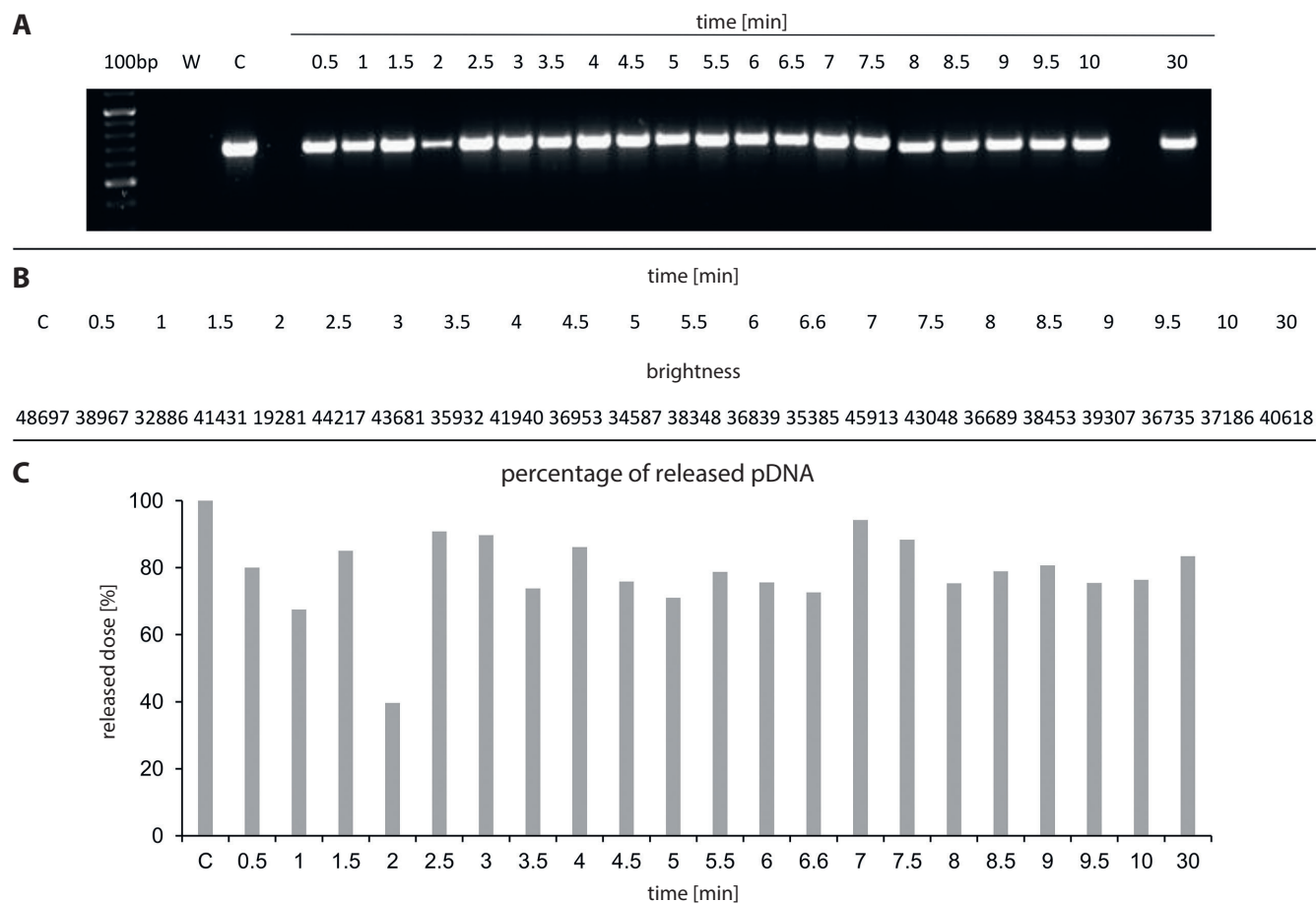


Fig. 3. Release conditions of pAAV/LacZ from the gene capsule. A beaker with 100 mL of acceptor fluid was placed in a shaking incubator and maintained at 37°C. The gene capsule was placed in the acceptor fluid and shaking was set at 100 rpm. Samples (8 µL) were collected every 30 s for 10 min and after 30 min. Lastly, polymerase chain reaction (PCR) and electrophoresis were carried out



**Fig. 4.** Release of pAAV/LacZ from the gene capsule within 30 min. **A.** Agarose gel photo of electrophoretic separation after polymerase chain reaction (PCR). The pAAV/LacZ primers ( $T_m = 42.1^\circ\text{C}$ , 35 cycles), 1.8% SYBR Safe gel, 676 bp product visualized, W – negative control, C – positive control (pAAV/LacZ), 100 bp – size marker; **B.** The values used for the calculations of the percentage of released plasmid DNA (pDNA); **C.** The percentage of released pDNA calculated by comparing the brightness of the C band (positive control) and the bands representing pDNA release within 30 min

## PCR and electrophoresis

In the present study, the gene encoding ampicillin resistance cloned into the used plasmid was amplified. Primers with the following sequence were designed: 5'ATAGTTGCCT-GACTCC3' and 5'GTTACATCGAACTGGA3'. The reaction mixture (20  $\mu\text{L}$ ) contained 8  $\mu\text{L}$  of collected sample, 10  $\mu\text{L}$  of Master Mix 2 $\times$  complete PCR buffer (Thermo Fisher Scientific, Waltham, USA), and 1  $\mu\text{L}$  of each primer. The following PCR thermal profile was selected: 5 min at  $94.0^\circ\text{C}$ ; 35 cycles (30 s at  $94.0^\circ\text{C}$ , 30 s at  $42.1^\circ\text{C}$ , 40 s at  $72.0^\circ\text{C}$ ); and 10 min at  $72.0^\circ\text{C}$ . After the PCR, the samples were subjected to electrophoretic separation on 1.5% agarose gel enriched with SYBR Safe (Thermo Fisher), which is a cyanine dye that binds to DNA. Gene Ruler 100 bp Plus DNA Ladder (Thermo Fisher) was used as the size marker. The separated product was visualized and photographed under UV light using a ChemiDoc MP Imaging System (Bio-Rad, Hercules, USA) (Fig. 4A). In order to assess how much of the active substance (DNA) was released from gene capsule within 30 min, the brightness intensity of the bands in agarose gel was analyzed using ImageJ software (National Institutes of Health

(NIH), Bethesda, USA). The values used for the calculations of the released pDNA percentage are presented in Fig. 4B.

## Stability of gene capsules

A method to test the stability of hard gelatin capsules containing lactose and pAAV/LacZ was designed. The obtained gene capsules and placebo capsules were stored at  $4^\circ\text{C}$  and room temperature (RT) for 1 day, 7 days, 14 days, 30 days, 3 months, and 6 months. After the indicated times, the capsules were dissolved in 250 mL beakers containing 100 mL of water and placed in a shaking incubator at  $37^\circ\text{C}$  and 100 rpm. The 8- $\mu\text{L}$  samples were collected and PCR was performed using 2 types of designed primers. The 1<sup>st</sup> primer pair, as in the release test, allowed the amplification of the ampicillin resistance gene, while the 2<sup>nd</sup> pair of primers was complementary to the ITR LacZ coding fragment (primers annealing temperature of  $54.9^\circ\text{C}$ , sequences: 5'CATCTGCTGCACGCGAAGAA3', 5'GAGGGAGTG-GCCAACTCCAT3'). The PCR products were separated with electrophoresis. These methods were described in the above section titled "PCR and electrophoresis".





**Table 4.** Disintegration time of empty, placebo and gene capsules at 35°C in water or HCl solution. The disintegration time of all capsules at 35°C was 210 s (bold)

Time [s]	Disintegration [%] at 35°C					
	water			HCl		
	empty capsule	placebo	gene capsule	empty capsule	placebo	gene capsule
45	20	35	30	25	45	40
90	40	60	60	50	70	70
<b>210</b>	<b>80</b>	<b>90</b>	<b>90</b>	<b>80</b>	<b>90</b>	<b>90</b>
1800	100	100	100	100	100	100

filled with lactose or lactose with plasmid at the same time were disintegrated in 90% (Table 4, Fig. 2).

### Assessment of pDNA release from gene capsules

This study was performed with gene capsules containing 50 µg of plasmid each. The analyzed samples (8 µL) were collected every 30 s for 10 min and after 30 min (Fig. 3). The PCR was performed. Then, the resulting products underwent electrophoretic separation in agarose gel. Plasmid release from the capsules was observed in the indicated time. After only 30 s in the sample, pAAV/LacZ was released. After 30 min, the band corresponding to the presence of pAAV/LacZ was also visible. Electrophoresis revealed that pDNA maintains the correct structure and was present in each sample. Moreover, the absence of a band in the sample marked as negative control (W) proved that the reaction was performed correctly (Fig. 4A). Additionally, to assess the amount of DNA released from capsules within 30 min, the brightness intensity of the bands in the agarose gel was analyzed. The brightness values

of the C band (positive control) and the other bands (showing release of pAAV/LacZ from the gene capsule within 30 min) were compared (Fig. 4A). After 30 min, 83% of the DNA dose contained in the capsule was observed in the acceptor fluid (Fig. 4C).

### Stability of gene capsules

The aim of this experiment was to assess the stability and durability of the prepared capsules under the following conditions. The gene and placebo capsules were stored for 1 day, 7 days, 14 days, 30 days, 3 months, and 6 months at 4°C and room temperature (RT). After the stated times, the capsules were dissolved in water at 37°C. Seven capsules containing plasmid DNA (pAAV/LacZ) and 7 placebo capsules with only lactose were tested at each of the mentioned time intervals at both temperatures. Next, 8 µL samples were collected and PCR was performed using the 2 designed primers. Then, the samples then underwent electrophoretic separation on 1.5% agarose gel. The active substance (pAAV/LacZ) did not degrade at the 2 tested temperatures and after the indicated times, as confirmed

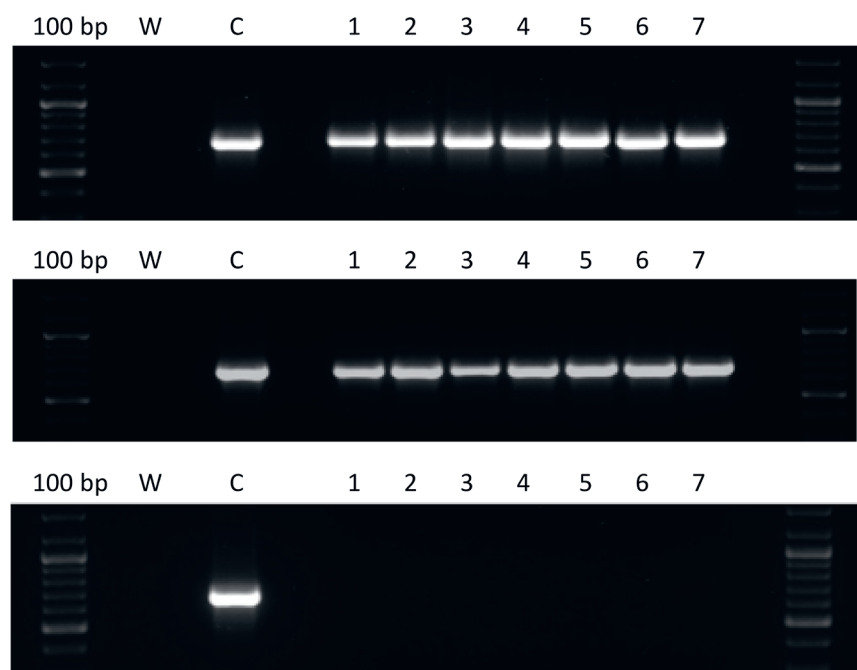


**Fig. 5.** Stability of gene capsules after 1 day of storage at the following temperatures: A – 4°C; B – room temperature; C – placebo. Electrophoretic separation after polymerase chain reaction (PCR). The pAAV/LacZ primers ( $T_m = 42.1^\circ\text{C}$ , 35 cycles), 676 bp product visualized, 100 bp – size marker, W – water, C – control (pAAV/LacZ). The numbers 1–7 indicate the samples collected from the 7 separately dissolved capsules

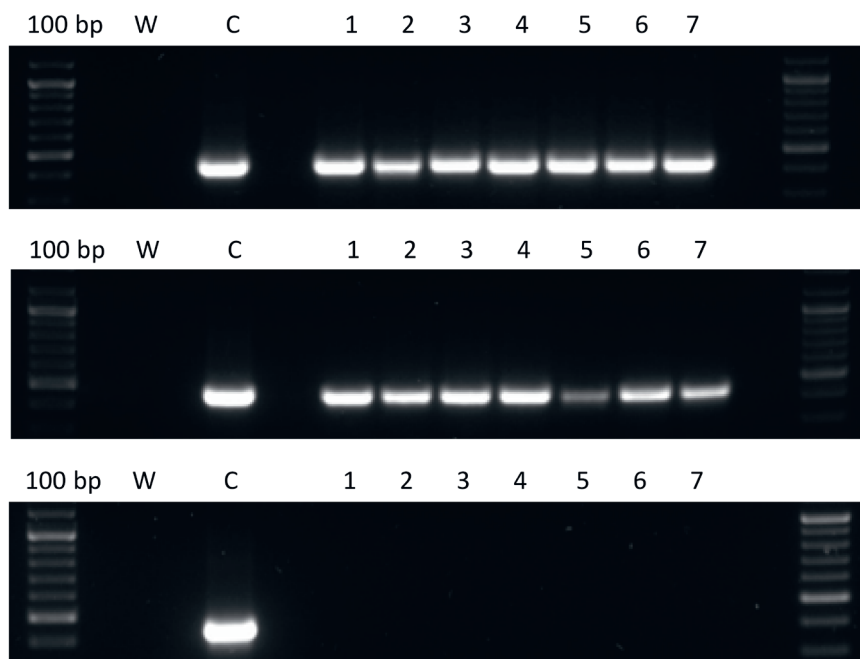


**Fig. 6.** Stability of gene capsules after 6 months of storage at the following temperatures: A – 4°C; B – room temperature; C – placebo. Electrophoretic separation after polymerase chain reaction (PCR). The LacZ ITR primers ( $T_m = 54.9^\circ\text{C}$ , 35 cycles), 436 bp product visualized, 100 bp – size marker, W – water, C – control (pAAV/LacZ). The numbers 1–7 indicate the samples collected from the 7 separately dissolved capsules

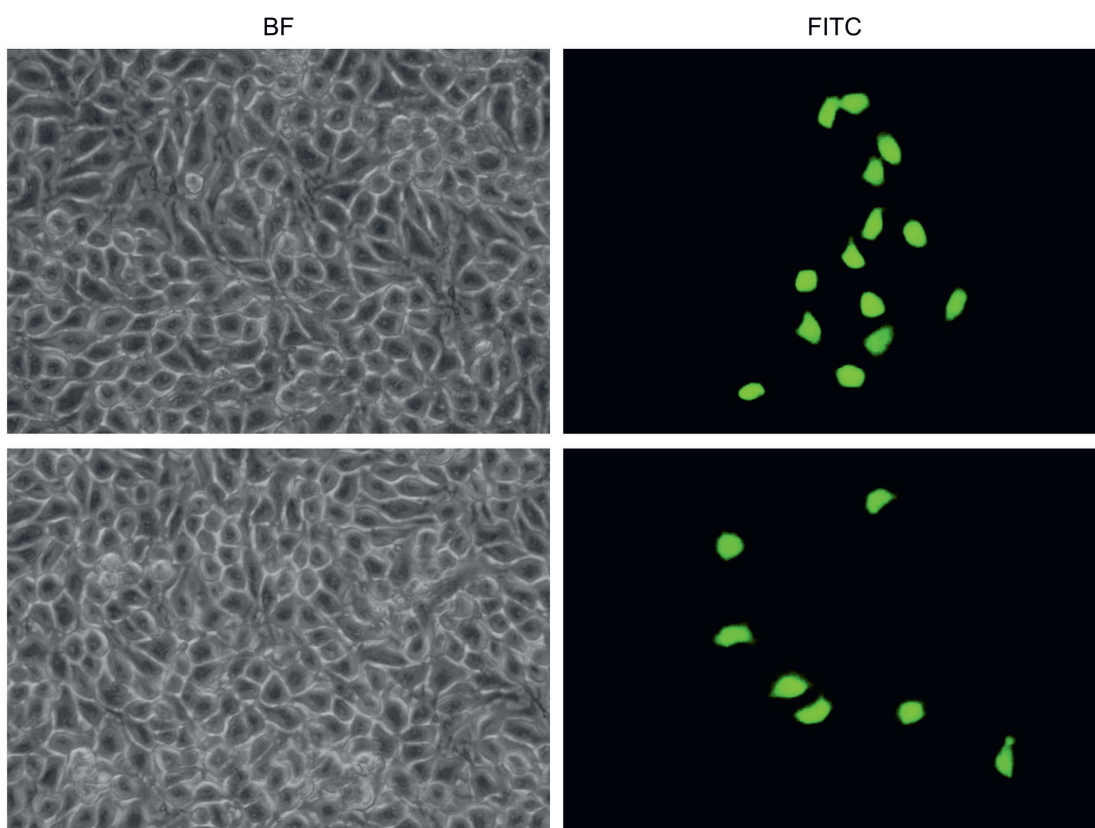


**Fig. 7.** The B16-F10 cell transduction with recombinant adeno-associated virus (rAAV) vectors. Photographs of representative rAAV transduced cells expressing green fluorescent protein (GFP) were taken at  $\times 10$  magnification using an inverted microscope. The GFP+ cells formed groups in which 4–14 cells were observed. BF – pictures collected in bright field; FITC – pictures collected using a fluorescein isothiocyanate (FITC) filter

by electrophoresis for each group. Figure 5 and Fig. 6 show representative images after 1 day and 6 months, respectively, with use of the 2 types of primers.

### Transduction activity of gene capsules

The transduction efficiency of B16-F10 cells was assessed with inverted fluorescence microscopy. Cell evaluation

was performed on the 7<sup>th</sup> day of the experiment. The results are shown in Fig. 7. As shown, the cells were successfully transduced with rAAV vectors released from capsules. The GFP-positive (GFP+) cells were grouped. From 4 to 14 GFP+ cells were observed in the microscope field of view. Effective transduction was documented in Fig. 7, proving that the vectors carrying the reporter gene were not damaged during the overall procedure of transduction

from gene capsules. During gene capsule preparation and release from the drug formulation, the rAAV vectors maintained their structure and managed to enter into the cells. The originally designed transduction procedure was successful. Moreover, the introduction of additional steps preceding transduction did not adversely affect the cell culture, as it was not infected with bacteria or fungi. These findings demonstrate the safety of the conditions used.

## Discussion

Gene therapy is a promising method in medicine. Currently, gene therapy is mainly based on lentivirus or adeno-associated virus vectors, or the method of localization and repair of damaged *CRISPR-Cas9* genes.<sup>24</sup> New medicinal products delivering therapeutic genes, such as Glybera, Strimvelis, Kymriah, Yescarta, Luxturna, Zolgensma, and Zynteglo,<sup>16</sup> have demonstrated the success of this treatment method and they encourage further intensive research. Considering the routes of administration of gene preparations, it seems that – apart from parenteral administration – oral, intranasal and transdermal forms may be particularly useful. Oral gene delivery is an extremely interesting therapeutic option due to the possibility of systematic and repeated administration of the drug, limited hospitalization and the features of the gastrointestinal tract. Since the intestines are easily accessible orally, rectally or endoscopically, it is not necessary to perform invasive surgery. The digestive tract has an unusually large surface area, which means there is a huge population of cells that can accept genes. There are also stem cells in the intestinal glands (e.g., Lieberkühn's crypts) that are important for certain types of therapy. At the same time, it is worth emphasizing that the intestinal epithelium is highly vascularized, which may allow the efficient passage of newly synthesized proteins (resulting from gene transfer) into the bloodstream and, as a consequence, enable the treatment of systemic diseases.<sup>25</sup> Studies have shown that therapeutic genes can be used in the treatment of inflammatory bowel disease (IBD)<sup>20</sup> and colorectal cancer,<sup>26</sup> as well as systemic diseases such as hemophilia.<sup>27</sup> However, the efficient delivery of genes via the gastrointestinal tract poses anatomical and physiological challenges for researchers, such as the presence of an acidic pH in the stomach, intestinal enzymes and bacterial flora.<sup>26</sup> Oral systems should be designed to overcome the various conditions present in the digestive tract that may inactivate a sensitive substance like DNA. Therefore, it is important to design and carefully select materials for oral gene delivery. Recent achievements in oral gene therapy include strategies improving the efficiency of gene transfer, cell targeting and stability, as well as the adaptation of the drug form to the conditions present in the gastrointestinal tract.<sup>20,28–30</sup> One example of improving oral gene therapy

is the functionalization of delivery carriers to enhance gastric stability and particle uptake or to target the active substance to the desirable cells. In a study by He et al., mannose-modified trimethyl chitosan-cysteine nanoparticles were used.<sup>28</sup> This system allowed for targeted delivery of siRNA to intestinal macrophages and was effective in both, gastric and intestinal conditions. Promising targeted delivery methods include systems with bile acid conjugates that increase the stability of the active substance in the stomach and improve the uptake by intestinal enterocytes through bile acid transporters.<sup>20</sup> In order to overcome the difficult conditions in the digestive tract, dual material particulate systems that combine various properties of materials to protect, release and deliver cargo to cells, can be prepared.<sup>29</sup> Another interesting idea is smart delivery systems that can adapt to the local conditions in the digestive tract. An excellent example is enzyme and pH responsive nanogels. This system allows the nanogel to collapse and protects the payload under low pH conditions, yet expands under the higher pH conditions of the intestine to be degraded by intestinal enzymes to release cargo.<sup>30</sup> Therefore, appropriate carriers are required to protect nucleic acids against the hostile environment of the gastrointestinal tract. Previous studies have used microspheres, chitosan, modified silica, and modified micelles.<sup>20–23</sup> Bhavsar and Amiji attempted to treat IBD by administering a plasmid encoding IL-10, which was incorporated in microspheres.<sup>20</sup> Local expression of IL-10 reduced the levels of pro-inflammatory factors (e.g., interferon  $\alpha$  (IFN- $\alpha$ ), tumor necrosis factor  $\alpha$  (TNF- $\alpha$ ), IL-1, and IL-12). Moreover, the therapy resulted in an increase in body weight, restoration of colon length and mass, and inhibition of the inflammatory response. Guliyeva et al. developed chitosan microparticles containing plasmid DNA.<sup>21</sup> The in vitro release of pDNA was pH-dependent: at the same time that the pH increased, the release rate decreased. In in vivo studies, after oral administration of pDNA-chitosan microparticles, the expression of the reporter gene was observed in histological sections of the stomach and small intestine. In another study, Li et al. conducted oral gene delivery tests using poly-L-lysine modified silica nanoparticles.<sup>22</sup> This vehicle has low intestinal toxicity in BALB/C mice. The efficient expression of the reporter gene was detected in the stomach, and the expression in the intestine was mainly seen in mucosal cells. In the work of Guo et al., the ability of poly(allylamine)-based amphiphilic polymer micelles to deliver siRNA through the gastrointestinal tract was assessed.<sup>23</sup> The physicochemical profiles showed that the transfection molecules self-assemble into complexes with nanometric diameters (150–300 nm) and a cationic surface charge (+20–30 mV). The transfection complexes were stable in the presence of saline solutions and simulated gastrointestinal fluids. The authors achieved up to 35% cellular uptake in in vitro studies, with successful release of siRNA from endosomes/lysosomes.

The presented research examples emphasize the potential and functionality of different substances for oral gene delivery in gene therapy.

The rAAV/GFP contains rAAV-DJ as a vector, which delivers the *GFP* reporter gene. The well-characterized rAAV-DJ is a recombinant mosaic vector made from the DNA of 8 AAV serotypes that efficiently transduce cells from various cancer lines. Our previous studies revealed the high transduction activity of rAAV-DJ in the B16-F10 cell line.<sup>31,32</sup>

Both viral and non-viral vectors were used in this study. Plasmids, adenoviral vectors and retroviral vectors are the most frequently used gene delivery vectors in clinical trials of gene therapy.<sup>33,34</sup> The AAVs are widely used in gene therapy as vectors due to their ability to ensure long-term gene expression and the lack of pathogenicity; thus, they are developed for gene delivery applications.<sup>31,35</sup> The AAV vectors are currently the most common type of viral vectors used in clinical trials of gene therapy.<sup>36</sup>

The aim of this study was to develop hard gelatin gene capsules based on lactose. Lactose monohydrate, popular in pharmacy recipes, was used. Lactose is a disaccharide composed of D-galactose and D-glucose linked by a  $\beta$ -1,4-glycosidic bond. It is nontoxic and does not have any pharmaceutical or pharmacodynamic interactions with other drug components.<sup>1,12</sup> Lactose is the most common diluent in tablets and capsules due to its good physical stability and water solubility, availability, and cost-effectiveness.<sup>37</sup>

A manual capsule filling machine was used to prepare the capsules (Fig. 1), which facilitates and improves the preparation of divided powders in modern pharmacy recipes. It enables precise dosing of powder into hard gelatin capsules without weighing individual doses. The capsule machine ensures maximum purity of the drug and the esthetics of the final form. In this study, 100 placebo capsules were obtained and the mass uniformity test of single-dose preparations was performed based on the Ph Pol XI.<sup>1</sup> The results met the requirements of the Ph Pol XI, i.e., a maximum 2 of 20 capsules slightly exceeded the permissible deviation, which for capsules weighing less than 300 mg can be  $\pm 10\%$  (Table 1). We prepared 100 gene capsules that contained lactose and the active substance in the form of 10  $\mu$ L of pAAV/LacZ solution in a concentration of 5  $\mu$ g/ $\mu$ L per capsule (50  $\mu$ g pDNA/capsule). Preparation of powder mass to fill the capsules containing pAAV/LacZ required care for the cleanliness of the workplace, as well as special care was required when combining the plasmid DNA with lactose. The tested gene capsules also met the requirements of the Ph Pol XI in terms of mass uniformity, i.e., a maximum 2 out of 20 gene capsules slightly exceeded the permissible deviation (Table 2).<sup>1</sup>

The capsules disintegrated, according to definition in the Ph Pol XI,<sup>1</sup> in 45 s at 37°C and in 210 s at 35°C. The difference of 2°C slowed the disintegration of all capsules (empty, gene and placebo). According to the Ph

Pol XI, the disintegration time should not be longer than 30 min. After this time, all tested capsules were completely dissolved. The short disintegration time of the capsules allows quick release and a rapid effect of the active substance.

In gene therapy research, it is important to determine the transduction efficiency of gene preparations, which is associated with the mechanism of DNA release from the drug. Therefore, the gene capsules were tested for active ingredient (DNA) release. Due to the experimental form of the tested drug as well as the type and specificity of the active substance used in the capsules (plasmid DNA), the original changes of the test conditions were introduced. This allowed the observation of pAAV/LacZ released from the capsules (as described in the Materials and Methods section). As shown in Fig. 4, the presence of pDNA in the acceptor fluid was observed after 30 s, and DNA was detected in each of the collected samples. After 30 min, 83% of the dose contained in the capsule was observed.

To characterize the obtained gene capsules, stability experiments were also performed. The aim was to determine whether pAAV/LacZ in combination with lactose was stable under certain storage conditions and time. Assuming that the gene capsules are in the form of a prescription drug, pharmacists should determine their shelf life. Medicines that patients receive must have adequate quality and activity in the prescribed period. In accordance with the chapter “Medicines prepared in a pharmacy” in the National Monographs of Ph Pol XI, vol. 3,<sup>1</sup> it is assumed that the maximum period of use of non-sterile solid preparations prepared with the use of prescription substances, when properly stored (temperature up to 25°C, protected from light, well-sealed containers), is not longer than 3 months.<sup>1</sup> In our study, the active substance was not a prescribed substance. As the prepared form of the drug is experimental, it was tested for a much longer period of time. Interesting results were obtained in the stability assessment, which showed the extraordinary stability of pDNA. The released pDNA was stable for 6 months, both at a reduced temperature and RT. This is important information indicating that it is possible to prepare capsules for a patient for a longer period of dosing without fear of DNA inactivation.

In the context of the therapeutic potential of designed gene capsules, an important part of this study was the transduction of B16-F10 cancer cells using the viral vector from the gene capsules. The B16-F10 murine melanoma is one of the most commonly used cell lines in cancer research.<sup>38</sup> The active ingredient in the capsules, which was used for B16-F10 cell transduction, was rAAV/GFP. The results are promising and indicate the possibility of introducing genes from viral vectors enclosed in a solid drug form. In vitro experiments (Fig. 7) confirmed that the DNA released from the capsule was able to enter the cells, was expressed in the cells, and behaved as an active substance. The *GFP* + cells clearly confirmed the bioavailability of DNA from the capsule.

## Limitations

The clinical utility of our results would be enhanced if *in vivo* animal studies would be conducted. Additionally, the proposed composition of the gene capsule does not include excipients commonly used in enteral formulations. In future research, it would be worth considering excipients that ensure an enteral form.

## Conclusions

With reference to prior works about non-viral gene carriers taken orally,<sup>20–23</sup> this work has shown that viral vectors should be considered for the treatment of diseases, using orally administered gene therapy. Moreover, the performed experiments demonstrated that it is possible to obtain a solid form of a gene drug that combines gene therapy with a pharmacy recipe. The obtained gene capsules demonstrate the potential of gene therapy in increasing the availability of gene preparations for patients.

### ORCID iDs

Edyta Banaczowska-Duda  <https://orcid.org/0000-0002-9538-8129>  
 Alicja Bieńkowska-Tokarczyk  <https://orcid.org/0000-0002-7675-0428>  
 Maciej Małecki  <https://orcid.org/0000-0002-7078-4918>

### References

1. Urząd Rejestracji Produktów Leczniczych. *Farmakopea Polska XI*. 11<sup>th</sup> ed. Warszawa, Poland: Urząd Rejestracji Produktów Leczniczych, Wyrobów Medycznych i Produktów Biobójczych; 2017.
2. Forough AS, Lau ETL, Steadman K, et al. A spoonful of sugar helps the medicine go down? A review of strategies for making pills easier to swallow. *Patient Prefer Adherence*. 2018;12:1337–1346. doi:10.2147/PPA.S164406
3. Allen LV Jr. Basics of compounding: Capsules. *Int J Pharm Compd*. 2016;20(2):125–134. PMID:27323424
4. Ibrahim IR, Ibrahim MI, Al-Haddad MS. The influence of consumers' preferences and perceptions of oral solid dosage forms on their treatment. *Int J Clin Pharm*. 2012;34(5):728–732. doi:10.1007/s11096-012-9667-6
5. Gullapalli RP, Mazzitelli CL. Gelatin and non-gelatin capsule dosage forms. *J Pharm Sci*. 2017;106(6):1453–1465. doi:10.1016/j.xphs.2017.02.006
6. Sultana M, Butt MA, Saeed T, et al. Effect of rheology and poloxamers properties on release of drugs from silicon dioxide gel-filled hard gelatin capsules: A further enhancement of viability of liquid semi-solid matrix technology. *AAPS PharmSciTech*. 2017;18(6):1998–2010. doi:10.1208/s12249-016-0674-0
7. Allen LV Jr. Basics of compounding: Clinical pharmaceuticals. Part 2. *Int J Pharm Compd*. 2016;20(6):485–493. PMID:28339388
8. Bonhoeffer B, Kwade A, Juhnke M. Alternative manufacturing concepts for solid oral dosage forms from drug nanosuspensions using fluid dispensing and forced drying technology. *J Pharm Sci*. 2018;107(3):909–921. doi:10.1016/j.xphs.2017.11.007
9. Allen LV Jr. Basics of compounding: Clinical pharmaceuticals. Part 1. *Int J Pharm Compd*. 2016;20(5):389–396. PMID:28339374
10. Helin-Tanninen M, Pinto J. Oral solids. In: Bouwman-Boer Y, Fenton-May V, Brun P, eds. *Practical Pharmaceutics: An International Guideline for the Preparation, Care and Use of Medicinal Products*. Berlin, Germany: Springer; 2015: 51–75.
11. Sznitowska M. *Farmacja stosowana: technologia postaci leku*. Warszawa, Poland: PZWL Wydawnictwo Lekarskie; 2017.
12. Darji MA, Lalge RM, Marathe SP, et al. Excipient stability in oral solid dosage forms: A review. *AAPS PharmSciTech*. 2018;19(1):12–26. doi:10.1208/s12249-017-0864-4
13. Małecki M. Preparaty plazmidowe w terapii genowej. *Wspolczesna Onkol*. 2004;8(7):321–327. <https://www.termedia.pl/Plasmid-preparations-in-gene-therapy,3,2581,1,1.html>. Accessed September 17, 2021.
14. Mali S. Delivery systems for gene therapy. *Indian J Hum Genet*. 2013;19(1):3–8. doi:10.4103/0971-6866.112870
15. Keeler AM, ElMallah MK, Flotte TR. Gene therapy 2017: Progress and future directions. *Clin Transl Sci*. 2017;10(4):242–248. doi:10.1111/cts.12466
16. Shahryari A, Saghaeian JM, Mohammadi S, et al. Development and clinical translation of approved gene therapy products for genetic disorders. *Front Genet*. 2019;10:868. doi:10.3389/fgene.2019.00868
17. European Medicines Agency. Summary of product characteristics: Glybera. [https://www.ema.europa.eu/en/documents/product-information/glybera-epar-product-information\\_en.pdf](https://www.ema.europa.eu/en/documents/product-information/glybera-epar-product-information_en.pdf). Accessed January 18, 2021.
18. European Medicines Agency. Summary of product characteristics: Luxturna. [https://www.ema.europa.eu/en/documents/product-information/luxturna-epar-product-information\\_en.pdf](https://www.ema.europa.eu/en/documents/product-information/luxturna-epar-product-information_en.pdf). Accessed January 18, 2021.
19. European Medicines Agency. Summary of product characteristics: Zolgensma. [https://www.ema.europa.eu/en/documents/product-information/zolgensma-epar-product-information\\_en.pdf](https://www.ema.europa.eu/en/documents/product-information/zolgensma-epar-product-information_en.pdf). Accessed January 18, 2021.
20. Bhavsar MD, Amiji MM. Oral IL-10 gene delivery in a microsphere-based formulation for local transfection and therapeutic efficacy in inflammatory bowel disease. *Gene Ther*. 2008;15(17):1200–1209. doi:10.1038/gt.2008.67
21. Guliyeva U, Oner F, Ozsoy S, Haziroglu R. Chitosan microparticles containing plasmid DNA as potential oral gene delivery system. *Eur J Pharm Biopharm*. 2006;62(1):17–25. doi:10.1016/j.ejpb.2005.08.006
22. Li Z, Zhu SG, Gan K, et al. Poly-L-lysine-modified silica nanoparticles: A potential oral gene delivery system. *J Nanosci Nanotechnol*. 2005;5(8):1199–1203. doi:10.1166/jnn.2005.220
23. Guo J, O'Mahony AM, Cheng WP, O'Driscoll CM. Amphiphilic polyallylamine based polymeric micelles for siRNA delivery to the gastrointestinal tract: In vitro investigations. *Int J Pharm*. 2013;447(1–2):150–157. doi:10.1016/j.ijpharm.2013.02.050
24. Dunbar CE, High KA, Joung JK, Kohn DB, Ozawa K, Sadelain M. Gene therapy comes of age. *Science*. 2018;359(6372):eaan4672. doi:10.1126/science.aan4672
25. Lozier JN, Yankaskas JR, Ramsey WJ, Chen L, Berschneider H, Morgan RA. Gut epithelial cells as targets for gene therapy of hemophilia. *Human Gene Ther*. 1997;8(12):1481–1490. doi:10.1089/hum.1997.8.12-1481
26. O'Neill MJ, Bourre L, Melgar S, O'Driscoll CM. Intestinal delivery of non-viral gene therapeutics: Physiological barriers and preclinical models. *Drug Discov Today*. 2011;16(5–6):203–218. doi:10.1016/j.drudis.2011.01.003
27. Bowman K, Sarkar R, Raut S, Leong KW. Gene transfer to hemophilia A mice via oral delivery of FVIII-chitosan nanoparticles. *J Control Release*. 2008;132(3):252–259. doi:10.1016/j.jconrel.2008.06.019
28. He C, Yin L, Song Y, Tang C, Yin C. Optimization of multifunctional chitosan-siRNA nanoparticles for oral delivery applications, targeting TNF- $\alpha$  silencing in rats. *Acta Biomater*. 2015;17:98–106. doi:10.1016/j.actbio.2015.01.041
29. Nurunnabi M, Lee SA, Revuri V, et al. Oral delivery of a therapeutic gene encoding glucagon-like peptide 1 to treat high fat diet-induced diabetes. *J Control Release*. 2017;268:305–313. doi:10.1016/j.jconrel.2017.08.035
30. Knipe JM, Strong LE, Peppas NA. Enzyme- and pH-responsive microencapsulated nanogels for oral delivery of siRNA to induce TNF- $\alpha$  knockdown in the intestine. *Biomacromolecules*. 2016;17(3):788–797. doi:10.1021/acs.biomac.5b01518
31. Mao Y, Wang X, Yan R, et al. Single point mutation in adeno-associated viral vectors: DJ capsid leads to improvement for gene delivery *in vivo*. *BMC Biotechnol*. 2016;16(1):1–8. doi:10.1186/s12896-015-0230-0
32. Czajka M, Zajkowska A, Gawlak M, Bujalska-Zadrozny M, Malecki M. Mosaic recombinant adeno-associated virus vector rAAV/DJ/CAG for targeted gene delivery to melanoma cells metastasized to the lung. *Anticancer Res*. 2020;40(8):4425–4444. doi:10.21873/anticancer.14448
33. Wirth T, Parker N, Yla-Herttua S. History of gene therapy. *Gene*. 2013;525(2):162–169. doi:10.1016/j.gene.2013.03.137
34. Schmeer M, Bucholtz T, Schleef M. Plasmid DNA manufacturing for indirect and direct clinical applications. *Hum Gene Ther*. 2017;28(10):856–861. doi:10.1089/hum.2017.159

35. Kurian JJ, Lakshmanan R, Chmely WM, et al. Adeno-associated virus VP1u exhibits protease activity. *Viruses*. 2019;11(5):399. doi:10.3390/v11050399
36. Lotfinia M, Abdollahpour-Alitappeh M, Hatami B, Zali MR, Karimi-poor M. Adeno-associated virus as a gene therapy vector: Strategies to neutralize the neutralizing antibodies. *Clin Exp Med*. 2019;19(3): 289–298. doi:10.1007/s10238-019-00557-8
37. Lamešič D, Planinšek O, Lavrič Z, Ilič I. Spherical agglomerates of lactose with enhanced mechanical properties. *Int J Pharm*. 2017;516(1–2): 247–257. doi:10.1016/j.ijpharm. 2016.11.040
38. Giavazzi R, Decio A. Syngeneic murine metastasis models: B16 melanoma. *Methods Mol Biol*. 2014;1070:131–140. doi:10.1007/978-1-4614-8244-4\_10





# Non-secretory multiple myeloma: Diagnosis and management

Grzegorz Charliński<sup>1,2,A–F</sup>, Artur Jurczyszyn<sup>3,E,F</sup>

<sup>1</sup> Department of Internal Medicine, University of Warmia and Mazury, Olsztyn, Poland

<sup>2</sup> Department of Hematology, Warmian-Masurian Cancer Center of The Ministry of The Interior and Administration's Hospital, Olsztyn, Poland

<sup>3</sup> Plasma Cell Dyscrasias Center, Department of Hematology, Faculty of Medicine, Jagiellonian University College of Medicine, Kraków, Poland

A – research concept and design; B – collection and/or assembly of data; C – data analysis and interpretation;

D – writing the article; E – critical revision of the article; F – final approval of the article

Advances in Clinical and Experimental Medicine, ISSN 1899–5276 (print), ISSN 2451–2680 (online)

*Adv Clin Exp Med.* 2022;31(1):95–100

## Address for correspondence

Grzegorz Charliński

E-mail: grzegorzcharlinski0508@gmail.com

## Funding sources

None declared

## Conflict of interest

None declared

Received on May 28, 2021

Reviewed on August 16, 2021

Accepted on August 19, 2021

Published online on October 12, 2021

## Abstract

Multiple myeloma (MM) is one of the most commonly diagnosed blood cancers. One criterion for the diagnosis of MM is serum and/or urine monoclonal protein produced by clonal plasmocytes. However, about 1–2% of MM cases do not have monoclonal protein. If other diagnostic criteria are present, the possibility of a diagnosis of non-secretory MM should be considered. As the different types of non-secretory MM depend on the underlying cause, the current definition is considered insufficient. Currently, both the diagnosis and treatment of non-secretory MM are the same as those of secretory MM. Due to the rarity of non-secretory MM, most findings are from retrospective studies on small groups of patients and case reports. The method of monitoring the effectiveness of MM treatment remains a problem, as it is usually based on the assessment of the percentage of clonal plasma cells in the bone marrow and imaging studies.

**Key words:** diagnosis, management, non-secretory multiple myeloma

## Cite as

Charliński G, Jurczyszyn A. Non-secretory multiple myeloma: Diagnosis and management. *Adv Clin Exp Med.* 2022;31(1):95–100. doi:10.17219/acem/141455

## DOI

10.17219/acem/141455

## Copyright

© 2022 by Wrocław Medical University

This is an article distributed under the terms of the Creative Commons Attribution 3.0 Unported (CC BY 3.0) (<https://creativecommons.org/licenses/by/3.0/>)

## Introduction

Multiple myeloma (MM) is a blood cancer that arises from clonal plasmocytes (CP) that accumulate in the bone marrow (BM) and, in most cases, produce monoclonal (M) protein. Infiltration of CP may occur at extramedullary sites and/or in peripheral blood during disease progression.<sup>1</sup> Multiple myeloma is the 2<sup>nd</sup> most frequently diagnosed hematologic malignancy and accounts for 10–15% of all blood cancers and 1–1.8% of all cancers. The incidence of MM in Europe is 4.5–6.0/100,000/year.<sup>2</sup> According to the National Health Fund (Narodowy Fundusz Zdrowia (NFZ)) data, there were nearly 2600 new MM cases in Poland in 2016.<sup>3</sup> The median age at MM diagnosis is 72 years.<sup>2</sup> Over 90% of patients are >50 years old at MM diagnosis, while only 2% of patients are younger than 40 years.<sup>4</sup> Currently, the median overall survival (OS) of MM patients is approx. 6 years.<sup>5</sup> In the subgroup of patients treated with high-dose (HD) chemotherapy with

autologous stem cell transplantation (ASCT), the median OS is approx. 8 years.<sup>6</sup> In comparison, it is shorter in the subgroup of patients >75 years of age and amounts to approx. 5 years.<sup>5</sup> In 2014, the criteria for the diagnosis of MM were modified (Table 1).<sup>7</sup> One of the primary criteria for the diagnosis of MM are CP that produce M-protein. This is typically M-protein of the immunoglobulin (Ig) G, IgA or free light chains (FLCs) of the kappa or lambda type, which account for 54%, 21% and 16% of all MM cases, respectively.<sup>8</sup> Monoclonal IgD protein is found in less than 2% of MM patients. Notably, M-protein is not present in serum or urine in approx. 3–5% of patients meeting the criteria for MM diagnosis.<sup>9</sup> These types of MM are generally referred to as non-secretory (NS) MM. The introduction of serum FLC (sFLC) as part of laboratory diagnostics has confirmed both, the prevalence and change in the definition of NSMM. Currently, it is believed that approx. 2% of MM patients are diagnosed with true NSMM in which M-protein is not found by standard testing.<sup>10</sup>

**Table 1.** Revised IMWG diagnostic criteria for monoclonal gammopathy of undetermined significance, smoldering multiple myeloma and multiple myeloma itself<sup>7</sup>

Definition of monoclonal gammopathy of undetermined significance
Both criteria must be met: – serum M-protein (IgG or IgA) <3 g/dL and/or urinary <500 mg/24 h and – clonal plasmocytes (CP) in bone marrow <10%
– absence of organ damage resulting from proliferation of clonal plasmocytes or amyloidosis
Definition of smoldering multiple myeloma
Both criteria must be met: – serum M-protein (IgG or IgA) ≥3 g/dL and/or urinary ≥500 mg/24 h and/or – clonal plasmocytes in bone marrow 10–60%
– absence of organ damage resulting from proliferation of clonal plasmocytes or amyloidosis
Definition of multiple myeloma
Both criteria must be met: – clonal plasmocytes in bone marrow ≥10% or extramedullary plasmacytoma – ≥1 of the following types of organ damage resulting from CP proliferation:
– organ damage resulting from the proliferation of CP, specifically: • hypercalcemia: serum calcium >0.25 mmol/L (>1 mg/dL) higher than upper limit of normal or >2.75 mmol (>11 mg/dL) • renal insufficiency: creatinine clearance <40 mL/min or serum creatinine >177 μmol/L (>2 mg/dL) • anemia: hemoglobin concentration >2 g/dL below the lower limit of normal, or a hemoglobin concentration <10 g/dL • bone lesion(s): ≥1 osteolytic lesion on skeletal radiography, CT or PET/CT
– ≥1 of the following biomarkers of malignancy (SLiM): • clonal plasmocytes in bone marrow ≥60% • involved: uninvolved sFLCr ≥100 • >1 focal lesions (≥5 mm in size) on MRI

CT – computed tomography; IgG – immunoglobulin G; IMWG – International Myeloma Working Group; M-protein – monoclonal protein; MRI – magnetic resonance imaging; PET/CT – positron emission tomography/computed tomography; sFLCr – serum free light chain ratio.

## Objectives

This article aims to present the current terminology and principles of diagnosis and treatment of patients with NSMM.

## Methodology

Data on the diagnosis and treatment of NSMM presented in this article are based on published studies available in the PubMed online database. Based on selected keywords, we identified 358 articles related to NSMM. After reviewing them, 52 full papers were included, 14 of which are included in this article. The PRISMA flow diagram is presented as Fig. 1.

## Mechanisms of monoclonal protein production

The M-protein found in the serum and/or urine of patients with MM may take the following forms<sup>11</sup>:

1. high concentration of whole Ig molecules composed of heavy and light chains;
2. high concentration of whole Ig molecules with an additional high concentration of light chains not associated with heavy chains;
3. free light chains in the presence of very little or even no total Ig; and
4. free heavy chains in the absence of associated light chains.

The reasons for the inhibition of M-protein production, or secretion by CP, are not fully understood. One cause of true NSMM is the loss of the ability of CP

PRISMA 2020 flow diagram for updated systematic reviews which included searches of databases, registers and other sources

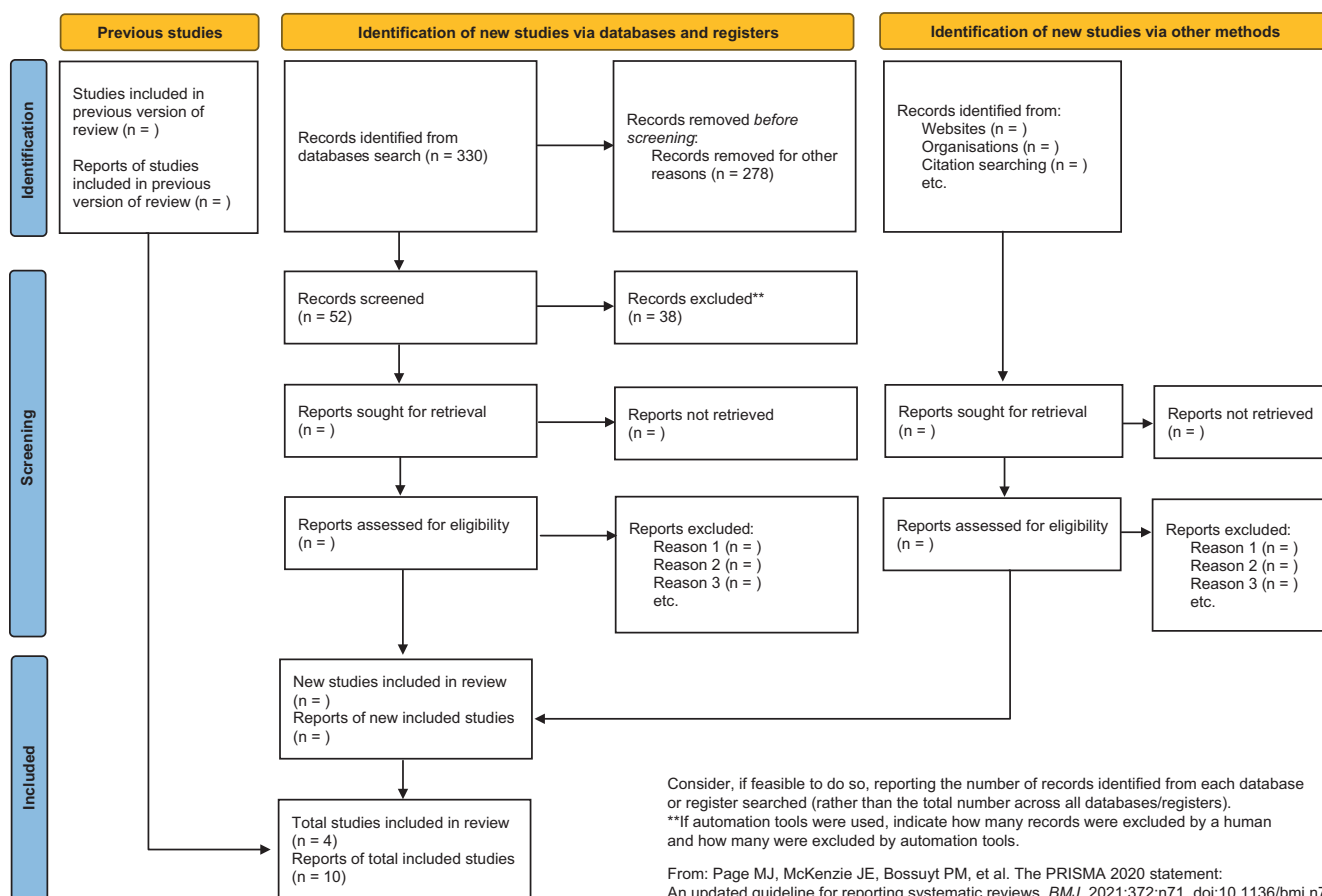


Fig. 1. PRISMA flow diagram

to initially secrete heavy chains and then light chains of Ig.<sup>12</sup> Other possible causes and hypotheses include: the loss of the polyadenylation site necessary for extracellular Ig secretion<sup>13</sup>; loss of the heavy chain V domain, which leads to the decreased secretion and increased intracellular Ig destruction<sup>14</sup>; loss of the ability to produce M-protein due to the mutation of the Ig light chain<sup>14</sup>; the secretion of heavy chains (which are considered toxic to plasmocytes) by plasmocytes which may promote their survival during clonal evolution in MM.<sup>15</sup>

## Types of NSMM

The International Myeloma Working Group (IMWG) defines NSMM as MM in the absence of M-protein in the serum and/or urine protein immunofixation assay.<sup>7,16</sup> Thus, this definition does not include MM with light chains only detected with the sFLC assay.<sup>9,17</sup> For this reason, the current definition is insufficient. As CP secretes the Ig component, cases of NSMM can be further classified into at least 2 distinct categories with subcategories<sup>18</sup>:

1. non-secretory MMs (85% of cases):

- oligo-secretory/FLC-restricted MMs: in most cases, the light chains are detected using the sFLC assay. In cases of oligo-secretory MM, serum M-protein <1.0 g/dL, urine M-protein <200 mg/24 h and sFLC values <100 mg/L are common;
- true NSMMs: CP produces M-protein, but is unable to secrete it into the extracellular space;
- false NSMMs: the immunofluorescence test shows the presence of M-protein inside CP, but no extracellular M-protein is found using standard laboratory tests;

2. non-producing MMs (15% of cases): no Ig production by CP is found.

Figure 2 shows the infiltration of CP in the BM of a patient with NSMM.

## Diagnosis and monitoring of NSMM

The diagnostic tests recommended for patients with suspected NSMM are the same as those recommended for patients with secreting MM. Besides diagnosing NSMM, one purpose of these tests is to identify the presence

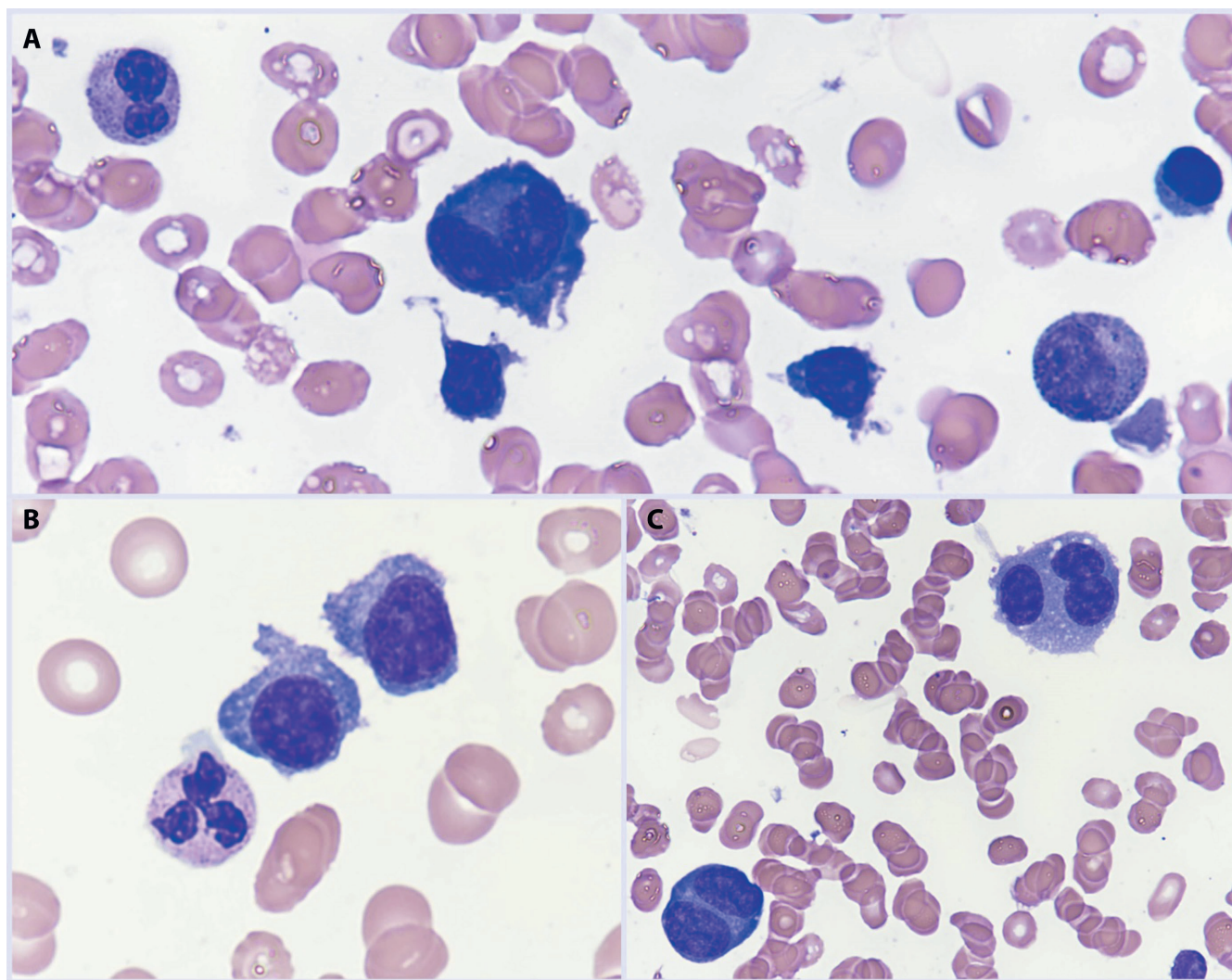


Fig. 2. Bone marrow aspirate smears showing plasma cells, including atypical binucleate (A) and trinucleate plasma cells (B,C). Wright's staining,  $\times 1000$  magnification. Courtesy of Marta Szostek, PhD

of symptoms of end organ damage, such as hypercalcemia, anemia or bone damage, to distinguish asymptomatic from symptomatic cases.<sup>16</sup> Initial laboratory investigation for NSMM should include complete blood count (CBC), serum protein electrophoresis (SPEP), immunofixation electrophoresis (IFE), sFLC assay, and quantitative Ig levels including IgD and IgE. Urinalysis for initial workup should include a 24-hour urine test with protein quantification and IFE. In addition, a baseline metabolic panel should be performed to assess coagulation factors, renal and liver function, serum calcium level,  $\beta$ -2-microglobulin, and lactate dehydrogenase (LDH). All patients with suspected NSMM require a BM biopsy for cytology, histopathology, multiparameter flow cytometry (MPF) and CD138 fluorescence in situ hybridization (FISH). The most frequently observed primary cytogenetic abnormality in NSMM patients is t(11,14) (q13,q32), which occurs in about 60–80% of patients with NSMM.<sup>19,20</sup> Table 2 lists the diagnostic tests recommended for patients with suspected or diagnosed NSMM. Figure 3 shows the diagnostic algorithm for NSMM.

Table 2. The diagnostic tests recommended for patients with suspected or diagnosed non-secretory multiple myeloma<sup>18</sup>

Initial diagnostic tests for non-secretory multiple myeloma
– CBC with peripheral blood smear
– routine chemistry, including serum calcium, $\beta$ -2 microglobulin, LDH, creatinine clearance (and/or serum creatinine), electrolytes, and liver function tests
– SPEP with IFE
– serum quantitative immunoglobulins (including IgD or IgE if suspected)
– 24-hour UPEP with IFE and M-protein quantification
– sFLC assay and sFLCr
– PET/CT scan

CBC – complete blood count; IFE – immunofixation electrophoresis; LDH – lactate dehydrogenase; M-protein – monoclonal protein; PET/CT – positron emission tomography/computed tomography; sFLC – serum free light chain; sFLCr – serum free light chain ratio; SPEP – serum protein electrophoresis; UPEP – urine protein electrophoresis; IgD – immunoglobulin D; IgE – immunoglobulin E.

If true NSMM is suspected, staining should be performed to assess the intracellular presence of Ig. True cases of NSMM typically lack easy parameters for evaluating

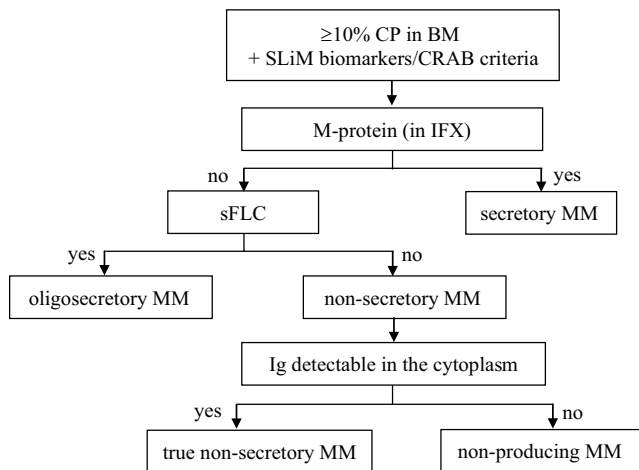


Fig. 3. Algorithm for the diagnosis of non-secretory multiple myeloma

CP – clonal plasmocytes; sFLC – serum free light chain; MM – multiple myeloma; BM – bone marrow; IFX – immunofixation; Ig – immunoglobulin.

treatment efficacy. For this reason, sensitive skeletal examinations, including positron emission tomography (PET)/computed tomography (CT), are recommended. It is thought that by performing PET/CT together with BM examination, the effectiveness of the applied NSMM treatment can be objectively assessed.<sup>21</sup> In general, monitoring the response of NSMM treatment is a challenge for both, hematologists and oncologists. The abovementioned methods are currently considered the “gold standard” for monitoring responses in all MM types, including BM aspiration in NSMM cases and MM tumor biopsy. The primary method used to monitor treatment response in patients with oligosecretory MM is the sFLC assay. A more sensitive test used to assess BM cells, including CP, is MPF.<sup>22</sup> Simultaneous BM examination with MPF and sensitive imaging (e.g., magnetic resonance imaging (MRI) or PET/CT) is currently the best way to assess the effectiveness of treatment in patients with NSMM.<sup>23,24</sup>

During induction treatment of patients with NSMM, it is recommended to repeat BM biopsy every 3–6 months and whole body PET/CT examination every 6–12 weeks, especially for cases of true NSMM. For patients who achieve remission after treatment or during maintenance treatment, it is recommended to repeat BM biopsy and PET/CT scan every 3–6 months.<sup>25</sup>

## Treatment of NSMM

Considering the rarity of NSMM and the ineligibility of patients with NSMM for clinical trials, its clinical course and prognosis are not fully known. We do not have conclusive data to suggest that the efficacy of NSMM treatment differs from that of secreting MM. The literature is dominated by case reports and retrospective analyses of small groups of NSMM patients. In 2020, PubMed published 8 case reports and 1 retrospective treatment analysis

Table 3. Treatment outcomes of non-secretory myeloma in selected retrospective studies

References	Number of patients with NSMM	Median OS [months]	Median PFS [months]
Chawla et al. <sup>26</sup>	124	49.3	28.6
Kumar et al. <sup>27</sup>	110	62	30
Smith et al. <sup>28</sup>	13	46	N/A
Terpos et al. <sup>29</sup>	6	four-year: 100%	36.1

NSMM – non-secretory multiple myeloma; OS – overall survival; PFS – progression free survival; N/A – not applicable.

of patients with NSMM. Retrospective studies investigated standard treatments for NSMM patients with conventional chemotherapy and HD chemotherapy followed by ASCT. In one of the largest retrospective studies, Chawla et al. examined the survival and prognosis of 124 patients with NSMM. The median progression-free survival (PFS) was 28.6 months and the median OS was 49.3 months. Investigators found that the time to progression, PFS, and OS before 2001 were all comparable to those for patients with secretory MM.<sup>26</sup> There has been a significant improvement in patient outcomes: median survival was 43.8 months before 2001 compared to 99.2 months for 2001–2012 ( $p < 0.001$ ). For patients diagnosed in the period of 2001–2012, OS was better in NSMM cases than in secretory MM cases (median survival of 8.3 years vs 5.4 years,  $p = 0.03$ ). There were no survival differences in patients treated with HD chemotherapy followed by ASCT.<sup>26</sup> In a study by Kumar et al., of 110 patients with NSMM treated with ASCT, the median PFS and OS were 30 months and 69 months, respectively. Three-year PFS in NSMM and secretory MM cases was 40% and 33%, respectively ( $p = 0.05$ ), while three-year OS was 66% and 61%, respectively ( $p = 0.26$ ).<sup>27</sup> Due to the higher occurrence of t(11,14) in NSMM, a change in treatment is expected in the near future. Studies by Smith et al.<sup>28</sup> and Terpos et al.<sup>29</sup> found longer survival times (PFS, OS) in patients with NSMM. The results of selected retrospective studies of patients with NSMM are presented in Table 3.

## Conclusions

Non-secretory MM is a rare type of MM. We lack data to determine the prevalence of NSMM in Poland. Extrapolating data obtained from other countries, we can expect approx. 25–50 new NSMM cases per year in Poland.

Given the subtypes and pathogenesis of NSMM, the definition of this form of MM is likely to change in the near future. Due to the difficulties in assessing the effectiveness of treatment, patients with NSMM usually do not qualify for prospective clinical trials. As a result, the available data are typically the results of retrospective studies or case reports. Currently, treatments for NSMM are the same

as those for secretory MM. Given the higher incidence of t(11,14), we may soon see a change in the treatment for this subgroup of MM. There is undoubtedly a need for more research into this rare type of MM.

### ORCID iDs

Grzegorz Charliński  <https://orcid.org/0000-0002-0595-5864>

Artur Jurczyszyn  <https://orcid.org/0000-0001-9796-8365>

### References

- Kumar SK, Rajkumar SV, Kyle RA, et al. Multiple myeloma. *Nat Rev Dis Primers*. 2017;3:17046. doi:10.1038/nrdp.2017.46
- Palumbo A, Bringhen S, Ludwig H, et al. Personalized therapy in multiple myeloma according to patient age and vulnerability: A report of the European Myeloma Network (EMN). *Blood*. 2011;118(17):4519–4529. doi:10.1182/blood-2011-06-358812
- Narodowy Fundusz Zdrowia. Szpiczak plazmocytowy (mnogi). Ocena jakości informacyjnej rejestru kontraktowego. <https://www.nfz.gov.pl/aktualnosci/aktualnosci-centrali/nowy-raport-nfz-szpiczak-plazmocytowy,7543.html>. Accessed June 29, 2021.
- Jurczyszyn A, Nahi H, Avivi I, et al. Characteristics and outcomes of patients with multiple myeloma aged 21–40 years versus 41–60 years: A multi-institutional case-control study. *Br J Haematol*. 2016;175(5):884–891. doi:10.1111/bjh.14328
- Durie BGM, Hoering A, Abidi M, et al. Bortezomib with lenalidomide and dexamethasone versus lenalidomide and dexamethasone alone in patients with newly diagnosed myeloma without intent for immediate autologous stem-cell transplant (SWOG S0777): A randomised, open-label, phase 3 trial. *Lancet*. 2017;389(10068):519–527. doi:10.1016/S0140-6736(16)31594-X
- Attal M, Lauwers-Cances V, Hulin C, et al. Lenalidomide, bortezomib, and dexamethasone with transplantation for myeloma. *N Engl J Med*. 2017;376(14):1311–1320. doi:10.1056/NEJMoa1611750
- Rajkumar SV, Dimopoulos M, Palumbo A, et al. International myeloma working group updated criteria for the diagnosis of multiple myeloma. *Lancet Oncol*. 2014;15(12):e538–e548. doi:10.1016/S1470-2045(14)70442-5
- Sharma A, Binazir T, Sintow A, Lee CC, Shaharyar S, Tache J. An extremely rare manifestation of multiple myeloma: An immunoglobulin D secreting testicular plasmacytoma. *Cureus*. 2017;9(6):e1400–e1406. doi:10.7759/cureus.1400
- Lonial S, Kaufman JL. Non-secretory myeloma: A clinician's guide. *Oncology*. 2013;27(9):924–930. PMID:24282993
- Rajkumar SV. Multiple myeloma: 2020 update on diagnosis, risk-stratification and management. *Am J Hematol*. 2020;95(5):548–567. doi:10.1002/ajh.25791
- Corso A, Mangiacavalli S. Non-secretory myeloma: Ready for a new definition? *Mediterr J Hematol Infect Dis*. 2017;9(1):e2017053. doi:10.4084/MJHID.2017.053
- Preud'Homme JL, Hurez D, Danon F, Brouet JC, Sligmann M. Intracytoplasmic and surface-bound immunoglobulins in "nonsecretory" and Bence-Jones myeloma. *Clin Exp Immunol*. 1976;25(3):428–436. PMID:822974
- Cogné M, Preud'Homme JL. Gene deletions force nonsecretory alpha-chain disease plasma cells to produce membrane-form alpha-chain only. *J Immunol*. 1990;145(8):2455–2458. PMID:2120331
- Cogné M, Guglielmi P. Exon skipping without splice site mutation accounting for abnormal immunoglobulin chains in nonsecretory human myeloma. *Eur J Immunol*. 1993;23(6):1289–1293. doi:10.1002/eji.1830230615
- Decourt C, Galea HR, Sirac C, Cogné M. Immunologic basis for the rare occurrence of true nonsecretory plasma cell dyscrasias. *J Leukoc Biol*. 2004;76(3):528–536. doi:10.1189/jlb.0803382
- The International Myeloma Working Group. Criteria for the classification of monoclonal gammopathies, multiple myeloma, and related disorders: A report of the International Myeloma Working Group. *Br J Haematol*. 2003;121(5):749–757. PMID:12780789
- Lonial S, Kaufman JL. Non-secretory myeloma: A clinician's guide. *Oncology*. 2013;27(9):924–928. PMID:24282993
- Dupuis MM, Tuchman SA. Non-secretory multiple myeloma: From biology to clinical management. *Onco Targets Ther*. 2016;15(9):7583–7590. doi:10.2147/OTT.S122241
- Dimopoulos MA, Moreau P, Terpos E, et al. Multiple myeloma: EHA-ESMO Clinical Practice Guidelines for diagnosis, treatment, and follow-up. *Ann Oncol*. 2021;32(3):309–322. doi:10.1016/j.annonc.2020.11.014
- Avet-Loiseau H, Garand R, Lodé L, Harousseau JL, Bataille R; Intergroupe Francophone du Myélome. Translocation t(11;14)(q13;q32) is the hallmark of IgM, IgE, and nonsecretory multiple myeloma variants. *Blood*. 2003;101(4):1570–1571. doi:10.1182/blood-2002-08-2436
- Nandakumar B, Kumar SK, Dispenzieri A, et al. Cytogenetic features and clinical outcomes of patients with non-secretory multiple myeloma in the era of novel agent induction therapy. *Clin Lymphoma Myeloma Leuk*. 2020;20(1):53–56. doi:10.1016/j.clml.2019.09.624
- Zamagni E, Cavo M. The role of imaging techniques in the management of multiple myeloma. *Br J Haematol*. 2012;159(5):499–513. doi:10.1111/bjh.12007
- Paiva B, Martinez-Lopez J, Vidrales MB, et al. Comparison of immunofixation, serum-free light chain, and immunophenotyping for response evaluation and prognostication in multiple myeloma. *J Clin Oncol*. 2011;29(12):1627–1633. doi:10.1200/JCO.2010.33.1967
- Durie BGM, Harousseau JL, Miguel JS, et al. International uniform response criteria for multiple myeloma. *Leukemia*. 2006;20(9):1467–1473. doi:10.1038/sj.leu.2404284
- Regelink JC, Minnema MC, Terpos E, et al. Comparison of modern and conventional imaging techniques in establishing multiple myeloma-related bone disease: A systematic review. *Br J Haematol*. 2013;162(1):50–61. doi:10.1111/bjh.12346
- Chawla SS, Kumar SK, Dispenzieri A, et al. Clinical course and prognosis of non-secretory multiple myeloma. *Eur J Haematol*. 2015;95(1):57–64. doi:10.1111/ejh.12478
- Kumar S, Perez WS, Zhang MJ, et al. Comparable outcomes in non-secretory and secretory multiple myeloma after autologous stem cell transplantation. *Biol Blood Marrow Transplant*. 2008;14(10):1134–1140. doi:10.1016/j.bbmt.2008.07.011
- Smith DB, Harris M, Gowland E, Chang J, Scarffe JH. Non-secretory multiple myeloma: A report of 13 cases with a review of the literature. *Hematol Oncol*. 1986;4(4):307–313. doi:10.1002/hon.2900040407
- Terpos E, Apperley JF, Samson D, et al. Autologous stem cell transplantation in multiple myeloma: Improved survival in nonsecretory multiple myeloma but lack of influence of age, status at transplant, previous treatment and conditioning regimen. A single-centre experience in 127 patients. *Bone Marrow Transplant*. 2003;31:163–170. doi:10.1038/sj.bmt.1703818